Fabrication of Novel Hydrogel Films for Drug Delivery Applications: Influence of Crosslinker and Nanomaterials on Film Properties

A Thesis Submitted to
Indian Institute of Technology Guwahati
for the Degree of

Doctor of Philosophy

By

K. Dharmalingam

Department of Chemical Engineering
Indian Institute of Technology Guwahati
Assam, India
February 2020

INDIAN INSTITUTE OF TECHNOLOGY GUWAHATI
Department of Chemical Engineering
Guwahati – 781039

STATEMENT

The present thesis entitled, "**Fabrication of Novel Hydrogel Films for Drug Delivery Applications: Influence of Crosslinker and Nanomaterials on Film Properties**" has been carried out by me under the supervision of Dr. R. Anandalakshmi, Department of Chemical Engineering, Indian Institute of Technology Guwahati. This work has not been submitted elsewhere for the award of any degree.

February, 2020.

(**K. Dharmalingam**)
Department of Chemical Engineering,
Indian Institute of Technology Guwahati,
Guwahati – 781 039

INDIAN INSTITUTE OF TECHNOLOGY GUWAHATI
Department of Chemical Engineering
Guwahati – 781039

CERTIFICATE

It is certified that the work described in this thesis, entitled "**Fabrication of Novel Hydrogel Films for Drug Delivery Applications: Influence of Crosslinker and Nanomaterials on Film Properties**", done by Mr. **K. Dharmalingam**, a Ph.D. student of Department of Chemical Engineering, Indian Institute of Technology Guwahati, for the award of degree of *Doctor of Philosophy* has been carried out under my supervision. This work has not been submitted elsewhere for the award of any degree.

February, 2020.

Dr. R. Anandalakshmi
Associate Professor
Department of Chemical Engineering
Indian Institute of Technology Guwahati
Guwahati – 781 039

Dedicated to my beloved Parents

ACKNOWLEDGEMENTS

First, I thank God Almighty, who is the Alpha and the Omega, the Beginning and the End, for all His blessings in my life especially in this PhD journey.

I express my sincere gratitude to my research supervisor Dr. R. Anandalakshmi for her constant support, guidance, encouragement, advice, and valuable discussions, which helped me to improve an understanding of the subject along with skills and the successful culmination of my thesis work. I must acknowledge her for providing the unconditional freedom to work, think and express on whatever I have done in my research work by keeping the faith on my capabilities.

I am highly thankful to my doctoral committee members, Prof. G. Pugazhenthi (Chairman), Dr. Partho Sarathi Gooh Pattader and Dr. S. Senthilkumar for their continuous academic guidance and checking my work progress and seminars during my Ph.D. Their valuable discussions and suggestions helped me to understand the basics of the subject and along with skills and also improve the quality of my research work.

I would like to express my sincere gratitude to the Head of the Department of the Chemical Engineering for giving me the opportunity to work in the department and to use departmental facilities. I am also grateful to all the faculty members of the Chemical Engineering department. I would also like to thank Mr. Harsaraj Biswanath for his technical assistance and friendly discussions. My special thanks to all scientific officers and staff members in our department and central instruments facility.

My sincere thanks to collaborators Prof. Ajaikumar B. Kunnumakkara, Prof. Vibin Ramakrishnan and Dr. Lalit Mohan Pandey (Deapartment of Biosciences and Bioengineering, IITG) for providing facilities and suggestions.

The financial support for this thesis is provided by the Indian Institute of Technology Guwahati and Ministry of Human Resource and Development, India is highly acknowledged.

I would like to thank my research team members and colleagues Dr. Pankaj Jha, Mr. Aditya, Mr. Abhishek, Mrs. Suhas and Mr. Bhowmik for their help, suggestions and enjoyable company.

I would like to thank my best friends in IIT Guwahti Mr. Philip, Mr. Arul, Mr. Ankur, Mr. Sunil, Mr. Kaniska, Mr. Aniruddha, Ms. Prerona, Mr. Ujwal, Mr. Rajsekar, Mr. Suresh, Mr. Vijay, Mr. Sathishraj, Dr. Atul Kumar, Mr. Arun, Mr. Muthuvel, Mr. Anil Kumar, Dr. Devivash, Dr. Padma, Ms. Harsha, Dr. Hassan, Mr. Srinivas, Mr. Piyal, Mr. Bikas, Ms. Barnali, Mr. Kuldeep, Mr. Rupam and Mr. Pritam for their support in every step of my life.

I sincerely submit my due respect to my beloved parents Mr. C. Koodalingam and Mrs. K. Jeya as well as my wife Dr. M.K. Yogeswari and my son Master Nathan Samuel for their unfailing love and affection without would not which I would not be what I am.

I express my deep sense of gratitude to my father-in-law Mr. M.G. Krishnamoorthi, my mother-in-law Mrs. K. Indhumathi, my brother-in-law Mr. K.R.Arun Kumar, my sister-in-law Mrs. K. Gowri Gayathri and my niece Ms. A.G. Akshara who provided their help to me in all the time.

I would like to thank my brothers and sisters in Christ Mr. Stephen Vijaykumar, Mrs. Ruby Grace Stephan Vijay, Mr. Gnanaprakasam, Mrs. Lizzie Gnanaprakasam, Mr. Sam Israel, Dr. Magdalene, Mr. Josiah, Mrs. Joy Josaih, Mr. Joseph, Dr. Nissi Paul Joseph, Mr. John Karuna, Mrs. Joyce Karuna, Mr. Divakar, Mr. Senthilkumar, Dr. John Irudaya Raj, Mr. Raja, Mr. Krishna and Mr. Pandi for their prayers and constant support.

Finally, I would like to express my deepest gratitude to all my relatives who gave constant suppot and help throught this PhD journey.

K. Dharmalingam

Abstract

Hydrogels are made up of hydrophilic polymers or hydrophilic monomers, which are crosslinked as three-dimensional networks to hold ample amount of water. Thus, the hydrogels can swell in water media without dissolving. Since human body contains almost 60% water, hydrogels, which can imbibe plenty of water into their network structure, are found to be a good candidate in biomedical field. Therefore, the potential applications of the fabricated hydrogels have been investigated for wound healing and drug delivery applications in the current work.

In the present study, chapters first, second and third provides a brief introduction about hydrogels and their preparation methods, a comprehensive review of sodium carboxymethylcellulose (NaCMC) and hydroxypropylmethylcellulose (HPMC) based hydrogels for various applications and materials and methods for fabricating various hydrogel films, respectively.

Fourth chapter mainly focuses on preparation of hydrogel films from NaCMC and HPMC using citric acid (CA) as a crosslinker. Various properties of fabricated NaCMC-HPMC/CA hydrogel films were studied in detail. The chemical crosslinking (ester bond) between NaCMC and HPMC was confirmed by FTIR analysis. It was found that swelling ratio, crystallinity and water contact angle of the hydrogel films based on NaCMC-HPMC (2 wt.%) decreased with increase in CA from 5% to 20% (by weight). The increase in glass transition temperature (T_g) and decrease in initial decomposition temperature were observed with increase in CA concentration in NaCMC-HPMC films and were confirmed by DSC and TGA analysis, respectively. Tensile strength of hydrogel films decreased while elongation (%) increased with increase in CA. Highly interconnected nanoporous network and decrease in average pore diameter from micron to nanosize in cryofixed hydrogel films were found by

FESEM and mercury intrusion porosimetry, respectively. The drug loading efficiency of hydrogel films was significantly higher for methylene blue compared to tetracycline. It was observed that hydrogel films released the drugs in sustained manner for 72 h. The hydrogel films showed significant antibacterial activity after three days of release at 37°C in PBS (pH 7.4).

Fifth chapter focuses on fabrication of hydrogel films comprising of NaCMC, HPMC, CA and zinc oxide nanoparticles (ZnO NPs) by solution casting method. XRD patterns showed that crystallinity of films was decreased and also ZnO crystalline peaks were disappeared with increase in CA concentrations (5-20 wt.%). FTIR and micro-Raman analysis confirmed the absence of Zn-O vibration. It was found that swelling ratio, tensile strength and initial decomposition temperature of the films decreased with increase in CA. As CA concentration increased, the agglomeration of the nanoparticle increased according to FESEM and FETEM analysis. FETEM-EDX elemental mapping showed that the nanoparticle composed of C, O and Zn. The prepared films released zinc and showed significant antibacterial activity against *Escherichia coli* MTCC 1610 and *Staphylococcus aureus* MTCC 6538. The fabricated films exhibited biocompatibility with HaCaT cells.

Sixth chapter explains about influence of CA on hydrogel films composed of NaCMC, HPMC and copper oxide nanoflakes (CuO NFs) and the physico-chemical, mechanical, thermal and antibacterial properties of fabricated hydrogel films were comprehensively studied. XRD patterns showed that the prepared hydrogel films revealed the crystalline phase for cupric oxide/cuprous oxide/copper ($CuO/Cu_2O/Cu$) at 20% CA concentration. Laser micro-Raman spectroscopy confirmed the presence of CuO and Cu_2O in the films. Increase in CA concentration decreased the swelling ratio and tensile strength and increased the decomposition temperature of NaCMC, HPMC and CuO.

According to FESEM and FETEM results, shape and size of CuO nanoflakes were completely changed into spherical nanoparticles with increase in CA concentration. HRTEM and inverse FFT images showed that the d-spacing of CuO (0.252 nm), Cu_2O (0.24 nm) and Cu (0.20 nm) were in exact match with XRD results. The prepared hydrogel films exhibited significant antibacterial activity and biocompatibility against HaCaT cells.

Seventh chapter describes about the influence of grapefruit seed extract (GFSE), which possess natural antimicrobial and antioxidant constituents, on CA and ZnO NPs incorporated cellulose-based hydrogel films containing NaCMC and HPMC. The effect of GFSE (0.25-1.0%, v/v) on hydrogel films was examined for their physico-chemical, mechanical, thermal, antioxidant and antibacterial properties. The swelling ratio, tensile strength and thermal stability of hydrogel films decreased with increase in GFSE concentrations. On the other hand, elongation (%) and antioxidant activity of hydrogel films were found to be 34-60% and 25-79%, respectively for increasing amounts of GFSE. FESEM and FETEM clearly showed that two different types of nanoparticles (50-90 nm and 5-10 nm) were present in GFSE incorporated films. The release of polyphenolic compounds and zinc from hydrogel films was in sustained manner. Furthermore, the fabricated hydrogel films exhibited antibacterial activity against both *E. coli* and *S. aureus*.

Overall conclusions and significance of findings are listed in chapter eight of this thesis.

All these results suggest that the preprared hydrogel films could find their potential applications in wound healing and drug delivery applications, especially in treating chronic wounds.

Keywords: Sodium carboxymethylcellulose, Hydroxypropylmethylcellulose, Citric acid, Zinc oxide nanoparticles, Zinc oxide complexes, Copper oxide nanoflakes, Grapefruit seed extract, Antioxidant, Wound healing, Drug delivery, Biocompatibility.

CONTENTS

LIST OF TABLES

LIST OF FIGURES

ABBREVIATIONS

AA or AAc	acrylic acid
AMPS	acrylic polymer 2-acrylamido-2-methylpropanesulfonic acid
AE	allylic ethers
ABA	antibacterial activity
AOA	antioxidant activity
APS	ammonium persulfate
AIBN	2,2-azo-isobutyronitrile
BPO	benzoyl peroxide
β-CD	β-cyclodextrin
CMCS	carboxymethylchitosan
CAS	ceric ammonium sulfate
CS	chitosan
CA	citric acid
$CuCl_2$	copper chloride
CuO	cupric oxide
Cu_2O	cuprous oxide
Cu	copper
MTT	3-(4,5-dimethylthiazol-2-yl)-2,5-diphenyl tetrazolium bromide
DPPH	2,2-diphenyl-1-picrylhydrazyl
DVS	divinylsulphone
DADMAC	diallyldimethylammonium chloride
EPH	epichlorohydrin
E. coli	*Escherichia coli*
EDGE	ethyleneglycoldiglycidyl ether
EHA	2-ethylhexyl acrylate
EDGMA	ethylene glycol dimethacrylate
EDGE	ethyleneglycol diglycidyl ether
FFT	fast Fourier transform
FA	fumaric acid
GA	gallic acid
GTA or GLA	glutaraldehyde
GO-Ag	graphene oxide silver nanoparticles
GQD	graphene quantum dot
HCl	hydrochloric acid
HPC	hydroxypropylcellulose
HEC	hydroxylethylcellulose
HPMC	hydroxypropylmethylcellulose
LDH	layered double hydroxides
MA	malic acid
MC	methyl cellulose
MB	methylene blue
MBA	N,N'-methylene bis acrylamide
TEMED	N,N,N',N'-tetramethylethylenediamine

NIPA	N-isopropylacrylamide
NVP	N-vinyl-2-pyrrolidone
DCC	N,N'-dicyclohexylcarbodiimide
E (%)	percentage elongation
PDMAEMA	poly(2-dimethylaminoethyl methacrylate)
PVP	poly(vinyl pyrrolidone)
PVA	poly(vinyl alcohol)
PAAc	poly(acrylic acid)
PEG	poly(ethylene glycol)
PAAm or PAM	poly(acrylamide)
PAN	poly(acrylonitrile)
PHEMA	poly-2-hydroxyethylmethacrylate
PMMA	poly(methyl methacrylate)
PHFIM	poly(hexa-fluoroisopropyl methacrylate)
PEO	poly(ethyleneoxide)
PPO	poly(propyleneoxide)
PLA	poly(lactide)
PGA	poly(glycolide)
PF	poly(propylene fumarate)
PHB	poly(hydroxy butyrate)
PVAc	poly(vinyl acetate)
PNIPAAm	poly(N-isopropylacrylamide)
PHPMA	poly(hydroxypropylmethacrylamide)
KPS	potassium persulfate
AgNPs	silver nanoparticles
NaCMC	sodium carboxymethyl cellulose
Na-Alg	sodium alginate
S. aureus	*staphylococcus aureus*
SNP	sulfur nanoparticles
SR	swelling ratio
TS	tensile strength
TC	tetracycline hydrochloride
ZnO	zinc oxide
ZnO-MCM-41	zinc oxide impregnated mesoporous silica

Chapter 1

Introduction

1.1. Hydrogel

In recent years, hydrogels have gained more attention due to their excellent water absorption and retention ability and their wide-spread applications in agriculture, drug delivery systems, pharmaceuticals, hygienic products, contact lenses, food packaging, tissue engineering, catalysis, artificial organs, waste water treatment and textile industry. Hydrogels are made up of hydrophilic monomers or hydrophilic polymers to retain large quantity of water or biological fluids in their physically or chemically crosslinked three-dimensional polymeric network structures (Arica, 2000; Fei et al., 2000, 2000; Gorgieva and Kokol, 2011; Ibrahim et al., 2013; Kok et al., 1999; Mahinroosta et al., 2018; Pourjavadi et al., 2006; Roy et al., 2012; Sarkar and Singh, 2017; Shahbazi et al., 2016; Tran et al., 2017). The capability of hydrogels to absorb or retain water is due to the presence of large number of hydrophilic groups in the polymeric backbone. It is not dissolved in water or biological fluids because of their higher crosslinking degree (Ahmed, 2015). The fluid holding capacity of the hydrogels mainly depends on nature of the polymer(s) and crosslinking density. Hydrogels can be engineered with tailored properties such as chemical and biological response to stimuli (Fig. 1.1), mechanical strength and biodegradation (Ahmed, 2015; Burkert at al., 2007).

1.2. Hydrogel preparation

In general, hydrogels can be prepared by physical and chemical methods (Mahinroosta et al., 2018).

Physical methods

Physical synthesis involves crosslinking of polymers by hydrogen bonding or ionic bonding or hydrophobic forces, which plays main role in forming the hydrogel network.

Physical hydrogel preparation can be done in several ways, which include (a) warming or cooling a polymer solution to form a gel, (b) crosslinking the polymers in solutions using freeze-thaw cycles, (c) lowering pH of two different polymers in aqueous solutions to make strong hydrogen bonding, (d) mixing of polyanion and polycation solutions to form a gel and (e) mixing of polyelectrolyte solution with a multivalent ion of opposite charge to form a gel. If the environmental conditions such as pH, temperature and ionic strength of solution change, the physically crosslinked gels dissolve considerably (Fig. 1.1). Also, mechanical properties are poor in the case of physical hydrogels (Caló and Khutoryanskiy, 2015; Hoffman, 2012; Ma et al., 2015).

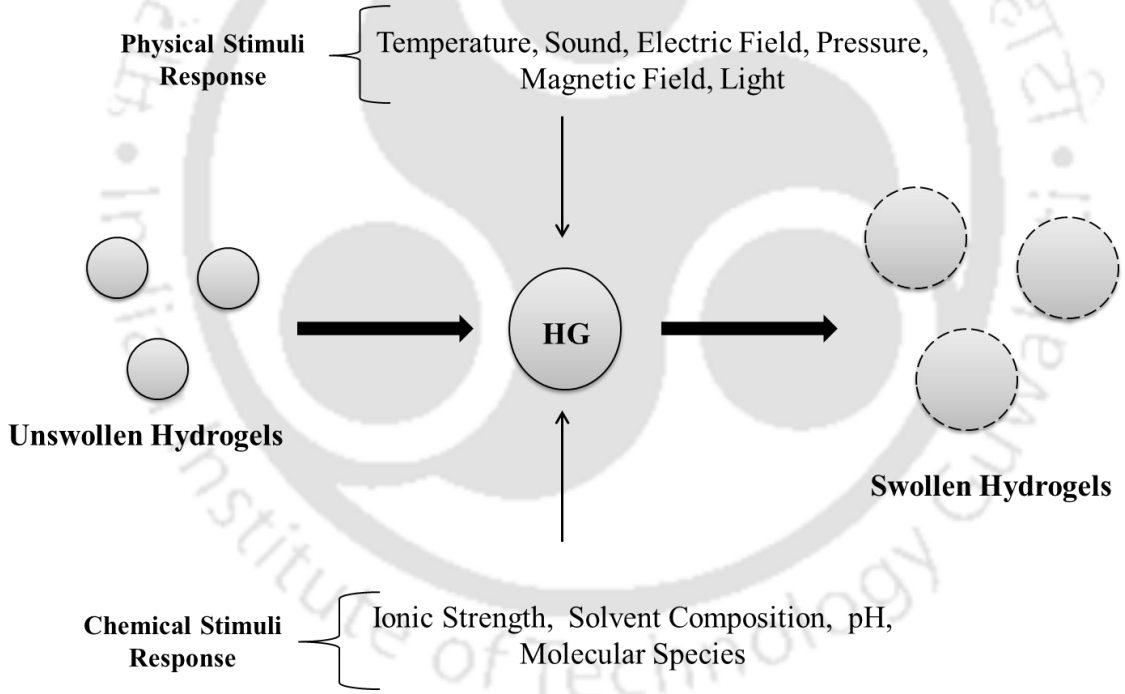

Figure 1.1: Physical and chemical stimuli response of hydrogels.

Chemical methods

In chemical synthesis, the formation of covalent linkages is achieved by crosslinking of polymers in dry state or in solution state to make chemical hydrogels. The resultant

hydrogels may undergo different swelling rate based on pH, temperature and ionic strength used for crosslinking.

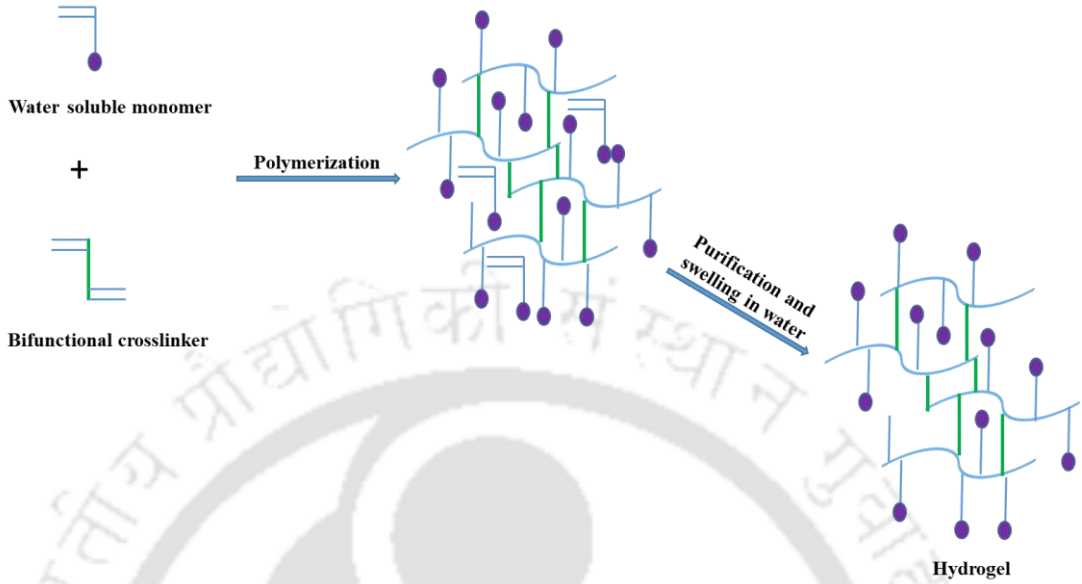

Figure 1.2: Synthesis of chemical hydrogels by polymerization.

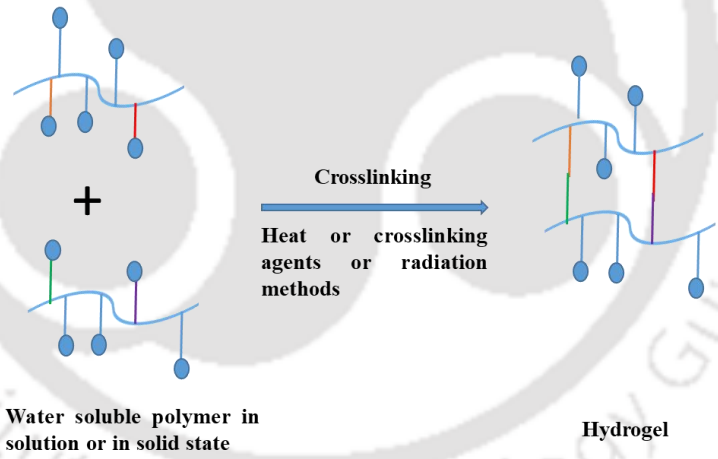

Figure 1.3: Synthesis of chemical hydrogels by crosslinking of water-soluble polymers.

The shape of the chemically crosslinked hydrogels may change when it is exposed to an electric field. Preparation of chemically crosslinked hydrogels can be further classified into two categories: (a) three-dimensional polymerization – hydrophilic monomer is polymerized using polyfunctional crosslinking agents (AE, MBA, TEMED, EDGE, EGDMA, etc.) and free radical generating compounds (BPO, KPS,

AIBN, APS, UV-, gamma- or electron irradiation) (Fig. 1.2) and (b) direct cross-linking of water-soluble polymers using crosslinking agents (GTA, EPH, DVS, DCC, FA, CA and MA), electron beam and gamma radiation (Fig. 1.3).

The main disadvantage of three-dimensional polymerization method is the presence of unreacted monomers, often toxic, in the final product. Hence, the monomers need to be purified thoroughly. This purification step is often time-consuming and it may extend up to few weeks in comparison with direct crosslinking methods in which the final product is purified shortly (Bajpai and Giri, 2003; Buhus et al., 2007; Caló and Khutoryanskiy, 2015; Chatterji and Kaur, 1992; Demitri et al., 2008; Ghorpade et al., 2017; Hashem et al., 2013; Pourjavadi et al., 2006, 2007; Sannino et al., 2003, 2006; Sarkar and Singh, 2017; Wach et al., 2001; Wang et al., 2007). There are other ways to classify hydrogels based on physical structure, ionic charge, synthesis route, size, mechanical and structural properties (Fig. 1.4) (Mahinroosta et al., 2018).

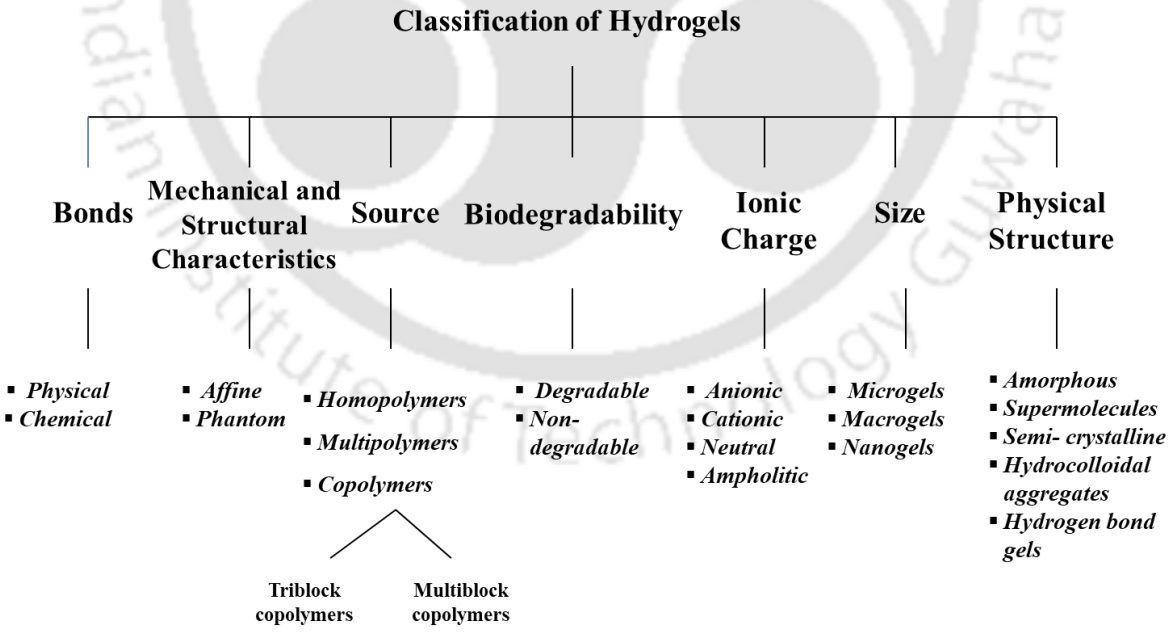

Figure 1.4: Classification of hydrogels based on different parameters.

1.3. Polymers for hydrogels

In the recent past, hydrogels, derived from natural polymers and their derivatives (Table 1.1) have been largely used in drug delivery systems and tissue engineering applications (Bao et al., 2014a; Hoffman, 2012).

Table 1.1: Natural/synthetic polymers used for synthesizing hydrogel matrices (Caló and Khutoryanskiy, 2015; Hennink and van Nostrum, 2012; Hoffman, 2012).

Natural polymers and their derivatives	**Synthetic polymers and their derivatives[a]**
agar, agarose, alginate, carrageenan, cellulose, chitin, chitosan, collagen, dextran, fibrin, gelatin, hyaluronic acid, pectin, polylysine, pullulan, starch , carboxymethyl chitin, MC, HPC, HEC, HPMC, NaCMC, chondroitin sulfate, dextran sulfate.	PVP, PVA, PAAc, PEG, PAAm, PAN, PHEMA, PMMA, PHFIM, NVP, PEO, PPO, PLA, PGA, PF, PHB, PVAc, PNIPAAm, PHPMA

[a]Refer abbreviations for expansion.

Amongst all polymers, cellulose is the world's abundant natural, renewable, non-toxic and biodegradable polymer and it has been used to prepare cellulose-based hydrogels by physical or chemical cross-linking methods for various applications (Deng et al., 2008; Guo and Chu, 2005a; Raucci et al., 2015; Weng et al., 2004a).

1.4. Cellulose based derivatives

Sodium carboxymethylcellulose

Carboxymethylcellulose (CMC), commonly known as sodium salt of NaCMC, is one of the most widely used ether derivative of celluloses and hydrophilic in nature.

NaCMC is an anionic polyelectrolyte, which is sensitive to pH and ionic strength variations (Lopez et al., 2015). It possesses biocompatibility, biodegradability, film forming ability and excellent viscodynamic elasticity. It is used as a stabilizer and thickener in food industry. The presence of large number of hydroxyl (-OH) and carboxyl (-COOH) groups makes the NaCMC polymer as versatile material for various applications such as pharmaceutical, food, personal care/cosmetic and paper industries. The molecular structure of NaCMC is shown in Fig. 1.5. The degree of substitution (DS) of NaCMC is defined as an average number of carboxymethyl (-CH_2-COOH) groups substituted per monomer molecule. It is generally ranged between 0 and 3 with the remaining R = H. Furthermore, swelling rate and equilibrium water uptake of NaCMC is higher than other cellulose based hydrogels (Ma et al., 2015; Ghorpade et al., 2017).

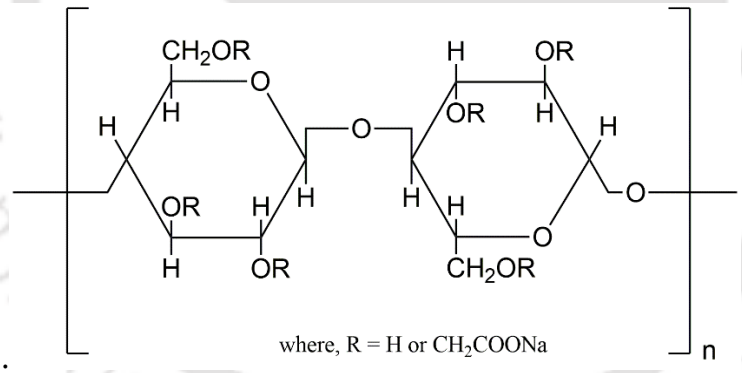

Figure 1.5: Molecular structure of NaCMC.

A number of research works have been reported on preparation of NaCMC based hydrogels by physical or chemical crosslinking (Capanema et al., 2018a; Javanbakht and Namazi, 2018; Joorabloo et al., 2019; Liu et al., 2002; Wach et al., 2003). However, hydrogels fabricated from NaCMC alone had poor mechanical strength in swollen state, which restricted their applications in wound dressing and drug delivery materials (Qiu

et al., 2007; Wang et al., 2007). The presence of -COOH groups led to enhanced pore sizes in the swollen state due to strong electronic repulsions. Consequently, drug loaded into NaCMC based hydrogel cannot be used for controlled drug delivery (Shen et al., 2015).

Hydroxypropylmethylcellulose

Hydroxypropylmethylcellulose (HPMC) is an ether derivative of cellulose which is water soluble, tasteless and odorless. It is prepared by substituting hydroxypropyl ($CH_3CH(OH)CH_2$) and methyl ($-CH_3$) groups to primary and secondary hydroxyl (-OH) groups of cellulose (Joshi, 2011). The molecular structure of HPMC is shown in Fig. 1.6. Commercially, it is available in different grades such as HPMC E, F, J and K based on their molecular weight. The properties of HPMC depend on its molecular weight, methyl and hydroxypropyl content. HPMC is frequently used for controlled release of drugs due to the presence of hydrophobic (methyl) and hydrophilic (hydroxypropyl) moiety. It possesses good swelling and gelation capability (Chopra et al., 2007; Joshi, 2011; Marani et al., 2015; Siepmann and Peppas, 2012). FDA approved HPMC as a non-toxic substance to human body (Marani et al., 2015; Mujtaba and Kohli, 2016). HPMC is an alternative to gelatin because of its emulsifying and thickening property.

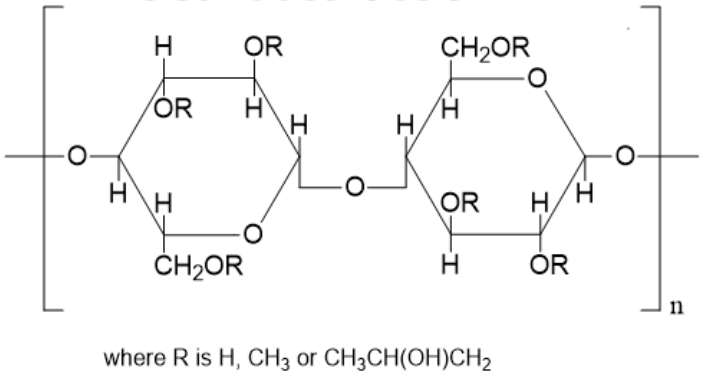

Figure 1.6: Molecular structure of HPMC.

The films prepared using HPMC are tougher, elastic and bioadhesive and also stable in the presence of light and heat or reasonable levels of moisture (Peh and Wong, 1999). Due to its film forming nature, gelation property, controlled release of drugs and mechanical properties, considerable attention has been given on HPMC based hydrogels for food packaging, drug delivery and tissue engineering applications (Barros et al., 2015; Liu et al., 2009; Peh and Wong, 1999).

1.5. Crosslinking agents

Various crosslinking agents have been used to synthesize hydrogels such as FA, DVS, DCC, EPH, CA, GTA and MA. Although there are several crosslinking agents available, CA has gained more attention due to its non-toxicity and lower price. Furthermore, CA is produced as an intermediate metabolite in human body via Krebs cycle (Demitri et al., 2008; Dharmalingam and Anandalakshmi, 2019).

Citric acid

Citric acid ($C_6H_8O_7$) is widely used in pharmaceutical and food industries. It is used as an acidity regulator in oral medicaments. It is regarded as a tricarboxylic acid, which has three dissociation constants at pKa = 3.13, 4.76 and 6.40. It shows different degree of deprotonation and protonation (Krukowski et al., 2017) in a specific pH as shown in Fig. 1.7. Welch (1988) reported that polycarboxylic acids (1,2,3,4-butanetetracarboxylic acid, BTCA) were able to crosslink the cotton cellulose effectively for textile applications.

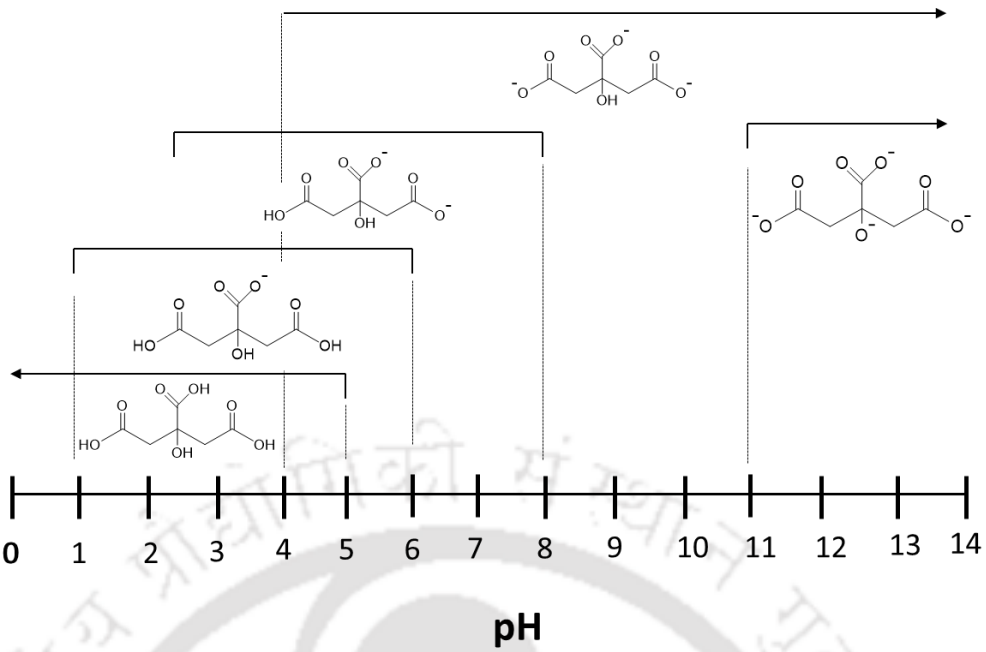

Figure 1.7: Different degrees of deprotonation and protonation of citric acid in a specific pH.

Citric acid was also identified as a crosslinking agent for cellulose based hydrogels for textile applications by Andrews (1989). Yang (1993) and Yang and Wang (1996) identified that almost 17 different polycarboxylic acids were able to crosslink the cotton fabric via cyclic anhydride intermediates. The concept of using citric acid as a crosslinker for producing CMC based superabsorbent hydrogels for personal care, agriculture and drug delivery systems was first reported by Demitri et al. (2008).

1.6. Nanomaterials

Accelerating the wound healing process is a major challenge encountered by surgeons and is an important area of research. Many methods have been suggested by various research groups since the 1990s. Nowadays, nanomaterials have opened a new gateway to fasten the wound healing process. Nanoparticles possess a higher surface-to-volume ratio and have been efficiently employed in numerous biomedical applications,

including wound healing therapies (Mihai et al., 2019). In the field of wound healing, there are several nanomaterials such as silver, zinc, copper, gold and lipid based nanoparticles are being currently used. The mechanism of nanomaterials in hastening the wound healing process include antimicrobial, antinflammatory, extra cellular matrix production, promoting cell proliferation and improving growth factors (Du and Wong, 2019).

1.7. Wounds

Wound is formed by physical or thermal damage, resulting in disintegration of anatomical structure and function of the skin. Based on repairing process, wounds are generally classified into acute and chronic wounds. The causes of acute wounds include burns, surgical and mechanical injuries while chronic wounds are due to ulcers (foot and diabetic), persistent infections, malignancies and untreated primary wounds. The duration for acute wound healing is faster (~8-12 weeks) compared to chronic wounds (> 12 weeks). Besides, acute wound leaves minimal scars (Boateng et al., 2008; Vijayakumar et al., 2019). Wounds can also be classified as superficial wounds, partial thickness wounds and full thickness wounds based on the area of the skin affected and number of skin layers. Superficial wounds occur on epidermal surface only. Injury on both epidermal and dermal layers including blood vessels, hair follicles and sweat glands is called as partial thickness wounds while injury on subcutaneous and deeper tissues is described as full thickness wounds (Boateng et al., 2008; Krasner et al., 1993).

1.8. Wound healing

The biological process of wound healing is related to growth and tissue regeneration. In order to repair the damaged tissue, a series of interdependent and overlapping phases occur. The four phases of wound healing are hemostasis phase, inflammatory phase, proliferation phase and maturation phase (Fig. 1.8). Discontinuation of wound healing

in any phases may lead to chronic wounds. The factors which impair the wound healing phases are degree of infection, poor nutrition, ageing and diabetic, resulting in prolonged healing times (Boateng et al., 2008; Vijayakumar et al., 2019).

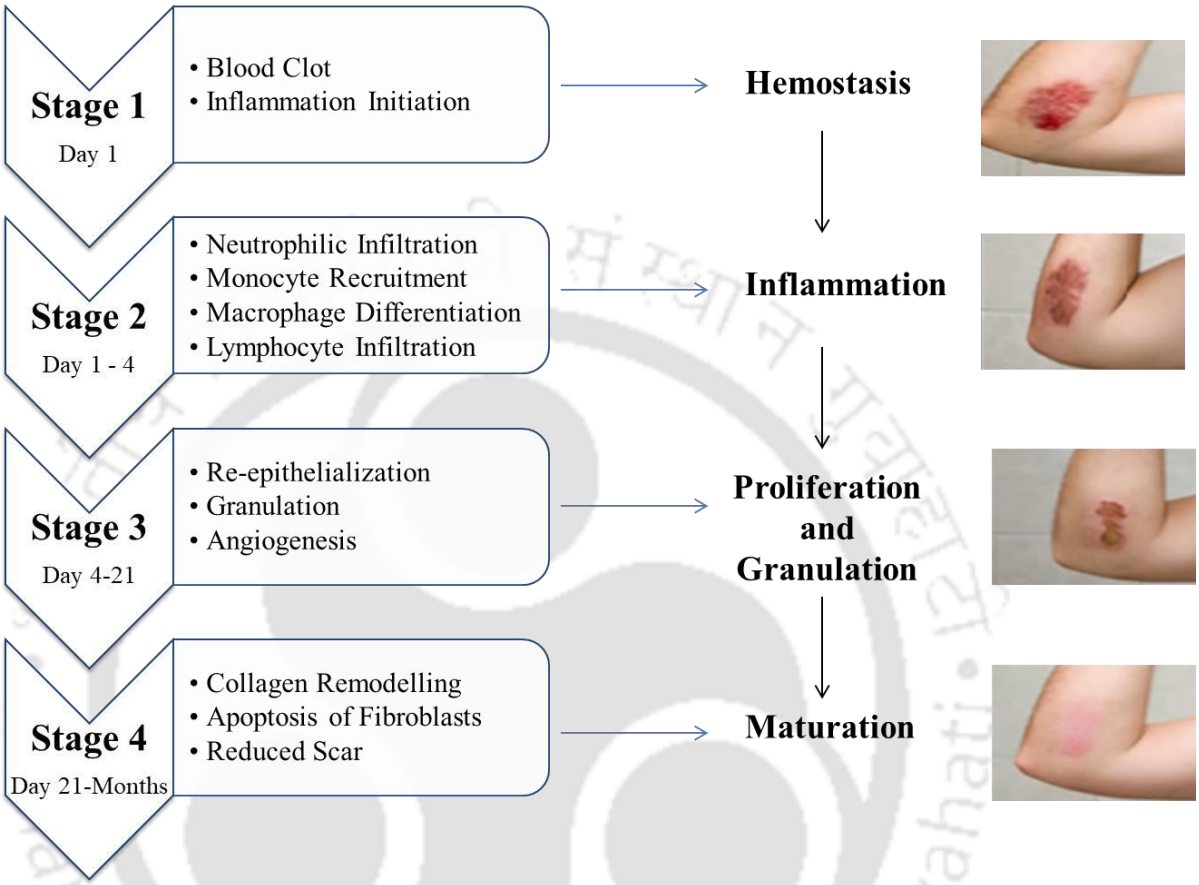

Figure 1.8: Different stages of wound healing.

1.9. Wound dressings

The primary function of a wound dressing material is to maintain the wound dry by permitting evaporation of wound exudates and inhibiting the entry of pathogenic microbes into the wound. In order to manage the wounds, traditional dressings such as gauzes, cotton, lint and bandages were used. Modern wound dressing materials are developed based on providing optimum environment, including a moist environment, vapor permeability, oxygen circulation and minimal bacterial load, to allow cells to progress into different phases. The modern dressing materials are hydrocolloids,

hydrogels and alginates. Commonly, hydrogels are produced in the form of gels or thin films or foam sheets (Boateng et al., 2008).

1.10. Hydrogel dressings

Hydrogels are swellable hydrophilic materials, which are insoluble due to crosslinking. Hydrogels can be applied over wound area either as an amorphous gel or film or solid sheet.

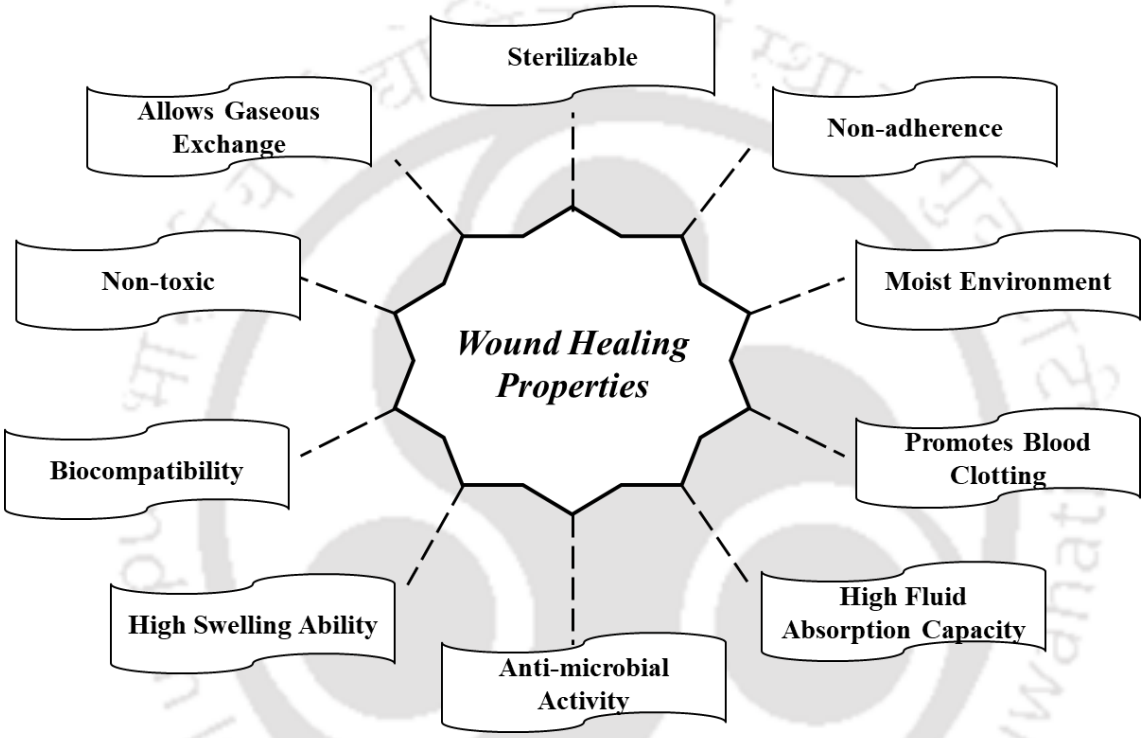

Figure 1.9: Properties of ideal wound dressing materials.

The hydrogel sheets are fabricated by physical crosslinking of polymers and thus it physically entraps the water molecules in their network structure. Because of its physical crosslinking, hydrogel sheets absorb large amounts of water upon contacting with wound exudates. The application of amorphous gels on the wound often requires secondary covering (Boateng et al., 2008). The hydrogel films can be prepared either in dry or wet form. The wet form of hydrogel dressings cannot absorb much exudates, leading to fluid accumulation and followed by skin maceration and bacterial growth. However, dry form of hydrogel films possesses ideal characteristics of a wound

dressing material such as cleansing of wound (debridement), maintaining a moist environment, removing of excess exudates and blood, exchanging water vapor and air, preventing infection, providing thermal insulation, creating low adherence and coming up with cost effective materials (Fig. 1.9) (Boateng et al., 2008; Vijayakumar et al., 2019).

1.11. Controlled drug delivery dressings

Controlled release of drugs to the wound site prolongs its action by allowing continual release from wound dressing material (Robinson and Lee, 1987) The application of hydrophilic polymers has great promise for controlled release of drugs due to their potential advantages. Controlled delivery dressings provide drugs to the target site in a consistent and sustained fashion for prolonged time and thus avoiding frequent dressing change (Boateng et al., 2008). Drug release from wound dressing material is controlled by following physical processes: (i) hydration of polymer or polymer matrix upon contacting with water or fluids, (ii) swelling to form a gel, (iii) diffusion of drug from polymer dosage and (iv) erosion of the polymer gel or matrix (Boateng et al., 2008; Korsmeyer et al., 1983; Papadimitriou et al., 1993).

The polymeric films containing drugs adhere to biological membranes, when the films are in contact with water or mucus, are called as bioadhesives or mucoadhesives. These films were started developing in mid 1980s and nowadays they have been used to release the drugs for specific localization of the human body (Lehr, 2000; Movassaghian et al., 2011). Mostly, cellulose derivatives containing drugs (caffeine, nicotine, ketoconazole, chloramphenicol, tetracycline and methylene blue) are used in bioadhesives for buccal, transdermal, nasal, ocular and vaginal delivery (Grabovac et al., 2005). Among all cellulose derivatives, NaCMC and HPMC has received special

attention as bioadhesives. The bioadhesive characteristics of NaCMC and HPMC make the resulting hydrogels attractive for various applications (Sannino et al., 2009).

Current work aims to fabricate hydrogel films containing two ether cellulose derivatives such as NaCMC and HPMC using citric acid as a crosslinking agent for wound healing and drug delivery systems. The aim of this thesis is to gain fundamental knowledge in synthesizing novel hydrogel films using new combinations of hydrophilic polymers (NaCMC and HPMC) and characterizing hydrogel films for their potential applications in wound healing and drug delivery systems. Furthermore, the main goal of the present work is to study mechanistic insights into various properties of hydrogel films.

1.12. Organization of the thesis

The thesis has been presented in eight chapters including the introduction section and review of literature. The outline of each chapter is as follows:

Chapter 1 provides a brief introduction about hydrogels and their preparation methods. A brief overview of polymers (especially NaCMC and HPMC), citric acid (crosslinker), types of wound and ideal requirements of a wound dressing materials is also presented along with controlled drug delivery dressings.

Chapter 2 presents a comprehensive review of NaCMC and HPMC based hydrogels for various applications including wound dressing applications. The scope and objectives of the current work are also provided.

Chapter 3 presents materials and methods to fabricate various hydrogel films. A detailed characterization techniques are also provided.

Chapter 4 presents the physical, chemical, thermal and mechanical properties of various concentrations of citric acid crosslinked NaCMC and HPMC hydrogel films. Also, the drug (methylene blue and tetracycline) loading efficiency and drug release studies of the fabricated films are provided.

Chapter 5 presents the physico-chemical, thermal, mechanical and antibacterial properties of various concentrations of citric acid crosslinked NaCMC-HPMC hydrogel films in the presence of ZnO nanoparticles (NPs). Zinc release studies and biocompatibility of the prepared hydrogel films are also presented.

Chapter 6 presents the physical, chemical, thermal, mechanical and antibacterial properties of various concentrations of citric acid crosslinked NaCMC-HPMC hydrogel films in the presence of CuO nanoflakes. Copper release studies and biocompatibility of the prepared hydrogel films are also presented.

Chapter 7 provides physico-chemical, mechanical, thermal, antioxidant and antibacterial properties of various concentrations of grapefruit seed extract (GFSE) incorporated into NaCMC-HPMC-ZnO/CA (optimized) hydrogel films. Zinc and polyphenolic compound release studies of the prepared hydrogel films are also presented.

Chapter 8 provides the overall conclusions and the scope for future studies.

1.13. Closure

This chapter presents about hydrogels and their preparation methods. A brief overview of NaCMC and HPMC polymers, citric acid, nanomaterials, types of wound and ideal requirements of a wound dressing material is also outlined along with controlled drug delivery dressings. In the next chapter (Chapter 2), the review of literature related to NaCMC and HPMC hydrogels are presented comprehensively.

भारतीय प्रौद्योगिकी संस्थान गुवाहाटी
Indian Institute of Technology Guwahati

Chapter 2

Review of literature

In this chapter, preparation, characterization and applications of NaCMC and HPMC based hydrogels are reviewed to comprehend the research progress on hydrogels.

2.1 NaCMC based hydrogels

First time, Chatterjii and Kaur (1992) initiated the preparation of CMC based hydrogels by chemical crosslinking of glutaraldehyde. A series of crosslinked gelatin-CMC semi interpenetrating networks (IPN) were prepared. It was found that the swelling properties of IPN are as a function of CMC content. Several combinations of hydrogel films were also prepared and it was found that gelatin (protein component) plays a vital role in the mechanical properties of the films. The shape of the gel was observed to change when electric stimulus was applied. The prepared hydrogels find its potential applications in cartilage tissue associated problems.

Kök et al. (1999) prepared aldicarb (water soluble, pesticide) loaded CMC-lignin crosslinked hydrogel microspheres with Al^{3+} ions. In this study, lignin was added as a filler to regulate the pesticide release in controlled manner. The rate of release of pesticide was affected by lignin - CMC and pesticide-CMC ratios. The release of pesticide from hydrogel microspheres was found to be Fickian diffusion. The prepared hydrogel microspheres can be used in agriculture, where controlled pesticide release is necessary.

Fei et al. (2000) synthesized CMC hydrogels without any additives by radiation (γ-ray) crosslinking. A series of hydrogels of CMC with a degree of substitution (DS) ranging from 0.7 to 2.2 were synthesized at various irradiation dosages. Higher crosslinking and higher swelling was found with a high DS of 2.2 at lower dosage of irradiation and high

concentration of CMC (20%). The hydrogels with DS of 2.2 showed swelling ratio of 165 and 78 (g water/g dried gel) in water and in 0.9% NaCl solution, respectively. The synthesized hydrogels can be used in cosmetics, medical, hygienic materials and agriculture.

Yakup Arica (2000) investigated the preparation of CMC hydrogel beads in the presence of Fe^{3+} ions. Polyphenol oxidase (PPO, enzyme) was covalently immobilized with CMC hydrogel beads using epichlorohydrin. The prepared hydrogel beads were thermally stable and showed excellent stability during storage period due to covalent attachment of enzyme with CMC beads. The optimum reaction temperature was 40°C and 45°C for free and immobilized enzyme, respectively. The optimum pH was 6.5 and 7.0 for free and immobilized enzyme, respectively. The hydrogel immobilized enzyme can be used to detoxify the phenolic compounds of industrial origin.

Wach et al. (2001) synthesized NaCMC (DS of 2.2) hydrogels by radiation techniques (γ-ray and electron beam). Various concentrations of NaCMC such as 10%, 20%, 30%, 40%, 50% and 60% were studied to investigate the effect of gel fraction and swelling capability in the prepared hydrogels. The gel fraction and swelling were up to 95% and 800 (g of water/g of dried gel), respectively for 50% NaCMC concentration. Moreover, the study proved that the obtained crosslinked CMC was degraded by cellulase enzyme and therefore the hydrogel had no harmful effect on environment. The synthesized hydrogel finds its applications in pharmaceutical and biomedical fields.

Liu et al. (2002) prepared NaCMC (more than 20% concentration) hydrogels by radiation technique (γ-ray) in the presence of N_2 or N_2O. The effect of various reaction conditions such as acidic, basic, inorganic salt and temperature on swelling performance of CMC hydrogels was comprehensively studied. It was found that the

swelling ratio was minimum at strong acidity (pH<5), strong basicity (pH>8), lower valence (Na^+) of inorganic salt and lower temperature. The prepared NaCMC based hydrogels can extensively be used in biomedical materials and agriculture.

Bajpai and Giri (2003) investigated grafting of acrylamide (AM) onto NaCMC via radical polymerization method in the presence of MBA as a crosslinker and KPS as a free radical initiator to synthesize NaCMC-*g*-PAM hydrogels. It was observed that the swelling of hydrogels decreases with increasing concentration of CMC, AM and MBA. The swelling kinetics was also studied with respect to composition of hydrogels and pH of swelling medium. The prepared hydrogels were loaded with KNO_3 as a model agrochemical and the agrochemical was released in controlled manner.

Lenzi et al. (2003) probed the degree of crosslinking for CMC-HEC network structure (hydrogel) by various approaches such as ^{13}C CP-MAS NMR, free swelling equilibrium and uniaxial compression. In this study, divinylsulphone (DVS) was used as a chemical crosslinker to synthesize CMC-HEC hydrogels. Among three approaches, NMR technique was able to detect only chemically effective crosslinks while the other two approaches were able to detect elastically effective physical and chemical crosslinks. The prepared hydrogels can be used in biomedical and agricultural fields.

Wach et al. (2003) investigated CMC (20%, 30% and 50% in aqueous solution) based hydrogel formation by radiation (γ-ray). The prepared hydrogels exhibited pH dependent swelling behavior and their swelling was higher at neutral and basic pH. It was found that tensile strength of hydrogels (50% CMC with DS of 2.2) was 0.91 and 30 MPa, respectively at relaxed and dried state. Moreover, the elongation was 80% for 50% CMC.

Sannino et al. (2003) probed chemical crosslinking of cellulose derivatives such as NaCMC and HEC using divinylsulphone (DVS) to prepare superabsorbent hydrogels for the treatment of edemas (body water elimination). Reduction in swelling capacity was observed with increase in pH and NaCl concentrations. Estimation of degree of crosslinking in hydrogels was performed by ^{13}C CP-MAS NMR. The prepared hydrogels were biocompatible and not induced inflammatory response according to cytotoxicity assay and nitric oxide (NO) measurement study. These hydrogels can be administered orally to absorb water from intestine without disturbing body functions.

Sannino and Nicolais (2005) prepared cellulose derivatives (NaCMC and HEC) based microporous superabsorbent hydrogels using divinylsulphone (DVS) as a crosslinker. In this study, effect of microporosity of hydrogels on swelling capability was studied. The dry xerogel was obtained from three different desiccation methods such as desiccation at atmospheric conditions, under vacuum and extraction with acetone. The presence of microporosity was related to the desiccation method and affected the swelling behavior at different ionic concentrations (0.01-1 mol/l of NaCl) and pHs. These properties are suitable in the field of personal care absorbent.

Sannino et al. (2005) synthesized HEC, NaCMC and HA based superabsorbent hydrogels using water-soluble carbodiimide (WSC) as a crosslinker and citric acid as a catalyst. Different weight ratios of HEC, NaCMC and HA at fixed chemical crosslinker concentrations (5%) and catalyst (1%) were formulated. The chemical compositions significantly affected the equilibrium water uptake. Also, dehydration method by acetone extraction induced microporous structure, which further affected sorption properties. Finally, uniaxial compression tests and dynamic-mechanical measurements were probed to evaluate elastically effective degree of crosslinking. The synthesized

hydrogels can be used as bulking agents or stomach fillers in dietary regimes to reduce hunger and helping patients to eat low amount of food.

Sannino et al. (2006) prepared NaCMC and HEC based hydrogels using water-soluble carbodiimide (WSC) as a crosslinker and citric acid as a catalyst. This study mainly focused on biocompatibility of the prepared materials by transepithelial electrical resistance (TEER) measurements and lactate dehydrogenase (LDH) assay. These results revealed that NaCMC- HEC based hydrogels maintained functional integrity with epithelial tissues and they can be used as stomach fillers for hypocaloric diets.

El-Rehim et al. (2006) prepared electron beam irradiation crosslinked super-porous hydrogels from NaCMC and PAAm. Ammonium carbonate was used as porogens during copolymerization of NaCMC/PAAm. It was found that gel content and swelling properties increased with irradiation dosage and/or PAAm concentration. The swelling ability of the prepared hydrogels was also studied in simulated urine solutions and compared with commercial products. The features of the prepared hydrogels make its application into personal care product industry.

Pourjavadi et al. (2006) investigated radical crosslinking of Na-Alg/NaCMC using MBA as a crosslinker and APS as an initiator. The optimum conditions for highest water absorbency was found to be 0.54 weight ratio of Na-Alg/NaCMC, 0.015 mol/L of MBA, 0.00486 mol/L of APS and 85°C reaction temperature. It was observed that swelling ratio reduced with increasing concentration of MBA, APS and NaCl. The water absorbency was in the order NaCl> $CaCl_2$> $AlCl_3$ (at fixed 0.15 mol/L concentration of NaCl, $CaCl_2$ and $AlCl_3$) for various salt solutions and in the order LiCl>NaCl>KCl for monovalent cations in salt solutions. The prepared hydrogels can be used in drug delivery systems.

Abd El-Mohdy (2007) probed free radical polymerization (γ-radiation) method to synthesize CMC/PAM hydrogels. The synthesized hydrogels imbibed 40-700 g of water/g of dry gel based on their varying compositions of CMC/PAM (50/50, 30/70, 20/80, 10/90, 0/100 wt.%) and irradiation dosages. The gel content of hydrogels increased with PAM content and irradiation dosages whereas swelling properties decreased with the gel content. The swelling properties of hydrogels also varied with pH, temperature and ionic strength of medium. The hydrogels were loaded with KNO_3 as an agrochemical and its release rate was increased with agrochemical loading (0.5-3.5%) and reduced with increase in PAM content and irradiation dosages.

Buhus et al. (2007) developed CMC-PVA based hydrogels using epichlorohydrine as a crosslinker for sustained drug release systems. The hydrogels were developed with different degrees of crosslinking, which further influenced the degree of drug loading. The hydrogel was loaded with hydrosoluble drug namely chloramphenicol. The drug release kinetics was found to be zero order. The prepared hydrogel system showed antibacterial activity.

El Salmawi (2007) prepared PVC-CMC based hydrogels by freezing and thawing, electron beam irradiation or combination of two methods. It was found that gel fraction percentage and swelling percentage were higher for combined methods (freezing and thawing, electron beam irradiation) than individual method. It was observed that swelling percentage increased with temperature and decreased with increase in concentration of salt fertilizers. The developed hydrogels have a wide range of applications in biomedical materials and agriculture.

Ogushi et al. (2007) synthesized NaCMC based hydrogels by enzymatic (horseradish peroxidase (HRP) and hydrogen peroxide (H_2O_2)). reaction. Initially, tyramine was

covalently coupled with NaCMC using carbodiimide to prepare NaCMC with phenol moieties (NaCMC-Ph). Then, HRP enzyme was used to crosslink NaCMC-Ph via oxidation reaction. The gelation of NaCMC-Ph depends on HRP and H_2O_2 concentrations (0-300 mM). It was evaluated that the viability of mammalian cells inside the hydrogels was 80%. This type of hydrogels can be used for various biomedical applications.

Popa et al. (2007) prepared NaCMC based hydrogel crosslinked with epichlorohydrin (EPC) and stable microparticles of acetylphthalylcellulose (APC) for sustained release of isosorbide dinitrate (Ik, drug). The drug was loaded into CMC based hydrogels through diffusion (ethanol-water system). The microparticles (Ik-ACP) were prepared by co-precipitation technique. The drug release followed zero order kinetics with respect to CMC based hydrogels as well as APC based hydrogels. The prepared hydrogels can be applied for heart disease treatment.

Pourjavadi et al. (2007) investigated graft copolymerization of acrylic acid onto CMC using MBA as a crosslinker and APS as an initiator to synthesize hydrogels. Mineral powders of celite were mixed with CMC to obtain CMC-*g*-poly(acrylic acid)/celite hydrogels. Taguchi experimental design method was used for optimization of hydrogel synthesis based on its swelling properties. It was found that the optimized final product imbibes 310 g of water/g of dried gel. These super-swelling properties of these hydrogels make its usefulness in personal care products and agriculture.

Qiu et al. (2007) synthesized hybrid hydrogels of CMC/activated carbon (AC) using γ-radiation method. According to this study, addition of AC significantly improves gel fraction, gel strength, swelling percentage and thermal stability when compared to pure CMC hydrogels. Also, hybrid hydrogels possess good flexibility and elasticity. These

excellent properties make them suitable for absorbents, wound covers and mattresses in medical fields.

Spin coating of CMC/HEC based superabsorbent hydrogels on Quartz crystal microbalance plates using divinylsulphone (DVS) as a crosslinker was performed by Sannino et al. (2007). The prepared hydrogels were in the form of a thin layer, which is sensitive to changes in ionic strength (0-0.5 mol/l of water), pH and change in mass. This macromolecular hydrogel based sensors and actuators are highly useful to study hydrogel swelling kinetics.

Wang et al. (2007) prepared CMC/PVP based hydrogels by γ-ray irradiation. The properties of CMC/PVP blend were enhanced in terms of flexibility, mechanical strength and transparency compared to pure CMC based hydrogels. Gel fraction of CMC/PVP hydrogels increased with the concentration of PVP and decreased with swelling rate. The moisture retention capability of CMC/PVP hydrogels was similar to commercially available wound dressing hydrogels but the swelling rate was higher for CMC/PVP based hydrogels. Better mechanical strength and water retention capability make CMC/PVP as an ideal candidate for wound dressing materials.

First time, citric acid (CA) was used as a crosslinking agent to prepare NaCMC/HEC based superabsorbent hydrogels by Demitri et al. (2008). In this study, CA was added at various concentrations (1.75%, 2.75%, 3.75%, 10%, and 20%) for fixed NaCMC/HEC weight ratio (3/1). HEC was used to promote intermolecular crosslinking. The crosslinking reaction was carried out at 80°C, which was sufficient to form cyclic anhydride from CA. But, crosslinking time was varied from 0 to 24 h to study crosslinking rate and swelling ratio. The maximum swelling ratio was 900 g of swollen hydrogel/g of dried gel at CA concentration of 3.75%. Weak crosslinking with

insufficient mechanical properties was observed when CA concentration lower than 1.75%. The prepared supersorbent hydrogels can be a good candidate for agricultural applications.

Don et al. (2008) prepared CMC based hydrogel membranes composed of three copolymer microgels such as poly(AA-*co*-SA), poly(AA-*co*-EHA), poly(NIPAAm-*co*-AA). The copolymers were synthesized through emulsion polymerization and mixed together with CMC to prepare hydrogel membranes. In this study, CMC and poly(AA-*co*-SA) were used as a matrix and poly(AA-*co*-EHA) as an adhesive component. The prepared hydrogel membrane showed thermo-responsive behavior due to the presence of poly(NIPAAm-*co*-AA). Caffeine was loaded into the hydrogel and its release behavior was studied. The release of caffeine was controlled by swelling of the hydrogel membranes. The developed hydrogel membranes can be used for transdermal drug delivery systems.

El-Hag Ali et al. (2008) synthesized a series of CMC/AAc hydrogels by γ-radiation induced copolymerization. The hydrogel was loaded with theophylline drug to study the swelling kinetics (CMC/AAc). The synthesized hydrogels showed pH dependent swelling behavior from pH 1 to 7. Swelling kinetics study showed that the hydrogel displayed Fickian diffusion at pH 1 whereas non-Fickian diffusion at pH 7. The prepared hydrogels can be served as colon-specific drug carrier.

Li et al. (2008) prepared iron (III) crosslinked CMC/clay based hydrogels containing herbicide acetochlor. The influence of different types of modified clays such as Na-clay, Fe-clay, Su-clay, Al-clay and Cta-clay on swelling ratio and herbicide release was comprehensively studied. According to this study, Na-clay showed maximum swelling ratio and higher release rate whereas Al-clay showed higher sorption capacity and

slower release rate. The release of acetochlor from CMC/clay hydrogels was controlled by diffusion mechanism. The formulated hydrogels possess potential applications to enhance the efficiency of herbicide in agriculture.

Ma et al. (2008) designed CMC/PNIPA/clay semi-IPN (interpenetrating polymer networks) hydrogels using TEMD as an activator and KPS as an initiator. The synthesized hydrogels showed faster swelling at pH 7.4 (non-Fickian diffusion) and slower swelling at pH 1.2 (Fickian diffusion). The hydrogels displayed higher deswelling rates and it was described by first-order kinetics equation. The increasing concentration of clay (Laponite XLG) decreased the deswelling rate. Higher tensile strength (approx. 50 kPa) and elongation percentage (1280) was exhibited by the prepared hydrogels. The hydrogels with improved mechanical properties and stimuli-sensitivity makes its potential applications in biomedical industry.

Sadeghi and Hosseinzadeh (2008) prepared CMC–poly(NaAA-*co*-AAm) superabsorbent hydrogels by alkaline (NaOH) hydrolysis of CMC and PAN physical mixture. The maximum swelling capacity of hydrogels was 559 g of water/g of dried gel under optimum conditions. The hydrogels showed swelling-deswelling behavior, which is suitable for drug delivery applications. This study owns several advantages such as simple method to form hydrogels, no initiator and no expensive crosslinker used (green process) and no radical polymerization involved.

Xiao et al. (2009) prepared dual-crosslinked Fe-CMC/PVA microparticles (hydrogels) by ferric ion crosslinking and freezing-thawing cycles. The size of microparticles was in the range of 0.2-1.2 µm. These microparticles showed pH-sensitive release behavior and could be effective for pH-sensitive applications. Thus, synthesized microparticles were able to maintain stability of hemoglobin proteins in an acidic environment.

Sakai et al. (2009) developed CMC-tyramine (Ph) conjugate hydrogels via peroxidase enzymatic crosslinking method. The hydrogels were probed for cellular adhesion and proliferation. Almost 76.9% of L929 fibroblast cells were adhered on CMC-tyramine (Ph) conjugate hydrogels within 4 h of seeding and were proliferated as a confluent monolayer on the gel after 168 h of culturing. The cells of fibroblast were harvested using cellulase from the gel and proliferated after transferring to culture dish. The morphology of the cells remained same in both cases. The conjugated hydrogels showed the possibility of its application in cell sheet technology (tissue engineering).

Chang et al. (2010) synthesized a series of CMC/cellulose based superabsorbent hydrogels using epichlorohydrin (ECH) as a crosslinker in NaOH/urea aqueous systems. The hydrogels showed an exciting swelling ratio of 1000 g of water/g of dried gel. It also exhibited smart swelling and deswelling in NaCl or $CaCl_2$ ionic medium. The BSA protein was loaded by deswelling the dried gel and the release of the protein was controlled by varying CMC concentrations. These properties make the hydrogels as an ideal candidate in the field of biomaterials.

Bao et al. (2011) prepared cellulose-g-P(AA-co-AM-co-AMPS)/MMT superabsorbent hydrogels by graft copolymerization method in the presence of MBA and KPS. The thermal properties of the prepared hydrogels were investigated by TGA to characterize the weight loss and grafting information. The SEM study showed that porous crosslinked structure present between MMT and CMC. The swelling capability of the hydrogels was dependent on pH, particle size and the concentration of the cationic salt solutions. The effect of salt solutions on the swelling ratio had the following rank: $K^+ > Na^+ > Ca^{2+} > Mg^{2+}$. The developed hydrogels find their potential applications in agricultural and biomedical area.

Chang et al. (2011) synthesized amphoteric hydrogels from quaternized cellulose (QC) and CMC via epichlorohydrine (ECH) chemical crosslinking method. The weight ratio of QC to CMC influenced the swelling ratio. It was found that the swelling ratio increased (from 8.6 to 498 g of water/g of dried gel) with weight ratio of QC/CMC (from 3:1 to 1:3). The hydrogels showed smart swelling behavior from pH 1 to 13. Also, hydrogels exhibited an excellent swelling behavior in NaCl, $CaCl_2$ and $FeCl_3$ ionic solutions. Due to their pH and salt responsive swelling behaviors, the prepared hydrogels can be used in agriculture, food and biomedical areas.

Gorgieva and Kokol (2011) developed temperature-responsive hydrogel films from CMC/HEC using citric acid (CA) as a crosslinker. The weight ratios of CMC/HEC were varied from 3:1 to 1:1 using different CA concentrations such as 1.75%, 2.75%, 3.75%, 5.75%, 10% and 20% (w/w) of polymers (CMC and HEC). In the preparation method, the hydrogel samples were pre-dried for 24 h at 30°C and then crosslinked for another 24 h at 80°C to obtain hydrogel films. The formed ester bond during the crosslinking process and glass transition temperature of hydrogels was characterized by FTIR and DSC, respectively. Degree of crosslinking and swelling behavior decreased with increase in weight ratios of HEC. All the prepared hydrogels were showed temperature dependent swelling capability. The developed temperature-responsive hydrogels can be used in textile industry for functional finishing of cotton knitwear.

Ni et al. (2011) probed slow release of nitrogen fertilizers on the basis of attapulgite (APT) as matrix and ethyl cellulose (EC) film and CMC/HEC hydrogels as coatings. A series of different weigh ratios of CMC/HEC hydrogels were initially prepared by citric acid crosslinking method and then fertilizers were loaded on them. The release of nitrogen fertilizers such as urea, ammonium sulfate and ammonium chloride in soil were investigated. The slow-release of fertilizers was examined for 20 days at room

temperature. It was found that more than 95% of nitrogen fertilizers released from hydrogels. The lowest diffusion coefficient (D) of nitrogen was found as 0.0029 mm^2/day for ammonium chloride. The release rate was slow for all the nitrogen fertilizers due to the presence of APT. The highest water absorbency was found for 3:1 ratio of CMC/HEC and 3.5% CA concentrations. The developed hydrogels have excellent ability to reduce nutrient loss and water loss in drought-prone environments.

Bao et al. (2012) developed a series of superabsorbent composites from cellulose, acrylic polymer and inorganic particles such as SiO_2, TiO_2, ZnO, Al_2O_3 and montmorillonite (MMT) by graft copolymerization method. The effect of cellulose derivatives (CMC, HPMC, MC and HEC) and inorganic particles on swelling rate and equilibrium water absorbency was investigated and the order was found to be CMC > without cellulose > HPMC > MC > HEC in water as well as in saline environment. It was concluded that inorganic particles with low isoelectric points (IEP) such as ZnO or Al_2O_3 exhibited low water absorbency whereas high IEP (SiO_2 or TiO_2 or MMT) showed high water absorbency. The prepared hydrogels can be effectively used in agricultural and biomedical fields.

Raafat et al. (2012) synthesized superabsorbent hydrogels from CMC/PVP by γ-irradiation crosslinking process. It was found that increase in ionic radius decreased swelling ratio due to penetration difficulty of ions into the hydrogels. Hence, the effect of salt solutions on swelling ratio of the hydrogels was in the order of Na^+> K^+> Mg^{2+}> Ca^{2+}. Swelling ratio of hydrogels decreased with increase in irradiation dosages. It was observed from SEM study that porous structure decreased with increase in PVP content. Urea, as a nitrogen source, was loaded into the hydrogels. The amount of urea release was directly proportional to the loading percent of urea in the hydrogels. These

characteristics of the hydrogels make its applications in agricultural area for increasing water-holding capacity and/or retaining nutrients.

Roy et al. (2012) prepared flexible and transparent PVP-CMC hydrogel films by heat (15 Psi, 120°C for 20 min) induced physical crosslinking process. A series of hydrogel films were prepared by solution casting technique. Among the prepared hydrogel films, PVP and CMC in a ratio of 20:80 showed excellent mechanical properties. Biodegradation of the hydrogel films were investigated in liquid state for 8 weeks. The weight loss of hydrogel films was about 38% at the end of 8 weeks. The developed hydrogel films can be used in food packaging materials, mainly for food stuffs, vegetables and fresh fruits.

Hashem et al. (2013) developed CMC hydrogels using polycarboxylic acids (malic or succinic or citric acid) as crosslinking agents. The synthesized hydrogels were incorporated with ZnO nanoparticles by in situ process to obtain CMC-hydrogel-ZnO-nanocomposites. The hydrogels containing ZnO nanoparticles showed antibacterial activity against *E. coli*, *P. aeruginosa*, *S. aureus* and *B. subtilis*. The hydrogels with excellent swelling ratio was obtained using 0.5% succinic acid as a crosslinker. The prepared hydrogels have their applications in medical field.

CMC hydrogels loaded with Ag nanoparticles were synthesized by Hebeish et al. (2013). The CMC based hydrogels were obtained using epichlorohydrin as a crosslinker in alkaline medium. In this study, AgNPs were synthesized by two different approaches: (i) the preformed hydrogel matrix acted as a stabilizing medium and trisodium citrate for assisting CMC to reduce Ag^{+} to AgNPs and (ii) CMC hydrogel assisted in situ preparation. The prepared hydrogels containing AgNPs were

characterized for their physical, chemical, morphological and antibacterial properties. These hydrogels can serve as potential candidates for medical applications.

Ibrahim et al. (2013) developed hydrogel membranes from cellulose, CMC and PVA. In this study cellulose was isolated from rice straw and then converted to CMC. Membranes of PVA/cellulose and PVA/CMC were prepared by radical copolymerization method using ceric ammonium sulfate (CAS) as a free radial generator. The prepared membranes were probed by desalination test (0.2% NaCl). The cellulose and CMC containing PVP membranes were capable of reducing NaCl concentration by 25% and 15%, respectively. The membranes were characterized by FTIR, TGA, DSC, SEM and water vapor transmission rate and chemical vapor transmission rate of hydrogel membranes were also determined. The prepared membranes can be used in desalination process.

Mandal et al. (2016) developed a series of hybrid nanocomposite hydrogels from CMC and multi-walled carbon nanotube (MWCNT) by ultrasonication. An anti-inflammatory drug namely diclofenac sodium was loaded for controlled release as transdermal device. The optimized nanocomposite hydrogels showed lower swelling percentage, higher gel strength, higher stability (about three months) and controlled drug release when compared to pure CMC. Biocompatibility of prepared nanocomposite hydrogels was studied using primary rat fibroblasts. Also, prepared nanocomposites were characterized by FTIR, TGA, FESEM, AFM and TEM analyses in detail.

Wang et al. (2013) synthesized CMC-*g*-poly(AA-*co*-AMPS) superabsorbent hydrogels via free radical graft copolymerization method using MBA as a crosslinker and APS as a free radical initiator. The synthesized hydrogels showed swelling ability at various

pHs and saline solutions. The addition of AMPS significantly improved the swelling ratio and salt-resistance properties. The hydrogels exhibited swelling-deswelling behavior in pH, ranging between 2.0 and 7.0. The smart swelling properties and salt-resistance properties make these hydrogels as potential candidates for drug delivery systems.

Abd El-Mohdy (2014) investigated graft copolymerization method to synthesize CMC-*g*-PAG hydrogels using γ-radiation. Grafting between CMC and PAG was proved by FTIR and XRD results. The synthesized hydrogels showed higher thermal stability than pure CMC as confirmed by TGA. The swelling ratio of hydrogels was higher at pH 12 whereas it was lower at pH 2. The maximum swelling ratio was found to be 700 g of water/g of dried gel. The swelling behavior of hydrogels in salt solutions had the following rank: $Na^{+} > Ca^{2+} > Fe^{3+}$. The hydrogels also showed swelling and deswelling behavior between pH ranging between 12 and 2. The synthesized hydrogels have a wide application in drug delivery systems, agriculture and personal care products.

Bao et al. (2014) probed double crosslinking mechanisms to synthesize hydrogel films from carboxymethylchitosan (CMCS) and CMC using $CaSO_4$ as an ionic crosslinker and genipin as a covalent crosslinker. It was observed that the double crosslinked hydrogel films showed higher swelling ratio between pH 3 and 7. It was found that toughness and max load were affected by ionic and covalent crosslinking in hydrogel films, respectively. The cells were cultured on hydrogel films, which did not elicit any toxic substances to cellular growth. The prepared hydrogel films can be used in drug delivery vehicles and skin tissue engineering.

Fekete et al. (2014) synthesized hydrogels from four cellulose derivatives such as NaCMC, MC, HPC and HEC by γ-radiation. It was observed that the gel fraction

increased with irradiation dosages and decreased with increasing polymer concentrations. The swelling ratio was found to be higher for CMC hydrogels, while HPC and MC based hydrogels showed lowest swelling ratio. The diffusion mechanism of water into hydrogels was proved to be anomalous. The synthesized hydrogels have a potential application in wound dressing materials and diapers.

Ibrahim et al. (2014) prepared hydrogel beads from CMC and sodium alginate (Na-Alg) using Ca^{2+} as a crosslinker and then prepared hydrogel beads were irradiated by γ-irradiation. It was found that addition of CMC, Na-Alg and crosslinker affected beads formation and swelling percentage. The optimum combination of polymer and crosslinker compositions was found to be 1:3 of CMC/SA and 3% crosslinker, respectively. The beads were characterized using FTIR, SEM and TGA. The hydrogel beads were loaded with ammonium nitrate as a model agrochemical and release of nitrate salt increased with pH of the medium and loading percentage of the salt. The hydrogel beads can be a viable candidate for controlled release of ammonium nitrate in agriculture.

Tang et al. (2014) studied synthesis of superabsorbent hydrogels from chitin and CMC using epichlorohydrin as a crosslinking agent. It was observed from SEM study that chitin was responsible for homogeneous porous structure in chitin/CMC hydrogels. The hydrogels showed an excellent swelling and shrinking behaviors in physical saline water, inorganic salt solution and synthetic urine. The maximum swelling ratio was found to be 1300 g of water/g of dried gel. The prepared hydrogels can be used as biomaterials.

Yu et al. (2014) investigated graft copolymerization method in the presence of MBA as a crosslinker to synthesize AA/CMC superabsorbent hydrogels by glow-discharge

electrolysis plasma (GDEP). The optimum conditions to synthesize hydrogels were found to be 9:1 of AA/CMC mass ratio, 0.3% of MBA and 60% of degree of neutralization. The grafting was confirmed by FTIR and XRD studies. The thermal stability of hydrogels was enhanced by grafting. The highest swelling ratio in distilled water was found to be 1330 g/g. The swelling behavior of the hydrogels in ionic aqueous solutions followed the order as $K^+ > Na^+ > Mg^{2+} > Ca^{2+} > Al^{3+} > Fe^{3+}$. Moreover, the hydrogels exhibited on-off switching swelling behaviors between pH 6.5 and 2.0. These hydrogels can have potential applications in drug delivery systems, personal care products and agriculture.

Zhang et al. (2014) probed free radical polymerization method in the presence of MBA and APS to synthesize nanocomposite hydrogels from grapheme oxide (GO), AM and CMC. The prepared hydrogels were also crosslinked by Al^{3+} ions. The compressive strength (2.87 MPa) of the nanocomposite hydrogels was significantly enhanced with addition of 1.6 wt.% GO sheets. It was confirmed by FTIR that hydrogen bond forms between oxygen of GO sheets and N-H group of PAM. The swelling kinetics of hydrogels follows pseudo-second-order equation. The ternary nanocomposite hydrogels can be used in drug delivery system and bioengineering.

Abou-Yousef and Kamel (2015) developed CMC hydrogels using polycarboxylic acids (maleic, succinic, or citric acids) as crosslinking agents. It was found that water uptake was higher for citric acid crosslinked hydrogels than the one produced from other acids. AgNPs were loaded *in situ* during hydrogel preparation using polycarboxylic acids as crosslinkers. Citric acid crosslinked hydrogels containing AgNPs showed highest antimicrobial activity for *S. aureus*, *P. aeruginosa*, *C. albicans*. It was concluded that distribution of AgNPs is influenced by structure of hydrogel networks. The prepared hydrogels can be used in biomedical applications.

Bozaci et al. (2015) synthesized CMC/Ag nanocomposite hydrogels using fumaric acid (FA) as a crosslinker and the hydrogels were coated on cotton fabric. It showed 99.9% antibacterial activity against *S. aureus* and *K. pneumonia*. Uniform distribution of AgNPs on cotton fabrics was confirmed by AFM and SEM. The treated cotton fabric was also characterized for its physical, chemical, thermal and mechanical properties. The prepared cotton fabric containing CMC/Ag nanocomposite hydrogels can be used as wound dressing materials.

Hebeish and Sharaf (2015) prepared MBA crosslinked nanocomposite hydrogels from diallyldimethylammonium chloride (DADMAC) and CMC by graft copolymerization method in the presence of APS as a free radical initiator. The prepared hydrogels were incorporated with CuO nanoparticles by *in situ* process. It was found that swelling ratio increased with concentration of DADMAC monomer. The maximum swelling was observed at pH 7. The nanocomposite hydrogels containing CuO showed antibacterial activities against *E. coli*, *S. aureus*, *P. aeuognos*, *B. subtilis* and it showed higher antibacterial activity than pure Ag/CMC-DAMAC nanocomposite hydrogels. The synthesized nanocomposite hydrogels can be a viable candidate for drug delivery and wound dressing applications.

Raucci et al. (2015) designed citric acid crosslinked CMC-HEC hydrogel films to study the surface material properties and osteoblast cellular responses. It was found that hydrophilicity and roughness were higher for citric acid crosslinked hydrogel films when compared to pure CMC and HEC films. Osteoblastic cell attachment, cell proliferation and differentiation were observed for crosslinked hydrogels. The developed hydrogels can have potential applications as fillers in bone repair treatment.

Yadollahi et al. (2015) prepared layered double hydroxides (LDH) crosslinked CMC nanocomposite hydrogels with simultaneous in situ formation of AgNPs. Crosslinking of LDH was confirmed by XRD and FTIR studies. It was observed that AgNPs were uniformly dispersed within CMC-LDH hydrogels. The swelling properties of Ag/CMC-LDH increased with pH when compared to CMC-LDH nanocomposite hydrogels. It was shown that AgNPs containing CMC-LDH hydrogels proved their antibacterial activity against *E. coli* and *S. aureus*. The prepared antibacterial nanocomposite hydrogels were stable more than one month and can be used as wound dressing materials.

Wen et al. (2015) synthesized chemical crosslinked NaCMC/HEC hydrogels using MBA and APS and then BSA protein was loaded into hydrogels. The crosslinked hydrogels were characterized by XRD, FTIR and SEM. The hydrogels exhibited swelling-deswelling behavior and the swelling behavior was confirmed at various pH and salt solutions. The BSA release was studied to simulate gastrointestinal environments at various pHs. The amount of drug release was found to be 85.2% and 17.8% at pH 7.4 and 1.2, respectively. The smart swelling behavior and high drug release percentage of these hydrogels make its application in controlled release of oral medication.

Alshehri et al. (2016) prepared CMC/PVA hydrogels using ethylene glycol diglycidyl ether (EGDE) as a crosslinker with simultaneous in situ formation of AgNPs by microwave radiation. The synthesized AgNPs in the hydrogels were spherical with size ranging from 8 to 14 nm according to SEM and TEM results. XRD results confirmed that the AgNPs had all phases of silver with FCC crystal system. It was observed that storage modulus was higher than loss modulus. The prepared Ag/CMC-PVP nanocomposite hydrogels exhibited antibacterial activity against *E. coli, K. pneumonia,*

P. aeruginosa, *P. vulgaris*, *S. aureus*, and *P. mirabilis*. The synthesized hydrogels can be used for treating urinary tract infection (UTI) pathogens.

Dilaver and Yurdakoc (2016) investigated fumaric acid (FA) crosslinked NaCMC/PVA hydrogel films. The hydrogel films were prepared from 3:1 ratio of CMC:PVA (2%) with varying FA concentrations such as 10, 15, 20, and 25 wt.% and followed by crosslinking in vacuum oven at 60°C. The prepared films were characterized by FTIR, TGA, XRD and SEM. Swelling of hydrogels in water was found to be increased with pH and the maximum swelling percentage was observed for 10% FA. The hydrogels also showed on-off switching swelling behavior between pH 2.6 and 8. The developed hydrogel films can be used as drug delivery vehicle for intestinal area.

Fekete et al. (2016) probed γ-radiation-induced crosslinking to synthesize superabsorbent hydrogels from CMC and AAc. Higher gel fraction was observed with lower irradiation dosages and increasing AAc concentrations. The highest swelling properties and gel fractions were found for 5:7.5 w/w percentage of CMC/AAc. The gel fraction and swelling capability of CMC/AAc hydrogels were higher than pure CMC hydrogels. The synthesized hydrogels have a wide application in biomedical and agricultural areas.

Namazi et al. (2016) prepared citric acid crosslinked CMC/MCM-41 nanocomposite hydrogel films and tetracycline and methylene blue were loaded through swelling in PBS. It was found that incorporation of mesoporous silica nanoparticles (MCM-41) enhances the swelling properties, tetracycline release, water vapor permeability and oxygen permeability. The prepared hydrogel films showed antibacterial activity against *S. aureus*. These characteristics of the hydrogel films make them suitable for wound healing applications.

Salama et al. (2016) developed CMC-*g*-PDMAEMA hydrogels using ethylene glycol diglycidyl ether (EGDE) as a crosslinker. In this study, biomimetic calcium phosphate was synthesized in the developed hydrogels and BSA was loaded through imbibition. Calcium phosphate containing hydrogels exhibited lower swelling percentage than pure hydrogels at pH 2.1 and 7.4. It was observed that calcium phosphate mineralized hydrogels released BSA in a sustained manner. The synthesized hydrogels can be effectively used for bone tissue repair.

Sarkar et al. (2016) investigated free radical polymerization technique to synthesize CMC-*g*-*cl*-Poly(AAm) hydrogels containing boron for slow release. It was observed that boron extensively crosslinked with cellulose during polymerization reaction, resulting in high strength composite hydrogels. The release of boron from hydrogels was followed Fickian diffusion mechanisms. It was found that reduction in water absorbency and high storage modulus led to slow release of boron. The developed hydrogels can be useful in agriculture for improving crop health.

Shahbazi et al. (2016) probed photo- and chemical crosslinking of CMC hydrogel films for food packaging applications. The photo- and chemical crosslinking were performed by UV irradiation/sodium benzoate and glutaraldehyde vapor/gelatin, respectively. It was observed that photo-crosslinked films exhibited higher crystallinity, higher water barrier property, lower solubility and higher tensile strength than chemically crosslinked one. The prepared hydrogel films did not elicit cytotoxicity for L-929 fibroblast cells.

Zare-Akbari et al. (2016) fabricated bionanocomposite hydrogel beads from CMC and ZnO using Fe^{3+} ionic crosslinking method for sustained and controlled delivery of propranolol hydrochloride (hydrophilic drug). It was found that CMC/ZnO hydrogel

beads showed higher thermal stability and higher swelling ratio than pure CMC hydrogels. Drug release was decreased with increasing concentration of ZnO nanoparticles and thus exhibited a controlled release in PBS buffer at pH 6.8.

Ghorpade et al. (2017) investigated crosslinking of citric acid to synthesize hydrogel films from β-cyclodextrin (βCD) and CMC for controlled release of hydrophobic drug such as ketoconazole. It was observed that βCD-CMC hydrogel films exhibited higher swelling ratio and higher drug loading than pure CMC hydrogel films. The burst release was minimized due to the presence of βCD. The comprehensive structural characterization was performed using solid state ^{13}C NMR, FTIR, TGA and DSC. Moreover, the hydrogel films were found to be biocompatible according to hemolytic assay.

Rakhshaei and Namazi (2017) synthesized a flexible citric acid crosslinked CMC hydrogel films containing ZnO modified mesoporous silica MCM-41 and tetracycline was loaded via post-impregnation. It was shown that CMC/ZnO-MCM-41 hydrogel films exhibited higher swelling ratio, higher drug loading and prolonged and controlled release of tetracycline than CMC/ZnO. The prepared nanocomposite films showed higher water vapor permeability and higher oxygen permeability than neat CMC hydrogel films. Zeta potential study showed that the negative charge of MCM-41 was changed by positive charge of ZnO, resulting in positive surface charge (+9.3 ± 1.2 mV) of the films. The hydrogel films showed antibacterial activity due to inherent property of ZnO and tetracycline.

Sarkar and Singh (2017) prepared a series of citric acid crosslinked CMC hydrogels and bentonite reinforced hydrogels for base triggered release (TR) of thiamethoxam (insecticide). The hydrogel composites were comprehensively characterized by ^{1}H

NMR, FTIR, XRD and SEM-EDS. The thiamethoxam release was studied in aqueous solutions (pH 7-11) and burst release was observed at pH > 7. The release followed the Gallagher–Corrigan kinetic equation. These formulated hydrogels can be efficiently used to control insects, which have alkaline pH in their gut.

Tran et al. (2017) probed γ-radiation grafting to synthesize NaCMC/Sodium Styrene Sulfonate (SSS) for removal of heavy metal ions. It was found that ratio of CMC/SSS 1:0 (w/w) showed higher gel fraction. The swelling ability was dependent on SSS concentration. Water absorbency was higher for CMC/SSS hydrogels than neat CMC hydrogels. The grafted hydrogels showed its capability to remove heavy metal ions such as Cr, Fe and Pb efficiently. The kinetics study revealed that monolayer formation takes place on the surface of the hydrogels.

Novel bioengineered CMC-doxorubicin (DOX) hydrogel films were fabricated by Capanema et al. (2018a) for melanoma skin cancer applications. In this study, CMC with two DS of 0.77 and 1.22 was employed to prepare hydrogels such as CMC-0.77_DOX and CMC-1.22_DOX. The bioconjugates of CMC-DOX were crosslinked by citric acid (15% m/m of CMC-drug) and the crosslinking was confirmed by FTIR study. Results showed that swelling behavior, gel fraction and DOX release were dependent on DS of CMC. Furthermore, confocal laser scanning microscopy revealed that CMC-DOX hydrogels killed cancer cells and reduced acute effects in normal cells.

Capanema et al. (2018b) fabricated antimicrobial and biocompatible CMC-AgNPs nanocomposite hydrogel membranes for wound dressing. Various concentrations of citric acid were used as crosslinker to prepare CMC-AgNPs superabsorbent hydrogels. It was found that swelling and degradation behavior was influenced by citric acid concentrations. The prepared nanocomposite hydrogels were biocompatible with

human embryonic kidney cells (HEK293T). Besides, the developed hydrogels exhibited a strong antibacterial activity against Gram positive (S*taphylococcus aureus*) than Gram negative (*Escherichia coli* and *Pseudomonas aeruginosa).*

Capanema et al. (2018c) prepared citric acid (10-25%, m/m% of polymers weight) crosslinked CMC with PEG based superabsorbent hydrogel films for wound dressing applications. Results showed that increase in citric acid concentrations in hydrogel films drastically decreased swelling ratio from 5000% to 100%. The citric acid crosslinking was confirmed by FTIR analysis. It was observed that the absorption intensity at 1730-1715 cm^{-1} was gradually increased with increase in citric acid concentrations, confirmed crosslinking reaction. Surface nanomechanical analysis showed that addition of PEG increased the elastic modulus from 0.08 GPa (CMC films) to 1.9 GPa (CMC-PEG films). The MTT assay demonstrated that the fabricated hydrogels were biocompatible with human embryonic kidney cells (HEK293T).

Javanbakht and Namazi (2018) developed epichlorohydrin (ECH) crosslinked doxorubicin (DOX) loaded CMC/GQD (graphene quantum dot) nanocomposite hydrogel films for anticancer and drug delivery systems. Results showed that increase in GQD (10-30%) decreased the elongation at break (7-5%) while tensile strength was increased from 50 to 55 MPa. According to water vapor permeability (WVP) results, the WVP increased with increase in GQD concentrations in the films. At high concentration of GQD (30%), the swelling ratio was found to be 150% at pH 7.4. The DOX loading into CMC/GQD nanocomposite hydrogels was dependent on GQD concentration. The high concentration of GQD (30%) incorporated films released high cumulative amount of DOX for prolonged time (400 h). Furthermore, MTT assay showed that CMC/GQD nanocomposite hydrogels did not elicit any cytotoxic to blood

cancer cells (K562) while CMC/GQD/DOX hydrogel films demonstrated their cytotoxic activity against K562 cells.

Joorabloo et al. (2019) fabricated porous hydrogels containing heparinized nano ZnO/PVA/CMC by freeze-thaw cycles for wound dressing applications. Artificial neural network (ANN) and response surface methodology (RSM) were applied to design and model the porous hydrogels. In order to achieve the favourable properties of WVTR and swelling ratio, ANN and RSM were utilized. Based on the optimum values of WVTR and DSR, the prepared hydrogels showed good mechanical and antibacterial properties. Besides, the fabricated porous hydrogels showed biocompatibility with L929 and HDF cells.

Jantrawut et al. (2019) prepared hydrogel films containing low methoxy pectin (LMP), gelatin and CMC using glutaraldehyde (Glu) and $CaCl_2$ as crosslinkers and glycerine (G) as a plasticizer for wound dressing applications. It was found that povidone iodine (PI) incorporated into F-Glu-Ca-G30-PI hydrogel films showed superior properties compared to F-Glu-Ca-G40, F-Glu-Ca-G30, F-Glu-Ca-G20 and F-Glu-Ca-G10 films in terms of elongation at break (32.80%), water vapor transmission rate (1889 g/m^2/day), water retention capacity (81.70% at 2 h) and fluid uptake ability (88.45% at 2 h). The drug (PI) containing F-Glu-Ca-G30-PI films showed an excellent antibacterial activity (zone of inhibition of 22.06 ± 3.44 mm) against *S. aureus*.

Functional hydrogels containing CMC and reduced graphene oxide (rGO) was developed by Ali et al. (2019) for wound dressing applications. The in vitro study showed that the prepared hydrogels (rGO of 100 µg/ml) inhibited biofilm formation by *P. aeruginosa* and *S. aureus*. Furthermore, the fabricated hydrogels were biocompatible with primary human dermal fibroblast cells.

Active and water resistant food packaging films containing CMC-PVA were developed by Kanatt et al. (2020). In this study, citric acid was used as a crosslinker while *Aloe vera* gel was incorporated to improve the functionality of the films. It was observed that incorporation of citric acid significantly enhanced the mechanical properties while it decreased the moisture content, water solubility and water vapour permeability of the prepared films. The swelling ratio results revealed that increase in citric acid concentration decreased the capability of a film to trap water molecules. The formation of ester bond due to crosslinking was confirmed by FTIR. It was found that the tensile strength of a film increased upto 5% citric acid concentration and further increase in citric acid from 6-10% resulted in decreased tensile strength. This effect of citric acid on tensile strength was described based on its plasticizing property due to its chemical structure (three carboxyl groups and one hydroxyl). Due to incorporation of *Aloe vera* gel, the prepared films showed 69% DPPH radical scavenging activity at the end of 24 h. The developed films also protected the minced chicken meat from UV light and delayed the lipid peroxidation along with reduction of microbial growth.

Raho et al. (2020) prepared AgNPs doped silk fibroin/CMC nanocomposite hydrogels for biomedical applications. The hydrogel without AgNPs exhibited a high swelling ratio of 59 ± 5 g/g while addition of AgNPs decreased swelling ratio of 20-30 g/g. AgNPs loaded nanocomposite hydrogels showed antimicrobial activity against *E. coli, S. epidermidis, S. aureus, C. albicans and P. aeruginosa.* Furthermore, the developed hydrogels showed cytocompatibility with rat bone marrow derived mesenchymal stem cells.

2.2 HPMC based hydrogels

Pekel et al. (2004) investigated electron beam crosslinking of HPMC hydrogels with various degrees of substitution (DS 1.9 and 1.4) and viscosity (4270 mPa.s and 4370 mPa.s) for biomedical applications. It was exhibited that the swelling percentage did not change significantly till pH = 7 and significant changes were observed from pH = 8.0. The swelling percentage of thermal-sensitive hydrogels was found to be 2000% in cold water and 500% at 60°C. It was observed that tensile strength of the hydrogels increased with irradiation dosages. It was found that HPMC hydrogels with low DS showed 95% weight loss up to 24 h based on enzymatic degradation study.

Liu et al. (2009) synthesized superporous HPMC gel beads using divinylsulphone (DVS) as a crosslinker and nano-$CaCO_3$ as a porogen through inversing phase suspension crosslinking. It was found that porogen affected the morphology of hydrogel beads and interpenetrate pores formed at 70% of porogen. The equilibrium swelling ratio increased with porogen dosages whereas equilibrium swelling time decreased with porogen dosages. The higher swelling ratio of the superporous gel beads was due to larger surface area and loose structure, which was created by higher dosages of porogen. The prepared superporous gel beads can be useful in drug delivery applications.

Barros et al. (2014) probed physical crosslinking of chitosan (CH) and HPMC by casting-solvent evaporation (SC) method or by freeze–thaw (FT) technique for textile applications. In this study, a series of different weight ratios of CH and HPMC was used to prepare the hydrogel films. The miscibility of the polymers was studied by FTIR, SEM and AFM analysis. It was found that the films containing high CH showed swelling capability of 1,172% and 7,323% for SC and FT preparations, respectively. Lower swelling percentage was found for equivalent concentration of both polymers.

The low critical solution temperature (LCST) was found to be between 85.2°C and 87.5°C for thermoreversible hydrogel films.

Barros et al. (2015) synthesized CH/HPMC hydrogel films via solvent casting (SC) and freeze–thaw (FT) techniques for textile applications. The thermal, mechanical and structural properties were evaluated by DSC and TGA, DMA and XRD, respectively. It was concluded from characterization studies that the films had good miscibility between both polymers. Decomposition temperature, glass transition temperature and tensile strength of 50:50 (CH/CMC) compositions were found to be >270°C, > 194°C and 7.07 MPa, respectively. The prepared hydrogel films are suitable candidates to release active species (fragrances and antiperspirants) when body temperature increases.

Das et al. (2015) fabricated ethylene glycol dimethacrylate (EGDMA) crosslinked PAAm/HPMC/Au nanocomposite hydrogels for colon targeted drug delivery. The nanocomposite hydrogels were comprehensively characterized by XRD, FTIR, TGA, ^{13}C NMR, FESEM/EDAX/elemental mapping and HR-TEM. It was found that inorganic fillers (Au) enhanced higher gel strength in the nanocomposite hydrogels than pure PAAm/HPMC crosslinked hydrogels. The swelling ratio was higher at pH 7.4 at 37°C. The hydrogels did not elicit any cytotoxicity towards human mesenchymal stem cells (hMSCs). The release of colonic drugs such as ornidazole and 5-ASA were found to be sustainable for nanocomposite hydrogels.

Ghorpade et al. (2016) prepared β-cyclodextrin (βCD) grafted HPMC hydrogel films using citric acid as a crosslinker for controlled release of hydrophobic drug (ketoconazole). In this study, FTIR and ^{13}C NMR were investigated to prove the ester crosslinking between βCD and HPMC. It was found that swelling ratio, drug loading

and drug release were mainly dependent on βCD content. The maximum drug release was found to be 64.99% at the end of 24 h and its release mechanism was non-Fickian. The hydrogel films showed good biocompatibility according to hemolytic assay.

Iohara et al. (2017) synthesized thermoresponsive hydrogels composed of cyclodextrins (CDs) and hydrophobically modified HPMC (HM-HPMC) for ocular drug delivery. The thermoresponsive behavior of the gel was due to addition of CDs which interacted with HM-HPMC. The potential use of the prepared hydrogels was tested on the eyes of a rabbit. The solution (HM-HPMC/α-CD) containing diclofenac sodium drug was absorbed by formation of a gel on the ocular surface.

Mut et al. (2018) developed topical hydrogels contained chitosan and HPMC as polymers and sucrose palmitate and sucrose laurate as penetration enhancers for fluconazole delivery. The prepared hydrogels were evaluated for their drug content, viscosity, pH, in vitro drug release and ex vivo drug permeation. It was observed that all developed hydrogels fulfilled the requirements of drug content, viscosity and pH. In vitro release study showed that high flux and drug release rate were observed for all fluconazole incorporated chitosan-HPMC based hydrogels. According to ex vivo drug permeation study, sucrose laurate was an effective penetration enhancer for fluconazole.

Zhang et al. (2019) investigated potential use of HPMC, which were seeded with human adipose-derived stromal cells (ADSCs) for constructing lymphoid nodes in vivo. The grown hADSCs combined with 13% (w/v) HPMC were injected into mice subcutaneously. It was found that lymphoid nodes were developed at the injected sites after eight weeks. This technique could be an alternative method for adjunctive therapy for malignancies or engineering immune organs or immunodeficiency diseases.

The advantages and disadvantages of various hydrogels containing nanomaterials were listed in Table 2.1.

Table 2.1: Advantages and disadvantages of various hydrogels containing nanomaterials.

S.No.	Hydrogel compositions	Advantages	Disadvantages	Reference
1.	NaCMC, diallyldimethylammonium chloride and MBA **Form**: Hydrogel coated cotton fabric **NPs**: CuO and Ag	Hydrogels exhibited excellent antibacterial activity and swelling ratio. It can be used for drug delivery and wound healing applications.	Graft polymerization was tedious process and involved toxic crosslinkers and initiators. Mechanical properties were not reported. Biocompatibility of hydrogels was not reported.	Hebeish and Sharaf (2015)
2.	NaCMC, PVA and ethylene glycol diglycidyl ether (EGDE). **Form**: Hydrogel **NPs**: Ag	Hydrogel showed excellent antibacterial activity. It can be used for wound healing applications.	Chemical crosslinking of EGDE by microwave radiation cannot be suitable for industry. EGDE was a toxic chemical crosslinker. Biocompatibility of hydrogels was not reported. It needed secondary wound dressing materials.	Alshehri et al. (2016)
3.	NaCMC and citric acid. **Form**: Hydrogel films. **NPs**: ZnO in MCM-41	The process was less cumbersome to fabricate films. It exhibited higher swelling ratio, higher drug loading and prolonged and controlled release of tetracycline. Films showed higher water vapor permeability and higher oxygen permeability. Films exhibited antibacterial activity. Films were biocompatible.	Elongation at break of films was 4% (not flexible films). Films did not possess antioxidant activity. In vitro wound closure study was not reported.	Rakhshaei and Namazi (2017)
4.	NaCMC and citric acid. **Form**: Hydrogel films. **NPs**: Ag	The process was less cumbersome to fabricate films. It showed excellent swelling ratio of approximately 420–1500%. Films showed antibacterial activity. Films were biocompatible.	Mechanical properties were not reported. It was less transparent. Films did not show antioxidant activity. In vitro wound closure study was not reported.	Capanema et al. (2018b)
5.	NaCMC and epichlorohydrin **Form**: Hydrogel films. **NPs**: Graphene	Swelling ratio was found to be 150% at pH 7.4. Films showed higher water vapor permeability. Tensile strength was found to be 50 – 55 MPa. Films were biocompatible.	Films were brittle. The crosslinker was a pungent liquid and moderately soluble in water. The films did not show any antibacterial activity or antioxidant activity.	Javanbakht and Namazi (2018)
6.	NaCMC and PVA. **Form**: Porous Hydrogel films.	Films showed excellent swelling ratio and higher water vapour transmission	Freeze-thaw cycles were energy and time consuming process.	Joorabloo et al. (2019)

	NPs: ZnO	rate. Films were highly flexible. Films showed antibacterial activity and biocompatibility. Films showed good performance in wound healing by scratch assay	Tensile strength was poor (approx. 0.5 MPa) due to physical crosslinking. The films did not show any antioxidant activity. In vitro wound closure study was not reported.	
7.	NaCMC and silk fibroin **Form**: Hydrogels. **NPs**: ZnO	The hydrogel exhibited a high swelling ratio of 2000% – 3000%. Hydrogels showed antimicrobial activity. Hydrogels were biocompatible.	In this study, the process of hydrogel fabrication needed a high temperature (122°C) for curing with minimum of 5 h. Requirement of many chemicals to fabricate hydrogels and complicated steps were involved. Hydrogels did not show antioxidant activity. In vitro wound closure study was not reported. It needed secondary wound dressing materials.	Raho et al. (2020)

2.3. Research gap: motivation and scope of the present work

The overview on CMC and HPMC based hydrogels from available literatures undoubtedly indicate how researchers from all over the world are actively involved in preparation and characterization of different types of hydrogels for various applications including wound healing and drug delivery. Traditional routes of administering drugs through oral and intravenous generally keep a maximum drug concentration initially and then decreases over time. Nowadays, smart drug delivery systems capable of releasing drugs on-demand, site-specific and controlled dosages with on-off have aroused in the midst of researchers.

For wound healing and drug delivery systems, hydrogels fabricated from single polymer may not satisfy the requirements completely because of their poor three dimensional molecular structure formed by limited intermolecular interactions. In order to overwhelm this shortcoming, blending of cellulose ethers may be used (Chopra et al., 2007) for controlled release of drug or metal ions. Combination of two polymers

often produces a new functional biomaterial with salient features for controlled release applications (Ibrahim et al., 2013). Furthermore, it is described that the hydrogels fabricated from CMC release the drug in a faster rate because of their high swelling capability and poor mechanical strength in the swollen state compared to composite materials (Mandal et al., 2016; Zare-Akbari et al., 2016).

Based on available literature, the effect of citric acid (chemical crosslinking) with or without metal oxide nanoparticles has not been studied extensively for NaCMC and HPMC based hydrogel films for wound healing and drug delivery applications. Moreover, the previous studies used high temperature to fabricate films and the manufacturing process was time consuming. These shortcomings may impede the industrial applications of hydrogel films. Hence, in the current work, simultaneous drying and crosslinking strategy is applied to produce a novel series of NaCMC-HPMC hydrogel films. The combination of cellulose derivatives such as NaCMC and HPMC using citric acid as crosslinking agent for producing hydrogel films for wound healing and drug delivery systems has not been yet studied.

Although numerous literatures available on hydrogel films for wound healing and drug delivery systems, it is still imperious to fabricate hydrogel films as drug carriers by improving the drawbacks associated with it, such as high drug loading efficiency, drug stability in the films, controlled release, biocompatibility, antibacterial activity against both Gram positive and Gram negative, antioxidant activity and cost.

2.4. Objectives

Motivated by the scope of applications of hydrogel films in wound healing and drug delivery systems, the thesis is aimed to study the influence of citric acid on physico-chemical, mechanical, thermal, antioxidant and antibacterial properties of NaCMC-

HPMC based hydrogel films with or without metal oxide nanoparticles and with or without natural antibacterial as well as antioxidant rich component. Besides, the prepared hydrogel films are aimed to examine their drug or metal ion or polyphenolic compound release. The specific objectives are as follows:

- To prepare and characterize citric acid crosslinked NaCMC-HPMC hydrogel films for wound healing and drug delivery applications and to study the drug release behavior of the prepared hydrogel films
- To prepare zinc oxide complexes in composite hydrogel films for potential wound healing applications and to investigate the zinc release behavior of the prepared hydrogel films
- To develop cellulose-based nanocomposite hydrogel films containing $CuO/Cu_2O/Cu$ (cupric oxide, cuprous oxide and copper) nanoparticles and to examine the copper release behavior of the prepared hydrogel films
- To fabricate functionalized cellulose-based hydrogel films with zinc oxide complex and grapefruit seed extract for potential applications in treating chronic wounds and to examine the zinc and polyphenolic compound release behavior of the prepared hydrogel films

2.5. Closure

In this chapter, a comprehensive survey of literature on NaCMC and HPMC based hydrogels for various applications are thoroughly reviewed. Furthermore, motivation and scope of the present work along with the objectives are presented. Next chapter (Chapter 3) describes materials and methods to fabricate various hydrogel films (NaCMC-HPMC/CA, NaCMC-HPMC-ZnO/CA, NaCMC-HPMC-CuO/CA, NaCMC-HPMC-ZnO/GFSE) and their characterization techniques in detail.

Chapter 3

Materials and methods

In this chapter, materials and methods are presented to fabricate citric acid crosslinked NaCMC and HPMC based hydrogel films containing nanoparticles of either ZnO or CuO/Cu_2O/Cu or NaCMC-GFSE. Detailed characterization techniques to study physical, chemical, thermal, mechanical, antibacterial, antioxidant, drug loading and drug releasing properties are provided along with biocompatibility of the fabricated hydrogel films.

3.1. Materials

Sodium carboxymethylcellulose (NaCMC, 400-800 cps at 2% water, 25°C), citric acid, tetracycline hydrochloride, zinc nitrate hexahydrate, potassium hydroxide, copper chloride dihydrate, sodium hydroxide, 2,2-diphenyl-1-picrylhydrazyl, ascorbic acid, ethanol, methylene blue and Mueller-Hinton agar and ampicillin disc (AMP – 25 µg) were purchased from HiMedia Laboratories Pvt. Ltd. (Mumbai, India). Hydroxypropylmethylcellulose (HPMC K15M) was procured from Dow Chemical International Pvt. Ltd. (Mumbai, India). Grapefruit seed extract (GFSE) was obtained from ABC Techno Inc. (Tokyo, Japan). All reagents were analytical grade and ultrapure water was obtained from Millipore Milli-Q UV water filtration system.

3.2. Methods

3.2.1. Preparation of NaCMC–HPMC hydrogel films

Hydrogel films were prepared by adding NaCMC and HPMC (3:1 wt. ratio) in 100 ml of water with citric acid (CA) as a crosslinker. In a typical experiment, to formulate a polymer of 2 wt.% concentration (NaCMC-HPMC at a ratio of 3:1), 0.5 g of HPMC powder was dissolved in water at 90^{o}C under magnetic stirring condition for 30 min

until the clear solution was observed. Then, the solution was allowed to cool at room temperature. The presence of HPMC is essential to encourage intermolecular crosslinking as well as to reduce the crosslinking between NaCMC macromolecules alone. An amount of 1.5 g NaCMC was slowly added into the above solution under vigorous magnetic stirring and was left at 900 rpm for 12 h to obtain a homogeneous mixture. Finally, various concentrations of crosslinking agent such as 5%, 10% and 20% was added into NaCMC-HPMC (w/w of 2 wt. % polymer concentrations) aqueous solutions. Air bubbles were removed completely in all the samples under vacuum and 100 ml of each sample was cast on a Petri dish of 18 cm diameter. All the samples were kept for 5 h at 80°C for CA crosslinking reaction. Neat NaCMC (2 wt.%) crosslinked with CA (5%) hydrogel films were also prepared using a similar procedure for comparison. Finally, the hydrogel films were stored in a vacuum desiccator for further analysis.

3.2.2. Preparation of zinc oxide nanoparticles

Zinc oxide nanoparticles (ZnO NPs) were prepared by precipitation method according to Akhtar et al. (2017) with slight modifications. Briefly, aqueous solutions of 0.2 M zinc nitrate hexahydrate ($Zn(NO_3)_2.6H_2O$) and 0.4 M potassium hydroxide (KOH) were initially prepared. The KOH solution from the burette was added dropwise to the beaker containing zinc nitrate solution with vigorous stirring at room temperature. The white product formed in the suspension upon addition of KOH was centrifuged at 5000 rpm for 10 min. The pellets were washed with water for three times followed by ethanol. Finally, the white precipitate was calcined at 500°C for 3 h to obtain ZnO NPs.

3.2.3. Preparation of NaCMC–HPMC–ZnO nanocomposite hydrogel films

The nanocomposite hydrogel films were prepared from ZnO NPs, NaCMC, HPMC and citric acid. Initially, 0.5 g of HPMC was dissolved in 100 ml of water at 90°C with

continuous stirring to obtain a clear solution. The solution was left to cool at room temperature. The addition of HPMC promotes intermolecular crosslinking as well as intermolecular interactions. Then, 50 mg of ZnO NPs were added into the above solution and sonicated (33 kHz, 50 W) for 30 min to disperse the nanoparticles. An amount of 1.5 g of NaCMC was gradually added into ZnO-HPMC solution under vigorous magnetic stirring (900 rpm) for 8 h to obtain a homogeneous mixture. Finally, different concentrations of citric acid (CA) such as 5%, 10% and 20% (w/w of 2 wt.% polymer concentrations) were added into the solution containing NaCMC-HPMC-ZnO. All the samples were kept in a vacuum to remove air bubbles. A volume of 100 ml of each sample was cast into a Petri dish of 18 cm diameter and was kept at 80°C for 5 h for CA crosslinking reaction. The control nanocomposite films were also prepared using a similar procedure without the addition of CA. The nanocomposite films prepared were stored in a vacuum desiccator for characterizations.

In order to compare the influence of CA on ZnO NPs, 1:1, 1:2, 1:4 and 1:8 weight ratios of ZnO NPs and citric acid were mixed in 100 ml water without addition of polymers and left at room temperature for 24 h.

3.2.4. Preparation of copper oxide nanoflakes

Copper oxide (CuO) nanoflakes were synthesized using the precursors of copper chloride dihydrate ($CuCl_2.2H_2O$) and sodium hydroxide (NaOH) according to Anandan and Yang (2007) with minor modifications. Briefly, aqueous solutions of 0.5 M $CuCl_2.2H_2O$ and 1 M NaOH were initially prepared. Then, the NaOH solution was added dropwise to the beaker containing $CuCl_2.2H_2O$ solution with constant stirring of 500 rpm at room temperature. While stirring, the black precipitate formed upon addition of NaOH. The solution was centrifuged at 7000 rpm for 15 min. The black pellets were washed with ample amount of water and followed by ethanol to remove NaCl (by-

product) and other unreacted precursors completely. Finally, the black precipitate was dried at 80°C for 12 h to obtain CuO nanoflakes.

3.2.5. Preparation of NaCMC–HPMC–CuO nanocomposite hydrogel films

The cellulose-based nanocomposite hydrogel films were fabricated from CuO nanoflakes, HPMC, NaCMC and CA (chemical crosslinker). Initially, in order to enhance intermolecular crosslinking and intermolecular interactions, 0.5g HPMC was added into 100 ml of water under magnetic stirring (700 rpm) at 90°C. After a few minutes, the HPMC polymer was dissolved completely and the clear solution was left to attain room temperature. Then, 50 mg of CuO nanoflakes were added into the polymer solution and left for 30 min. The above solution was fed with an amount of 1.5 g NaCMC at 900 rpm for 8 h. Finally, citric acid to the extent of 5%, 10% and 20% (w/w of total polymer) was added into the homogeneous mixture. Before pouring the samples into a Petri dish of 18 cm diameter, air bubbles in all the samples were carefully removed using a vacuum pump. All the Petri dishes were kept at 80°C for 5 h. The control films were made using a similar method without incorporation of citric acid. The fabricated films were kept in a vacuum desiccator for further characterizations.

3.2.6. Preparation of NaCMC–HPMC–ZnO/GFSE nanocomposite hydrogel films

The precursors of nanocomposite hydrogel films were NaCMC, HPMC, CA, ZnO NPs and GFSE. Initially, 0.5 g of HPMC polymer was slowly dissolved in 100 ml of water at 90°C and the mixture was continuously stirred at 700 rpm for an hour to obtain a clear solution. Then, 1.5 g of NaCMC was gradually added to the HPMC solution at 900 rpm and left for 8 h to get homogeneous mixture. An amount of 0.4 g of CA was incorporated into the mixture. After complete mixing of CA, 50 mg of ZnO NPs were supplemented to the above solution, which was left for 30 mins under vigorous stirring. Finally, various amounts of liquid GFSE (0%, 0.25%, 0.5% and 1% v/v) was fed into

the solution containing NaCMC, HPMC, CA and ZnO. The composition of the control film was without addition of GFSE. Air bubbles were completely removed from all the samples using vacuum desiccator followed by solution casting into a Petri dish (18 cm diameter) which was kept at 80°C for CA crosslinking reaction. After complete drying, the films were peeled off from the Petri dish and preserved in a vacuum desiccator for further characterizations.

3.3. Characterizations

3.3.1. Swelling ratio of hydrogel films

An equal size of hydrogel films was immersed in PBS, pH 7.4 at 37°C for 24 h. The swollen films were carefully taken out and excess surface water was removed using filter paper. The swollen films were weighed and the swelling ratio (SR) was calculated as defined below:

$$SR\ (\%) = (W_s - W_{i(d)})/W_{i(d)} \times 100$$

where W_s and $W_{i(d)}$ are the weights of swollen and initial dried hydrogel films, respectively.

3.3.2. X-ray diffraction

All the samples were analyzed for their crystalline phase using X-ray powder diffractometer (XRD) (Make: Rigaku, model: SmartLab, USA). The Ni-filtered Cu Kα radiation (λ = 0.15418 nm, 45 kV, 112 mA) was used in the range of 5–70° (2θ) with a step size of 0.01° (2θ) and scan rate of 20°/min.

3.3.3. Fourier transform infrared spectroscopy

The Fourier transform infrared spectroscopy (FTIR) (Make: Shimadzu, model: IRAffinity-1, Japan) was performed using attenuated total reflectance (ATR) method. Film samples were directly placed on ATR crystal. These films were investigated over an absorbance range of 4000–400 cm^{-1} by 60 scans at a resolution of 4 cm^{-1}.

3.3.4 Raman spectroscopy

Raman spectra for all the samples (NaCMC-HPMC-ZnO, NaCMC-HPMC-CuO and NaCMC-HPMC-ZnO/GFSE films) were recorded from 1500 to 50 cm^{-1} using a laser at λ=633 nm with 10 s acquisition time (Make: Horiba Jobin Vyon; Model: LabRam HR, France). In order to record Raman spectra from 2000 to 50 cm^{-1} for copper based samples laser micro Raman spectrometer with a laser at a wavelength of 488 nm and acquisition time 30 s was used.

3.3.5. Differential scanning calorimetry

Differential scanning calorimetry (DSC) was used to obtain glass transition temperature (T_g) of samples (NaCMC-HPMC films) at a heating rate of 5°C/min over a temperature range of 20–200°C (Make: Mettler Toledo, model: DSC 1, Switzerland). Nitrogen was used as a purge gas. In order to find out glass transition temperatures (T_g), the following thermal cycles were adopted as: (i) heating from 20°C to 120°C at 5°C/min; (ii) isotherm at 100°C for 3 min; (iii) cooling from 120°C to 20°C at 5°C/min; (iv) heating from 20°C to 200°C at 5°C/min; (v) isotherm at 200°C for 3 min and (vi) cooling from 200°C to room temperature. An empty aluminium pan was used as a reference.

3.3.6. Thermogravimetric analysis

The thermal behavior of the samples was studied by thermogravimetric analysis (TGA) (Make: NETZCH, model: TG 209 F1 Libra, Germany) with the following parameters: heating rate, 10°C/min; inert gas, nitrogen; purge gas flow rate, 40 ml/min; protective gas flow rate, 20 ml/min and crucible, alumina.

3.3.7. Field emission scanning electron microscopy

Field emission scanning electron microscopy (FESEM) (Make: Zeiss, model: Sigma, Germany) was used to examine the surface morphology of the samples. Before the

analysis, all the samples were made conducting by gold sputter coating under argon gas.

3.3.8. Field emission transmission electron microscopy

Field emission transmission electron microscopy (FETEM) with energy dispersive X-ray (EDX) (Make: JEOL; model: 2100F, Japan) was used to observe the morphology of nanoparticles as well as to map the elements. In order to extract the nanoparticles from hydrogels, an equal size of films was allowed to swell in 15 ml water for 24 h. Finally, 5 µl suspension was dropped on a copper grid and dried. The images were obtained at 200 kV and a beam current of 145 µA.

3.3.9. Cryofixation of hydrogel films

First, NaCMC-HPMC hydrogel films were kept to swell in 1X PBS, pH 7.4 for 24 h. Then, the swollen films were quickly frozen using liquid nitrogen. Finally, the frozen samples were kept in a freeze dryer (Make: Martin Christ, model: Alpha 2-4 LD, Germany) to sublime the solvent (water). The freeze-dried hydrogel films were used for morphology analysis and pore structure analysis.

3.3.10. Mercury intrusion porosimeter (MIP)

Pore sizes of freeze-dried NaCMC-HPMC hydrogel films were analyzed by mercury intrusion porosimeter (Make: PMI, model: AMP-60K-A-1, USA). An approximately 0.32 g of freeze-dried films were used for analysis. Pore sizes and surface area were directly calculated using Porwin software.

3.3.11. Contact angle measurement

Water contact angle on NaCMC-HPMC hydrogel films was measured by goniometer (Make: Holmarc, model: HO-IAD-CAM-01B, India) at room temperature. Five milliliters of deionized water was gently placed on sample surfaces. After a particular

time, the static contact angle was directly measured by goniometer. At least three readings on different places of film samples were averaged.

3.3.12. Thickness and mechanical properties of films

The film thickness was measured by digital micrometer (Mitutoyo, Japan) and mechanical properties were performed according to ASTM D882-12 by computerized tensile strength testing machine (Make: Globe Tex; model: GTI-TS110, India). All the films were preconditioned at 25°C and 65 ± 5% relative humidity for 24 h.

3.3.13. Point of zero charge measurement

The point of zero charge (pzc) of NaCMC-HPMC hydrogel films was determined according to the procedure reported by Moreno-Castilla et al. (2000) and Mittal et al. (2015). Briefly, 0.5 g of the hydrogel films were added into the 50 ml of different pH solutions in the range of 2 to 11. The solutions were agitated in a shaker for 24 h at 200 rpm and 25°C. The final pH of the solution was recorded and a graph of ΔpH vs. initial pH was plotted to find out pzc.

3.3.14. In vitro drug loading and release

An equally weighed sample of NaCMC-HPMC films was kept in 20 ml of PBS containing drug (either tetracycline or methylene blue) with initial concentrations of 0.1 mg/ml. The drug was allowed to diffuse into the hydrogel films for 24 h at 37°C. The drug loading efficiency of hydrogel films is the ratio of the difference between total amount of drug added and the free drug in the supernatant to the total amount of drug incorporated as shown below:

$$\text{Loading efficiency } (\%) = \frac{\text{Total amount of drug} - \text{Free drug in the supernatant}}{\text{Total amount of drug}} \times 100 \quad (1)$$

The drug concentration of tetracycline and methylene blue was measured at 274 and 291 nm, respectively using UV-vis spectrophotometer (Make: Shimadzu, model: UV-2600, Singapore). The drug release from the loaded hydrogel films was studied in 20 ml PBS, pH 7.4 at 37°C for three days. Aliquots of 1 mL of samples were taken out at different time intervals and then an equal amount (1 mL) of PBS was added to maintain a constant volume. The concentration of samples was analyzed using UV-vis spectrophotometer from predetermined calibration curve. All the experiments were repeated three times and data were represented in mean±SD.

3.3.15. Polyphenolic compounds release study

The release of polyphenolic compounds from NaCMC-HPMC-ZnO/GFSE based hydrogel films was studied by UV-Vis spectroscopy (Make: Shimadzu; model: UV-2600; Singapore). An equal size of 2 cm × 2 cm film was immersed in 20 ml buffer (PBS, pH 7.4). The samples were agitated at 100 rpm, 37°C. At predetermined time period (0.5, 1, 2, 4, 8, 12 and 24 h), 1 ml of samples was taken and the same amount of fresh buffer was replenished. The absorbance at 263 nm was fixed to monitor the release of polyphenolic compounds.

3.3.16. DPPH scavenging activity

The antioxidant activity of NaCMC-HPMC-ZnO/GFSE based hydrogel films was determined by DPPH (2,2-diphenyl-1-picrylhydrazyl) radical scavenging assay (Singh and Dhiman, 2016). First, 100 µM solution of DPPH was prepared in methanol. Then, an equal size of 3 cm × 3 cm film was dipped in 4 ml of DPPH solution and the reaction mixture was left at 37°C in the dark for 2 h. The colour change from violet to light yellow was measured at 517 nm by UV-Vis spectroscopy (Make: Shimadzu; model: UV-2600; Singapore). The control was DPPH in methanol while blank was film in

methanol. Ascorbic acid (vitamin C) was used as positive control. Finally, the inhibition (%) of DPPH free radical was estimated according to the following equation:

$$\text{DPPH scavenging activity (\%)} = 100 - \{[(Abs_{sample} - Abs_{blank}) \times 100]/Abs_{control}\}$$

3.3.17. Liquid chromatography-mass spectrometry (LC-MS/MS) analysis

An amount of 1mL of GFSE was diluted with HPLC grade acetonitrile and water (1:1 v/v). Constituents of the sample were analyzed by LC-MS/MS (Make: Waters, Model: Q-Tof premier, UK) with the following settings: negative mode, range *m*/*z* 80-1200, capillary 2.26 kV, extraction cone 3.1 V, sampling cone 30 V, source temperature 105°C, desolvation temperature 400°C, desolvation gas (nitrogen) flow 650 L/h and cone gas flow 50 L/h. The parameters were controlled and the *m*/*z* values were evaluated by MassLynx 4.1 software.

3.3.18. Particle size analysis

The GFSE based nanocomposite films of size 4×4 cm were dropped in a 5 mL tube filled with water. The tube was agitated at 150 rpm for 12 h to leach out the nanoparticles. Then, the solution was centrifuged at 15,000 rpm for 10 min. Finally, the particle size and zeta potential were determined by a particle size analyzer without sonication (Make: Beckman Coulter, Model: Delsa Nano C, Switzerland).

3.3.19. Zinc and copper release by atomic absorption spectroscopy

Zinc and copper release was estimated by atomic absorption spectroscopy (AAS) (Make: Varian; model: AA240, Netherlands). An equal weight of hydrogel film samples (0.1 g) was kept in 20 ml of PBS (pH 7.4). The solution containing films were agitated continuously at 100 rpm, 37°C. Aliquots of 1 ml of sample were taken out at predetermined time intervals of 0.5, 1, 2, 4, 6, 12 and 24 h while an equal amount (1 ml) of fresh buffer was replenished to maintain a constant volume. Then, 1 ml of the sample was made up to 10 ml for zinc and copper estimation. Before the analysis of

zinc and copper content, all the samples were centrifuged at 10,000 rpm for 30 min and filtered. The released zinc and copper content was calculated using the calibration curve for zinc and copper standards.

3.3.20. Antimicrobial activity

Disc diffusion method was chosen to investigate the antibacterial activity of the prepared films against Gram-positive (*Staphylococcus aureus* MTCC 6538) and Gram-negative (*Escherichia coli* MTCC 1610) microorganisms. A disk of 5 mm in diameter of various hydrogel films was placed on Mueller-Hinton agar plate, which was previously inoculated with bacterial concentration of 10^6 CFU/ml. In the case of methylene blue and tetracycline loaded hydrogel films, after three days of drug release in PBS, disks of 5 mm in diameter were subjected to antibacterial test. After 24 h incubation at 37°C, a clear zone around the disk was measured using a ruler. A disk containing ampicillin (25 µg) was used as positive control.

3.3.21. Cytotoxicity study

3.3.21.1. Cell culture

The HaCaT human keratinocyte cells obtained from NCCS, Pune, India were maintained in DMEM medium (Priya and Jeyajothi, 2019) (Gibco™; Life Technologies, NY, USA) supplemented with 10% FBS (Gibco®, NY, USA) and 1X Penstrep (Invitrogen, USA) at 37°C in a CO_2 incubator (5% CO_2 and 95% humidity).

3.3.21.1. MTT assay

The effect of prepared ZnO NPs, CuO nanoflakes and CA crosslinked films (NaCMC-HPMC-ZnO and NaCMC-HPMC-CuO films) on the proliferation of HaCaT cells was determined using MTT assay. Briefly, HaCaT cells were seeded at a density of 2000 cells/well in 96 well plates and incubated at 37°C in a CO_2 incubator for 24h. Erstwhile, "conditioned media" was prepared by incubating 10 mg of the films in 2 mL of serum

free DMEM media for 24 h, after which supernatant was collected and filtered with a 0.22 µm syringe filter (RanDisc^{TM}, India). Using the filtrates, 50% of each sample was prepared and added in previously seeded cells. The MTT assay was performed at predetermined period. After each time point, 10 µl of 5 mg/ml of MTT (Invitrogen, USA) was added to each well and incubated for 2 h. Following that, the culture medium of each well was replaced with 100 µl of DMSO (Merck, Germany) and then incubated at room temperature for 1 h. Finally, the absorbance was measured at 570 nm with a microplate reader (TECAN Infinite 200 PRO multimode reader, Switzerland). The effect on the proliferation of HaCaT cells due to the treatment of the samples was measured by normalizing the absorbance at predetermined period with 0 h, keeping the absorbance of control as 100%.

3.4. Statistical analysis

The data sets were evaluated using Origin software (version 8.5). The data were analyzed for paired comparison of individual data means by one-way ANOVA with Tukey Post-hoc analysis. A p-value less than 0.05 was considered statistically significant. All the experiments were conducted three times wherever required and data were represented in mean±SD.

3.5. Closure

In this chapter, materials and methods to prepare various hydrogel films are presented in detail along with characterization techniques. Next chapter (Chapter 4) presents the results and discussion of various amounts of citric acid (5-20 wt.% of polymer) crosslinked NaCMC and HPMC hydrogel films.

Chapter 4

Fabrication, characterization and drug loading efficiency of CA crosslinked NaCMC-HPMC hydrogel films for wound healing and drug delivery applications

In this chapter, the effect of CA on hydrogel films containing sodium carboxymethylcellulose (NaCMC) and hydroxypropylmethylcellulose (HPMC) was studied for their physical, chemical, thermal, mechanical and antibacterial properties as well as for their drug (methylene blue and tetracycline) loading efficiency and drug release properties.

4.1. Introduction

Hydrogels are physically or chemically crosslinked hydrophilic polymeric three-dimensional networks that can absorb and hold large amounts of water or biological fluids. Hydrogels have found wide variety of applications in drug delivery, tissue engineering, hygienic products, agriculture, wastewater treatment, textile and food packaging (Fei et al., 2000; Gorgieva and Kokol, 2011; Kök et al., 1999; Pourjavadi et al., 2007; Shahbazi et al., 2016; Tran et al., 2017; Wach et al., 2001). In the recent past, hydrogels derived from natural polymers and its derivatives have been largely used in drug delivery and tissue engineering applications (Bao et al., 2014; Hoffman, 2012). Amongst various polymers, cellulose is the world's most abundant, natural, renewable, non-toxic and biodegradable polymer and it is being used to prepare hydrogels for various applications (Deng et al., 2008; Guo and Chu, 2005; Raucci et al., 2015; Weng et al., 2004). Sodium carboxymethylcellulose (NaCMC) is an ether derivative of cellulose and is highly hydrophilic due to the presence of abundant hydroxyl (-OH) and carboxyl (-COOH) groups. NaCMC has been paid more attention in the preparation of hydrogels due to its good water-solubility, better biocompatibility, best swelling

capability, high abundance and low price (Ahmed, 2015). Amongst all cellulose-based hydrogels, NaCMC stands out in swelling rate (in distilled water and saline solutions) and equilibrium water uptake (Ghorpade et al., 2017; Ma et al., 2015). An extensive research has been done on the preparation of NaCMC based hydrogels by physical or chemical crosslinking (Arica, 2000; Fei et al., 2000; Kök et al., 1999; Wach et al., 2003, 2001). However, hydrogels prepared from NaCMC alone possess poor mechanical strength in the swollen state, limiting their applications in wound dressing and drug delivery materials (Qiu et al., 2007; Wang et al., 2007). Moreover, NaCMC hydrogel system possesses large swelling ratio due to the presence of carboxylic (-COOH) groups, which further leads to strong electronic repulsion resulting in enhanced pore size. Therefore, drug-loaded NaCMC hydrogel systems cannot be used for controlled drug delivery applications (Shen et al., 2015). Hence, NaCMC was combined with other polymeric materials (HEC, PVP and PVA), which are crosslinked by high energy irradiation, radical polymerization, enzymatic reactions and chemical reactions. This limitation has resulted in polymer composite matrix containing NaCMC crosslinked with different polymers (HEC, PVP and PVA) by either physical or chemical means (Abd El-Mohdy, 2007; Abd El-Rehim et al., 2006; Buhus et al., 2007; El Salmawi, 2007; Lenzi et al., 2003; Ogushi et al., 2007; Pourjavadi et al., 2006; Sannino et al., 2005, 2003, 2007, 2006; Sannino and Nicolais, 2005; Wang et al., 2007). Although many methods were reported to produce NaCMC based hydrogels, there may be some disadvantages due to high production cost, preparation time, crosslinking through toxic chemicals and high energy irradiation. In order to have non-toxic final product and safe manufacturing process, some of the researchers used non-toxic crosslinking agents to crosslink NaCMC with other polymers for various applications in agriculture, textile

and health care (Demitri et al., 2008; Gorgieva and Kokol, 2011; Ni et al., 2011; Raucci et al., 2015; Ullah et al., 2015).

Hydrogels prepared from single polymer can seldom completely satisfy the requirements of drug delivery systems due to their poor network structure formed by partial inter-chain (intra-chain) interactions. In order to overcome this disadvantage in drug delivery systems, mixtures of cellulose derivatives especially cellulose ethers were used for accomplishing controlled drug release (Chopra et al., 2007). Blending of different polymers offers a new structural material with attractive advantages for controlled release applications (Ibrahim et al., 2013). It was also reported that hydrogels prepared from CMC alone releases the drug in much faster rate due to its high swelling ratio. Further, it displayed low mechanical strength compared to composites (Mandal et al., 2016; Zare-Akbari et al., 2016).

Hydroxypropylmethylcellulose (HPMC) is a water-soluble, tasteless, odorless, off-white colored ether cellulose derivative. It has been approved by FDA as a non-toxic substance to the human body (Marani et al., 2015; Mujtaba and Kohli, 2016). It is used as a food additive, emulsifier, thickening agent and as an alternative to gelatin. HPMC films are stable in the presence of light, heat and reasonable levels of moisture. They are flexible in terms of incorporating additives into the film without difficulty. HPMC is often used for controlled release of drugs (Siepmann and Peppas, 2012). Due to the presence of polar (hydroxypropyl) and non-polar (methyl) groups in HPMC, it can be involved in the intermolecular, intramolecular and hydrophobic interactions (Chen et al., 2015). Based on the degree of substitution of polar and non-polar groups, HPMC exhibits different affinity towards water and drug (Kondaveeti et al., 2017).

Various chemical crosslinking agents were used to synthesize hydrogels namely GTA, EPH, DVS, DCC, CA and MA. Though there are several chemicals available for

crosslinking, CA has received considerable attention due to its non-toxicity and lower price. Also, the human body itself synthesizes citric acid as an intermediate product via Krebs cycle. The concept of using citric acid as a crosslinker for producing CMC based superabsorbent hydrogels for agriculture was first reported by Demitri et al. (2008). Cellulose ether derivatives of NaCMC and HPMC are frequently used as gelling agents in drug formulations and are less prone to microbial contamination compared to other gelling agents such as agar, pectin, acacia, gelatin and tragacanth (Shokri and Adibkia, 2013). The smart behavior of NaCMC and HPMC in response to change in pH, ionic strength and temperature (physiological variables) proved to be an attractive option for in vivo applications (Sannino et al., 2009).

The combination of cellulose ether derivatives such as NaCMC and HPMC using citric acid as a crosslinking agent for producing hydrogel films for wound dressing drug delivery applications has not yet been studied. Although numerous studies are available on hydrogel films for drug delivery systems, it is still imperious to develop hydrogel films as drug carriers with the characteristics like high drug loading efficiency, drug stability in the films, controlled release, biocompatibility and biodegradability. Also, effect of citric acid on physical, thermal and mechanical properties of the hydrogel films is not studied in detail. Besides, the drug loading capacity of citric acid crosslinked hydrogel films is not yet reported. The present chapter aims to fabricate and characterize hydrogel films of citric acid crosslinked NaCMC-HPMC. Finally, the developed hydrogel films were loaded with two model drugs such as methylene blue and tetracycline for wound healing and drug delivery applications.

4.2. Results and discussion

The mixing ratio of the polymers such as NaCMC and HPMC to develop hydrogel films was optimized/chosen based on their SR and a steady appearance in the swollen state

in PBS at 37°C and pH 7.4. According to DSC analysis, the dehydration process of citric acid leading to cyclic anhydride was evident at 60°C (minimum) (Fig. A1). The curing temperature (80°C) was optimized on the basis of SR of the prepared hydrogel films after 24 h in PBS at 37°C and pH 7.4. Furthermore, the temperature was optimized based on the characteristics of fast drying, flexible and easily peelable from Petri dishes.

4.2.1. Crosslinking mechanism of citric acid (CA)

Supersorbent hydrogels of CA crosslinked NaCMC and HEC were developed for agricultural applications and the CA crosslinking mechanism was also proposed by Demitri et al. (2008). First, CA forms cyclic anhydride after condensation reaction during heating. Ester bond was formed between cyclic anhydride moiety and hydroxyl groups of cellulosic chains. After esterification step, another cyclic anhydride moiety emerges during heating. Another ester bond formation occurs between second cyclic anhydride and cellulose hydroxyl groups. Thus, CA creates intermolecular crosslinking through cyclic anhydride between hydroxyl groups of cellulose, resulting in ester bonds.

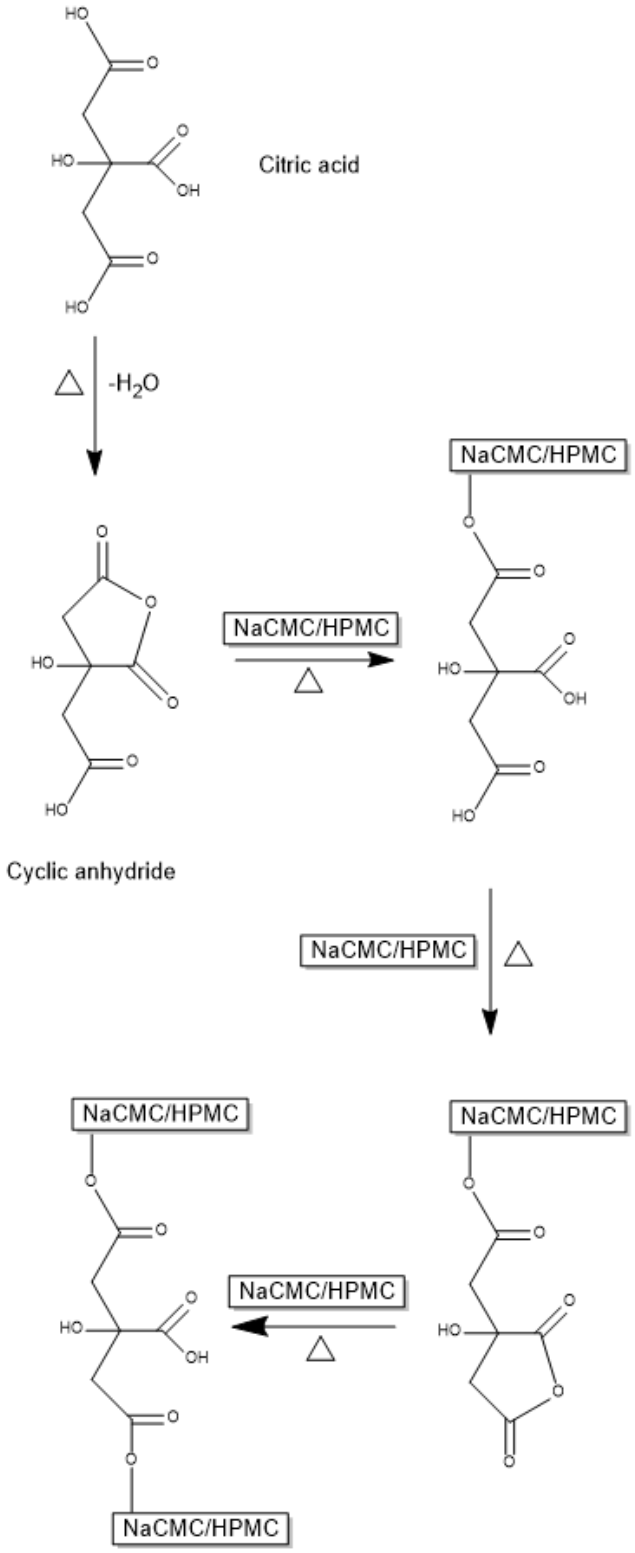

Figure 4.1. Possible sequential crosslinking reaction mechanism of CA as a crosslinker with NaCMC and HPMC.

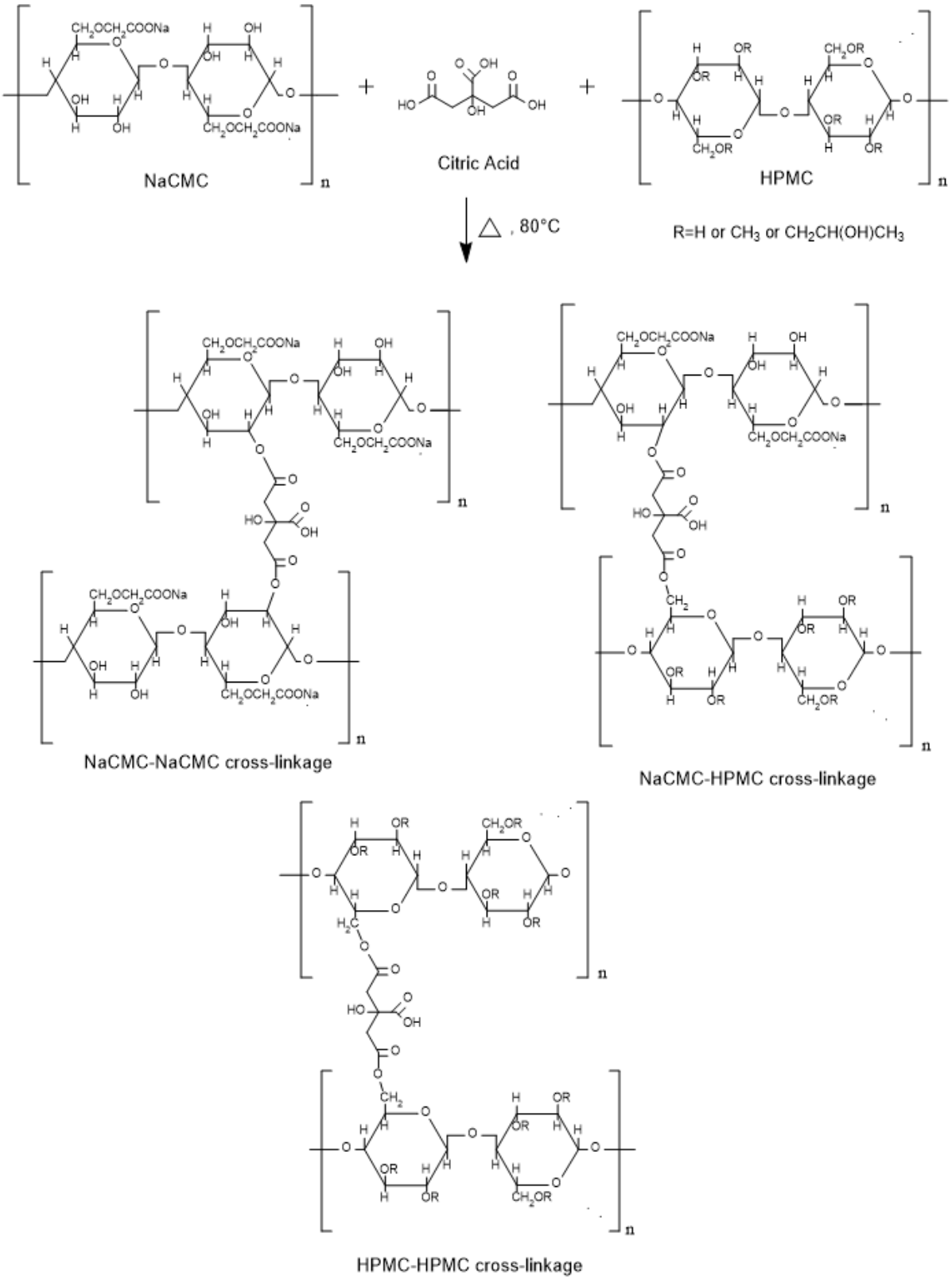

Figure 4.2. Proposed possible crosslinked structures of NaCMC and HPMC with CA molecule.

In the present study, the mechanism of CA crosslinking between NaCMC and HPMC is shown in Fig. 4.1. The final possible molecular structure of crosslinked NaCMC-NaCMC, HPMC-HPMC and NaCMC-HPMC is shown in Fig. 4.2.

4.2.2. FTIR spectra of hydrogel films

The FTIR spectra shows the ester bond formation in CA crosslinked NaCMC-NaCMC (Fig. 4.3A), HPMC-HPMC (Fig. 4.3B) and NaCMC-HPMC (Fig. 4.3C). The FTIR spectra of neat NaCMC is shown in Fig. 4.3C(a). The broad peaks at 1589 cm^{-1}, 1420 cm^{-1} and 1326 cm^{-1} are due to COO^- stretching vibrations, $–CH_2$ scissoring and –OH bending vibrations of NaCMC, respectively (Fig. 4.3C(a)). The sugar ring vibrations of NaCMC are observed from 1200 cm^{-1} to 1000 cm^{-1}. A small band with broadness at 895 cm^{-1} is attributed to C–O–C stretching vibrations of NaCMC (Fig. 4.3C(a)) (Gorgieva and Kokol, 2011; Qiu et al., 2007; Raucci et al., 2015; Wang et al., 2007). FTIR spectra of HPMC showed broad peaks at 1641 cm^{-1}, 1458 cm^{-1} and 1375 cm^{-1}, which are due to bending vibration of –OH group, asymmetric and symmetric bending vibrations of a methoxy group ($–OCH_3$), respectively. The characteristic peak at 1052 cm^{-1} can be assigned to C-O-C stretching vibration of HPMC (Fig. 4.3C(b)) (Ding et al., 2015; Gorgieva and Kokol, 2011; Maity et al., 2013). The presence of ester bond in NaCMC-HPMC blend films was not observed (Fig. 4.3C(c)). But, CA crosslinked films show ester bond formation between cyclic anhydride of CA and –OH groups of cellulose derivatives such as NaCMC and HPMC at around 1720-1735 cm^{-1} (Fig. 4.3A-C).

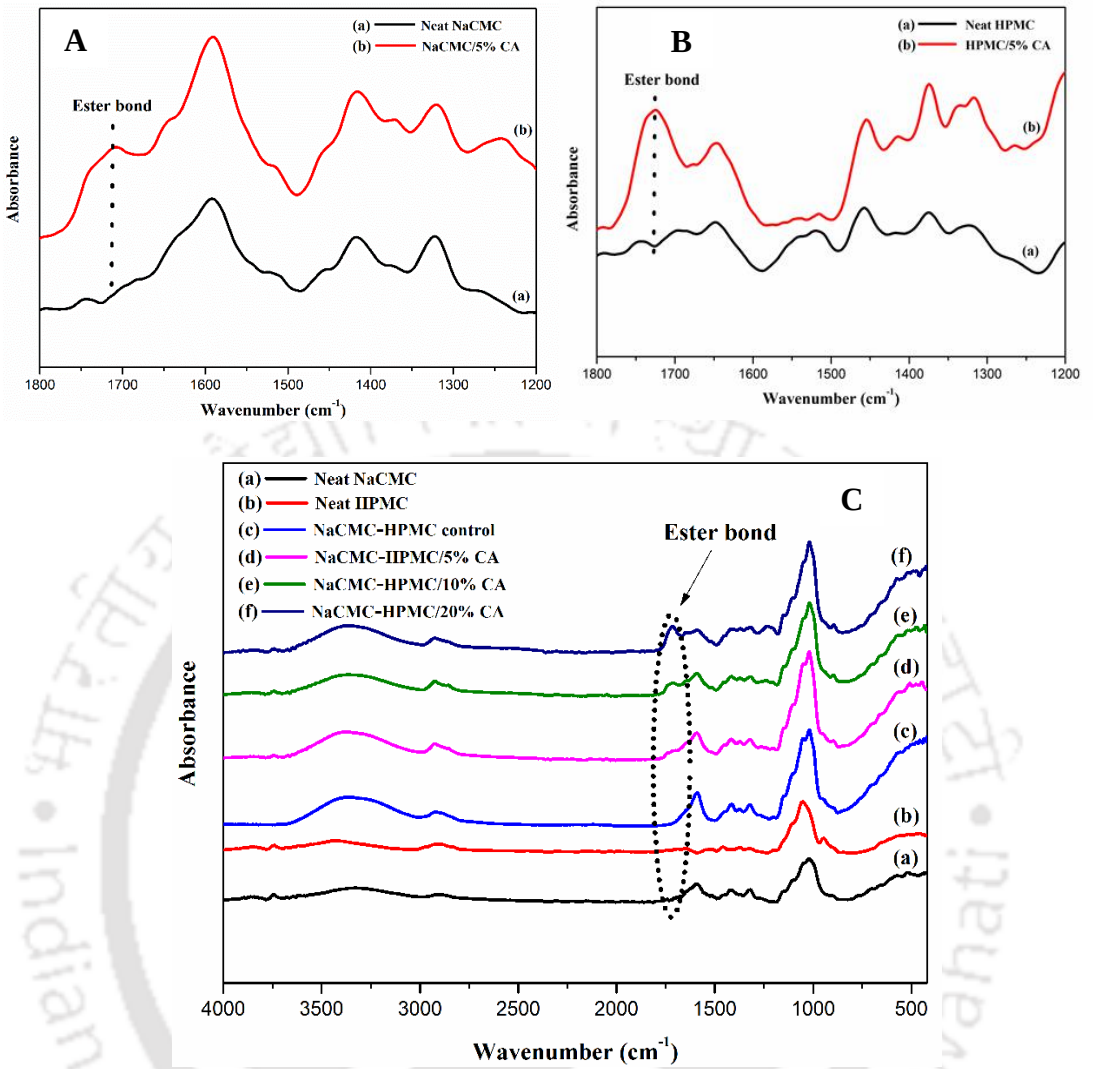

Figure 4.3. (A) FTIR pattern of (a) NaCMC and (b) NaCMC crosslinked with 5% CA. (B) FTIR pattern of (a) HPMC and (b) HPMC crosslinked with 5% CA. (C) FTIR pattern of (a) neat NaCMC, (b) neat HPMC, and NaCMC-HPMC hydrogel films of (c) control (blend), and crosslinked with (d) 5% CA (e) 10% CA and (f) 20% CA.

All films exhibited mixed characteristics of NaCMC and HPMC, but the intensity of ester bond increases with respect to CA concentrations (5%, 10% and 20%) due to higher degree of crosslinking (Fig. 4.3C(d-f)). Moreover, the area and intensity of asymmetric stretching of COO^- group increase in the crosslinked hydrogel films (Fig.

4.3C(d-f)). These results are in accordance with results of Gorgieva and Kokol (2011) and Demitri et al. (2008).

4.2.3. Swelling study of hydrogel films

SR of the prepared hydrogel films with various CA concentrations is shown in Fig. 4.4. It is known that the SR is inversely proportional to crosslinking density. FTIR analysis showed that the intensity of ester bond, which plays an essential role in crosslinking degree, increases with CA concentration.

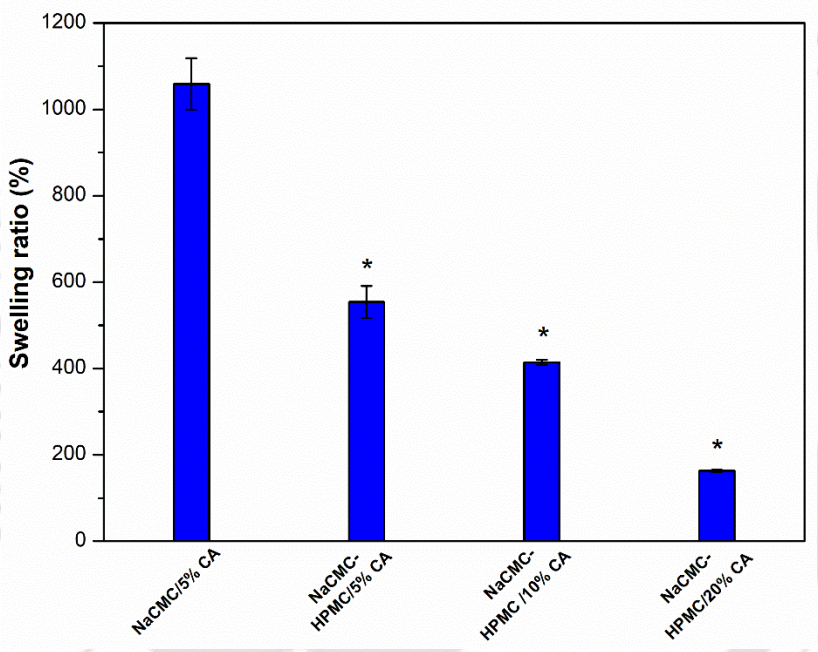

Figure 4.4. Swelling ratio (SR) (%) of NaCMC crosslinked with 5% CA and NaCMC-HPMC hydrogel films crosslinked with 5%, 10% and 20% CA concentrations after 24 h in PBS, pH 7.4 at 37°C (*P<0.05 is significant difference with respect to NaCMC/5% CA).

NaCMC (2 wt.%) crosslinked with 5% CA showed SR of 1058. 82 ± 59.88% (Fig. 4.4). This hydrogel film was unable to maintain its structure due to poor mechanical property. The addition of HPMC (0.5 wt.%) with NaCMC (1.5 wt.%) significantly

decreases the SR (Fig. 4.4). It may be either due to decrease in NaCMC concentration or increase in crosslinking density in NaCMC-HPMC mixtures or the formation of intermolecular hydrogen bond between NaCMC-HPMC. It was clearly observed that SR of NaCMC-HPMC (3:1 weight ratio) hydrogel films further decreases with increase in CA concentration (Fig. 4.4). It might be due to increase in crosslinking density, which further reduces the molecular space for water to enter into the network.

4.2.4. Effect of CA on crystallinity of hydrogel films

XRD pattern of neat NaCMC, neat HPMC, NaCMC-HPMC crosslinked with 5%, 10% and 20% CA is shown in Fig. 4.5(a-f).

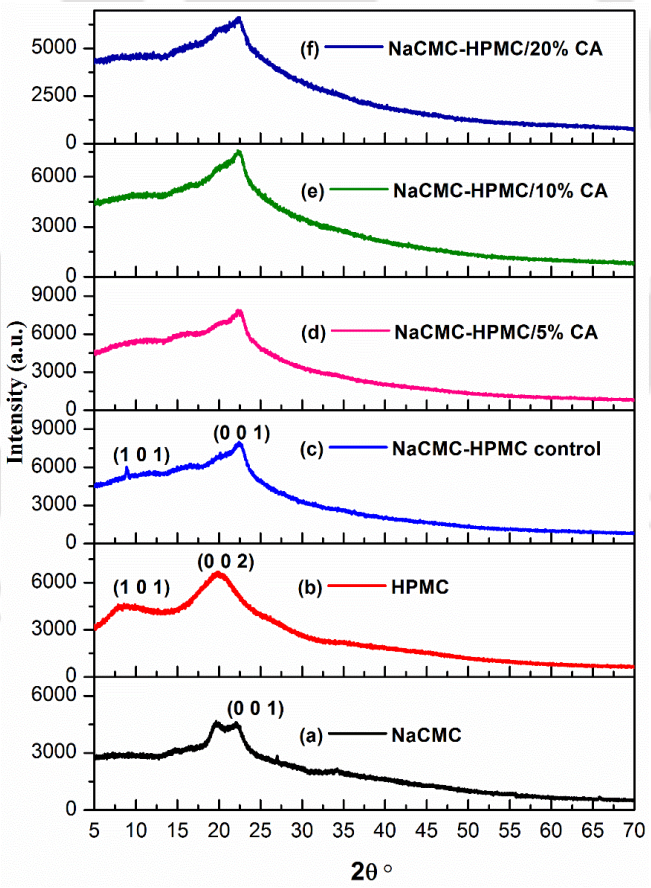

Figure 4.5. XRD pattern of (a) neat NaCMC, (b) neat HPMC, and NaCMC-HPMC hydrogel films of (c) control (blend), and crosslinked with (d) 5% CA (e) 10% CA and (f) 20% CA.

The neat NaCMC had diffraction peak at 2θ = 22.1° (Fig. 4.5a). The semi-crystalline behavior of HPMC was observed as broad peaks at a maximum peak intensity of 7.72° and 19.98° (2θ) (Fig. 4.5b). It is clear that both cellulose derivatives have appreciable crystallinity and not completely amorphous in nature. The blend films showed mixed characteristics of (0 0 1) and (1 0 1) crystalline planes for NaCMC and HPMC, respectively. However, the crystalline plane (0 0 2) for HPMC was not observed due to intermolecular interactions (Fig. 4.5c). The diffraction pattern of NaCMC-HPMC crosslinked with 5% CA showed a reduction in crystallinity and the HPMC crystalline plane (1 0 1) was disappeared because of its crosslinking with CA (Fig. 4.5d). The crystalline peaks were gradually broadened with increase in CA concentrations (10% and 20%) (Fig. 4.5e-f) compared to neat NaCMC, neat HPMC, NaCMC-HPMC blend films and NaCMC-HPMC crosslinked with 5% CA hydrogel films (Fig. 4.5a-d). It has been reported that peak broadening occurs with increasing amounts of crosslinking owing to added restrictions on polymer chain mobility (crystallite size) or development of imperfections or internal strain (Nielsen, 1969; Roberts and Mandelkern, 1960). The height of the peak was also decreased at 2θ = 22.1° with increase in CA. The decrease in the height of the peak was higher for 20% CA compared to 5% and 10% CA films. The decrease in height of the peak was also observed for fumaric acid (10% to 25%) crosslinked between NaCMC and PVA (Dilaver and Yurdakoc, 2016) and CA crosslinked starch/polyvinyl alcohol films (Shi et al., 2008).

4.2.5. Effect of CA on glass transition temperature of hydrogel films

DSC analysis was investigated to find out the effect of CA on glass transition temperature (T_g). The second heating cycle of neat NaCMC, neat HPMC, NaCMC-HPMC blend films and NaCMC-HPMC crosslinked with 5%, 10% and 20% CA hydrogel films is shown in Fig. 4.6(a-f). The T_g of NaCMC and HPMC were found to

be ~149°C (Fig. 4.6a) and ~146°C (Fig. 4.6b), respectively (Li et al., 2009; Meng et al., 2015). The blend films of NaCMC-HPMC showed T_g of ~142°C (Fig. 4.6c).

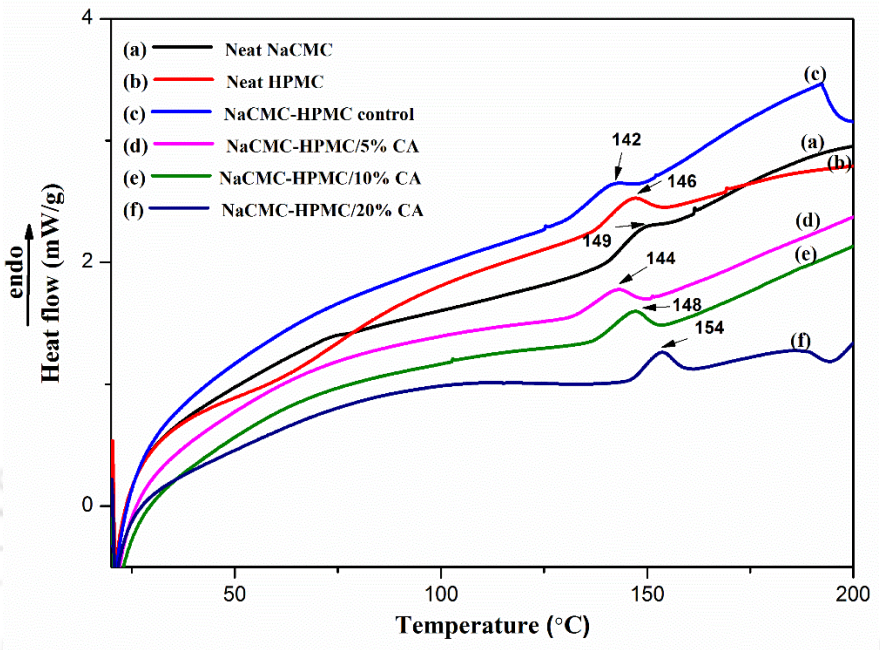

Figure 4.6. DSC analysis of (a) neat NaCMC, (b) neat HPMC, and NaCMC-HPMC hydrogel films of (c) control (blend), and crosslinked with (d) 5% CA (e) 10% CA and (f) 20% CA.

It is known that crosslinking restricts the molecular movements and increases the T_g. The T_g peak shift is small for low degree of crosslinking but is large for high degree of crosslinking (Nielsen, 1969). Moreover, CA crosslinking replaces the van der Waals interactions by covalent bonds (ester). Hence, the flow of heat is higher in the case of covalent bond interactions than weak force interactions. It was observed that the T_g was shifted to 144°C, 148°C and 154°C with increasing concentration of CA from 5%, 10% and 20%, respectively (Fig. 4.6d-f). The increase in T_g and decrease in SR (Fig. 4.4) with increasing CA suggest that crosslinking degree is increased. This further indicates

that the formed hydrogel acts as a single network due to crosslinking. The same results were observed for CA crosslinked starch/polyvinyl alcohol films (Shi et al., 2008).

4.2.6. Thermogravimetric analysis (TGA) of hydrogel films

TGA and derivative thermogravimetry (DTG) analysis for precursors of neat NaCMC, neat HPMC and neat CA are shown in Fig. 4.7A(a-c). Three-step weight losses were observed for neat NaCMC samples under N_2 flow rate (Fig. 4.7A(a)). An initial mass loss was observed between 30-180°C due to removal of moisture. The maximum weight loss of NaCMC was observed at 287°C in the second-step. Decarboxylation of NaCMC was observed at 357°C in the third-step (Fig. 4.7A(a)). HPMC showed two-step weight losses: (i) evaporation of loosely bound moisture at 70°C and (ii) actual decomposition of HPMC at 355°C (Fig. 4.7A(b)). CA decomposition was maximum at 206°C (Fig. 4.7A(c)).

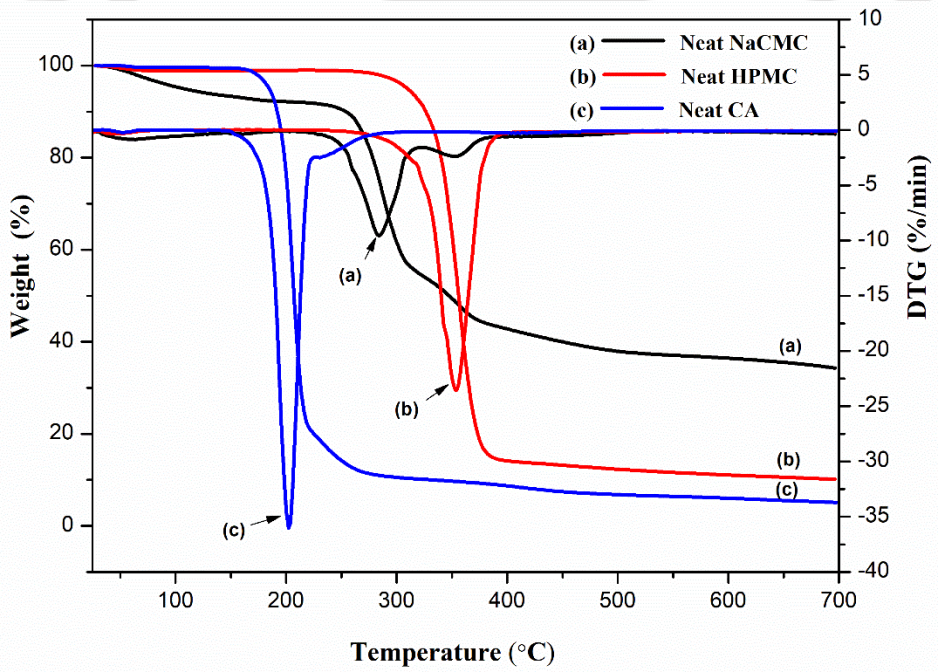

Figure 4.7A. TGA and DTG analysis of (a) neat NaCMC, (b) neat HPMC and (c) neat CA.

TGA and DTG analysis for NaCMC-HPMC blend films and NaCMC-HPMC crosslinked with 5%, 10 and 20% CA hydrogel films are shown in Fig. 4.7B(a-d). Three-step weight losses were observed in all films. An initial weight loss was observed at 120°C for all film samples. The blend films showed mixed decomposition characteristics of NaCMC and HPMC. Due to intermolecular interaction of HPMC with NaCMC, the maximum decomposition temperature of NaCMC in the blend films was observed at 292°C, which is higher than neat polymer (Fig. 4.7B(a)).

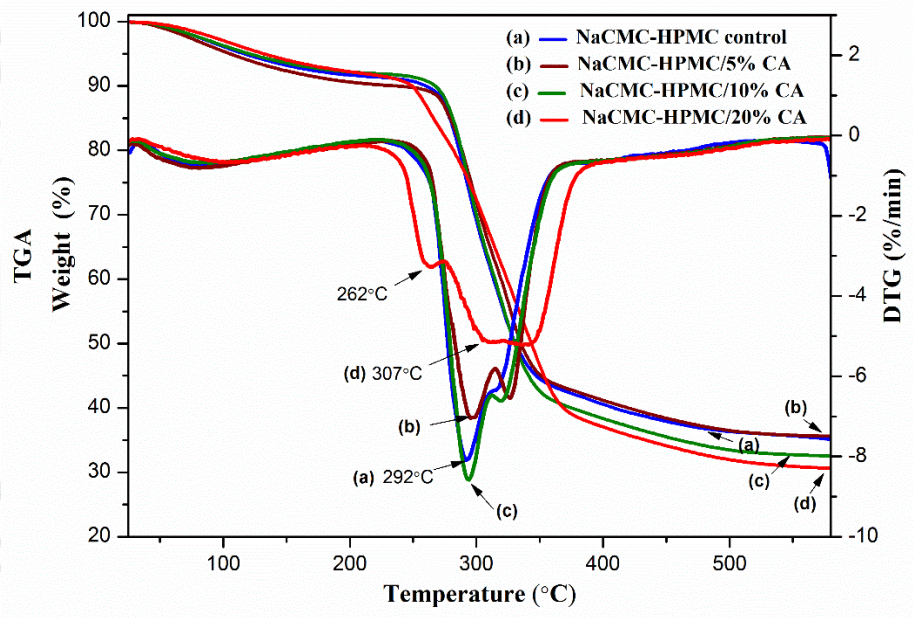

Figure 4.7B. TGA and DTG analysis of NaCMC-HPMC hydrogel films of (a) control (blend), and crosslinked with (b) 5% CA (c) 10% CA and (d) 20% CA.

The CA crosslinked films showed higher final decomposition temperature of NaCMC than neat polymer and blend films (Fig. 4.7B(b-d)). It suggests that crosslinking increases the final decomposition temperature of polymers. The NaCMC-HPMC

crosslinked with 20% CA showed one more shoulder peak at 262°C, which may be attributed to the excess amount of CA (Fig. 4.7B(d)).

4.2.7. Effect of CA on hydrophilicity of hydrogel films

The surface hydrophilicity of hydrogel films was investigated by contact angle measurement. The water contact angle of blend films and crosslinked films with various concentrations of CA is shown in Table 4.1 and Fig. 4.8.

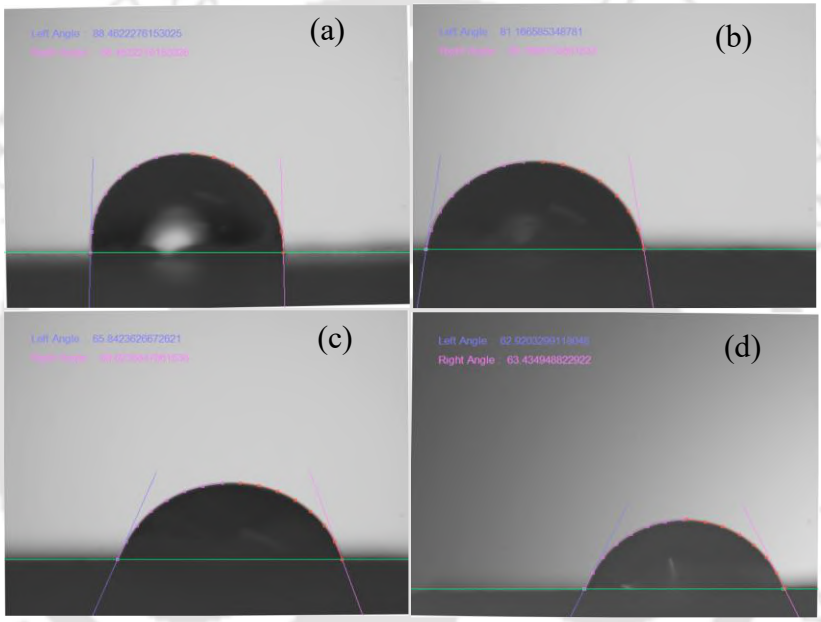

Figure 4.8. Water contact angle of NaCMC-HPMC hydrogel films of (a) control (blend), and crosslinked with (b) 5% CA (c) 10% CA and (d) 20% CA.

Table 4.1. Water contact angle of NaCMC-HPMC hydrogel films of control (blend) and crosslinked with different crosslinking concentrations.

Sample	Water contact angle
NaCMC-HPMC control	89.86 ± 1.55
NaCMC-HPMC/5% CA	81.27 ± 0.908*
NaCMC-HPMC/10% CA	67.29 ± 0.736*
NaCMC-HPMC/20% CA	62.43 ± 1.28*

*P<0.05 is significant difference with respect to control.

The blend films without crosslinking showed higher water contact angle of 89.86 ± 1.55° than CA crosslinked films (Fig. 4.8a-d), which is in accordance with crystallinity predicted from XRD results (Fig. 4.5c). Generally, water enters through amorphous regions. The contact angle decreases for CA crosslinked films (Fig. 4.8b-c) compared to non-crosslinked films (Fig. 4.8a) because of decrease in crystallinity (amorphous nature) with increase in CA. Moreover, increase in –COOH groups from CA, which contributes to surface hydrophilicity, decreases the contact angle of CA crosslinked films (Table 4.1). The same effect was observed for CA crosslinked hydroxyethyl cellulose (HEC-CA) and sodium salt of carboxymethyl cellulose (CMCNa-CA) (Raucci et al., 2015).

4.2.8. Morphology of hydrogel films by FESEM analysis

FESEM images of non-crosslinked and crosslinked film samples are shown in Fig. 4.9(a-h). The surface of NaCMC-HPMC blend films was rough as shown by FESEM (Fig. 4.9a). The interior morphology (50 KX magnification) of blend films showed the presence of microcracks (Fig. 4.9b). The addition of 5% CA as crosslinker shows relatively more smooth and uniform surface morphology due to the fact that CA creates covalent and intermolecular hydrogen bonds between polymer chains by crosslinking (Fig. 4.9c). The size of microcracks is also reduced for NaCMC-HPMC crosslinked with 5% CA films compared to blend films (Fig. 4.9a-d). Further increase in crosslinker concentration significantly reduces the surface roughness and size of microcracks (Fig. 4.9e-h). It is well known that crosslinking limits the molecular mobility and ties the polymers together. It was observed that the interior morphology is more rigid and compact for high CA concentration. Finally, slit-like nanocracks appeared for NaCMC-HPMC crosslinked with 20% CA films (Fig. 4.9h). The pore structure predicted by FESEM (Fig. 4.9a-h) are in accordance with SR, which decreased significantly for

increasing concentration of CA (Fig. 4.4). Pore structure played a crucial role in diffusion of water molecules

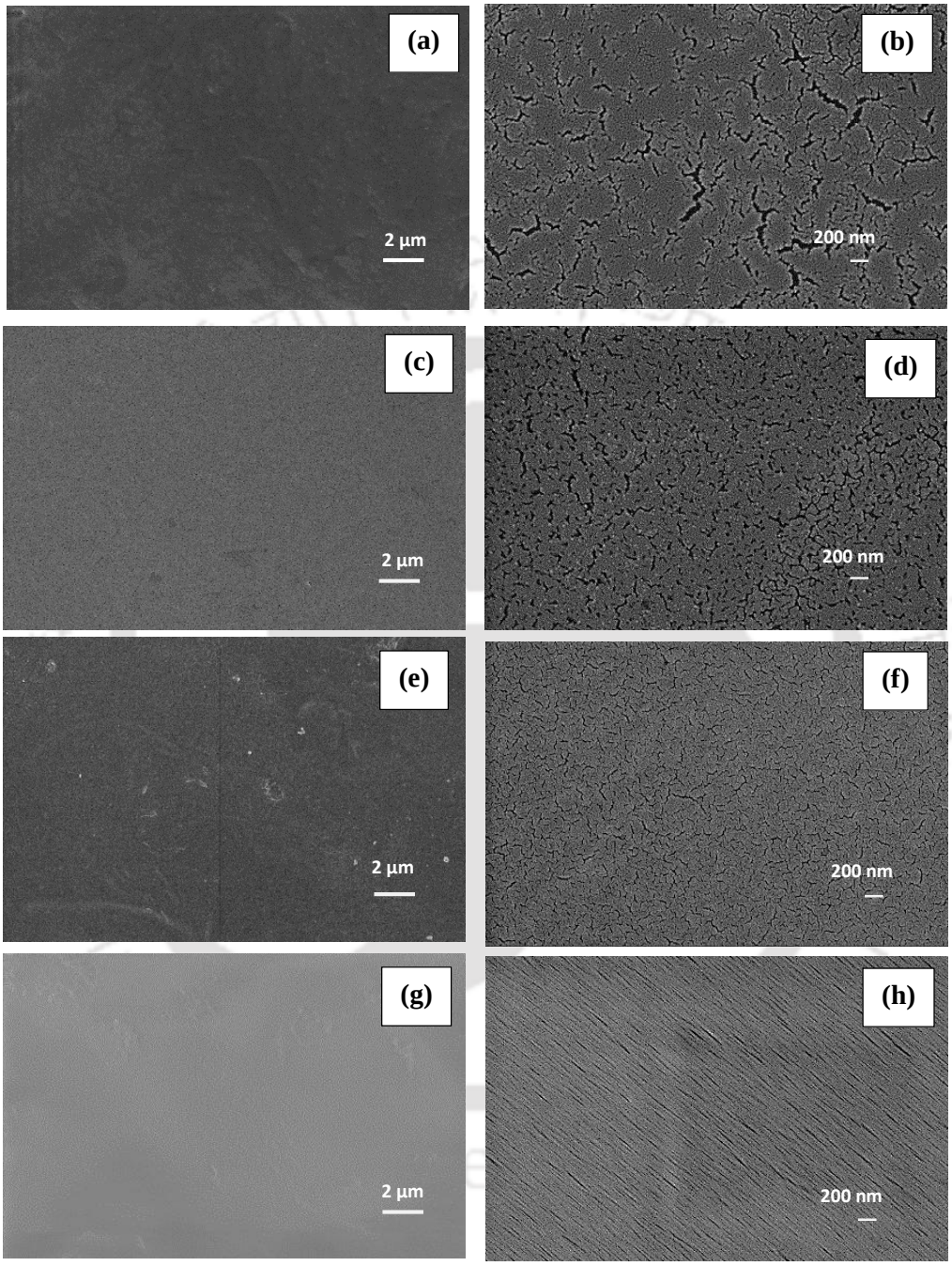

Figure 4.9. FESEM images of NaCMC-HPMC hydrogel films of (a,b) control (blend), and crosslinked with (c,d) 5% CA (e,f) 10% CA and (g,h) 20% CA at a magnification of 5000X (a,c,e and g) and 50KX (b,d,f and h).

The cryofixed swollen hydrogel film samples were also analyzed in order to identify the porous network morphology (Fig. 4.10a-c). This morphological analysis gives an idea about vital role played by concentration of CA in the network structure of the hydrogel films. The surface morphology showed different shapes of circular and elliptical pores for 5% CA swollen film (Fig. 4.10a).

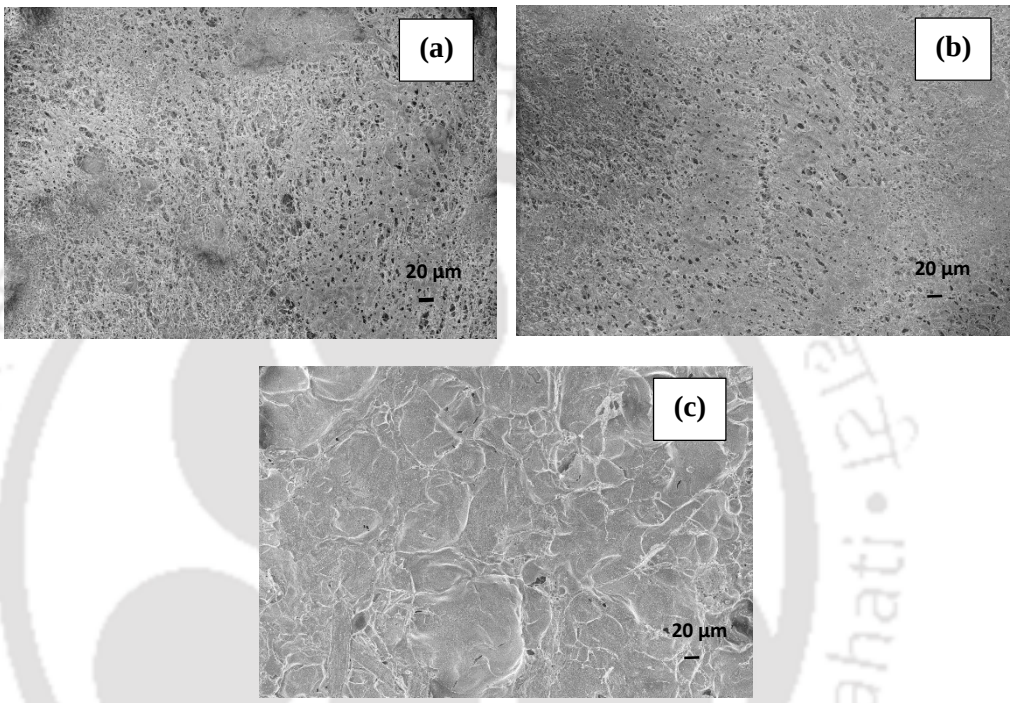

Figure 4.10. FESEM images of cryofixed NaCMC-HPMC hydrogel films crosslinked with (a) 5% CA (b) 10% CA and (c) 20% CA at 500X magnification.

Further increase in CA concentration to 10% showed the similar surface morphology of 5% CA with less pore size (Fig. 4.10b). A solid like structure without any noticeable micropores was observed for 20% CA crosslinked swollen films (Fig. 4.10c). On the other hand, nanopores were seen at higher magnifications (50 KX) suggesting that higher concentration of CA reduces the pore size (Fig. A2).

4.2.9. Pore analysis by MIP

MIP results of total pore area and average pore diameter of crosslinked hydrogel films are shown in Table 4.2. The pore distribution (%) vs. pore diameter (µm) of CA crosslinked hydrogel films is shown in Fig. A3.

Table 4.2. Mercury intrusion porosimetry (MIP) analysis of NaCMC-HPMC hydrogel films crosslinked with 5% CA, 10% CA and 20% CA.

S. No.	Sample	Total pore area (m^2/g)	Average pore diameter (4V/A, µm)
1.	NaCMC-HPMC/5% CA	53.0674 ± 2.353	0.3118 ± 0.044*
2.	NaCMC-HPMC/10% CA	61.795 ± 1.273	0.1731 ± 0.026*
3.	NaCMC-HPMC/20% CA	70.4721 ± 3.293	0.0774 ± 0.011*

*$P<0.05$ is significant difference from each other in the same column.

MIP measures the average pore diameter of surface as well as interior pores. The average pore diameter of crosslinked films significantly decreased with increase in CA concentration (Table 4.2) and the results are qualitatively matching with the morphology shown by FESEM (Fig. 4.10). However, MIP is more reliable to quantify the pores than the qualitative prediction by SEM (Kim and Chu, 2000). According to reported literature (Parwe et al., 2014), nanofiber mat with nanopores (65-102 nm) was prepared using electrospinning for better oxygen diffusion to the wound site and exudates removal. Presence of nanopores in the wound dressing material is an added advantage for preventing the invasion of pathogenic microorganism to the wound site. The prepared hydrogel films showed high total pore area and nanopores, which may facilitate the cell growth in the wound site (Table 4.2).

4.2.10. Mechanical properties of the hydrogel films

Tensile strength and percentage elongation (%) of blend films with and without CA are shown in Figs. 4.11 and 4.12. Generally, tensile strength increases and percentage elongation decreases with crosslinker concentration. On the other hand, the opposite result on tensile strength may be found with increase in plasticizer concentration. It was observed that CA played a dual role as a crosslinker and plasticizer especially in NaCMC-HPMC crosslinked with 20% CA hydrogel films. The blend films showed tensile strength and percentage elongation of 15.31 ± 1.15 MPa and 6.33 ± 0.57%, respectively (Figs. 4.11 and 4.12). The tensile strength of NaCMC-HPMC crosslinked with 5% CA was significantly higher than blend films due to crosslinking, which restricted the molecular motions resulting in an increased film strength (Figs. 4.11). The tensile strength was not significantly decreased ($P>0.05$) for 10% CA (Figs. 4.11). On the other hand, NaCMC-HPMC crosslinked with 20% CA showed significant decrease in tensile strength ($P<0.05$) (Fig. 4.11). This is due to the function of CA as the plasticizer, which reduced molecular interactions between NaCMC and HPMC, and results in decreased tensile strength. It is noted that 20% CA films showed an additional shoulder peak in the DTG curve (Fig. 4.7B(d)) due to the excess amount of CA which reduced the tensile strength significantly (Fig. 4.11). Although crosslinking degree increases with CA concentration, the number of –COOH groups, responsible for hydrophilicity also increases in the films. Hence, percentage elongation increased significantly with increase in surface hydrophilicity from 5-20% CA concentration (Fig. 4.12). Thus, crosslinking the blend films by CA increases the percentage elongation.

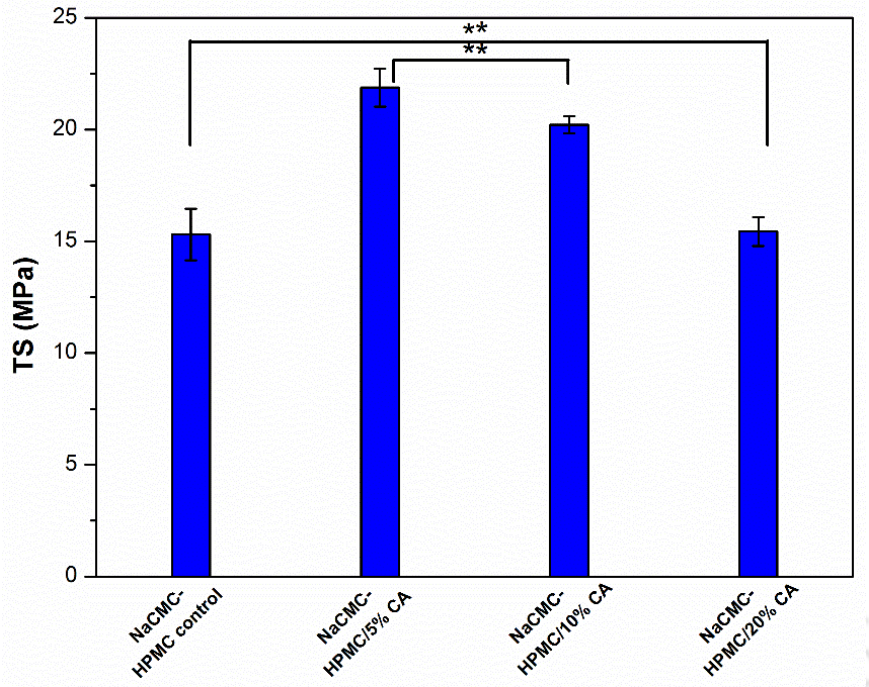

Figure 4.11. Tensile strength (TS) of NaCMC-HPMC hydrogel films of control (blend) and crosslinked with 5% CA, 10% CA and 20% CA (**P>0.05 is not significant difference between film samples).

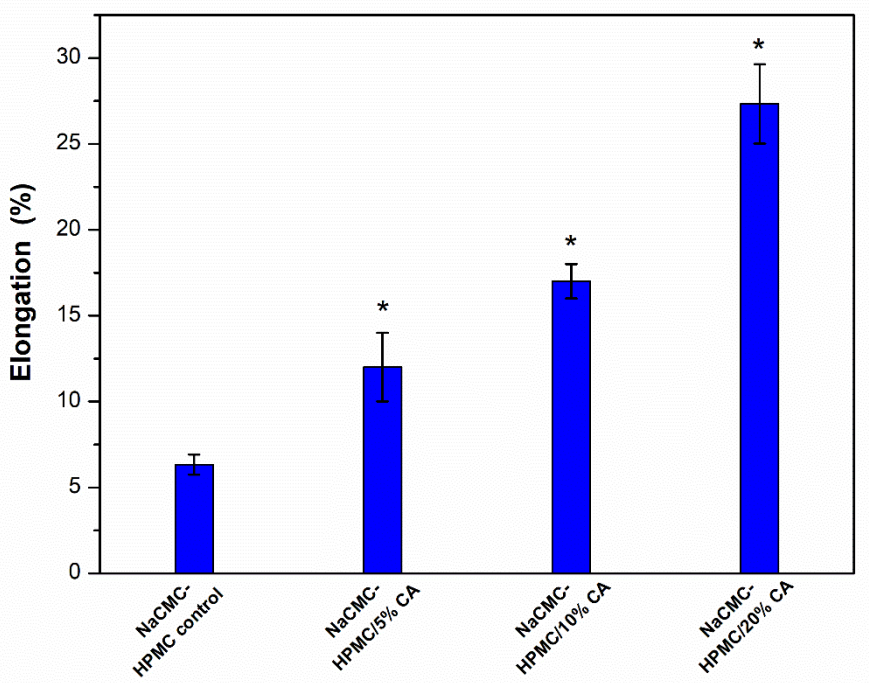

Figure 4.12. Elongation (%) of NaCMC-HPMC hydrogel films of control (blend) and crosslinked with 5% CA, 10% CA and 20% CA (*P<0.05 is significant difference with respect to control).

The same effect was observed in the CA crosslinked SP composites (starch/polyvinyl alcohol), in which increase in CA (5-30%) increased the percentage elongation and decreased the tensile strength (Shi et al., 2008).

4.2.11. Drug loading and drug release studies

4.2.11.1. Methylene blue loading and its release study

Fig. 4.13A shows the methylene blue loading efficiency (%) of crosslinked NaCMC-HPMC films in PBS, pH 7.4 at 37°C for 24 h. It was found that the addition of CA (5%, 10% and 20%) increased the methylene blue loading (Fig. 4.13A). The interaction between the hydrogel films and drug depends on the point of zero charge (pzc) of hydrogel films.

The pzc of hydrogel films is 4.98, 4.46 and 4.16 for 5% CA, 10% CA and 20% CA, respectively (Fig. 4.13B). The hydrogel film charge was negative at pH 7.4 (pH>pzc) which favored the adsorption of cation. Methylene blue shows a positive charge in PBS (pH 7.4). Hence, electrostatic interaction occurs between methylene blue and free $-COO^-$ groups of CA in the films. The methylene blue loading efficiency is greatly enhanced, which is approximately 23 times more when compared to CMC/MCM-41 nanocomposite films (Namazi et al., 2016).

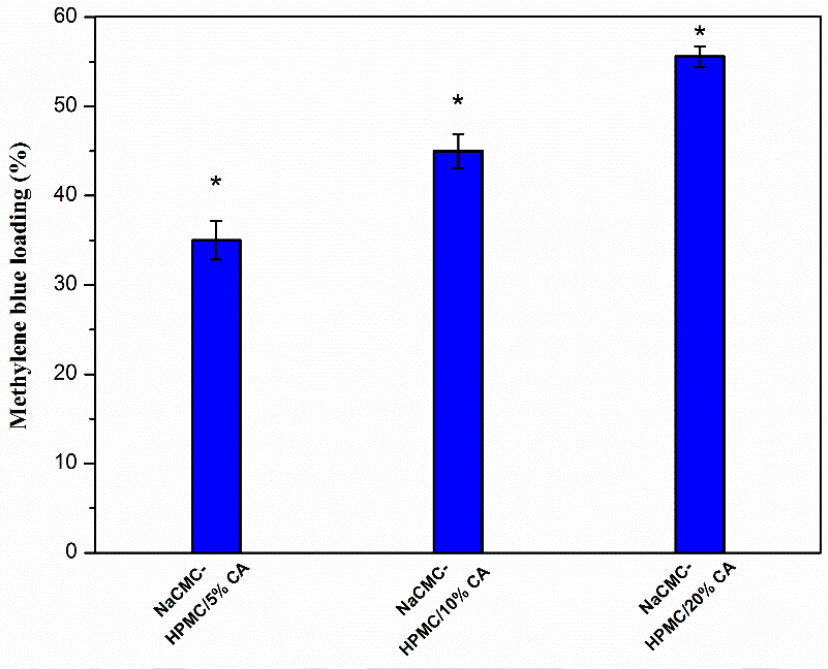

Figure 4.13A. Methylene blue loading efficiency (%) of NaCMC-HPMC hydrogel films crosslinked with 5%, 10% and 20% CA concentrations in PBS, pH 7.4 at 37°C for 24 h. (*P<0.05 is significant difference from each other).

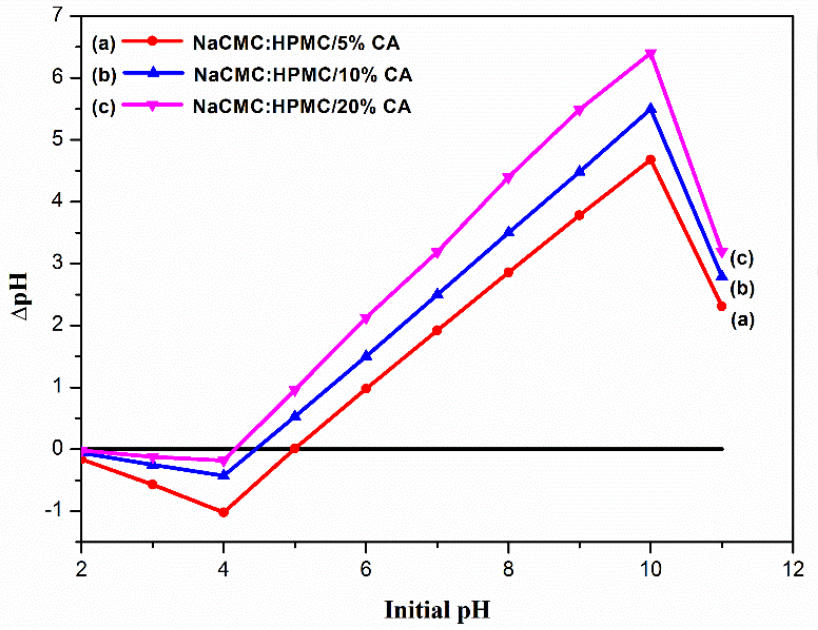

Figure 4.13B. The point of zero charge (pzc) of NaCMC-HPMC hydrogel films crosslinked with (a) 5%, (b) 10% and (c) 20% CA concentrations.

Methylene blue release profile is shown in Fig. 4.14. It was observed that the release pattern of methylene blue was significantly influenced by CA.

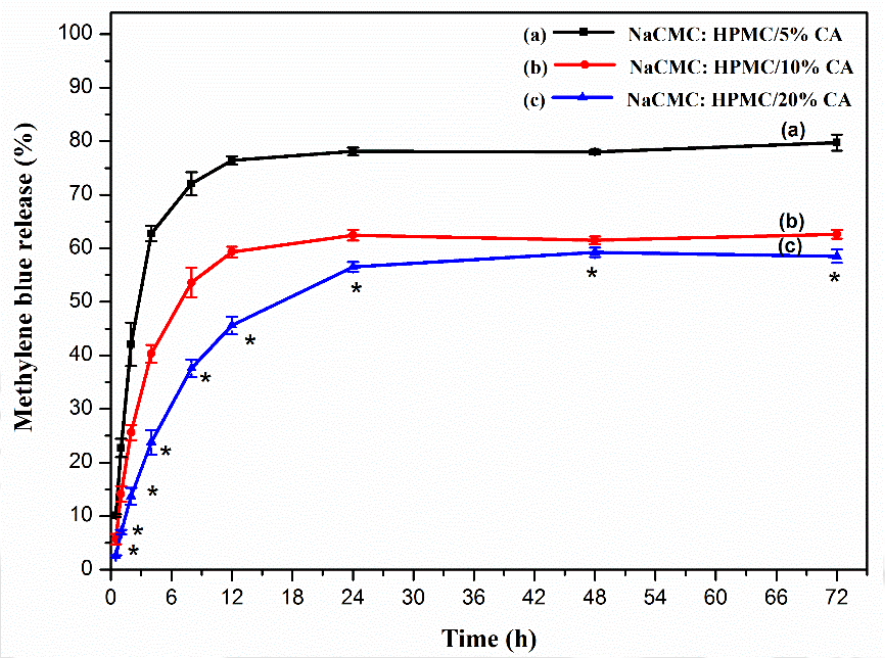

Figure 4.14. Methylene blue release (%) from NaCMC-HPMC hydrogel films crosslinked with (a) 5%, (b) 10% and (c) 20% CA concentrations in PBS, pH 7.4 at 37°C for 24 h (*P<0.05 is significant difference from 5% CA and 10% CA).

Due to less electrostatic attraction between NaCMC-HPMC/5% CA films and methylene blue, release of methylene blue was approximately 62.75 ± 1.40% within 4h. At the end of 12 h, methylene blue release reached a plateau value (Fig. 4.14a). Though the release was slow initially, 10% CA films reached a maximum release of 59.33± 0.98% after 12 h (Fig. 4.14b). Amongst all the crosslinked films, 20% CA films loaded with methylene blue showed a slow and steady release from 0.5 h to 48 h followed by a sustained release up to 72 h (Fig. 4.14c). Moreover, citric acid is a tri-

carboxylic acid which has three pKa values at pH 3.13, 4.76 and 6.40. At pH 7.4, the free –COOH groups of CA (Fig. 4.1) are fully deprotonated in NaCMC-HPMC crosslinked with 20% CA films. The slower release of drug can be attributed to increase in the number of free –COOH groups present in CA.

4.2.11.2. Tetracycline loading and its release study

Fig. 4.15 shows the tetracycline loading efficiency (%) of crosslinked NaCMC-HPMC films in PBS, pH 7.4 at 37°C for 24 h.

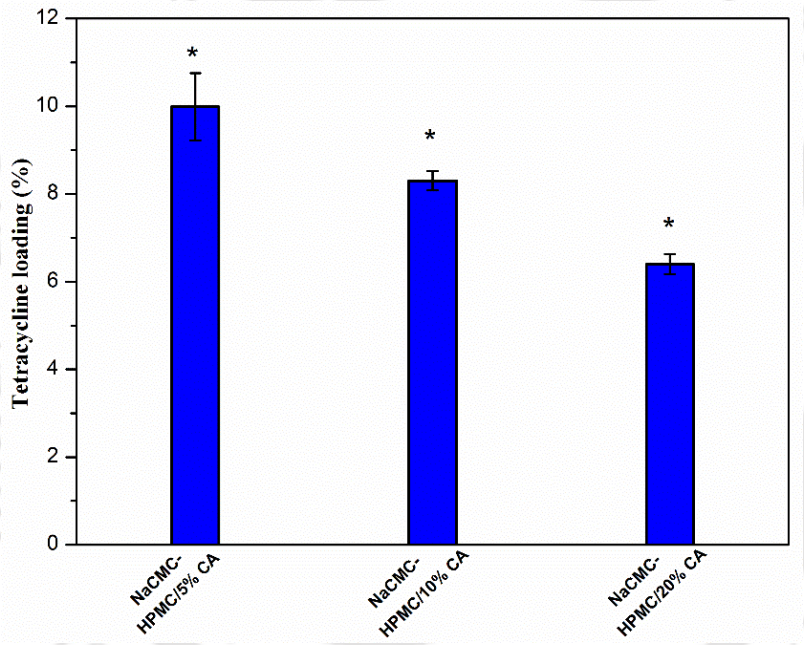

Figure 4.15. Tetracycline loading efficiency (%) of NaCMC-HPMC hydrogel films crosslinked with 5%, 10% and 20% CA concentrations in PBS, pH 7.4 at 37°C for 24 h (*P<0.05 is significant difference from each other).

Tetracycline molecule is mostly in zwitterion at pH 7.4 (Namazi et al., 2016). The tetracycline drug loading decreased with CA concentration due to repulsive force between free $–COO^-$ groups of CA (Fig. 4.1) and the drug. Tetracycline release profile

of hydrogel films is shown in Fig. 4.16. Since hydrophilicity of films increases with CA concentration, it was observed that 5% CA films release tetracycline in a slower rate up to 6 h (Fig. 4.16a).

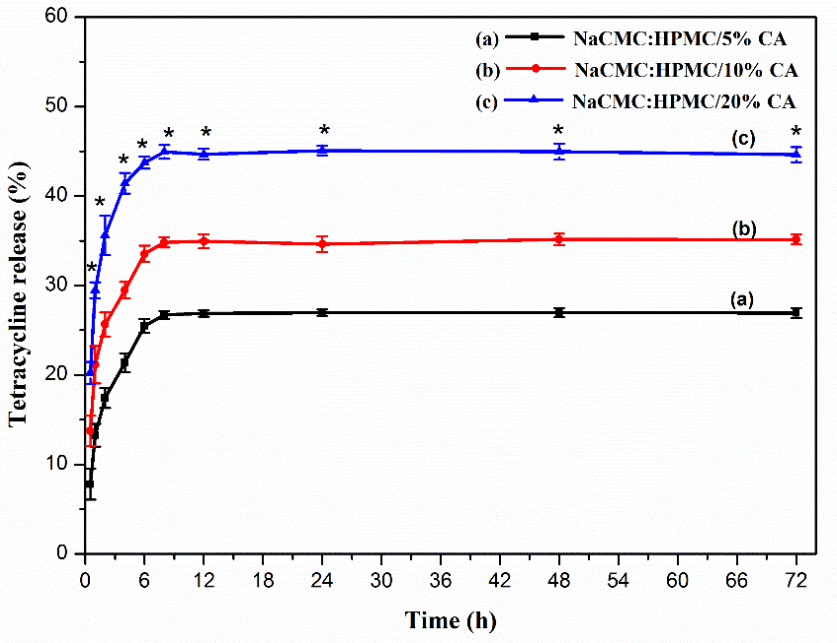

Figure 4.16. Tetracycline release (%) from NaCMC-HPMC hydrogel films crosslinked with (a) 5%, (b) 10% and (c) 20% CA concentrations in PBS, pH 7.4 at 37°C for 24 h (*P<0.05 is significant difference from 5% CA and 10% CA).

Moreover, the repulsive force between the free $–COO^-$ groups of CA and tetracycline molecules might be lesser in 5% CA films compared to 10% CA and 20% CA films (Fig. 4.16 a-c). The initial release of tetracycline for 10% CA films is slightly higher than 5% CA due to higher surface hydrophilicity and higher repulsive force between tetracycline and films containing free $–COO^-$ groups in the case of 10% CA films (Fig. 4.16b). The initial sudden release of tetracycline was observed within 1 h for 20% CA films (Fig. 4.16c). Amongst all crosslinked films, 20% CA films showed a maximum release of 45.07 ± 0.52% at the end of 6 h. As the concentration of CA increases, the

highest release of tetracycline was observed as a result of strong repulsion from increased number of free –COOH groups.

4.2.12. Antibacterial activity of hydrogel films

After three days of drug release in PBS, the antibacterial activity of methylene blue and tetracycline loaded hydrogel films against two pathogenic microorganisms such as *Staphylococcus aureus* and *Escherichia coli* was investigated (Table 4.3). If hydrogel films inhibit the bacterial growth up to three days, it is an added advantage for wound dressing materials. In the case of methylene blue loaded films, 20% CA films showed the highest zone of inhibition for *S. aureus* as well as *E. coli*. whereas tetracycline loaded films showed the highest inhibition zone for both pathogenic microbes in the case of 5% CA because of higher amount of remaining drug in the films.

Table 4.3. Inhibition zone of methylene blue and tetracycline loaded NaCMC-HPMC hydrogel films after three days of release in PBS, pH 7.4 at 37°C.

S.No.	**Sample**	**NaCMC-HPMC/5% CA** (mm)	**NaCMC-HPMC/10% CA** (mm)	**NaCMC-HPMC/20% CA** (mm)
1.	Methylene blue loaded films against *E.coli*	11.5 ± 0.5	13.5 ± 0.5	18.83 ± 0.28*
2.	Methylene blue loaded films against *S. aureus*	7.83 ± 0.28	10.83 ± 0.28	16.66 ± 0.57*
3.	Tetracycline loaded films against *E.coli*	23.33 ± 0.76*	15 ± 0.5	12.33 ± 1.15
4.	Tetracycline loaded films against *S. aureus*	19.83 ± 0.28*	12.5 ± 0.5	10.66 ± 0.57

*$P<0.05$ is significant difference with others in the same row.

4.3. Closure

In this chapter, the effect of CA on NaCMC-HPMC hydrogel films is discussed. The effect of CA on SR, contact angle of water (surface hydrophilicity), tensile strength, elongation (%) of hydrogel films is discussed. Further, the effect of CA on average pore diameter and point of zero charge (pzc) of hydrogel films is correlated along with loading of cationic drug (methylene blue) and anionic drug (tetracycline). Finally, the effect of CA on releasing the drugs and antibacterial activity of the films is discussed. In the next chapter (Chapter 5), the effect of CA on ZnO incorporated NaCMC-HPMC hydrogel films is discussed.

Chapter 5

Formation and characterization of ZnO complexes in nanocomposite hydrogel films for potential wound healing applications

The objective of this chapter is to study the effect of citric acid (CA) on sodium carboxymethylcellulose (NaCMC), hydroxypropylmethylcellulose (HPMC) and ZnO nanoparticles (NPs) based hydrogel films for their physico-chemical, thermal, mechanical and antibacterial properties as well as their zinc releasing property and biocompatibility.

5.1. Introduction

Hydrogels are three-dimensional networks, designed to create and maintain a moist environment by mimicking extracellular matrix of a skin. Besides, they absorb large amounts of water or biological fluids thereby preventing maceration while permitting the transport of nutrients, oxygen and metabolic products. These characteristics make hydrogels an excellent candidate for various biomedical applications, especially as a component in wound healing materials (Carrillo-Rodriguez et al., 2018; Gao et al., 2016; Lee et al., 2019). Among several polymers of cellulose derivatives, sodium carboxymethylcellulose (NaCMC) and hydroxypropylmethylcellulose (HPMC) have been widely investigated to fabricate hydrogels for wound healing applications (Ding et al., 2015; Ghorpade et al., 2016; Raucci et al., 2015; Zhong et al., 2019). Both polymers exhibit a higher swelling rate in saline solutions and distilled water in comparison to other cellulose ethers (Bao et al., 2012).

NaCMC is water-soluble, non-toxic, biodegradable, pH sensitive and an inexpensive cellulose derivative (Charpentier et al., 1997; Ullah et al., 2015). Due to the presence of anionic functional groups (–OH, – COO^-), it can be readily crosslinked either by a

physical or by a chemical method to produce hydrogels. However, NaCMC based hydrogels exhibit poor mechanical strength and strong electronic repulsion (in water and saline solutions) limiting their role in wound healing and in various biomedical applications that demand the controlled release of drug (Mandal et al., 2016; Qiu et al., 2007; Shen et al., 2015). In order to overcome above mentioned disadvantages, NaCMC was crosslinked with different polymers such as HEC, PVP and PVA by different crosslinking methods (El Salmawi, 2007; Raafat et al., 2012; Raucci et al., 2015; Wang et al., 2007). However, their applications may be limited as wound healing materials due to lack of antibacterial activity. Blending of HPMC with NaCMC may create a new structural material for wound healing applications. HPMC is a non-ionic, non-toxic, water-soluble, tasteless, odorless, white colored ether cellulose derivative. The characteristics of film forming ability, presence of hydrophilic and hydrophobic groups, stability at low pH, light and heat resistance make HPMC as a suitable material for preparing drug delivery matrix and its usage in controlled release of drug (Kondaveeti et al., 2017; Marani et al., 2015).

There has been much attention in the preparation of polymeric-inorganic nanocomposites for biomedical applications (Hashem et al., 2013; Zare-Akbari et al., 2016). The nanocomposite hydrogels exhibit improved properties compared to composites. Among inorganic materials, zinc oxide (ZnO) has attracted significant interest due to its thermal stability, antimicrobial action, less toxicity and UV-blocking properties (Zare-Akbari et al., 2016). ZnO demonstrated its antimicrobial against *Staphylococcus aureus*, *Escherichia coli*, *Pseudomonas aeruginosa*, *Bacillus subtilis*, *Bacillus megaterium*, *Sarcina lutea*, *Klebsiella pneumonia*, *Candida albicans*, *Pseudomonas vulgaris* and *Aspergillus niger* (Ahmed et al., 2019; Carrillo-Rodriguez *et al*., 2018; Shafiq et al., 2014). Furthermore, Zn^{2+} is an essential element for cell

proliferation. It has been reported that the concentration of Zn^{2+} is higher in wound tissue than healthy tissue. The deficiency of Zn^{2+} delays the process of wound healing (Li et al., 2017). The presence of ZnO nanoparticle enhances fibroblast attachment, induces keratinocyte migration, improves re-epithelialization. In addition, ZnO nanoparticles possess anti-inflammatory and antiseptic properties (Augustine et al., 2014; Mihai et al., 2019; Vijayakumar et al., 2019). However, the safe use of ZnO nanoparticle solely depends on its size, type of cells and concentration. Furthermore, the observed in vitro cytotoxic effects for ZnO nanoparticles occur at least one order of less magnitude when the nanoparticles exposed to human skin under realistic conditions (Mohammed et al., 2019).

Wound healing is a complex process, involving a series of distinct phases, which can be accelerated by stimulating angiogenesis, supplying adequate nutrient elements and inhibiting bacterial growth in the wound (Li et al., 2017). It is well known that the dispersion and stabilization of ZnO nanoparticle play a vital role in all of these wound healing phases with reduced cytotoxicity. Despite that high concentration of ZnO nanoparticle leads to mitochondrial dysfunction, production of reactive oxygen species, inhibition of the expression of glutathione peroxidase and superoxide dismutase genes in human cells (Hamdan et al., 2017; Mihai et al., 2019). In order to restrain these problems, various approaches such as Au@ZnO core-shell (Khan et al., 2019), silica coated ZnO nanorods (Sotiriou et al., 2014), iron doping into ZnO nanoparticle (George et al., 2009) and modification of surface and chemical structure of ZnO nanoparticle using organic solvents (Punnoose et al., 2014) have been proposed. In this study, an attempt has been made to form a complex consisting of ZnO and citric acid in the presence of cellulose ether to stabilize ZnO nanoparticles and to regulate sustained release of zinc. The stabilization of ZnO by citric acid present in the colloidal solution

of NaCMC-HPMC has not been investigated for wound healing applications. Accordingly, the present chapter aims to develop novel hydrogel films with citric acid acting as a crosslinker and also as a stabilizer for ZnO. Also, the effect of citric acid on physical, thermal and mechanical properties of the hydrogel films is studied in detail.

5.2. Results and discussion

5.2.1. Crosslinking mechanism of citric acid (CA) in the presence of ZnO

The CA crosslinking mechanism between two cellulose ether derivatives such as NaCMC and hydroxyethylcellulose (HEC) was proposed by Demitri et al. (2008). Briefly, upon heating a cyclic anhydride intermediate forms after condensation reaction between two carboxyl groups of CA (Fig. 5.1). Then, esterification reaction occurs between the first cyclic anhydride and cellulose hydroxyl group resulting in exposing a new carboxyl group in CA. After the first esterification step, the second cyclic anhydride emerges which involves in another esterification. Finally, a CA moiety creates two ester bonds with hydroxyl groups of cellulose. The possible CA crosslinked molecular structures of NaCMC and HPMC without ZnO were given in section 4.2.1 (Fig. 4.2). In the present study, the possible CA crosslinking mechanism in the presence of ZnO mechanism between NaCMC and HPMC is shown in Fig. 5.1. According to a Swanzy (2017), mixing of different molar ratios of zinc oxide and citric acid forms a complex particulate molecule. Thus, the addition of ZnO may impede the CA crosslinking mechanism between celluloses. The α-hydroxy acid group in CA plays the main role in the formation of cyclic anhydride. Attachment of ZnO with α-hydroxy acid group inhibits the CA crosslinking completely. However, the binding of ZnO with either one of two carboxyl groups of CA does not prevent the formation of a cyclic anhydride and at least one esterification step occurs as shown in Fig. 5.1.

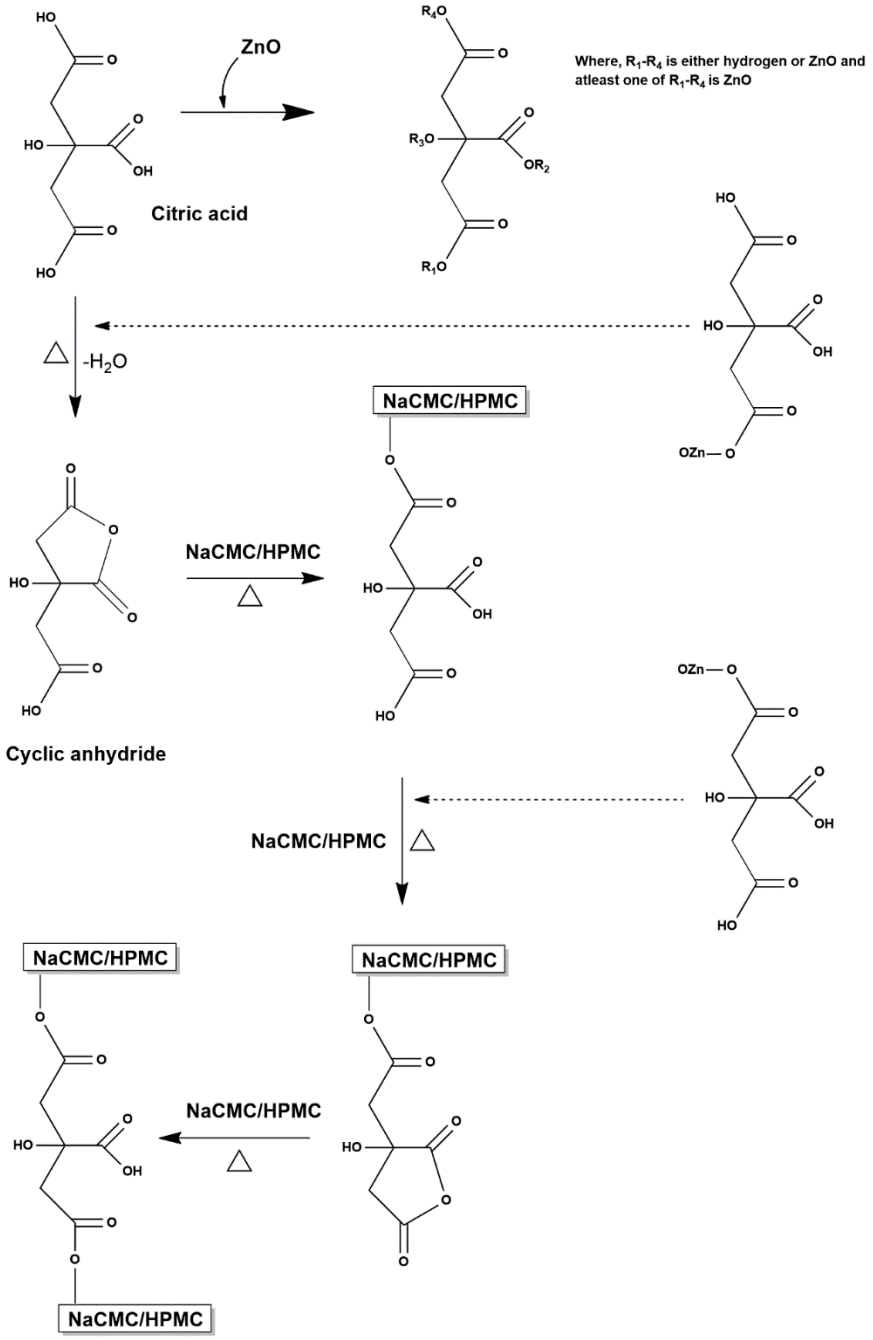

Figure 5.1. Possible sequential citric acid crosslinking mecahnism with NaCMC and HPMC in the presence of ZnO.

5.2.2. Effect of CA on crystallinity of hydrogel films

XRD pattern of synthesized ZnO NPs, NaCMC-HPMC-ZnO control films and various concentrations of CA (5-20%) crosslinked NaCMC-HPMC in the presence of ZnO is

shown in Fig. 5.2(a-e). Neat polymers of NaCMC and HPMC exhibited main diffraction peaks at 2θ = 22.1° and 19.98° (Fig. 4.5a,b).

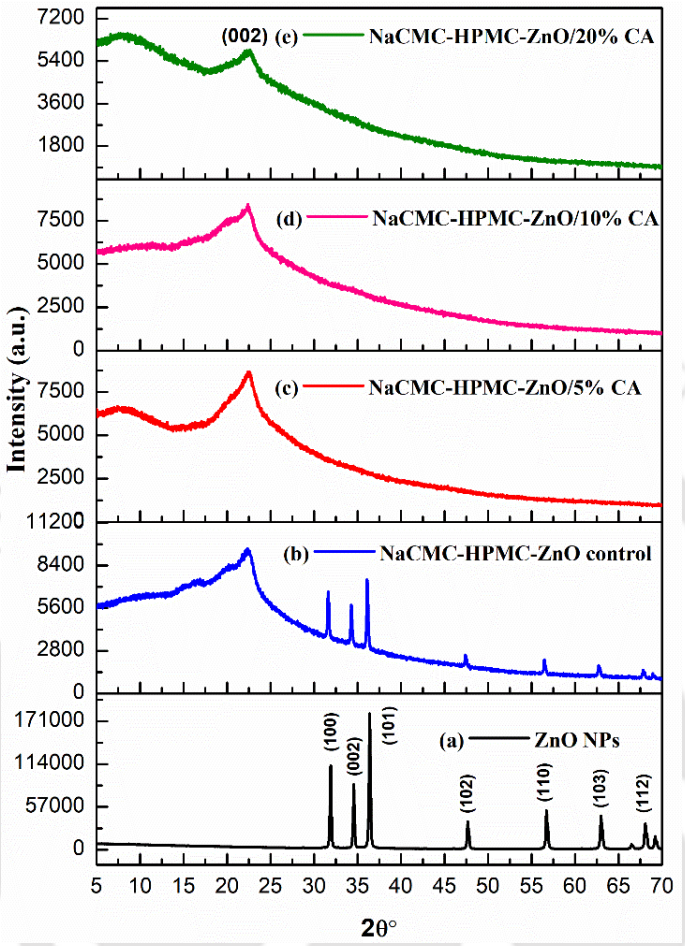

Figure 5.2. XRD pattern of (a) ZnO NPs and NaCMC-HPMC-ZnO hydrogel films of (b) control, and crosslinked with (c) 5% CA (d) 10% CA and (e) 20% CA.

It was observed that both polymers have appreciable crystallinity. Fig. 5.2(a) shows the crystalline phase of ZnO at 2θ = 31.74°, 34.44°, 36.27°, 47.69°, 56.72°, 62.80° and 68.7°. The diffraction pattern of synthesized ZnO has been indexed with hexagonal wurtzite structure (JCPDS #80-0075) (Dharmalingam et al., 2019). The NaCMC-HPMC-ZnO control films showed mixed characteristics of polymers and ZnO (Fig. 5.2b). The control films showed a broad peak at 2θ = 22.1° and all the crystalline phases of ZnO were present. However, the diffraction peak of HPMC was absent due to

destruction of crystallinity of HPMC at 90°C in film preparation. Thus, the control films showed mainly NaCMC crystallinity. All the crystalline phases of ZnO was disappeared in all CA incorporated NaCMC-HPMC hydrogel films (Fig. 5.2c-e). This may be due to CA complex formation with ZnO NPs (Bertoli et al., 2015; Farbun et al., 2007). The crystalline plane (0 0 2) was gradually widened with an increase in CA concentrations from 5% to 20% compared to control films. It has been reported that an increase in crosslinking degree broadens the peak due to decreased polymer chain mobility (crystallite size) or internal strain (Nielsen, 1969; Roberts and Mandelkern, 1960). A decrease in peak height ($2\theta = 22.1°$) was also observed for increase in CA concentrations. The decrease in peak height is in accordance with previous literatures (Dilaver and Yurdakoc, 2016; Shi et al., 2008).

5.2.3. FTIR and Raman spectra of hydrogel films

FTIR spectra of ZnO NPs, NaCMC-HPMC-ZnO control films and CA crosslinked hydrogel films are shown in Fig. 5.3A(a-e). A broad band at 412 cm^{-1} is attributed to Zn-O stretching vibration (Fig. 5.3A(a)) (Kannan and Saraswathi, 2017; Lakshmi Prasanna and Rajagopalan, 2016). All the characteristic vibrational modes are present for NaCMC, HPMC and ZnO in the control films (Fig. 5.3A(b)). The peaks at 1592 cm^{-1}, 1418 cm^{-1} and 1323 cm^{-1} correspond to COO^- stretching modes, $–CH_2$ scissoring and –OH bending modes in NaCMC, respectively. The presence of broad band from 1200 cm^{-1} to 1000 cm^{-1} is due to sugar ring vibrations. A small broad peak at 893 cm^{-1} is assigned to C–O–C stretching vibrations in NaCMC. The peaks at 1373 cm^{-1} and 1455 cm^{-1} are attributed to symmetric and asymmetric bending modes of $–OCH_3$ group in HPMC, respectively. A sharp peak at 1053 cm^{-1} is due to C-O-C stretching mode in HPMC (Ding et al., 2015; Gorgieva and Kokol, 2011; Qiu et al., 2007; Raucci et al.,

2015; Wang et al., 2007). A small shift in wavenumber of ZnO was observed in the control films due to interfacial interaction of ZnO between the polymers (Fig. 5.3A(b)).

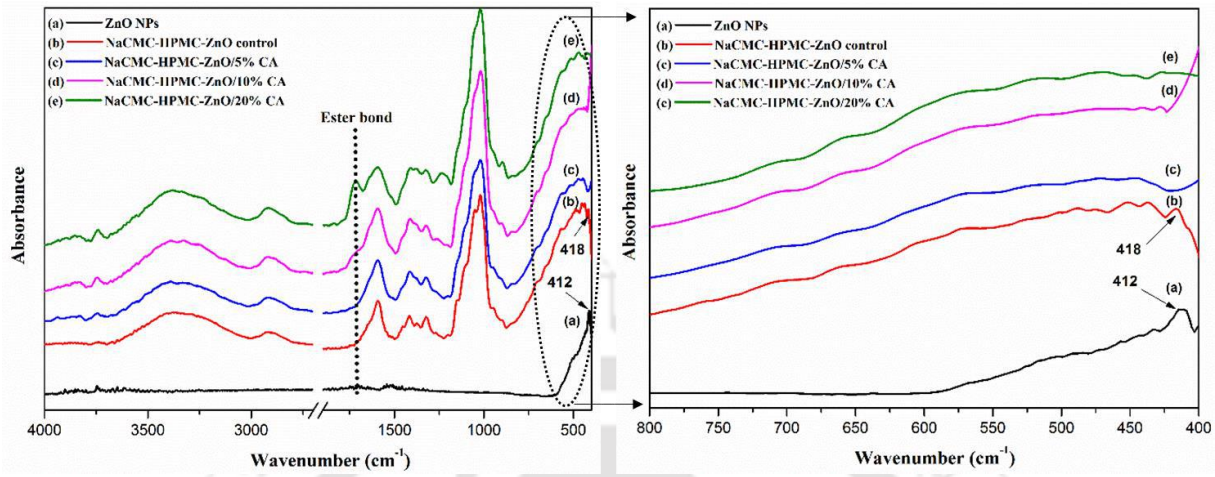

Figure 5.3A. FTIR pattern of (a) ZnO NPs and NaCMC-HPMC-ZnO hydrogel films of (b) control, and crosslinked with (c) 5% CA (d) 10% CA and (e) 20% CA.

However, different concentrations of CA added films did not show any peak for ZnO (Fig. 5.3A(c-e)). It may be attributed to complex formation between CA and ZnO resulting in disappearance of the ZnO characteristic peak. On the other hand, increase in CA increases the intensity of ester bond due to a high degree of crosslinking. The 10% and 20% CA crosslinked films exhibit ester bond formation at around 1720-1750 cm^{-1} while 5% CA films did not show noticeable ester bond due to poor crosslinking (Fig. 5.3A(c-e)). The increase in ester bond intensity with increase in crosslinker concentrations is in accordance with previous studies (Gorgieva and Kokol, 2011; Shi et al., 2008).

In order to investigate the effect of CA on ZnO NPs, micro-Raman spectroscopy was used for ZnO NPs, NaCMC-HPMC-ZnO control films and CA crosslinked films. It has been reported in several literatures that wurtzite ZnO has eight sets of individual optical

phonon modes according to group theory (Filippov et al., 2013; Handore et al., 2014; Sharma et al., 2011).

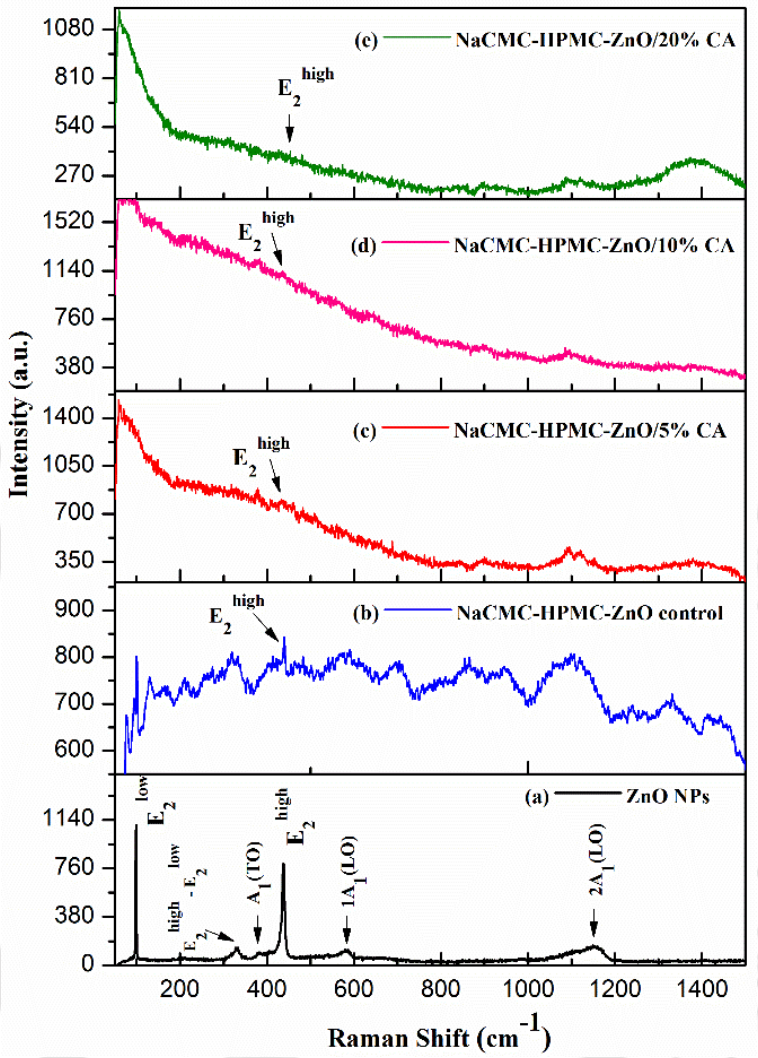

Figure 5.3B. Raman spectra of (a) ZnO NPs and NaCMC-HPMC-ZnO hydrogel films of (b) control, and crosslinked with (c) 5% CA (d) 10% CA and (e) 20% CA.

The peaks appear at 98 cm^{-1}, 331 cm^{-1}, 381 cm^{-1}, 437 cm^{-1}, 581 cm^{-1} and 1151 cm^{-1} is corresponded to E_2 (low), E_2 (high-low), A_1 (LO), E_2 (high), $1A_1$ (LO) and $2A_1$ (LO), respectively (Fig. 5.3B(a)). The control films showed the main characteristic peak of wurtzite ZnO at 437 cm^{-1} (E_2^{high}) but with reduced intensity, describes well dispersion of ZnO NPs in the polymeric films (Fig. 5.3B(b)). When CA concentration increases

from 5% to 20%, peak shifts (E_2^{high}) of few cm^{-1} and peak broadening were observed (Fig. 5.3B(c-e)). It may be either due to phonon confinement or phonon localization by surface impurities (Koutu et al., 2016). Besides, the addition of CA affected the change in polarizability of wurtzite ZnO by forming the complex. It is concluded from FTIR and micro-Raman studies that CA forms complex with ZnO in the presence of NaCMC and HPMC polymers. The conclusion from FTIR and micro-Raman studies is in well agreement with XRD studies (Fig. 5.2c-e).

5.2.4. Swelling of hydrogel films

The purpose of hydrogel films in wound dressing is to fasten the rate of healing by efficiently absorbing the wound exudates and thus preventing the wound from drying and bacterial infection (Goh et al., 2013). Therefore, the SR of the prepared hydrogel films was investigated for different concentrations of CA crosslinked NaCMC-HPMC-ZnO films as shown in Fig. 5.4. It is clear that increase in CA concentrations decreases the SR of NaCMC-HPMC-ZnO films. Because SR is inversely proportional to crosslinking density. According to FTIR results (Fig. 5.3A), the degree of crosslinking increases with increase in CA, which is in accordance with SR results. The NaCMC-HPMC-ZnO control films were completely dissolved at the end of 24 h due to lack of crosslinker. The SR of NaCMC-HPMC-ZnO/5% CA films showed approximately 2000% and finally became a gel. The SR of NaCMC-HPMC-ZnO/5% CA films was significantly higher than NaCMC-HPMC/5% CA (without ZnO) (Fig. 4.4). It is due to the presence of ZnO which forms a complex molecule (Fig. 5.1) with added CA and thus inhibiting the crosslinking mechanisms resulting in poor crosslinking density. However, SR was drastically decreased because of the higher amount of crosslinking density at higher CA concentrations (10% and 20%). It reveals that unreacted CA molecules with ZnO may participate in crosslinking at higher CA concentrations and

thereby increases crosslinking density. The similar observation of the effect of CA on the SR was found by previous studies (Namazi et al., 2016; Shi et al., 2008).

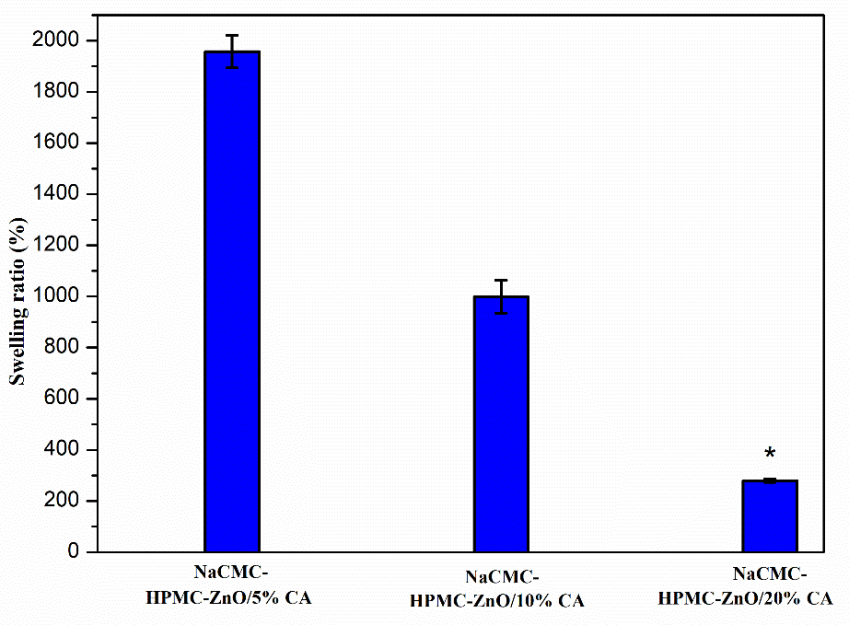

Figure 5.4. Swelling ratio (SR) (%) of NaCMC-HPMC-ZnO hydrogel films crosslinked with 5%, 10% and 20% CA concentrations (*P<0.05 is significant difference from 5% CA and 10% CA).

5.2.5. Thermal and mechanical properties of hydrogel films

TGA and DTG analysis of prepared ZnO NPs, control films and CA crosslinked films are shown in Fig. 5.5A(a-e). One-step weight loss was observed for ZnO NPs at 895°C under N_2 flow (Fig. 5.5A(a)) (Cao et al., 2014). TGA and DTG analysis for NaCMC, HPMC and CA are shown in Fig. 4.7A. The control films and CA crosslinked films exhibited a three-step weight losses from room temperature to 1000°C as follows: (i) removal of moisture up to 130°C, (ii) decomposition of polymers from 250°C to 500°C and (iii) decomposition of nanoparticles or CA complex nanoparticles from 670°C to 900°C (Fig. 5.5 A(b-e)). The control films showed mixed decomposition characteristics of polymers and ZnO NPs.

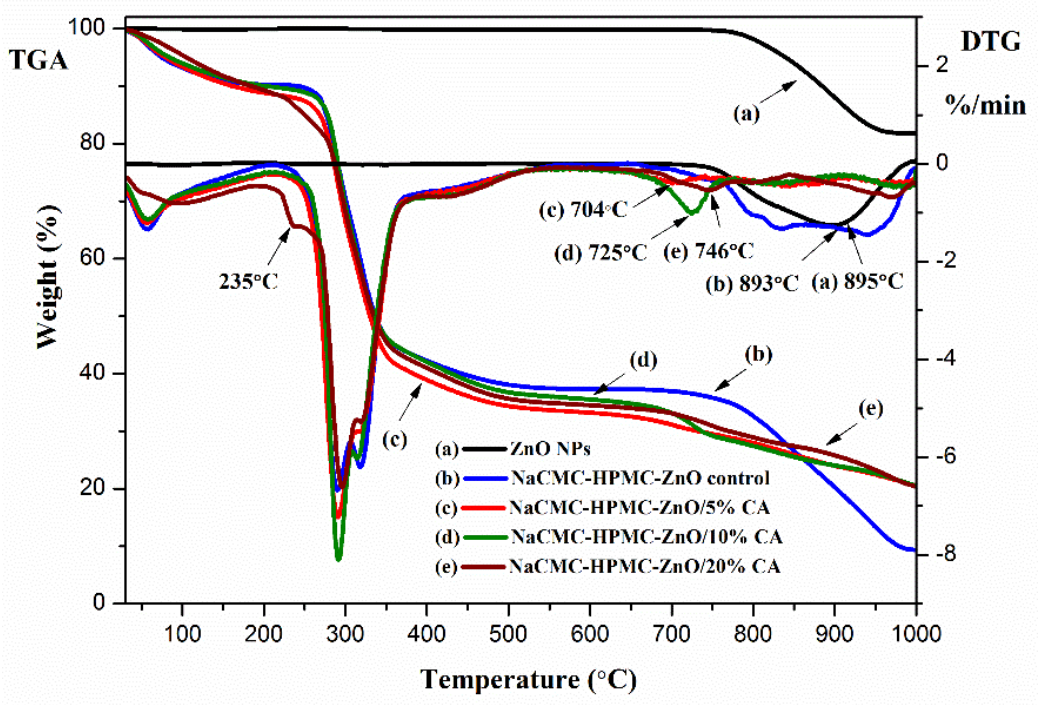

Figure 5.5A. TGA and DTG analysis of (a) ZnO NPs and NaCMC-HPMC-ZnO hydrogel films of (b) control, and crosslinked with (c) 5% CA (d) 10% CA and (e) 20% CA.

The decomposition temperature of ZnO NPs in the control films did not shift significantly (Fig. 5.5A(b)). However, NaCMC-HPMC-ZnO/5% CA films showed a drastic shift in decomposition temperature of ZnO to lower temperature at 704°C (Fig. 5.5A(c)). It can be attributed to the formation of ZnO complex with CA and thus reducing the decomposition temperature of ZnO. Also, increase in CA concentrations increased the decomposition temperature of the formed CA complex nanoparticles compared to 5% CA films (Fig. 5.5A(d,e)). All CA crosslinked films exhibited higher final decomposition temperature of polymers than control films. It reveals that increase in crosslinking density gradually increases the final decomposition temperature of NaCMC-HPMC polymers. A shoulder peak at 235°C was observed for NaCMC-HPMC-ZnO/20% CA due to the residual (unreacted) CA (Fig. 5.5A(e)).

Mechanical properties of prepared hydrogel films are shown in Fig. 5.5B. The control films showed tensile strength and elongation (%) of 19.27 ± 0.41 MPa and 21.33 ± 2.30%, respectively.

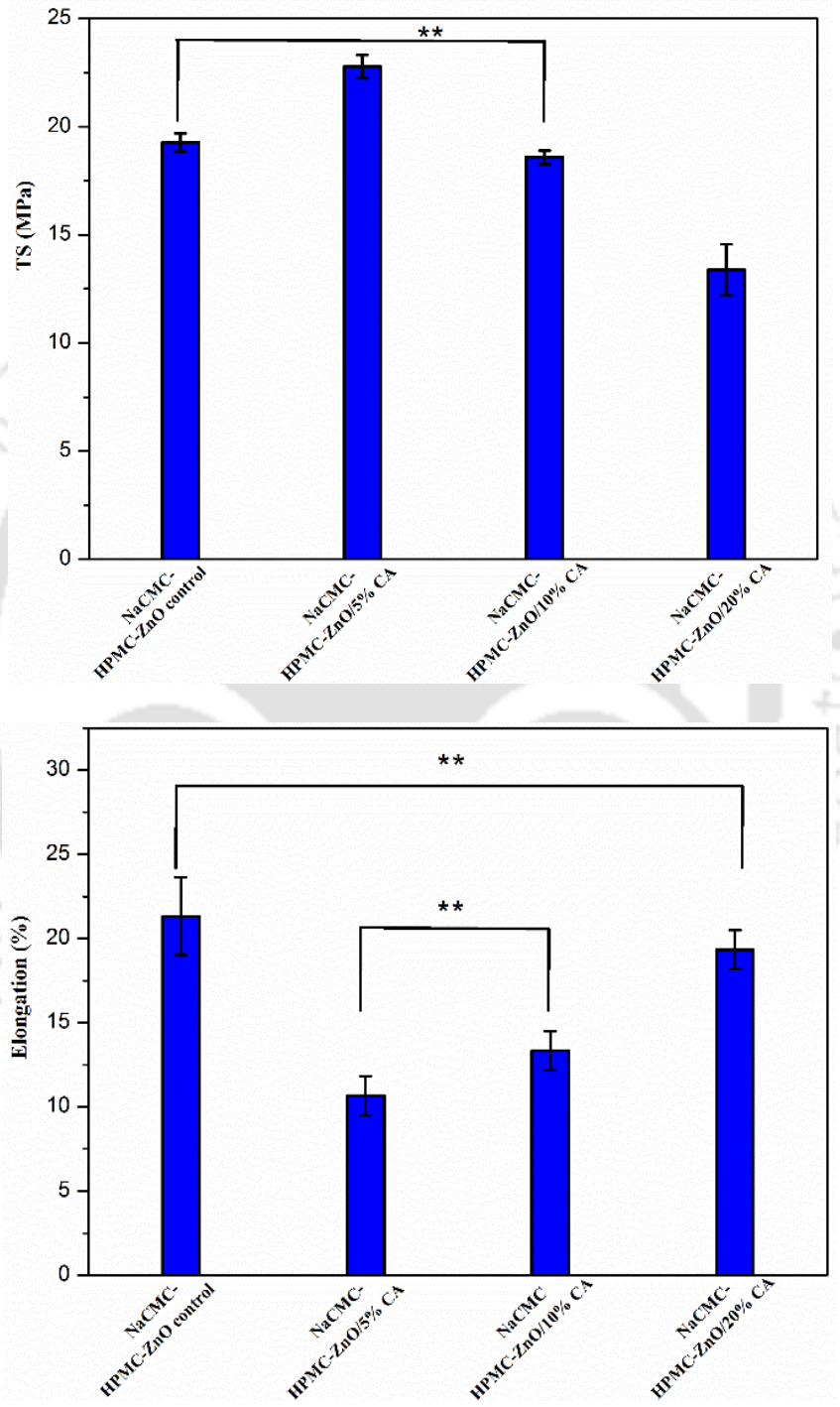

Figure 5.5B. Tensile strength (TS) and elongation (%) of NaCMC-HPMC-ZnO hydrogel films (**P>0.05 is not a significant difference between film samples).

It can be observed that increase in CA concentrations decreases tensile strength and increases elongation (%). It is in accordance with XRD results (Fig. 5.2) that the crystalline nature of the films decreases with respect to CA concentrations. According to TGA results (Fig. 5.5A(e)), the presence of significant residual CA in NaCMC-HPMC-ZnO/20% CA films reduced the molecular interactions and increased the polymer chain flexibility and thereby reduced the tensile strength. It is noted that the elongation (%) of NaCMC-HPMC-ZnO/20% CA is significantly higher than NaCMC-HPMC-ZnO/5% CA and NaCMC-HPMC-ZnO/10% CA due to the residual CA acted as a plasticizing agent. Shi et al. (2008) found the same effect of CA on starch/polyvinyl alcohol composite films.

5.2.6. Morphology study by FESEM and FETEM analysis

The FESEM and FETEM images of prepared ZnO NPs, NaCMC-HPMC-ZnO control and CA crosslinked films are shown in Fig. 5.6A(a-e) and Fig. 5.6B(a'-e'), respectively. In order to observe the effect of CA on ZnO NPs, the selective area electron diffraction (SAED) pattern is also shown in Fig. 5.6C(a"-e") for film samples mentioned above. The prepared ZnO NPs are mixtures of spherical and hexagonal with a diameter of 60-150 nm (Figs. 6A, B (a, a')). The SAED pattern of ZnO NPs shows that the prepared nanoparticles are highly crystalline (Fig. 5.6C(a")). All the film samples were magnified at 50 KX to observe the nanoparticles on the films' surface by FESEM. It was noted that the agglomeration of ZnO NPs is present in the NaCMC-HPMC-ZnO control films (Fig. 5.6A(b)). The extract of control film also showed the agglomeration of ZnO by FETEM (Fig. 5.6B(b')). Due to the presence of the polymers, the SAED pattern shows bright spots with a diffusive ring for NaCMC-HPMC-ZnO control ((Fig. 5.6C(b")). Increase in CA concentrations from 5% to 20%, the number of particles were increased as well as agglomerations due to CA complex with ZnO NPs (Fig. 5.6A(c-

e)). The extract of different concentrations of CA added films were also revealed the same results as shown in FESEM (Fig. A4) and FETEM (Fig. 6B(c'-e')) analysis. All the extracted nanoparticles from CA crosslinked hydrogel films exhibited only diffusive rings in SAED confirming their amorphous nature (Fig. 5.6C(c"-e")). The SAED results of ZnO NPs, control films and CA crosslinked films are in accordance with XRD results (Fig. 5.2(a-e)).

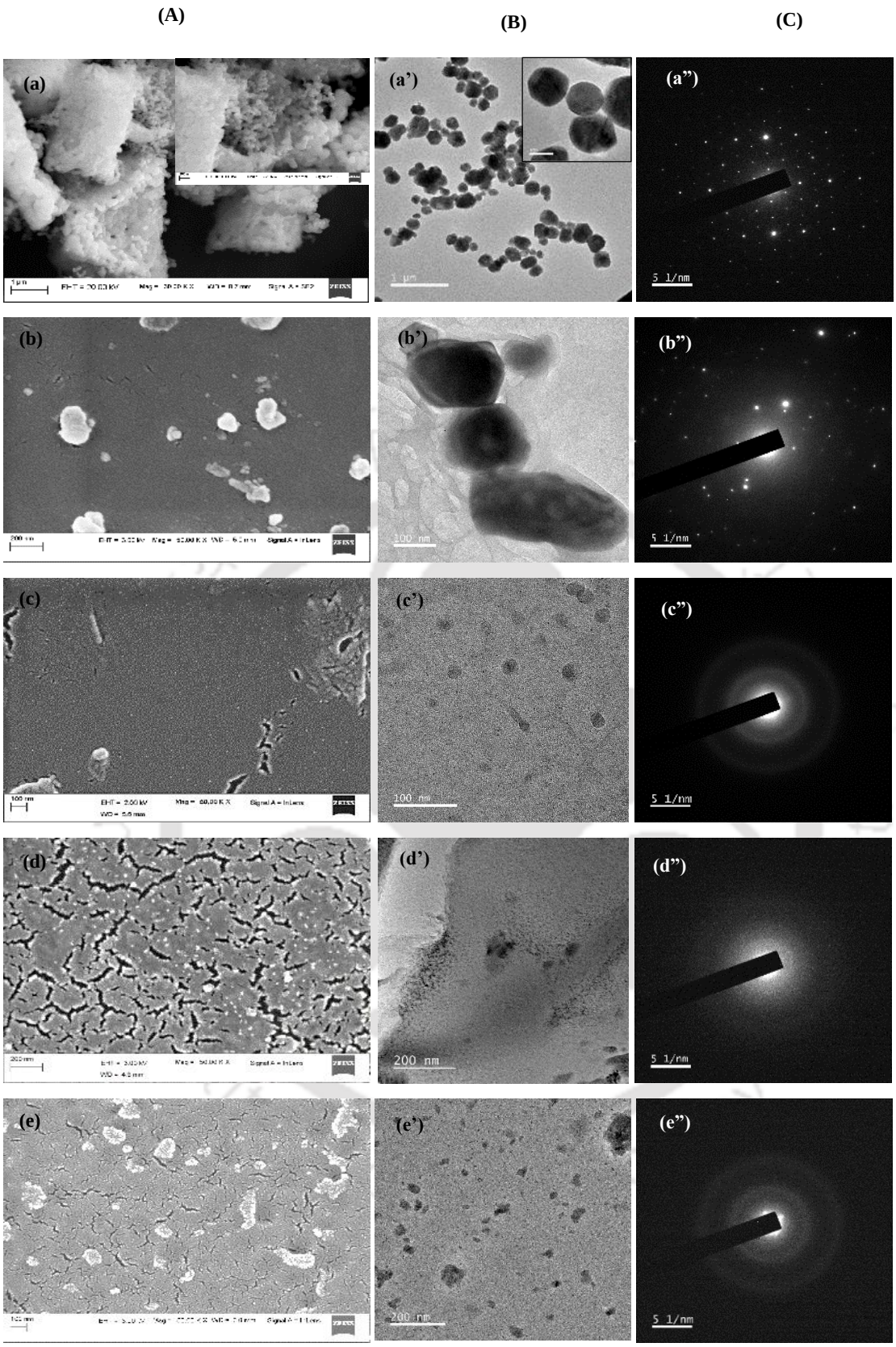

Figure 5.6(A-C). (A) FESEM images, (B) FETEM images and (C) SAED of (a, a', a") ZnO NPs (b, b", b") NaCMC-HPMC-ZnO control, and crosslinked with (c, c', c") 5% CA (d, d', d") 10% CA and (e, e', e") 20% CA at a magnification of 50KX (a-e).

Moreover, to observe the CA effect on ZnO NPs, different weight ratios (1:1, 1:2, 1:4 and 1:8) of ZnO NPs and citric acid were prepared without polymers. The morphology and SAED pattern of those samples are shown in Fig. A5(A, B). The particle size of ZnO complex increases with increase in CA (Fig. A5A(a-d)) and all weight ratios exhibited amorphous nature (Fig. A5B(b'-d')) in SAED except 1:1 ratio (Fig. A5B(a')). The concentration of CA was less to disturb the crystallinity of ZnO NPs in 1:1 ratio. The EDX spectra (Fig. A6) and elemental mapping (Fig. A7) showed that the formed complex is a combination of CA and ZnO.

5.2.7. Zinc release and antibacterial activities of hydrogel films

Zinc release profile is shown in Fig. 5.7A(a-d). In the case of control films, control films dissolved progressively and releasing zinc with respect to time. Hence, zinc release is slow up to 24 h (Fig. 5.7A(a)). A maximum release of zinc was found to be 1.24 mg/L at 24 h for the control films.

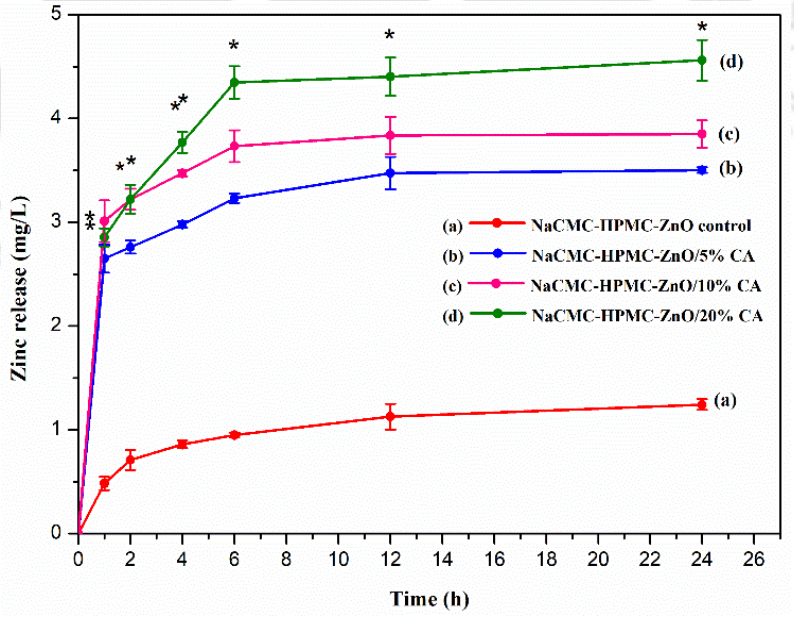

Figure 5.7A. Zinc release from (a) NaCMC-HPMC-ZnO control, and crosslinked with (b) 5% CA (c) 10% CA and (d) 20% CA in PBS, pH 7.4 at 37°C (*P<0.05 is significant

difference from control, 5% CA and 10% CA; **P>0.05 is not significant difference from 5% CA and 10% CA).

The fast release was found in the first hour for all the CA crosslinked films due to deprotonation of carboxyl groups in CA (Fig. 5.7A(b-d)). All the crosslinked films showed that slow and steady release of zinc from 1 h to 6 h and then their release become almost constant up to 24 h. But, NaCMC-HPMC-ZnO/20% CA films showed a higher release of zinc (4.56 mg/L) at 24 h compared to NaCMC-HPMC-ZnO/5% CA and NaCMC-HPMC-ZnO/10% CA. It can be attributed to increase in negative charge of the film with CA concentration. It is noteworthy that the released zinc concentration in this study are lower than the reported cytotoxicity level of 6.5 mg/L for mesenchymal stem cells (Straccia et al., 2015, 2014). However, the extent of cytotoxicity depends on the type of cell lines as well as the size of nanoparticles.

Inhibiting the bacterial growth in the wound is an added benefit for hydrogel films. Commonly, the Gram positive bacteria such as *Staphylococcus aureus* appear in the initial phase of chronic wound followed by Gram-negative species of *Escherichia coli* and *Pseudomonas* sp. in the advanced phases (Negut et al., 2018). Therefore, the antibacterial property of control films and CA crosslinked films against *E. coli* and *S. aureus* was analyzed by zone of inhibition method (Fig. 5.7(B, C), Fig. A8). Although the zinc release was higher for NaCMC-HPMC-ZnO/20% CA, it did not show significant bacterial inhibition against *E. coli* compared to NaCMC-HPMC-ZnO/5% CA and NaCMC-HPMC-ZnO/10% CA (Fig. 5.7B). However, NaCMC-HPMC-ZnO/20% CA films showed significant inhibition against *S. aureus* compared to control films and NaCMC-HPMC-ZnO/5% CA films (Fig. 5.7C). The released zinc from different hydrogel films is above the minimum inhibitory concentrations for *E. coli* and *S. aureus* (Ahrari et al., 2015; Straccia et al., 2014; Zarrindokht Emami-Karvani, 2012).

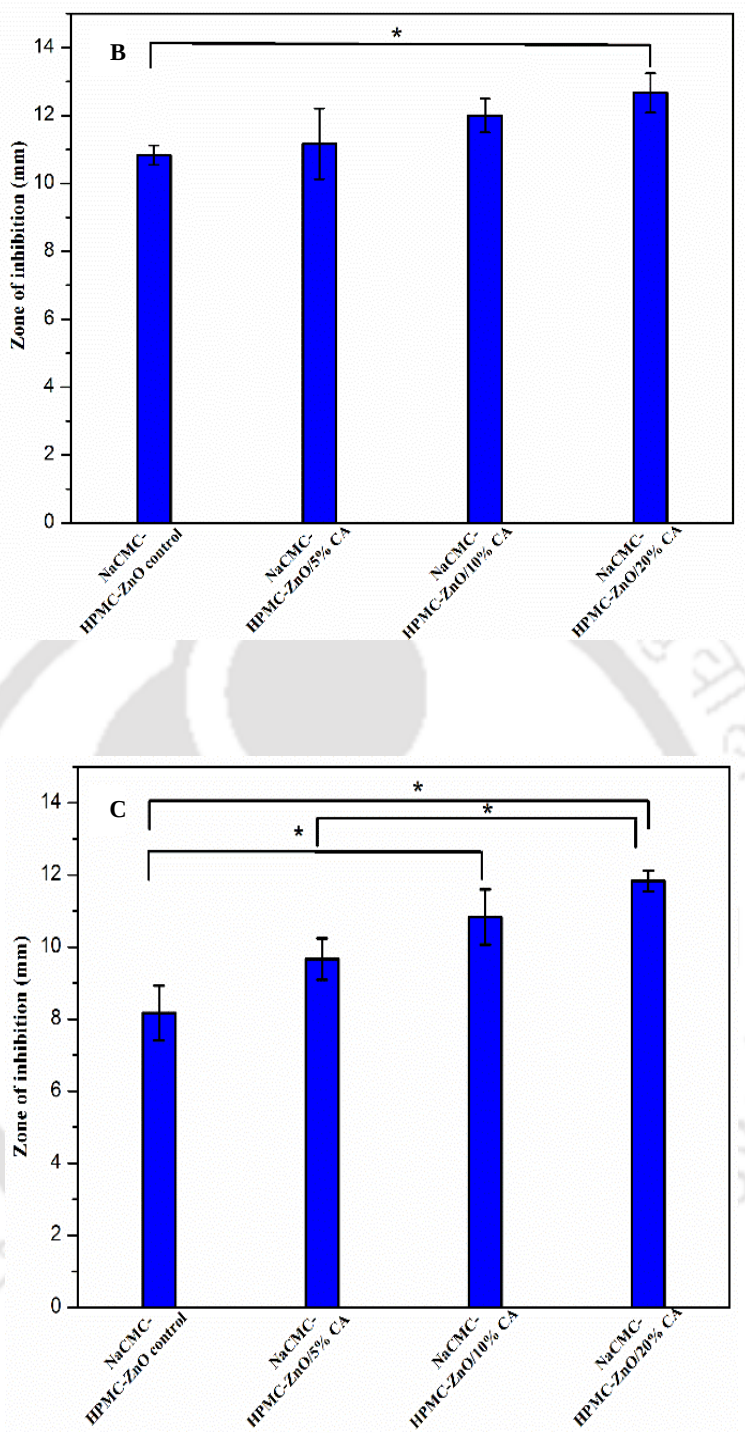

Figure 5.7(B, C). Zone of inhibition of control films and CA crosslinked films against (B) *E. coli* and (C) *S. aureus* (*P<0.05 is a significant difference between films).

The effect of ZnO complex (nanoparticle) can either be a surface or volume phenomenon. In the former case, the ZnO complex adsorbed on the cell surface

increases the porosity of outer cell membrane leading to the seepage of cytoplasmic contents. While the same occurs inside the cell due to the interaction of ZnO complex with bacterial cytosolic enzymes (Ahmed et al., 2019).

5.2.8. In vitro cytotoxicity

The prepared hydrogel films should be inert and biocompatible for wound healing applications.

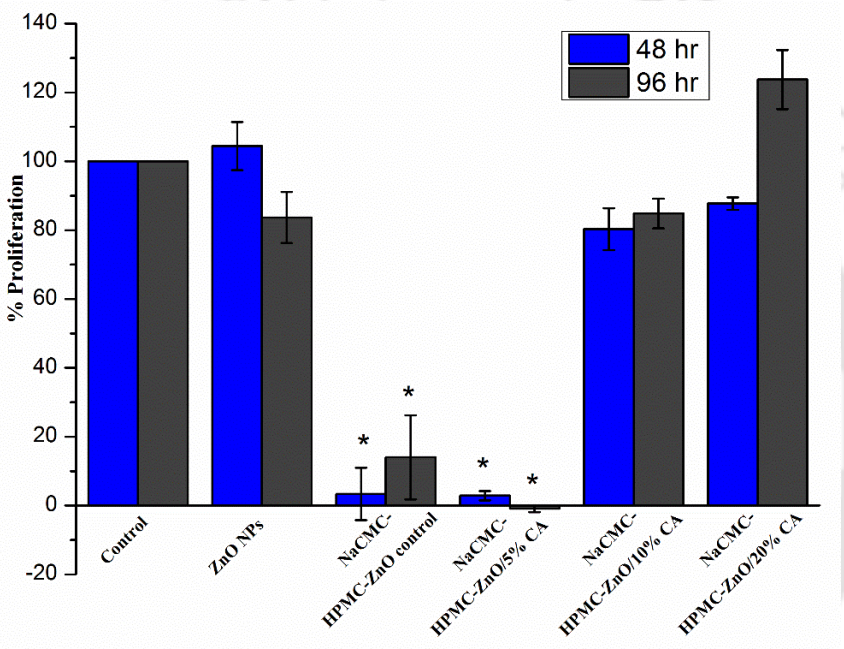

Figure 5.8. Percentage proliferation of ZnO NPs, control films and CA crosslinked films treated HaCaT cells evaluated using MTT assay. (*P<0.05 is a significant reduction in cell proliferation compared to control).

According to zinc release pattern (Fig. 5.7A), significant amount of zinc was released from all the hydrogel films. Hence, the supernatant from conditioned media was used to assess the cytotoxicity level. The MTT assay (Fig. 5.8) revealed that the prepared ZnO NPs and CA crosslinked films (NaCMC-HPMC-ZnO/10% CA and NaCMC-HPMC-ZnO/20% CA) did not significantly inhibit the proliferation of HaCaT human

keratinocyte cells. However, the higher cell proliferation of HaCaT cells in the case of ZnO NPs and NaCMC-HPMC-ZnO/20% CA compared to NaCMC-HPMC-ZnO/10% CA may be attributed to their particle size and specific surface area. Moreover, the different shape and size of ZnO would influence the cytotoxicity. Theoretically, the smaller ZnO NPs show higher cytotoxicity in terms of membrane damage and reactive oxygen species (ROS) generation than larger ZnO NPs (Huang et al., 2017). It was also shown that HaCaT cells can adapt ZnO NPs (upto 40 µg/ml) induced toxicity by Nrf-2 (nuclear factor (erythroid-derived 2)-like 2) proteasomal signal transduction, which can impart cytoprotective effects to the HaCaT cells against oxidative stress via ubiquitin-proteasome system (Wu et al., 2018). This oxidative balance mechanism is absent in bacteria resulting in bacterial death due to ROS generation.

The films of NaCMC-HPMC control and NaCMC-HPMC-ZnO/5% CA significantly reduced the proliferation of HaCaT cells. During the preparation of conditioned media, the formation of polymer nanospheres was observed in control and NaCMC-HPMC-ZnO/5% CA films (Fig. A9). Polymer nanospheres may enter into the cell, resulting in cell damage. Currently, the reaction mechanism for the formation of polymer nanospheres is unclear. This will be addressed in the near future.

5.3. Closure

In this chapter, the influence of CA on various physical, thermal and mechanical properties of NaCMC-HPMC-ZnO hydrogel films is discussed. The decrease in crystallinity, SR, initial decomposition temperature, tensile strength of hydrogel films is correlated with increase in CA concentration. The absence of ZnO peak is discussed using XRD, FTIR and micro-Raman results. The presence of nanoparticles on the hydrogel film surface and their composition are discussed. Further, the antibacterial

activity against *E. coli* and *S. aureus* and biocompatibility of the prepared hydrogel films is correlated with CA concentration. In the next chapter (Chapter 6), the effect of CA on NaCMC-HPMC hydrogel films containing CuO nanoflakes is discussed.

Chapter 6

Preparation and characterization of cellulose-based nanocomposite hydrogel films containing CuO/Cu_2O/Cu nanoparticles

In this chapter, the influence of citric acid (CA) on hydrogel films composed of sodium carboxymethylcellulose (NaCMC), hydroxypropylmethylcellulose (HPMC) and CuO nanoflakes is discussed to relate the CA effect on physico-chemical, mechanical, thermal and antibacterial properties of the fabricated hydrogel films.

6.1. Introduction

A wound can be defined as a discontinuity or defect in the skin which is the primary external defence system and the largest organ in the body. It is formed due to physical or thermal damage which disrupt the normal anatomical structure and function of the skin. In order to treat the wound, several traditional dressings such as cotton wool, bandages and gauzes have been used. However, these dressings do not offer a moist wound environment which plays a vital role for faster epithelialization and wound healing process. Evolution in polymer science attracted biomaterial scientists to replace the traditional dressings by hydrogels. Hydrogels are three-dimensional macromolecular networks which are formed by either physical or chemical crosslinking of hydrophilic polymers. Soft, flexible, hydrophilic, wettable, water-swellable, temperature and pH sensitive properties of hydrogels make them excellent candidate for wound healing applications. Among the polymeric dressings, hydrogels are the best choice for ideal wound dressing (Boateng et al., 2008; Cangul et al., 2006; Hasan et al., 2017; Kamoun et al., 2017).

In the recent past, a lot of natural and synthetic polymers were used to fabricate the hydrogels (Li et al., 2011; Pfister et al., 2007; Qiu et al., 2007; Raucci et al., 2015). Among the various polymers, cellulose derivatives such as sodium carboxymethylcellulose (NaCMC) and hydroxypropylmethylcellulose (HPMC) have been employed to design hydrogels for wound healing and drug delivery purposes (Demitri et al., 2008; Dharmalingam and Anandalakshmi, 2019; Ghorpade et al., 2016; Qiu et al., 2007). Besides, these polymers show higher swelling rate in distilled water and saline solutions compared to other cellulose ethers (Bao et al., 2012).

NaCMC is a polyelectrolyte (smart cellulose derivative) which is hydrophilic in nature, non-toxic, sensitive to ionic strength and pH variation, biocompatible and inexpensive (Sannino et al., 2009; Ullah et al., 2015). Despite the aforementioned advantages of NaCMC, the poor mechanical stability of the polymer at swollen state makes it unsuitable for drug delivery and wound healing applications. This disadvantage has been addressed by composite system. Hence, NaCMC is mixed with other polymers of polyvinyl alcohol, polyvinylpyrrolidone, hydroxyethylcellulose and hydroxypropylmethylcellulose (Dharmalingam and Anandalakshmi, 2019; El Salmawi, 2007; Raucci et al., 2015; Wang et al., 2007). However, the applications of these composite systems may be limited due to lack of inherent antibacterial property of the polymeric materials.

Composite hydrogel system incorporated with inorganic nanoparticles has been much considered in the field of biomedical engineering. The synergic effect can be obtained, when combining composite and inorganic materials, with tailor-made mechanical or functional properties. In this regard, different types of nanosized inorganic materials have been incorporated with NaCMC (Hebeish and Sharaf, 2015; Rakhshaei and Namazi, 2017; Zare-Akbari et al., 2016). Though there are various nanomaterials

available, copper-based nanoparticles have been paid much interest in the midst of researchers because of their wound healing ability, stimulation of vascular endothelial growth factors, induction of keratinocytes and fibroblast proliferation, anti-microbial and anti-inflammatory properties, stabilization of skin proteins (keratin and collagen) and also a long history of human usage (Cangul et al., 2006; Xiao et al., 2017). It is important to mention that the lethal dose (LD50) of copper ions via oral administration was found to be 110 mg/kg body weight of mice. According to the Hodge and Sterner Scale, the toxicity rating of copper ions falls on class 3, which are moderately toxic (Chen et al., 2006; Xiao et al., 2017). Furthermore, copper complexes accelerated the wound contraction and improved the acute wound environment than zinc oxide complexes (Cangul et al., 2006).

Although there are numerous studies have been investigated on copper-based hydrogels for wound healing applications, to the best of my knowledge, no study was undertaken pertaining to the influence of citric acid (non-toxic crosslinker) on the formation of Cu_2O/Cu nanoparticles from CuO nanoflakes in the presence of polymers (NaCMC and HPMC). Accordingly, the present chapter aims to fabricate novel hydrogel films with improved SR, mechanical properties and antibacterial activity along with sustained release of copper.

6.2. Results and discussion

6.2.1. Citric acid crosslinking and copper ion reduction

The citric acid (CA) crosslinked chemical structures of NaCMC and HPMC were elucidated in detail (Fig. 4.1). Briefly, CA is converted into a cyclic anhydride intermediate after condensation reaction. Then, the formed cyclic anhydride

intermediate reacts with a hydroxyl group of cellulose resulting in esterification reaction.

It is known that copper ion (Cu^{2+} of CuO) is prone to reduction to lower oxidation state (Cu^{+} of Cu_2O) or even to metallic copper (Cu^0) by a reducing agent. Initial hydroxylation of CuO on its surface is represented by the following chemical reaction (Eq. (6.1)).

$$\mathbf{CuO + H_2O \longleftrightarrow Cu(OH)_2} \quad (6.1)$$

The copper ion (Cu^{2+}) produced in Eq. (6.1) is not reduced to Cu^{+}/Cu^0 at low concentration of CA (Cu^{2+}: CA, 1:1) as shown in Eq. (6.2).

$$\mathbf{Cu(OH)_2 + C_6H_8O_7 \longrightarrow Cu^{2+} + C_6H_6O_7^{2-} + 2\,H_2O} \quad (6.2)$$

However, Cu^{2+} in Eq. (6.2) is further reduced into Cu^{+}/Cu^0 at high concentration of CA (1:4 and 1:8) as shown in Eqs. (6.3 and 6.4).

$$\mathbf{2Cu^{2+} + C_6H_6O_7^{2-} + H_2O \longrightarrow Cu_2O + C_6H_6O_7^{2-} + 2H^{+}} \quad (6.3)$$

$$\mathbf{Cu_2O + C_6H_6O_7^{2-} + 2H^{+} \longrightarrow 2Cu + C_6H_6O_7^{2-} + H_2O} \quad (6.4)$$

6.2.2. XRD analysis

XRD pattern of the synthesized CuO nanoflakes, control film of NaCMC-HPMC/CuO and NaCMC-HPMC/CuO hydrogel films with different concentrations (5 – 20%) of CA is presented in Fig. 6.1. The synthesized CuO nanoflakes exhibited crystalline phase at 2θ = 32.46°, 35.53°, 38.67°, 46.22°, 48.76°, 53.39°, 58.16°, 61.51°, 66.37° and 68.10° (Fig. 6.1a). The diffraction peaks of CuO nanoflakes have been indexed with monoclinic crystalline system (ICDD card no.: 01-085-7520). No other characteristic peaks of $CuCl_2$ or $Cu(OH)_2$ or precursors were observed, indicating the prepared CuO phase is pure. Both semicrystalline polymers of NaCMC and HPMC exhibited

diffraction peaks at 2θ = 22.1° and 2θ = 7.72° and 19.98°, respectively (Fig. 4.5a,b). In the case of control films (NaCMC-HPMC/CuO), a broad peak around 22° was observed, which confirmed the presence of NaCMC (Fig. 6.1b).

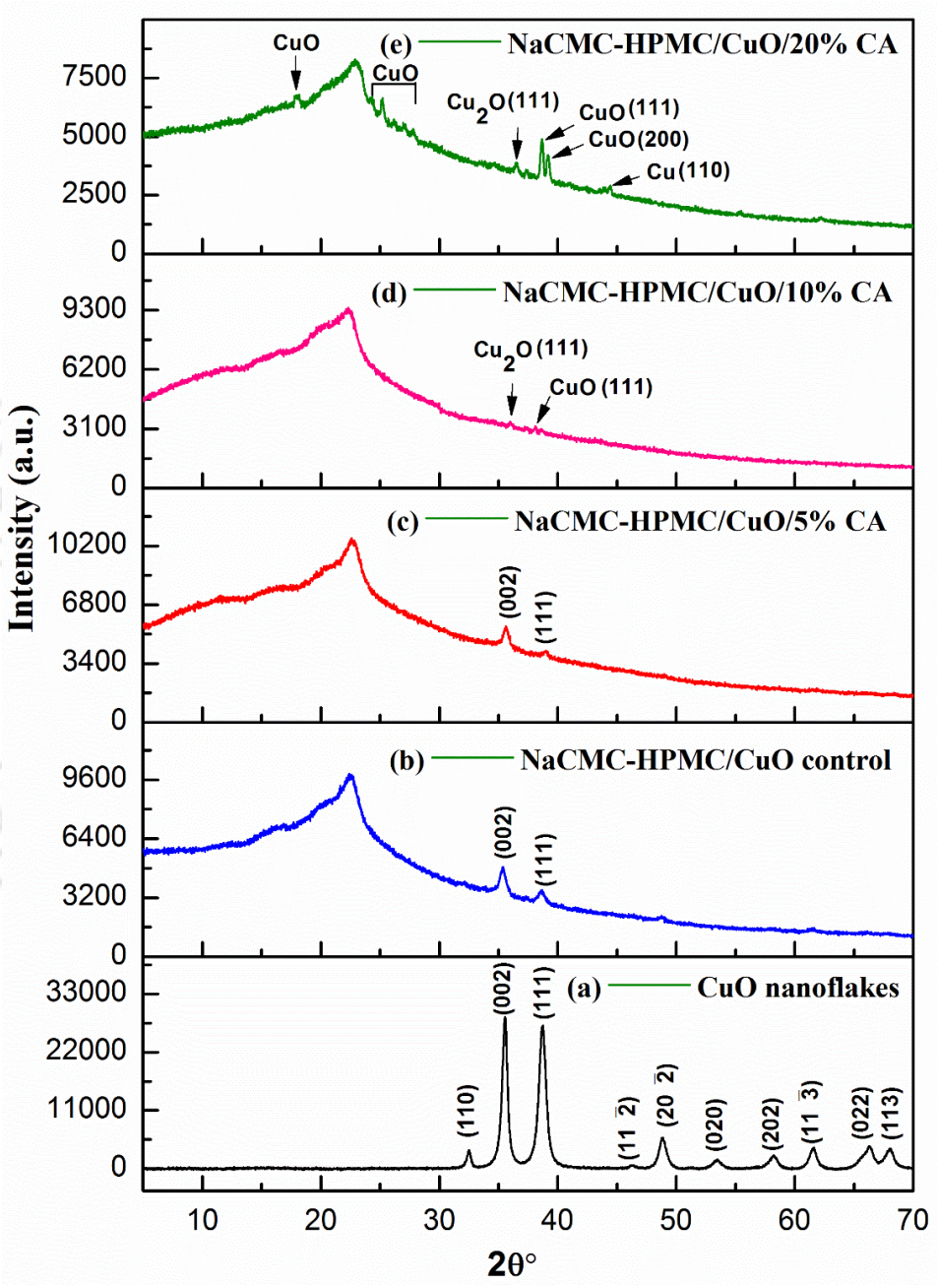

Figure 6.1. XRD patterns of (a) CuO nanoflakes and NaCMC-HPMC/CuO hydrogel films of (b) control and with different citric acid (CA) concentrations of (c) 5% (d) 10% and (e) 20%.

However, the diffraction peaks for HPMC were absent because of destruction of crystallinity during sample preparation as well as due to intermolecular interactions with NaCMC. The XRD pattern of control films depicts that the two polymers are compatible with each other. Besides, due to interaction with the polymer matrix, all the crystalline peaks of CuO nanoflakes were present in the control films with reduced intensity. Addition of 5% CA into NaCMC-HPMC/CuO hydrogel films increased the NaCMC peak intensity and many crystalline peaks of CuO were disappeared except the characteristic crystalline plane of (002) and (111) of CuO nanoflakes (Fig. 6.1c). Due to the reduction of copper (II) oxide to copper (I) oxide, a small peak (Cu_2O) was observed along with (111) plane of CuO for 10% CA films (Fig. 6.1d). Further increase in CA concentration (20%) resulted in mixtures of monoclinic CuO (ICDD card no.: 01-085-7520), unknown crystalline system of CuO (ICDD card no.: 00-003-0884), cubic Cu_2O (ICDD card no.: 01-071-3645) and cubic Cu phase (ICDD card no.: 01-080-5762) in the hydrogel films (Fig. 6.1e). It is known that citric acid can act as a reducing agent (Venkatesha and Ramesh, 2018). Thus, different oxidation states of copper (CuO, Cu_2O and Cu) were found in the hydrogel films when CA concentration increased from 5% to 20%.

6.2.3. FTIR analysis

The chemical interactions of synthesized CuO nanoflakes, NaCMC, HPMC and CA were analysed using FTIR spectra as shown in Fig. 6.2. As shown in Fig. 6.2a, the synthesized CuO nanoflakes showed that two prominent absorption peaks at 495 cm^{-1} and 607 cm^{-1} which are due to stretching vibrations of Cu-O in the monoclinic crystalline structure (Ethiraj and Kang, 2012; Siddiqui et al., 2014).

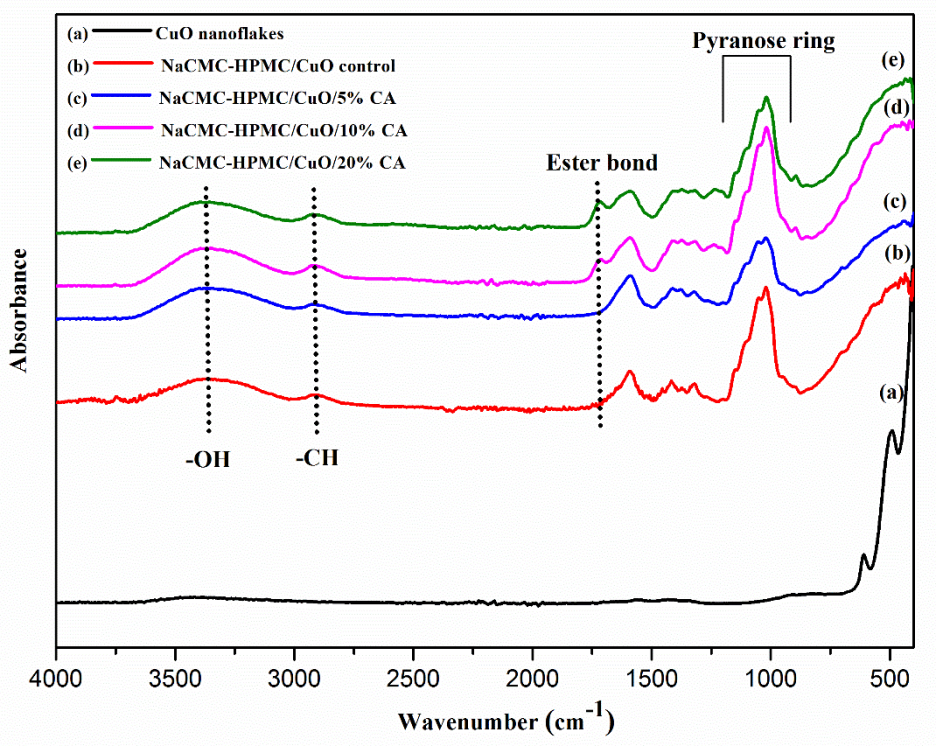

Figure 6.2. FTIR spectra of (a) CuO nanoflakes and NaCMC-HPMC/CuO hydrogel films of (b) control and with different citric acid (CA) concentrations of (c) 5% (d) 10% and (e) 20%.

The control film exhibited the distinctive vibrational modes of NaCMC and HPMC but not CuO nanoflakes (Fig. 6.2b). The peaks of NaCMC at 1596 cm^{-1} (COO^- stretching), 1419 cm^{-1} ($-CH_2$ scissoring), 1321 cm^{-1} (–OH bending) and 891 cm^{-1} (C–O–C stretching) were observed. The pyranose ring vibrations were found as a broad peak from 1200 cm^{-1} to 1000 cm^{-1}. Two small peaks at 1371 cm^{-1} and 1450 cm^{-1} are corresponded to symmetric and asymmetric bending vibrations of $-OCH_3$ group (methoxy) in HPMC, respectively. The C-O-C stretching vibration in HPMC was observed as a strong peak at 1052 cm^{-1} (Ding et al., 2015; Gorgieva and Kokol, 2011; Qiu et al., 2007; Raucci et al., 2015). Though the presence of CuO was confirmed in control films as well as for 5-20% CA incorporated films by XRD study (Fig. 6.1b-e), the characteristic peaks of CuO was not obvious in FTIR spectra (Fig. 6.2b-e). It might be due to well mixing of nanoparticles with polymer chains resulted in low intensity of

absorption band (Roy and Bhattacharya, 2014). Similarly, different concentrations of CA added films did not show any vibrational modes of CuO nanoflakes. However, increase in CA concentrations increases the ester bond intensity at 1725 cm^{-1} (Fig. 6.2c-e). It may be attributed due to increase in number of crosslinks. The previous studies (Gorgieva and Kokol, 2011; Shi et al., 2008) also confirmed that increase in crosslinker concentrations increases ester bond intensity due to crosslinking.

6.2.4. Raman spectroscopy analysis

Valuable information such as composition, crystalline system, energy shifts and a photon with low frequency modes in molecules could be inferred by Raman spectra. In order to elucidate the composition in the hydrogel films, Raman analysis was investigated as shown in Fig. 6.3. The monoclinic crystal structure of CuO belongs to the space group symmetry C^6_{2h}. Therefore, there are 12 zone center vibrational modes ($4A_u + 5B_u + A_g + 2B_g$). However, three Raman active modes (A_g, B^1_g, and B^2_g) were reported for CuO (Sahai et al., 2016; Wang et al., 2003). It was observed that the prepared CuO nanoflakes revealed three Raman peaks at 272 cm^{-1} (A_g), 318 cm^{-1} (B^1_g) and 611 cm^{-1} (B^2_g) as shown in Fig. 6.3a. In the case of control films (Fig. 6.3b), the Raman peaks of CuO were broadened and peak shifted because of phonon localization by surface impurities (polymers). Addition of 5% CA (Fig. 6.3c) did not change the Raman peaks as compared to control films (Fig. 6.3b). However, 10% and 20% CA films considerably broadened the Raman peaks with peak shifting (Fig. 6.3d,e). It may be ascribed to the quantum confinement effect of CuO nanoflakes (Wang et al., 2003). Besides, other peaks were also observed at 150 cm^{-1}, 528 cm^{-1} and 622 cm^{-1} for 10% and 20% CA added films (Fig. 6.3d,e), which confirmed the presence of Cu_2O phase (Chaurasiya et al., 2018; Deng et al., 2016; Niaura, 2000). Due to Raman inactive for Cu nanoparticles, no Raman peaks were found for 20% CA films.

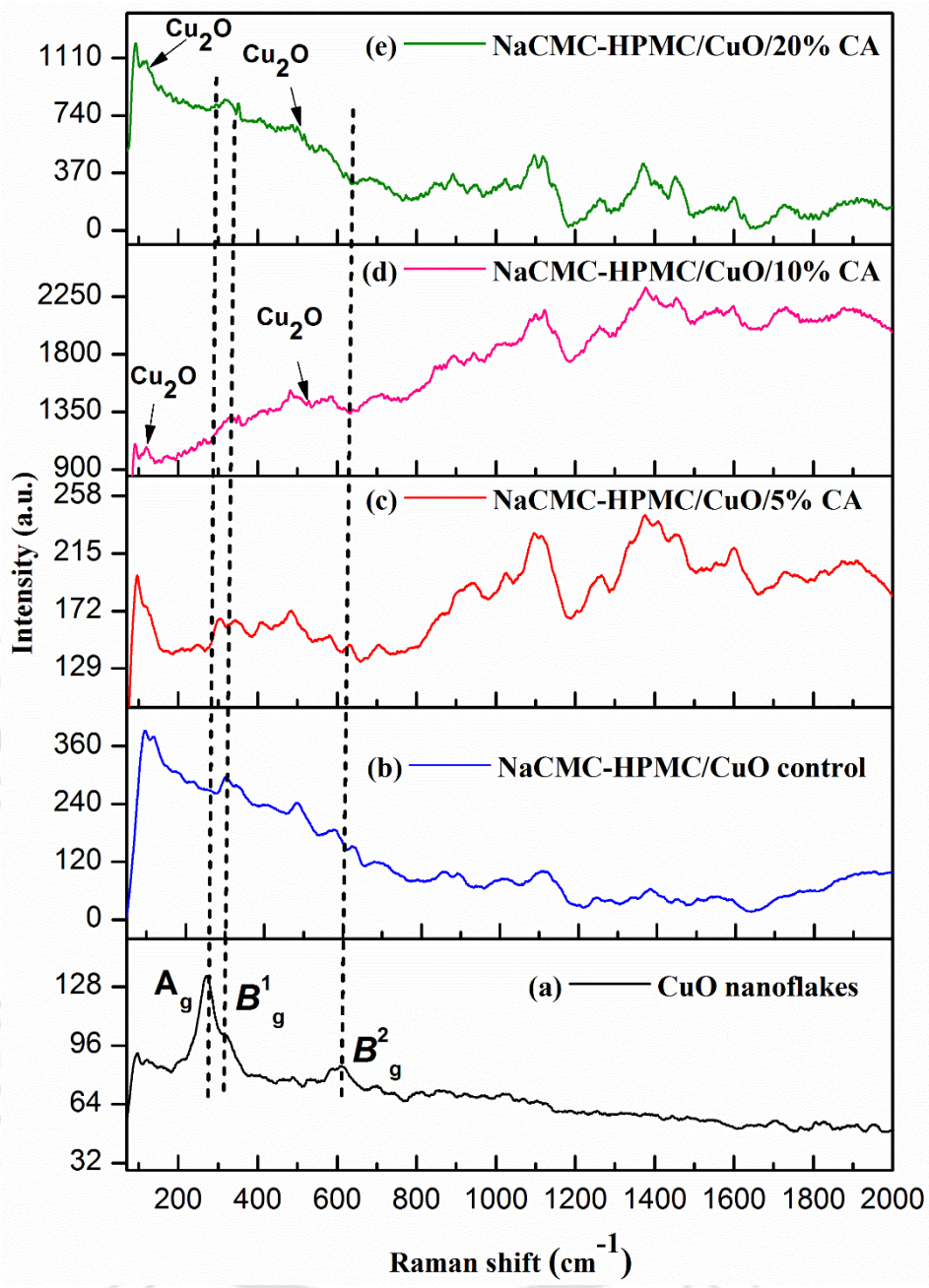

Figure 6.3. Raman spectra of (a) CuO nanoflakes and NaCMC-HPMC/CuO hydrogel films of (b) control and with different citric acid (CA) concentrations of (c) 5% (d) 10% and (e) 20%.

In addition to XRD analysis (Fig. 6.1), Raman spectroscopy analysis further confirmed the presence of mixed phases of CuO and Cu_2O in the 10% and 20% CA incorporated films.

6.2.5. Swelling ratio of hydrogel films

The release of exudate amount depends on types of wounds. One of the ideal characteristics of a wound dressing material is its exudate absorbing efficiency to provide a soothing and cooling effect over the wound bed. Therefore, the prepared hydrogel films were investigated for SR (Fig. 6.4).

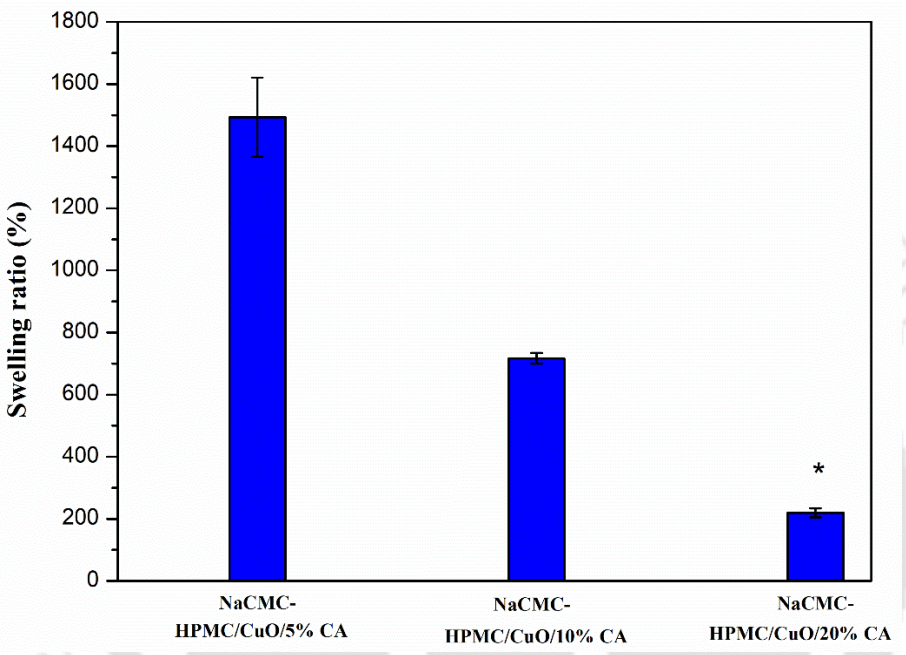

Figure 6.4. Swelling ratio (SR) (%) of NaCMC-HPMC/CuO hydrogel films crosslinked with different citric acid (CA) concentrations of 5%, 10% and 20% (*P<0.05 is significant difference with respect to 5% CA and 10% CA).

The control film (NaCMC-HPMC/CuO) was dissolved in PBS at 37°C because of the absence of crosslinking agent. The film of NaCMC-HPMC/CuO/5% CA exhibited a very high SR of approximately 1500% at the end of 24 h. The SR of NaCMC-HPMC/CuO/5% CA films is higher compared to NaCMC-HPMC/5% CA (Fig. 4.4) without CuO. The highest SR of NaCMC-HPMC/CuO/5% CA films is the result of poor crosslinking which was confirmed by FTIR analysis (Fig. 6.2c). It is known that

the swelling behavior is inversely proportional to crosslinking degree. As CA concentration increases, the SR of NaCMC-HPMC/CuO/10% CA and of NaCMC-HPMC/CuO/20% CA films significantly decreased due to increase in crosslinking degree. At higher CA concentrations, the unreacted CA molecules, which are not involved in reducing CuO nanoflakes into Cu_2O and Cu, crosslinked the polymers and thus increased the crosslinking degree. FTIR analysis confirmed that increase in CA concentration increases the absorption intensity of ester bond (crosslinking) (Fig. 6.2d,e). The previous literatures (Demitri et al., 2008; Ni et al., 2011) also confirmed that the increase in citric acid amount decreases the SR of hydrogel films.

6.2.6. Thermal analysis

Thermogravimetric (TG) and differential thermogravimetric (DTA) curves of synthesized CuO nanoflakes and CuO added hydrogel films are shown in Figs. 5(a-e) and 6(a-e). The decomposition temperature of citric acid, NaCMC and HPMC was found to be 205°C, 287°C and 355°C, respectively (Fig. 4.7A). As shown in Fig. 6.5a, the synthesized CuO nanoflakes showed a single-step decomposition at ~945°C (Fig. 6.6a) under nitrogen atmosphere (Svintsitskiy et al., 2013). The control film (Fig. 6.5b) and different concentrations of CA (Fig. 6.5c-e) added into control film exhibited four-stages and five-stages of decomposition, respectively. The weight loss of moisture, NaCMC, HPMC and CuO was found to be at 57°C, 284°C, 315°C and 955°C, respectively in the control films (Fig. 6.6b). The decrease in decomposition temperature of polymers (NaCMC and HPMC) and increase in decomposition temperature of CuO in the control film are due to interfacial interaction of CuO nanoflakes with polymers. The inclusion of different concentrations of CA (5-20%) into control film showed one more weight loss, which was corresponded to CA decomposition, including four-weight losses as observed in the control film.

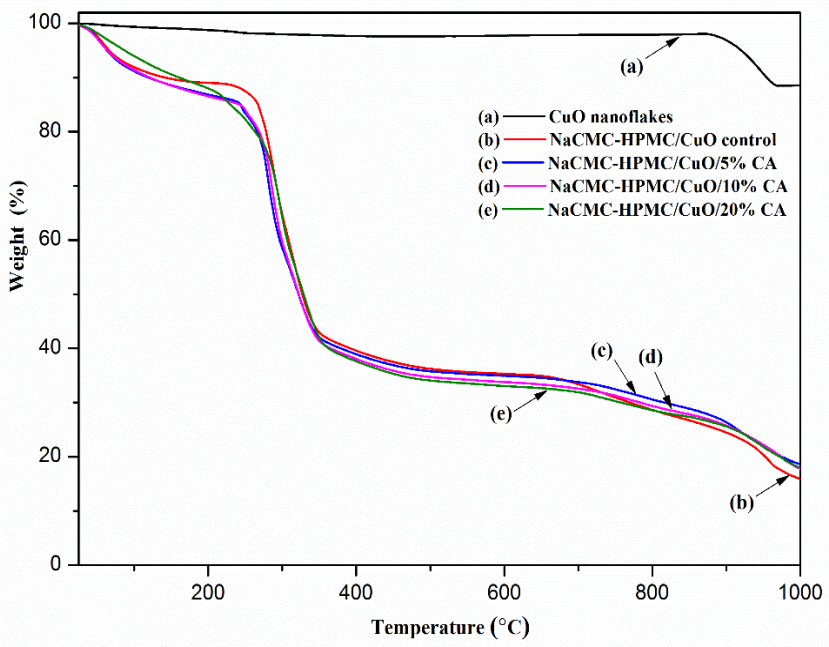

Figure 6.5. Thermogravimetric (TG) curves of (a) CuO nanoflakes and NaCMC-HPMC/CuO hydrogel films of (b) control and with different citric acid (CA) concentrations of (c) 5% (d) 10% and (e) 20%.

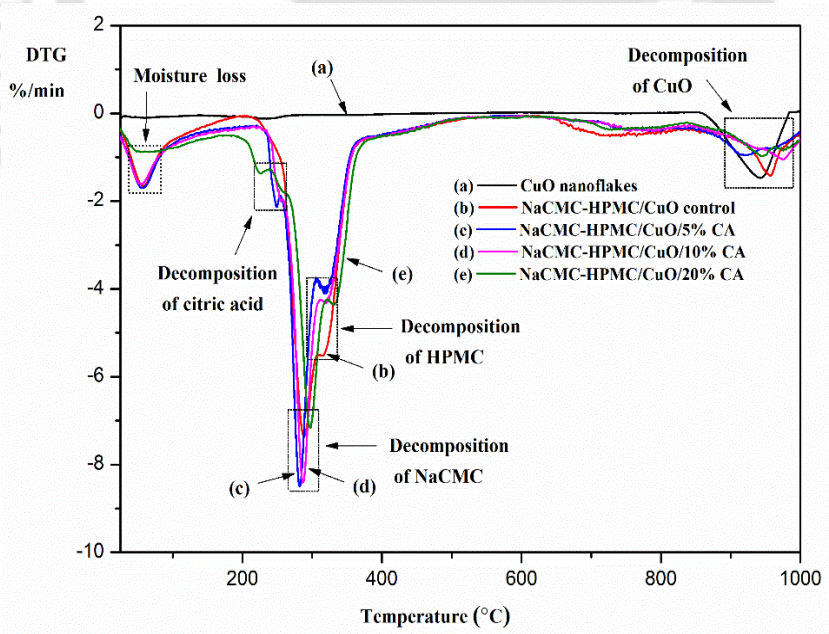

Figure 6.6. Differential thermogravimetric (DTG) curves of (a) CuO nanoflakes and NaCMC-HPMC/CuO hydrogel films of (b) control and with different citric acid (CA) concentrations of (c) 5% (d) 10% and (e) 20%.

The weight loss of CA was observed at 225-250°C for different concentrations of CA (Fig. 6.6c-e). However, the addition of 20% CA significantly lowered the decomposition temperature of CA compared to 5% and 10% CA. It might be due to the presence of residual amount of CA on the films (Figs. 5e and 6e). It was observed that the presence of mixture of CuO/Cu_2O/Cu particles, which were confirmed by XRD results (Fig. 6.1e), was found in NaCMC-HPMC/CuO/20% CA. Different sizes of particles may enhance the interfacial interactions with polymers. Hence, high concentration of CA (20%) significantly increased the decomposition temperature of NaCMC (297°C), HPMC (332°C) and CuO (979°C) compared to control films. Thermal analysis demonstrated that the films were composed of citric acid, NaCMC, HPMC and CuO. However, the decomposition step of Cu_2O was not observed in NaCMC-HPMC/CuO/10% CA and NaCMC-HPMC/CuO/20% CA films because of the nitrogen atmosphere.

6.2.7. Mechanical properties

The mechanical stability of hydrogel films over the wound site is one of the important characteristics. The hydrogel films should be soft, pliable, stress-resistant, durable and elastic because the different parts of the body may exert stress, specifically knees and elbows (Boateng et al., 2008; Güldiken et al., 2020). The incorporation of nanosize materials may enhance the mechanical properties. Thus, mechanical properties were investigated to ensure a balance between rigidity and flexibility of hydrogel films (Fig. 6.7).

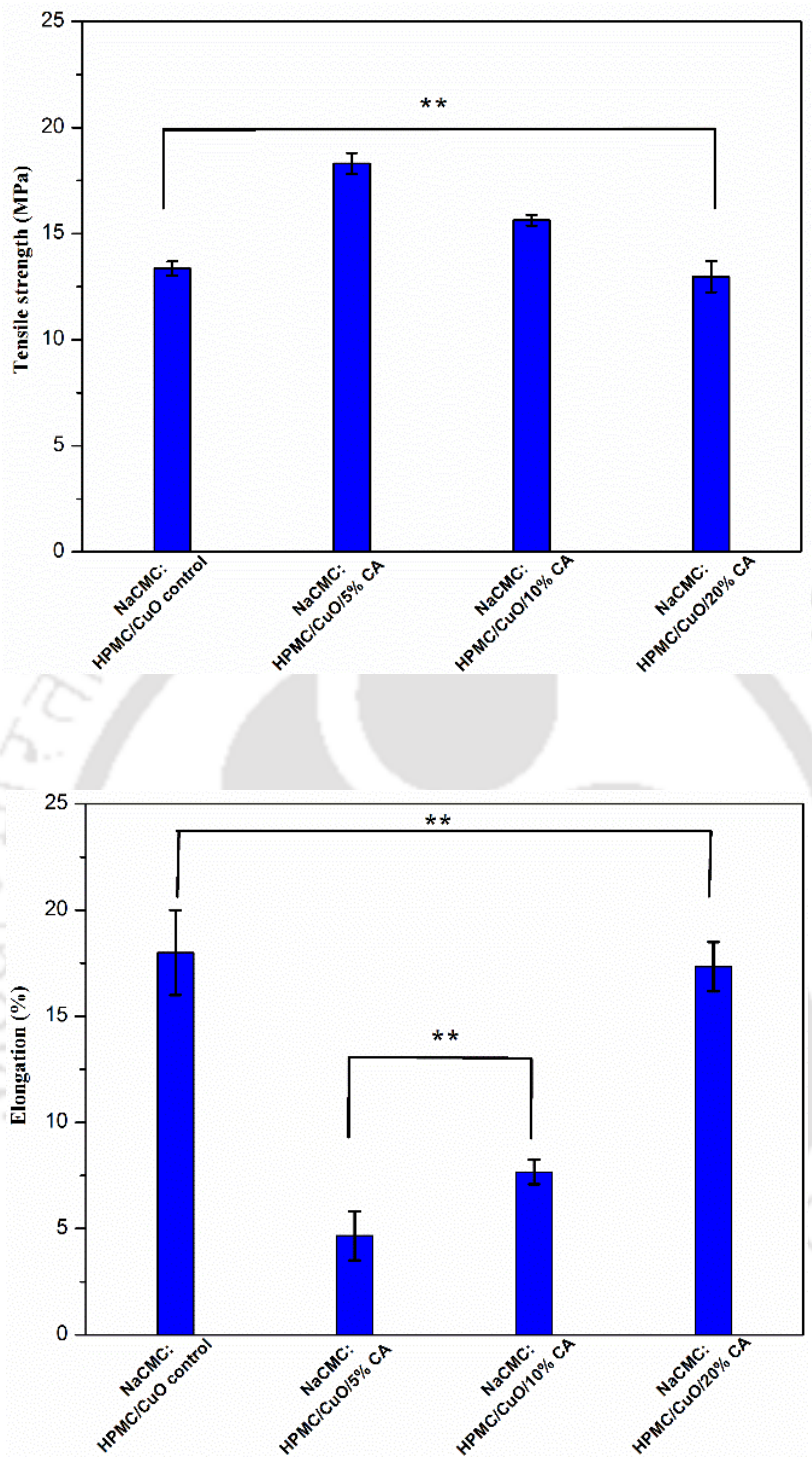

Figure 6.7. Mechanical properties of NaCMC-HPMC/CuO (control) films and different citric acid (CA) concentrations of 5%, 10% and 20% added films (**P>0.05 is not a significant difference between film samples).

The tensile strength and elongation (%) of control films were found to be 13.35 ± 0.33 MPa and 18 ± 2%, respectively. Addition of 5% CA into control films significantly increased the tensile strength (18.30 ± 0.48 MPa) and lowered elongation (4.66 ± 1.15%) due to increased crystalline intensity compared to control films (Fig. 6.1c). However, increase in CA concentrations (10% and 20%) significantly lowered the tensile strength and increased the elongation (%). It may be attributed to increase in CA concentrations decreased the crystallinity of films as shown in XRD results (Fig. 6.1d,e). The elongation (%) of 20% CA films was higher compared to 5% and 10% CA films because of residual amount of CA, which was confirmed by thermal analysis (Figs. 5 and 6e). In theory, it would anticipate tensile strength to increase with crosslinking when covalent bonds (strong) substitute Van der Waals' bonds (weak). But, decrease in tensile strength might be attributed to sub-microscopic cracks, which would develop from internal stresses, after the mobility of polymer chains decreased by crosslinking (Nielsen, 1969). The same observation was made for NaCMC-HPMC/20% CA films that the residual CA might act as a plasticizer in the films (Fig. 4.7B(d)). Furthermore, a higher tensile strength and lower elongation (%) of hydrogel films were reported by Javanbakht and Namazi (2018), Rakhshaei and Namazi (2017) and Jaiswal et al. (2019) compared to 20% CA films.

6.2.8. Morphological examinations

The morphology of as-prepared nanoparticles and the effect of CA on shape and size of the nanoparticles on the films are shown in Fig. 6.8(a-e). The TEM images of nanoparticles which were leached out from films and their selected area electron diffraction (SAED) pattern are presented in Fig. 6.8(a'-e') and Fig. 6.8(a"-e"), respectively. As shown in Fig. 6.8(a), the synthesized CuO was an agglomeration of nanoflakes.

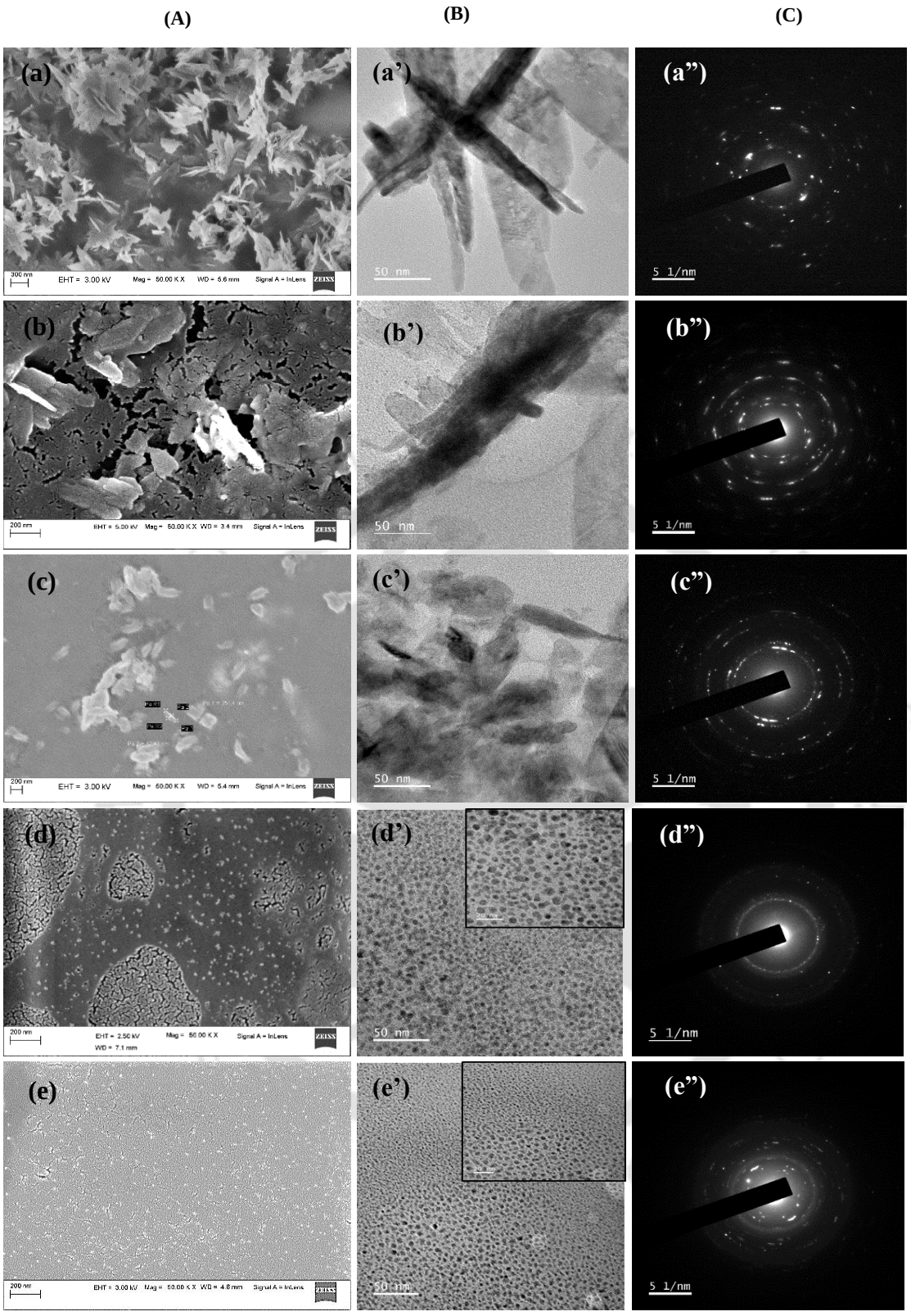

Figure 6.8. (A) FESEM (50 KX magnification) and (B) FETEM images and (C) SAED of (a, a', a") CuO nanoflakes and NaCMC-HPMC/CuO hydrogel films of (b, b', b") control, and different citric acid (CA) concentrations of (c, c', c") 5% (d, d', d") 10% and (e, e', e") 20%. Inset figure (d' and e') shows higher magnification in 20 nm scale.

The nanoflakes were clearly observed using TEM, which revealed that the nanoflakes had the approximate length and diameter of 200 nm and 15-30 nm (Fig. 6.8(a')), respectively. The SAED pattern of CuO exhibited a polycrystalline nature (Fig. 6.8(a")). The control film did not show any significant variation in shape, size and SAED pattern (Fig. 6.8(b-b")) as compared to as-synthesized CuO nanoflakes. The FESEM and FETEM images of 5% CA added films displayed that the shape of CuO nanoflakes in the films was not changed compared to control films but the size was significantly decreased to the length of approximately 100 nm and diameter of 10-20 nm due to the CA effect on CuO nanoflakes ((Fig. 6.8(c-c')). At higher concentrations of CA (10% and 20%), the shape and size of the nanoflakes on the films were completely changed as shown in Fig. 6.8(d,e). The increased citric acid concentration from 10-20% CA (Eqs. 6.5 and 6.6) led to the formation of more residual carbon, which reduced CuO significantly to Cu_2O and metallic Cu (Mahendraprabhu and Elumalai, 2016) according to the following reduction reactions

$$\mathbf{2CuO + C \longrightarrow Cu_2O + CO} \qquad (6.5)$$

$$\mathbf{CuO + C \longrightarrow Cu + CO} \qquad (6.6)$$

According to nucleation theory, the reaction rate and the solubility of the metal oxide nanoparticles play a vital role in determining the final size of the nanoparticles (Lane and Zimmerman, 2019). The formation of a new phase and new structure at higher CA concentrations (10% and 20%) might have occurred by nucleation. Because, increase in CA concentration also decreased the solution pH, which directed to coalescence as the principal form of growth and followed by Ostwald ripening (Thanh et al., 2014) to form uniform particle size of CuO, Cu_2O and Cu. Because of the change in shape and size of the nanoflakes which demonstrated quantum confinement effect in Raman spectra (Fig. 6.3d,e). The particle size of 10% CA films was in the range of almost 5-

10 nm and its SAED pattern also confirmed the polycrystalline nature of the nanoparticle (Fig. 6.8(d',d")). The FETEM images of 20% CA films evidently showed that two different sizes of nanoparticles were of approximately 2-4 nm and 5-10 nm (Fig. 6.8e'). It might be attributed to the high concentration of CA on CuO nanoflakes. The SAED pattern of nanoparticles of 20% CA films revealed that the nanoparticles are polycrystalline nature (Fig. 6.8e"). The SAED patterns are in accordance with XRD results that all the films showed different crystalline phases (Fig. 6.1b-e). HRTEM images with lattice fringes and inverse fast Fourier transform (FFT) images are presented in Fig. 6.9. The synthesized CuO nanoflakes, control films and 5% CA films showed d-spacing of 0.253 nm (Fig. 6.9a-c) which is corresponded to (002) crystalline plane of CuO (ICDD card no.: 01-085-7520). The d-spacing of 0.247 nm and 0.233 nm were observed for (111) plane of Cu_2O (ICDD card no.: 01-071-3645) and (111) plane of CuO (ICDD card no.: 01-085-7520), respectively, in 10% CA films (Fig. 6.9d,d').

The presence of Cu, Cu_2O and CuO phases were confirmed unambiguously in 20% CA films. It exhibited the d-spacing of 0.20 nm (ICDD card no.: 01-080-5762), 0.24 nm (ICDD card no.: 01-071-3645) and 0.252 nm (ICDD card no.: 01-085-7520) which are attributed to (110), (111) and (002) crystalline planes of Cu, Cu_2O and CuO, respectively (Fig. 6.9e-e"). Thus, HRTEM results and inverse FFT images further supported the XRD analysis (Fig. 6.1) and Raman spectra (Fig. 6.3).

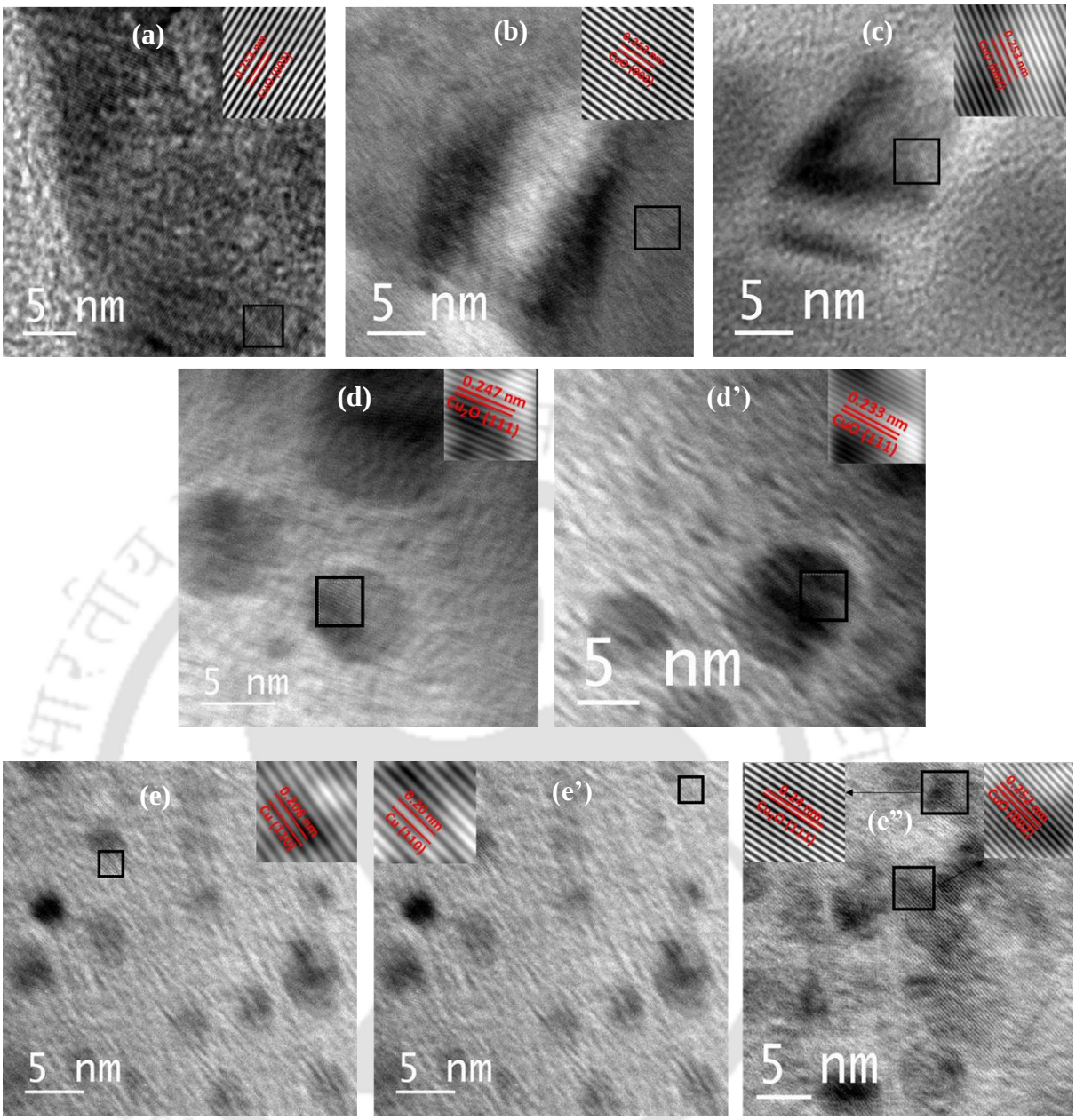

Figure 6.9. HRTEM images and inverse FFT (inset figure) of (a) CuO nanoflakes and NaCMC-HPMC/CuO hydrogel films of (b) control, and different citric acid (CA) concentrations of (c) 5% (d, d') 10% and (e, e', e") 20%.

6.2.9. Copper release

Copper release profile from CuO nanoflakes, control films and different concentrations (5-20%) of CA added films is shown in Fig. 6.10. The detected copper ions via atomic

absorption spectroscopy could come from either particulate form of CuO, Cu_2O and Cu or free copper ions. The prepared CuO nanoflakes and control films did not release ample amount of copper into PBS medium and release of copper was found to be maximum of 0.4 mg/L (Fig. 6.10a,b). All the CA (5-20%) added films released significantly higher amount of copper (Fig. 6.10c-e) than control films. Both 5% and 10% CA films released a maximum amount of copper of 7.53 mg/L and 8.89 mg/L, respectively within 1 h. Then, the release of copper was gradually decreased, which were significant, from 1 to 24 h. A maximum of copper release from 20% CA films was 9.79 mg/L which is higher than control films, 5% and 10% CA films. The release of copper was slightly decreased, which were not significant, from 1 to 6 h and followed by significant decrease from 6 to 24 h (Fig. 6.10e).

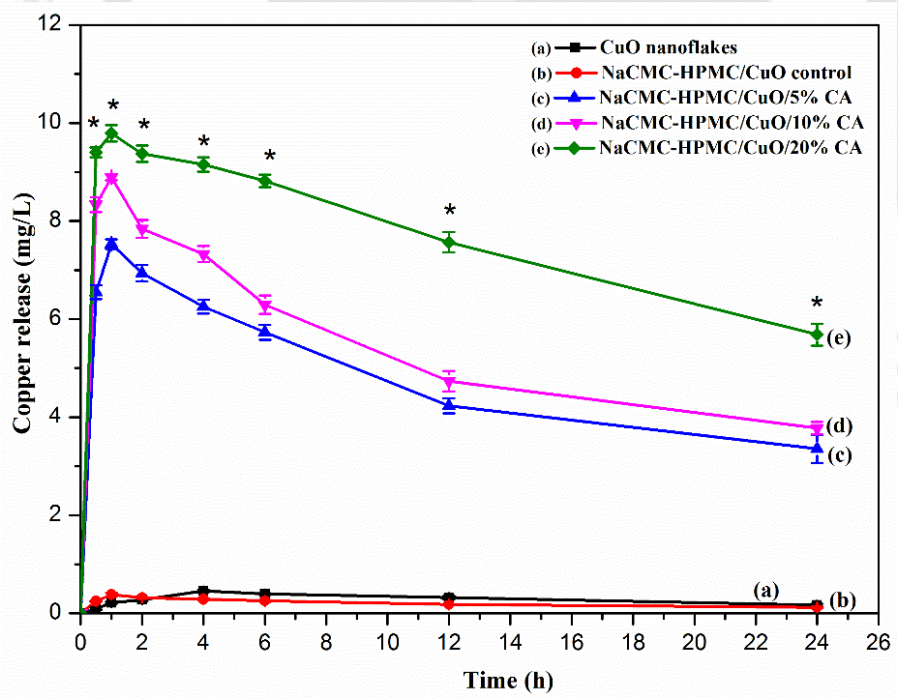

Figure 6.10. Copper release of (a) CuO nanoflakes and NaCMC-HPMC/CuO hydrogel films of (b) control, and different citric acid (CA) concentrations of (c) 5% (d) 10% and (e) 20% in PBS, pH 7.4 at 37°C (*P<0.05 is significant difference from other samples).

It can be deciphered that the amount of copper release increased with increase in CA concentrations. It might be due to high electrostatic repulsion between deprotonated COO^- groups of CA and COO^- groups of NaCMC polymer, which causes the diffusion of copper from hydrogel films in PBS medium.

6.2.10. Antibacterial activity

Hydrogel film with antibacterial activity is an added advantage in wound healing applications (Li et al., 2016; Rakhshaei et al., 2019). The zone of inhibition of control films and different concentration of CA incorporated hydrogel films against Gram-positive (*S. aureus*) and Gram-negative (*E. coli*) is shown in Fig. 6.11 and Fig. A10.

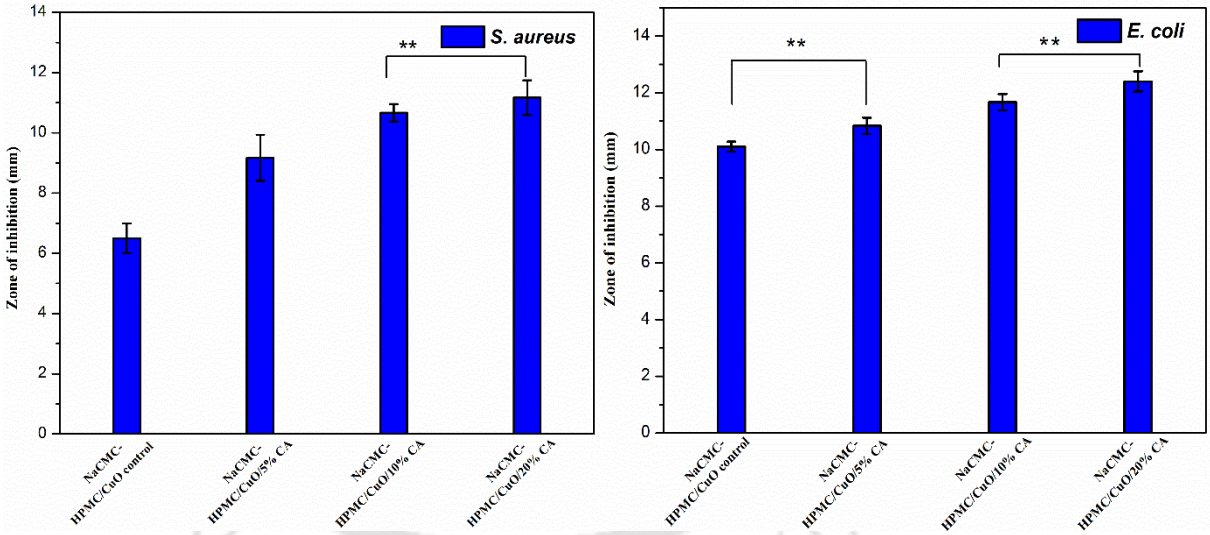

Figure 6.11. Zone of inhibition (mm) of control films and different citric acid (CA) concentrations (5-20%) for *S. aureus* and *E. coli* (**P>0.05 is not a significant difference between films).

The antibacterial activity of CuO incorporated hydrogel films was higher for *E. coli* than *S. aureus* due to the difference in the structure of the bacterial cell membrane. Besides, it might be difficult for CuO or Cu_2O or Cu to penetrate the thicker

peptidoglycan layer of *S. aureus* compared to *E. coli* (Padil and Černík, 2013). The zone of inhibition against both *S. aureus* and *E. coli* was significantly higher for 10% and 20% CA added films compared to control and 5% CA added films because of particle size and oxidation sate of copper. The surface activity of CuO differs with particle size which can exhibit different surface adsorption on bacterial membrane (Gao et al., 2009). It was observed that the bacterial protein has higher affinity towards Cu_2O (oxidation state I) than CuO (oxidation state II) (Meghana et al., 2015). The antibacterial mechanism of CuO might be due to generation of reactive oxygen species and lipid peroxidation which damages the bacterial cell membrane (Gajjar et al., 2009; Padil and Černík, 2013).

6.2.11. In vitro cytotoxicity

The amount of copper release was higher for CA incorporated hydrogel films than CuO nanoflakes and control films as shown in Fig. 6.10. Hence, the different extract amounts (supernatant) were collected from conditioned media and the cytotoxicity level was evaluated using MTT assay. In vitro cytotoxicity of as prepared CuO nanoflakes, control films and 5-20% CA added hydrogel films against HaCaT human keratinocyte cells is presented in Fig. 6.12. According to ISO 10993-5, “moderate” cell viability is from 60% to 40% (López-García et al., 2014). Although, the copper release was significantly lower for CuO nanoflakes and control films (0.4 mg/L) compared to CA added films (Fig. 6.10), a significant decrease in HaCaT cells viability was observed. However, 20% CA incorporated hydrogel films exhibited moderate HaCaT cell viability for 25% and 50% extract after four days in culture.

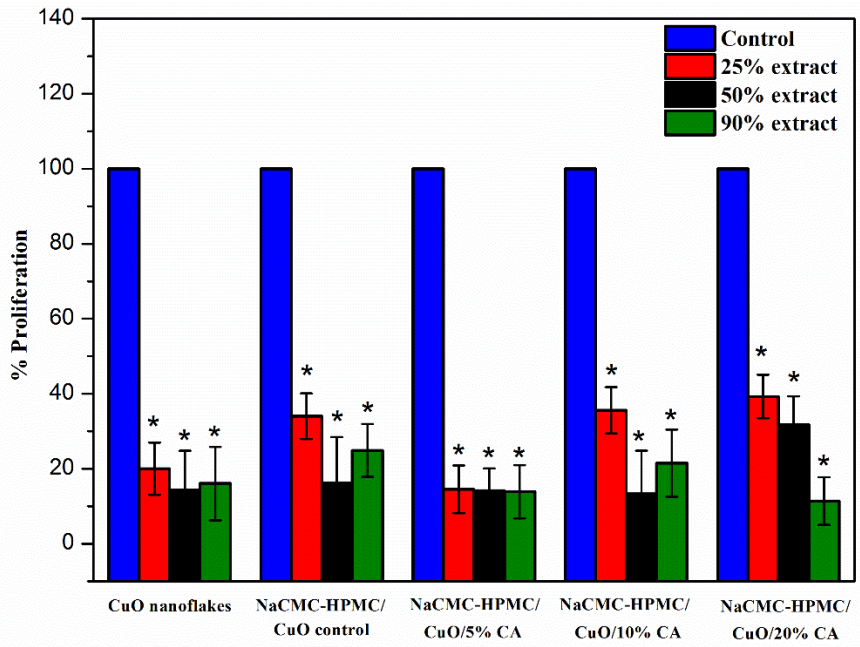

Figure 6.12. Proliferation (%) of HaCaT cells at 96 h in the presence of different extract concentrations from CuO nanoflakes, control films and 5-20% CA concentrations evaluated using MTT assay (*P<0.05 is a significant decrease in cell proliferation compared to control).

It could be attributed to particle size, morphology and chemical composition. It was observed in a previous study (Wongrakpanich et al., 2016) that smaller size CuO nanoparticles (4 nm) showed lesser toxic than larger nanoparticles (24 nm) due to the rate of entry of nanoparticles into the cell resulting in a differential influence on cytotoxicity.

6.3. Closure

In this chapter, the effect of CA on hydrogel films contained NaCMC, HPMC and CuO nanoflakes is discussed to get insight into their physical, chemical, thermal, mechanical and antibacterial properties. The synthesize of spherical nanoparticles of CuO/Cu_2O/Cu is correlated with CA concentration. The d-spacing of CuO, Cu_2O and Cu found by

HRTEM is interconnected with XRD results. Further, the biocompatibility of prepared hydrogel films for HaCaT cell proliferation and antibacterial activity against both Gram-positive and Gram-negative bacteria are discussed. In the next chapter (Chapter 7), the various properties of grapefruit seed extract (GFSE) incorporated NaCMC-HPMC-ZnO/CA (optimized) hydrogel films are presented.

Chapter 7

Functionalization of cellulose-based nanocomposite hydrogel films with ZnO complexes and GFSE for potential applications in chronic wound healing

In this chapter, the influence of grapefruit seed extract (GFSE), a natural antimicrobial and antioxidant liquid, on citric acid (CA) and zinc oxide nanoparticles (ZnO NPs) incorporated cellulose-based hydrogel films containing sodium carboxymethylcellulose (NaCMC) and hydroxypropylmethylcellulose (HPMC) is discussed. The various properties of fabricated hydrogel films are correlated with GFSE concentrations (0.25-1.0%, v/v).

7.1. Introduction

Skin is a physical-chemical barrier between the human body and environmental aggressions. It is the largest human organ and the first line of defence against pathogens (Boer et al., 2016; Pinho and Soares, 2018). Commonly, the human body is capable of repairing the wounds, which are due to physical or thermal damage, by a complex cascade of biochemical events (Gurtner et al., 2008). The healing process depends on infection, growth factors, oxygenation, hormones, diabetes and nutrition. The wound healing process occurs in four different phases such as hemostasis, inflammation, proliferation and remodelling. Any perturbation due to external and internal factors in the aforementioned phases can lead to chronic wounds (Guo and DiPietro, 2010; Vijayakumar et al., 2019). In order to restore skin integrity with minimal scars, many topical products have been developed to provide a moist environment with antibacterial activity. Nevertheless, chronic wound healing still endures a great challenge for biomaterial researchers because of multidrug-resistant microorganisms and bacterial biofilms (Mihai et al., 2019; Pinho and Soares, 2018).

In this facet, the nanotechnology and nanobiomaterials unlocked a new way to heal chronic wounds (Vijayakumar et al., 2019). Because, nanoparticles possess a higher surface-to-volume ratio and have been efficiently employed in numerous biomedical applications, including wound-healing therapies. Metal nanoparticles like zinc, silver and copper are increasingly being utilized in dermatology because of their potential effects on accelerating wound healing and also in treating and preventing microbial infections (Mihai et al., 2019). Amongst metal oxide nanoparticles, zinc oxide nanoparticles (ZnO NPs) contain essential mineral elements for wound healing and a trace amount of these elements showed strong activity. The topical application of ZnO NPs is generally used in skin creams due to their anti-inflammatory and antiseptic properties. The presence of ZnO NPs exhibits strong antibacterial activity and fastens the wound healing process by remaining at the wound site for prolonged period of time (Deepachitra et al., 2015; Mihai et al., 2019; Vijayakumar et al., 2019). Also, it stimulates keratinocyte migration and thus improving re-epithelialization (Mihai et al., 2019). However, the application and use of ZnO NPs exclusively depend on its concentration (Hussain et al., 2019; Siddiqi et al., 2018). In order to reduce the intrinsic toxicity of ZnO NPs, different researchers created Au@ZnO core-shell nanocomposites (Khan et al., 2019), silica-coated ZnO NPs (Sotiriou et al., 2014), iron-doped ZnO NPs (George et al., 2009) and complex of citric acid with ZnO NPs (zinc oxide complexes) (Swanzy, 2017).

Wound healing comprises of many difficult pathways, which also require a control balance between oxidative stress and antioxidants (Fitzmaurice et al., 2011). Antioxidants are capable of reducing oxidative stress at the wound site and thereby quickening the wound healing. Nowadays, antioxidants have been paid more attention

in polymer science and biomaterial due to their vital role in preventing or limiting the damage caused by reactive oxygen species (ROS) (Fitzmaurice et al., 2011; Kim et al., 2018). Also, antioxidants act as reducing agents and free radical scavengers. Amongst various natural antioxidants, polyphenolic compounds are well known for scavenging ROS and free radicals through their hydroxyl groups of aromatic rings (Fu et al., 2014; Kim et al., 2018).

One of such natural antioxidant substances is grapefruit seed extract (GFSE), which is extracted from pulp and seed of grapefruit. GFSE is rich in ascorbic acid, polyphenols, citric acid and lipids and classified as proanthocyanidins (PACs), which are flavonoid family (Cho et al., 1990; Kanmani and Rhim, 2014a). It demonstrated strong antibacterial and antifungal properties (Heggers et al., 2002). However, in spite of biocompatibility and low cost for food and pharmaceutical applications, it has several drawbacks such as instability and oxidation under ambient conditions. This can be overcome by entrapping antioxidant-rich GFSE in macromolecules or films, which mitigates the oxidation of antioxidants by limiting the oxygen access (Cho et al., 2011; Cirillo et al., 2010; Kim et al., 2018).

Recently, hydrogels have been emerged as a promising wound healing material for the development of functional biomaterials. Hydrogels are generally made from the hydrophilic polymeric materials, which are either physically or chemically crosslinked and can absorb and hold large amounts of biological fluids or water in their three dimensional network, thus providing a moist environment in the wound site (Hashem et al., 2013; Kim et al., 2018). The structural arrangement of crosslinked polymeric materials is similar to a typical skin, thus it is suitable for wound healing applications. There are different biopolymeric materials like starch, cellulose, collagen and chitosan employed to fabricate hydrogels to promote wound healing by fibrogenesis (Smith et

al., 2016; Vijayakumar et al., 2019). Amongst several biopolymers, sodium carboxymethylcellulose (NaCMC) and hydroxypropylmethylcellulose (HPMC) are ether derivatives of cellulose, which are hydrophilic in nature, biocompatible and biodegradable. Theses polymers show high swelling rate in water and biological fluids. The blending of these polymers produced a new biomaterial for wound healing applications (Dharmalingam and Anandalakshmi, 2019).

There are numerous reports in the development of polymeric-inorganic nanocomposite biomaterials for wound healing applications (Bajpai et al., 2017; Singla et al., 2017; Vijayakumar et al., 2019). However, in the current chapter, an attempt has been made to create functionalized hydrogel films with zinc oxide complex and GFSE. To the best of my knowledge, no study was investigated concerning to cellulose-based hydrogel films with zinc oxide complex and GFSE for potential wound healing applications. Therefore, the present chapter aims: (i) to reduce the inherent cytotoxicity of ZnO NPs by forming zinc oxide complex from ZnO NPs and citric acid (ii) to deliver the essential mineral element (zinc) in a sustained manner to the wound site (iii) to accelerate the wound healing process by balancing the oxidative stress via GFSE and (iv) to prevent the biofilm formation on the wound site via GFSE as well as zinc oxide complex. Furthermore, the effect of GFSE on the physicochemical and mechanical properties of the zinc oxide complex containing NaCMC-HPMC hydrogel films was comprehensively studied in detail.

7.2. Results and discussion

7.2.1. Citric acid (CA) crosslinking in the presence of zinc oxide (ZnO)

The ZnO and CA content for control film was optimized based on flexible in nature, peelable from Petri dishes, stable appearance after swelling in PBS buffer (pH 7.4) and

antibacterial activity (Chapter 6). The CA crosslinking of NaCMC and HPMC and their crosslinked molecular structures were shown in Figs. 4.1 and 4.2.

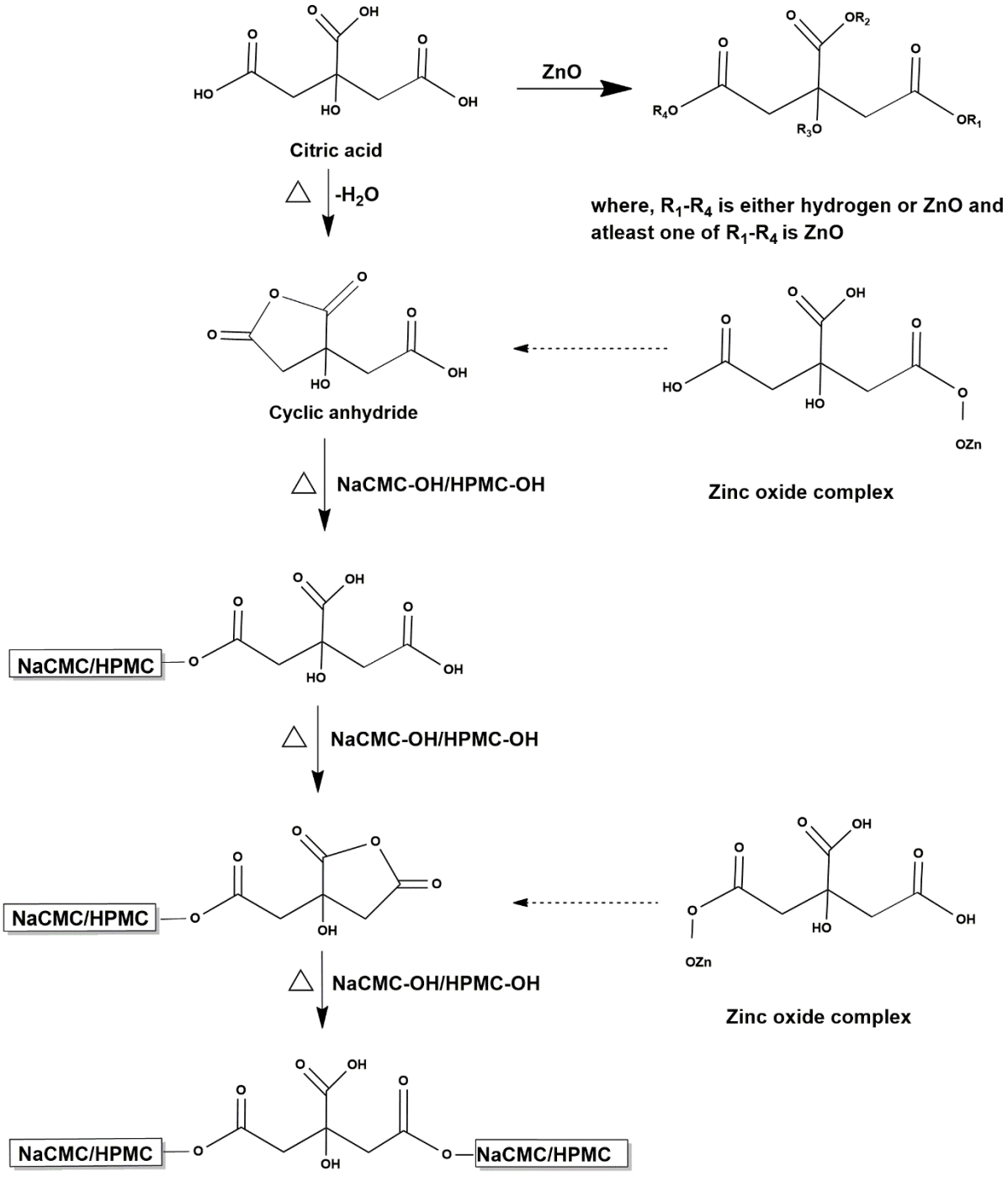

Figure 7.1. Possible mechanism of sequential crosslinking of NaCMC and HPMC by citric acid (CA) in the presence of ZnO.

Briefly, two carboxylic groups of CA form a cyclic anhydride with the removal of water upon heating. Then, the hydroxyl group of either NaCMC or HPMC reacts with cyclic anhydride resulting in esterification reaction and leaving α-hydroxy acid group to expose in CA. Likewise, the formation of second cyclic anhydride occurs followed by another esterification. A complex particulate molecule can be formed by mixing different molar ratios of ZnO and CA (Swanzy, 2017). Fig. 7.1 shows the sequential crosslinking steps of CA in the presence of ZnO and the absence of ZnO. The incorporation of ZnO may inhibit the sequential crosslinking steps of CA. There are four binding sites namely R_1-R_4 in CA for ZnO. If ZnO binds to α-hydroxy acid group in CA, the crosslinking ability of CA might be impeded. However, the binding of ZnO on R_1 or R_4 of CA cannot hinder the formation of at least one cyclic anhydride, thus one esterification step takes place as shown in Fig. 7.1.

7.2.2. Effect of GFSE on crystallinity of hydrogel films

XRD pattern of both NaCMC and HPMC polymers exhibits a broad peak at $2\theta = 22.1°$ and 19.98°, respectively (Fig. 4.5a,b). The synthesized ZnO showed hexagonal wurtzite structure (JCPDS #80-0075), which showed crystalline peak at 2θ = 31.73°, 34.42°, 36.25°, 47.68°, 56.71°, 62.82° and 68.5° (Fig. 5.2a). The compatibility of polymers can be observed from XRD pattern of the ZnO control film, which displayed mainly NaCMC peak due to inter- and intra-molecular hydrogen bonding with HPMC. The absence of ZnO peaks was found in the ZnO control film because of citric acid, which might be bound with ZnO (Fig. 7.1), and completely destroyed the ZnO crystallinity (Fig. 7.2a). Various concentrations of GFSE were added into the ZnO control film and their XRD patterns are presented in Fig. 7.2(b-d). There was no noticeable peak broadening in the main diffraction peak for 0.25% and 0.5% (v/v) GFSE addition (Fig.

7.2b,c) while it can be clearly seen that an increase in peak width for 1.0% (v/v) GFSE (Fig. 7.2d).

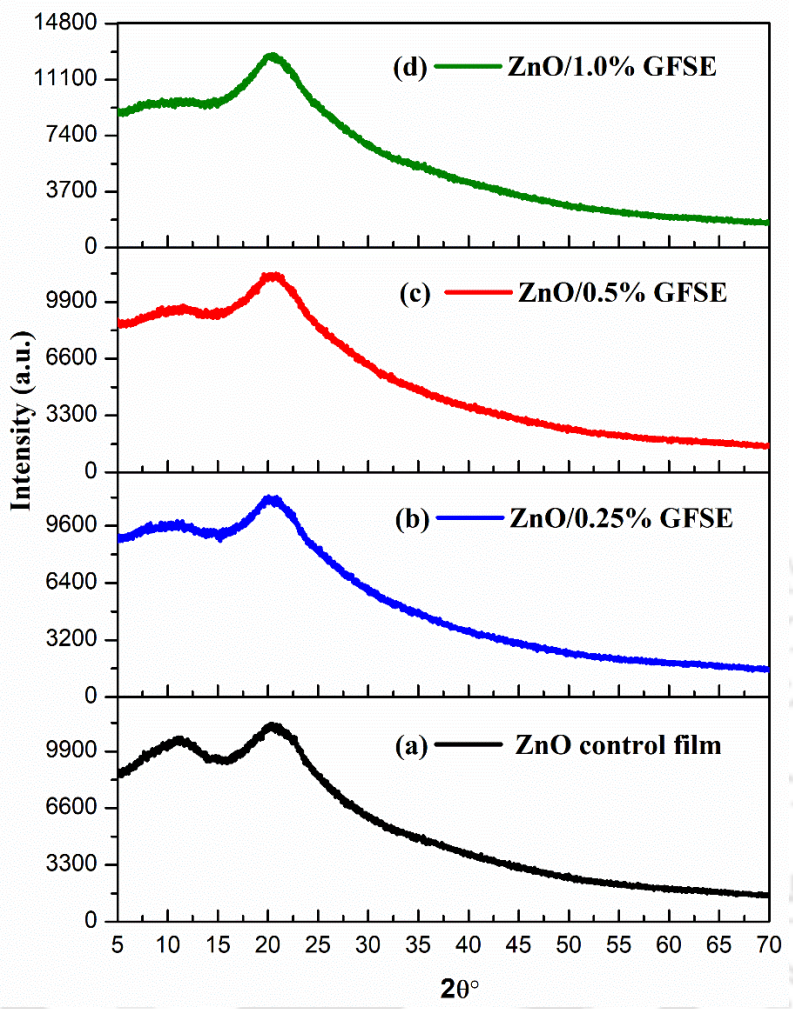

Figure 7.2. XRD pattern of citric acid crosslinked NaCMC-HPMC hydrogel films of (a) ZnO control, and various GFSE concentrations (v/v) of (b) 0.25% (c) 0.5% and (d) 1.0%.

It can be comprehended that a higher concentration of GFSE might decrease the internal strain of the polymers or mobility of the polymer chains and thus resulting in reduced crystallite size. Furthermore, an addition of GFSE did not shift the main crystalline peak as well as not produced any other peaks.

7.2.3. FTIR spectroscopy

Chemical interactions amongst the polymers (NaCMC and HPMC), citric acid, ZnO and GFSE were investigated using FTIR spectroscopy and their spectra are given in Fig. 7.3(a-f). A broad absorption peak between 400-590 cm^{-1} was assigned to ZnO vibrations (Fig. 7.3a) (Zare-Akbari et al., 2016). The spectra of GFSE (Fig. 7.3b) revealed the stretching of -OH (3300 cm^{-1}), asymmetric and symmetric stretching of CH_2 (2926 and 2855 cm^{-1}), bending vibrations of aliphatic $-CH_3$ and $-CH_2$ (1458 cm^{-1}), stretching of -C=O (1648 cm^{-1}) and in plane and out of plane bending of -CH (1200-1000 cm^{-1} and 1000-800 cm^{-1}) (Mohansrinivasan et al., 2015; Oliveira et al., 2016).

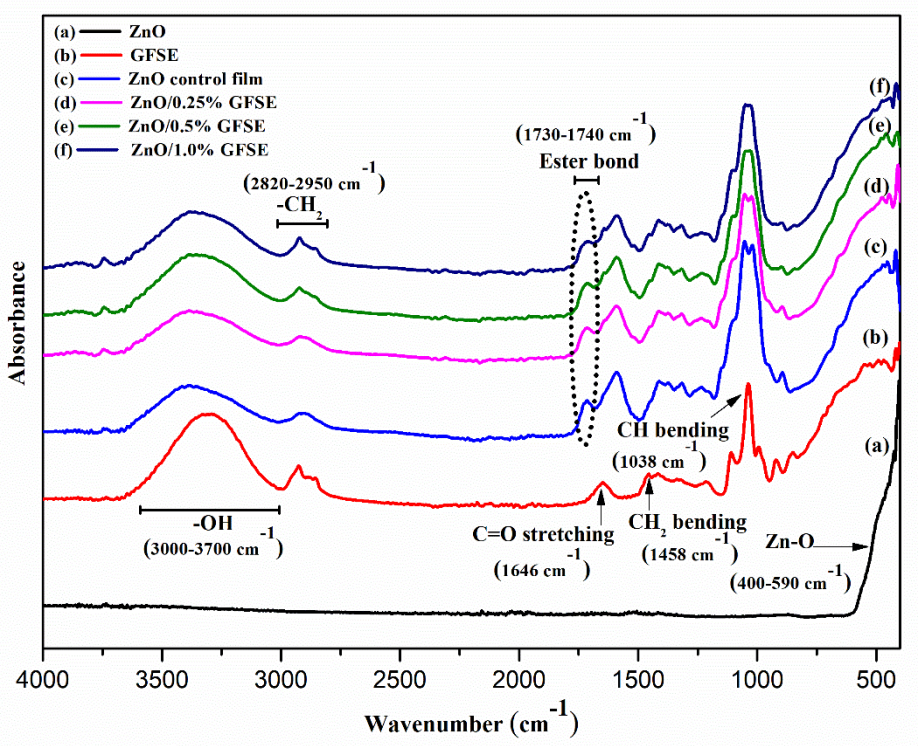

Figure 7.3. FTIR pattern of (a) ZnO, (b) GFSE and citric acid crosslinked NaCMC-HPMC hydrogel films of (c) ZnO control, and various GFSE concentrations (v/v) of (d) 0.25% (e) 0.5% and (f) 1.0%.

For citric acid incorporated ZnO control films, the presence of ester bond (1730 cm^{-1}) was observed (Fig. 7.3c) due to crosslinking between citric acid and polymers (Gorgieva and Kokol, 2011). However, the absence of the broad peak for ZnO was evident in the ZnO control films because of the formation of zinc oxide complex. Thus, the FTIR spectra is in accordance with XRD results for ZnO control films (Fig. 7.2a). Furthermore, other vibrational modes for NaCMC (-COOH stretching – 1589 cm^{-1}, -CH_2 scissoring – 1414 cm^{-1} and -OH bending – 1316 cm^{-1}) and HPMC (symmetric bending of -OCH_3 – 1374 cm^{-1} and asymmetric bending of -OCH_3 – 1454 cm^{-1}) were ascertained in the ZnO control films (Ding et al., 2015; Gorgieva and Kokol, 2011; Raucci et al., 2015). A typical broad absorption peak between 1200 cm^{-1} and 1000 cm^{-1} was seen in the ZnO control films due to sugar ring vibrations (Fig. 7.3c) (Raucci et al., 2015).

The FTIR spectra of the various concentrations of GFSE added hydrogel films (Fig. 7.3d-f) showed a similar spectral patterns compared to the ZnO control films. There was no noticeable difference between GFSE incorporated hydrogel films and ZnO control films. However, by having a closer view at the –CH_2 region (2820-2950 cm^{-1}) and ester band (1730-1740 cm^{-1}), it is clear that these peaks were slightly broader. It may be attributed due to increase in GFSE concentration. Deconvolution using a Gaussian function curve fitting analysis was applied to improve the resolution of the spectra from 1680-1790 cm^{-1}, which are corresponded to ester band and presented in Fig. A11 and Table A1. Peak fitting analysis showed that increase in GFSE concentration from 0.25% to 1.0% (v/v) shifted the ester band to higher wavenumber suggesting higher degree of crosslinking (Table A1). The previous study reported that higher number of crosslinks restricted the polymer chain mobility resulted in reduction of crystallite size (peak broadening). The ester band shifting to higher wavenumber

upon increasing GFSE concentrations is matched with peak broadening in XRD (Fig. 7.2b-d).

7.2.4. Raman spectra of hydrogel films

In order to investigate the effect of GFSE on the ZnO control films as well as citric acid on ZnO, micro-Raman spectroscopy was used and their spectra is given in Fig. 7.4(a-e). According to group theory, wurtzite ZnO has the following optical phonon modes such as E_2 (low), E_2 (high-low), A_1 (LO), E_2 (high) and $2A_1$ (LO). Amongst optical phonon modes, the mode of E_2 (high) is a main characteristic peak of wurtzite ZnO at 437 cm^{-1} (Filippov et al., 2013; Koutu et al., 2016; Sharma et al., 2011).

As shown in Fig. 7.4a, all the characteristic optical phonon modes were present for the prepared ZnO. However, an addition of CA shifted all the characteristic peaks of ZnO with peak broadening for the ZnO control films (Fig. 7.4b) because of phonon confinement or phonon localization (Koutu et al., 2016), which were imposed by surface impurities. Furthermore, the polarizability of ZnO might be changed due to addition of CA by forming the complex.

Incorporation of various concentrations of GFSE (Fig. 7.4c-e) did not shift or broaden the peaks of ZnO complex substantially compared to ZnO control films. Besides, no more additional peaks were observed in Raman spectra. It reveals that no significant effect of GFSE on ZnO complex and other precursors was evidently seen. In addition to XRD (Fig. 7.2) and FTIR (Fig. 7.3) analysis, micro-Raman study confirmed the absence of pure ZnO in all the prepared films.

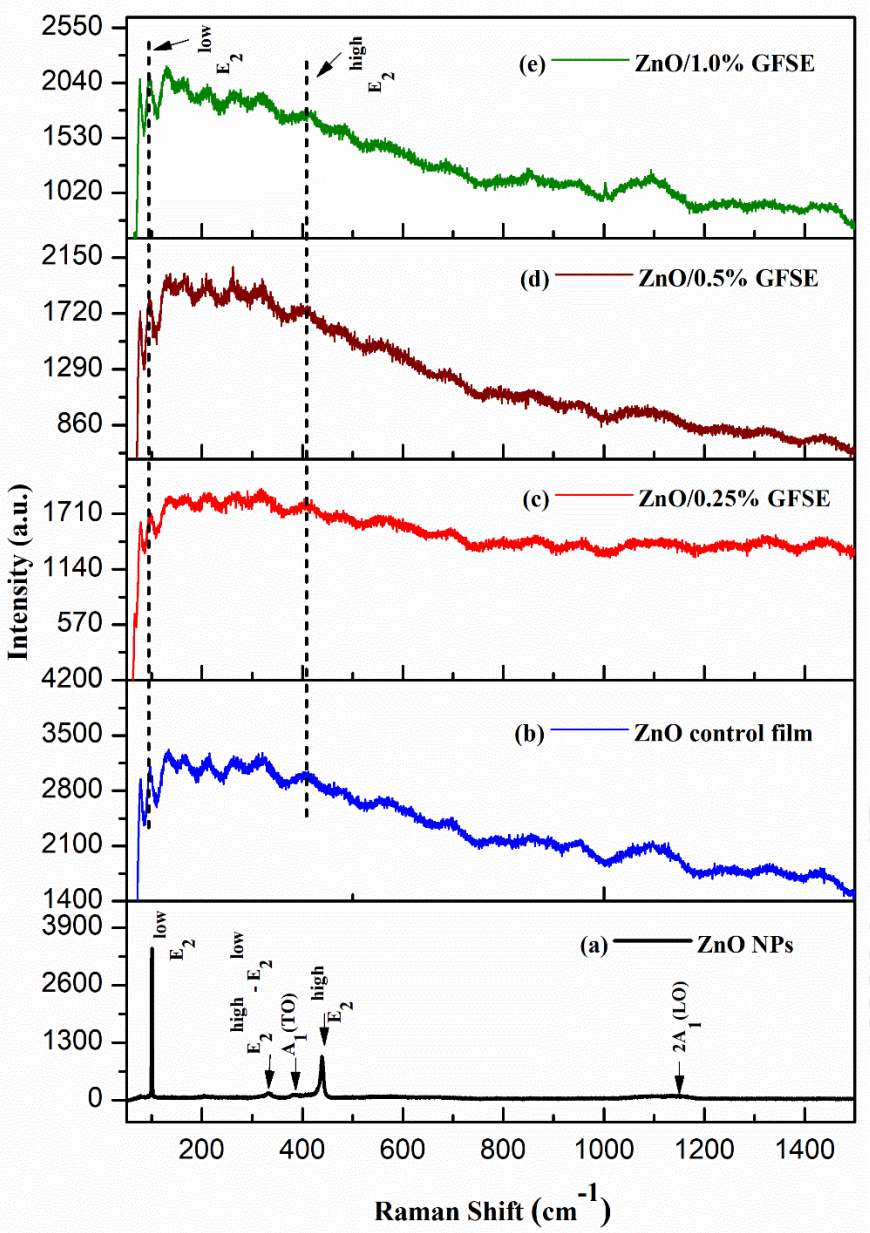

Figure 7.4. Raman spectra of (a) ZnO and citric acid crosslinked NaCMC-HPMC hydrogel films of (b) ZnO control, and various GFSE concentrations (v/v) of (c) 0.25% (d) 0.5% and (e) 1.0%.

7.2.5. Swelling ratio of hydrogel films

One of the most important ideal characteristics of a dressing material is SR. The application of a hydrogel film for different types of wounds depends on its SR. Therefore, the SR of ZnO control films and various amounts of GFSE added into the

ZnO control films was investigated and the capacity of each hydrogel film to swell in PBS (7.4) at 37°C is shown in Fig. 7.5.

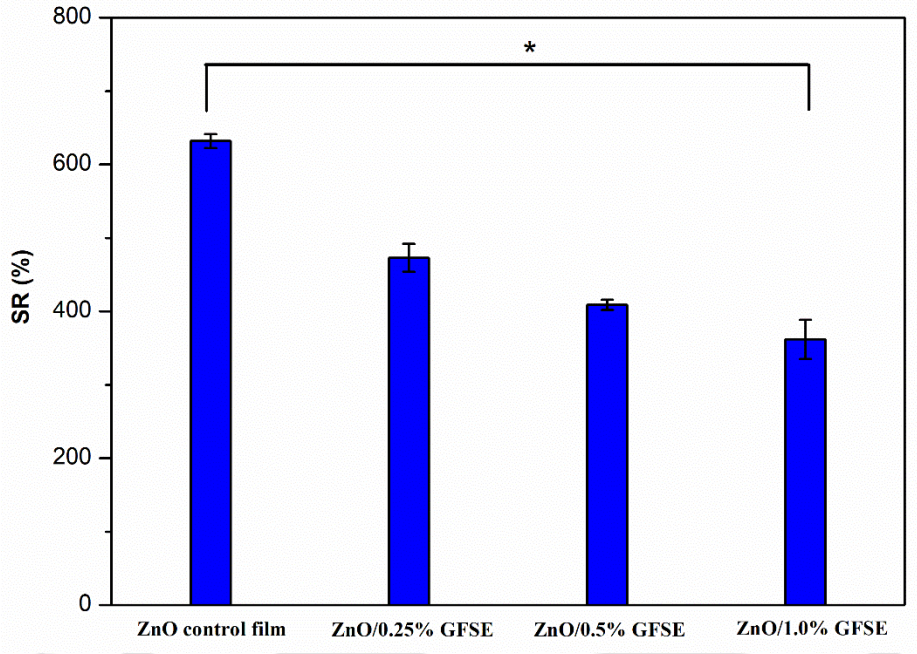

Figure 7.5. Swelling ratio (SR) of citric acid crosslinked NaCMC-HPMC hydrogel films of ZnO control and various GFSE concentrations (v/v) of 0.25%, 0.5% and 1.0% incorporated ZnO control films at 37°C in PBS (pH 7.4) for 24 h (*P<0.05 is significantly different amongst each other).

The ZnO control films showed a high SR of 632.03±9.52% at the end of 24 h. This is four times higher than the NaCMC-HPMC/20% CA films (Fig. 4.4). It might be due to the employment of CA in forming complex with ZnO, thus reducing the crosslinking degree of the polymers resulted in high SR. As the concentration of GFSE increased, the SR of the films decreased significantly (P<0.05) due to increase in crosslinking degree. The presence of citric acid, which can increase the crosslinking degree, in GFSE was confirmed by LCMS/MS analysis (Fig. A12). Hence, it is reasonable to argue that there is a possibility of GFSE components to involve in crosslinking. Also, FTIR

analysis confirmed that the accumulation of GFSE in the ZnO control films increases the ester bond to higher wavenumber due to increase in crosslinking (Table A1). The increase in crosslinking degree might be increased the hydrophobicity of films and decreased the molecular space thereby inhibiting the entry of water into the three dimensional crosslinked network.

7.2.6. Thermal property

Thermal property of synthesized ZnO powder and ZnO control films as well as GFSE incorporated hydrogel films was investigated and their TGA and DTA analysis is presented in Fig. 7.6(a-e). The decomposition temperature of CA, NaCMC and HPMC was found to be 206°C, 287°C and 355°C, respectively (Fig. 4.7A).

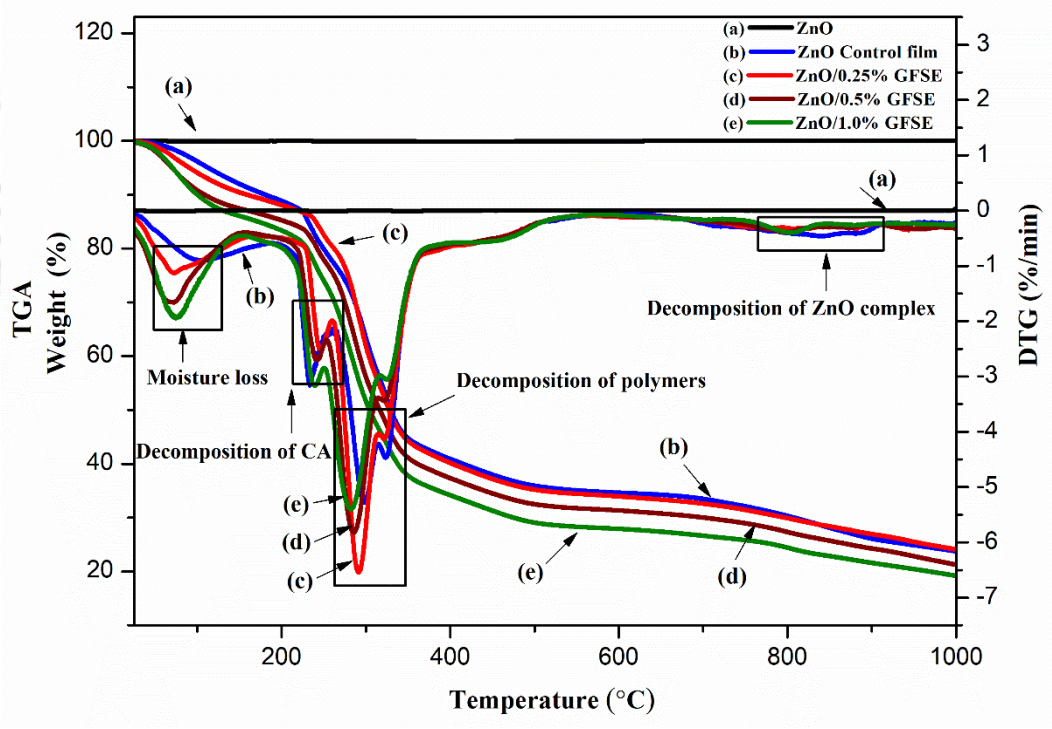

Figure 7.6. TGA and DTG analysis of (a) ZnO NPs and citric acid crosslinked NaCMC-HPMC hydrogel films of (b) ZnO control, and various GFSE concentrations (v/v) of (c) 0.25% (d) 0.5% and (e) 1.0%.

No decomposition step was observed for the synthesized ZnO from room temperature to 1000°C under N_2 atmosphere (Fig. 7.6a). The ZnO control films (Fig. 7.6b) revealed a four-step weight loss as follows: (i) evaporation of moisture upto 160°C, (ii) decomposition of CA from 230°C to 260°C, (iii) decomposition of NaCMC and HPMC from 260°C to 520°C and (iv) decomposition of ZnO complex from 710°C to 910°C. All the decomposition temperatures of ZnO control films were higher than the neat crosslinker and polymers because of the interaction amongst the precursors. All the four decomposition steps were observed for various concentrations of GFSE accumulated (Fig. 7.6c-e) ZnO control films. An amount of 0.25% GFSE (v/v) addition did not significantly change the onset decomposition temperature of CA and polymers as well as the residual mass at 1000°C (Fig. 7.6c) excluding the moisture decomposition step. However, for increasing accumulation of GFSE upto 1.0% (v/v) into the ZnO control films significantly decreased the onset decomposition temperature of CA, polymers and ZnO complex along with significant moisture loss (Fig. 7.6d,e). Furthermore, the residual mass of 0.5-1.0% GFSE added films was considerably lower compared to ZnO control films and ZnO/0.25% GFSE films. It is concluded that increasing amount of GFSE can decrease the thermal stability of films due to the presence of a large number of hydrophilic components in GFSE such as polyphenols and vitamins, which may interact with the precursor of the films. The same observation was found for GFSE incorporated agar-based films for food packaging applications (Kanmani and Rhim, 2014a).

7.2.7. Mechanical properties

It is required for a wound dressing to confirm a balance between rigidity and elasticity in order to encounter strains exerted at different body joints. Therefore, mechanical

properties of prepared hydrogel films were investigated and the results of tensile strength and elongation are shown in Figs. 7 and 8.

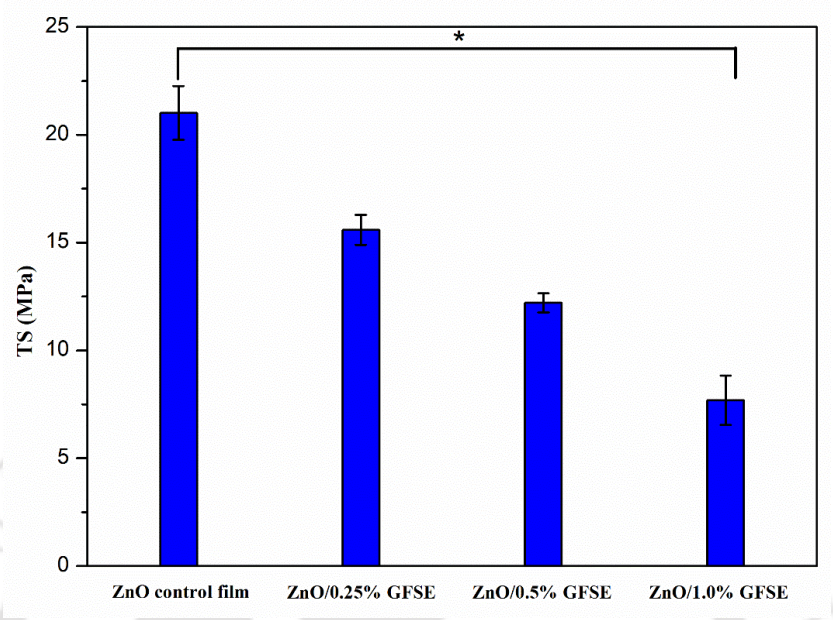

Figure 7.7. Tensile strength of citric acid crosslinked NaCMC-HPMC hydrogel films of ZnO control and various GFSE concentrations (v/v) of 0.25%, 0.5% and 1.0% incorporated ZnO control films (*P<0.05 is significantly different amongst each other).

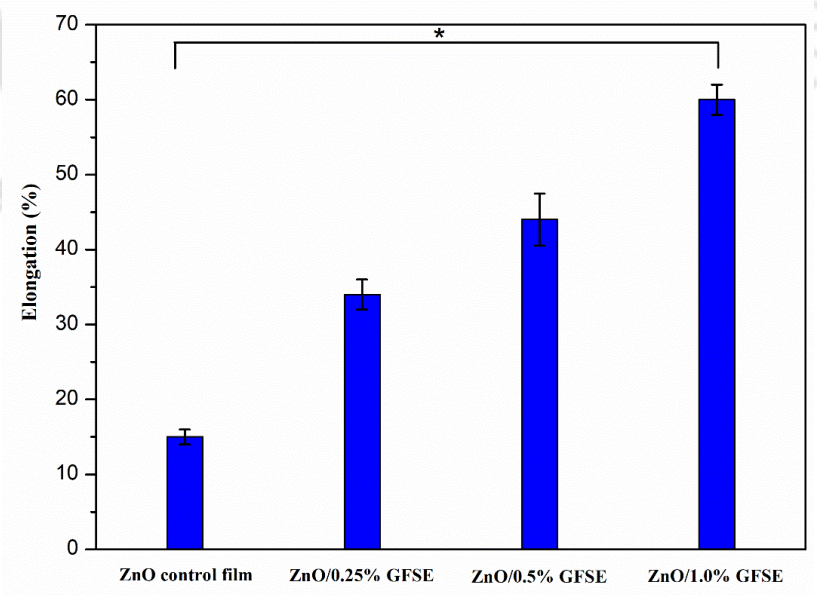

Figure 7.8. Elongation (%) of citric acid crosslinked NaCMC-HPMC hydrogel films of ZnO control and various GFSE concentrations (v/v) of 0.25%, 0.5% and 1.0% incorporated ZnO control films (*P<0.05 is significantly different amongst each other).

The ZnO control films showed tensile strength and elongation of 21.01±1.25 MPa and 15±1.09%, respectively. The incorporation of various amounts of GFSE (0.25-1.0%, v/v) significantly affected the tensile strength and elongation of hydrogel films. The addition of GFSE might have produced structural changes in the hydrogel films, resulted in decrease of tensile strength. Furthermore, decreasing of tensile strength might be attributed to decrease in the molecular interaction between the polymer (NaCMC and HPMC) strands and GFSE. The lowest value of tensile strength was found to be 7.69±1.14 MPa for 1.0% GFSE films. This drastic decrease in tensile strength could be attributed to partial replacement of stronger interactions between polymers by GFSE, which further resulted weaker polymer structures. Similar observations were made for carrageenan and chitosan-based films, which were incorporated with GFSE for packaging applications (Kanmani and Rhim, 2014b; Tan et al., 2015).

Elongation of a film reveals its flexibility. In contrast to tensile strength results, increase in GFSE concentration from 0.25% to 1.0% (v/v) dramatically increased the elongation of the hydrogel films. The highest elongation value (60±2.13%) was observed for 1.0% GFSE films. It could be attributed to the presence of polyphenolic compounds in GFSE, which might have contained repulsive charges to reduce the inter- and intra-molecular interactions of stronger polymer-polymer strands, resulting in an increased elongation of the films (Tan et al., 2015).

7.2.8. Morphology study by FESEM and FETEM analysis

The morphology of synthesized ZnO, ZnO control films and various concentrations of GFSE incorporated ZnO control films is shown in Fig. 7.9(a-e). The synthesized ZnO

showed different shapes with a diameter of 80-200 nm as shown in Fig. 7.9(a). In order to observe the nanoparticles, a higher magnification (50 KX) was used for all films.

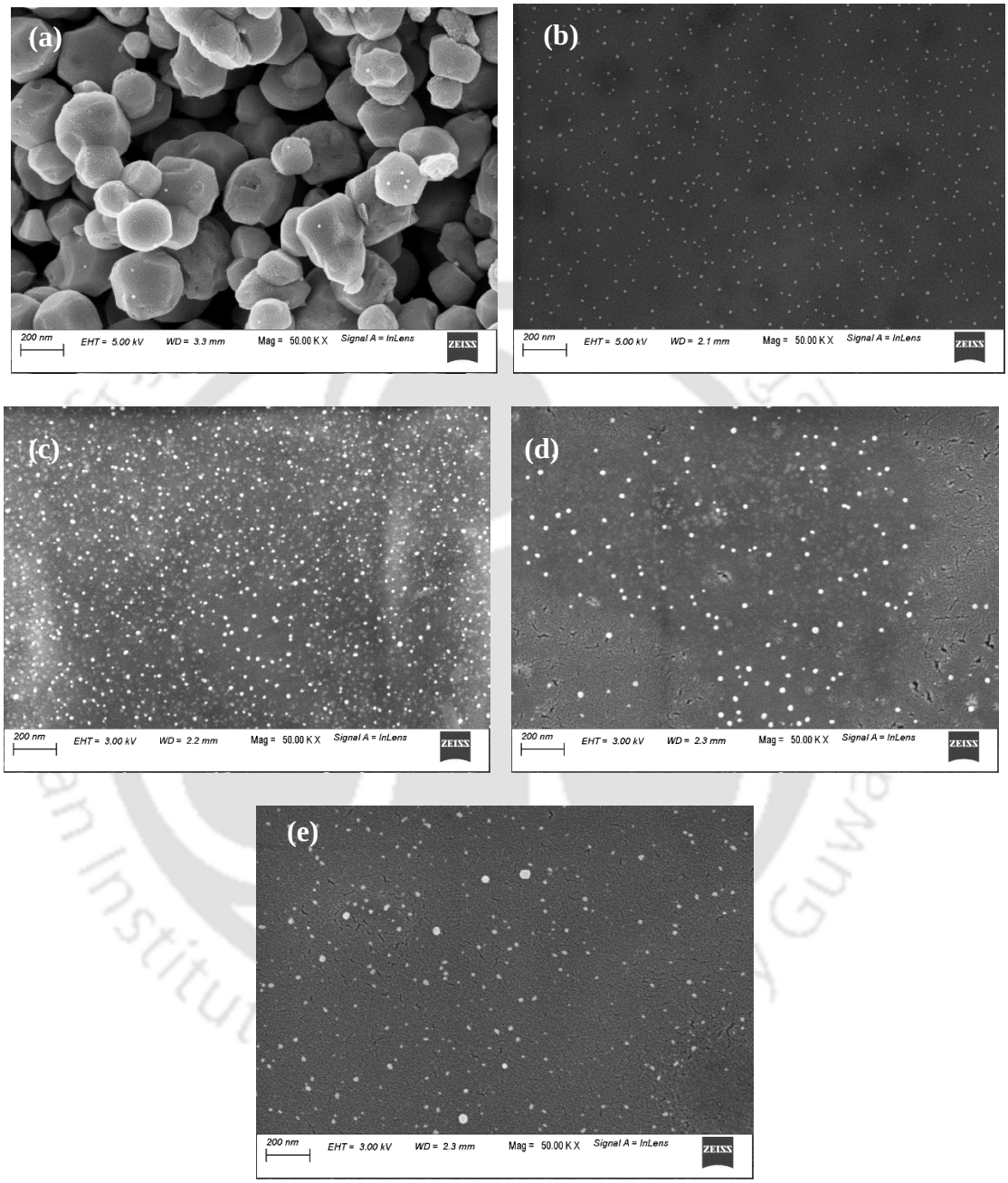

Figure 7.9. FESEM images of (a) ZnO and citric acid crosslinked NaCMC-HPMC hydrogel films of (b) ZnO control, and various GFSE concentrations (v/v) of (c) 0.25% (d) 0.5% and (e) 1.0%.

The size and shape of the nanoparticles in ZnO control films are significantly different compared to synthesized ZnO because of the CA effect on ZnO, resulting in zinc oxide complex. Two different kinds of nanoparticles were observed in all GFSE added films (Fig. 7.9c-e). For comparison, the presence of nanoparticles in GFSE incorporated hydrogel films in the absence of ZnO and citric acid is shown in Fig. A13. It is noteworthy to mention that the formation of nanoparticles was not observed in the previous studies (Kanmani and Rhim, 2014b; Tan et al., 2015).

The FETEM images of as-prepared ZnO is shown in Fig. 7.10(a). The leached out nanoparticles from ZnO control films and GFSE added films into water were examined by FETEM (Fig. 7.10b-c).

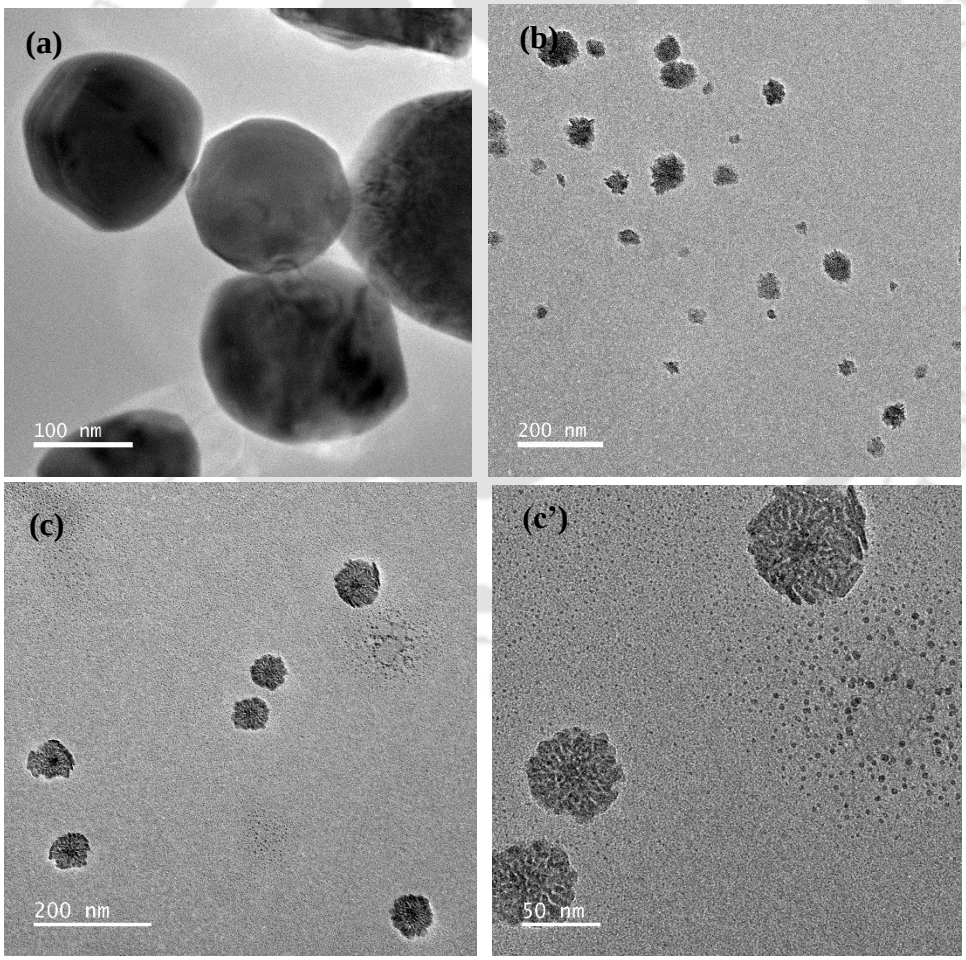

Figure 7.10. FETEM images of (a) ZnO and nanoparticles leached out from citric acid crosslinked NaCMC-HPMC hydrogel films of (b) ZnO control and (c and c') 0.25% GFSE.

An agglomeration of zinc oxide complex with particle sizes of approximately 30-100 nm was found for ZnO control films (Fig. 7.10b). The elemental mapping of zinc oxide complex is shown in Fig. A14. In order to distinguish between two different types of nanoparticles, the leached out nanoparticles from 0.25% GFSE films were carefully analysed. It is obvious from Fig. 7.10(c and c') that one type of nanoparticle showed micellar structures of 50-90 nm while other type showed spherical nanoparticles of 5-10 nm. The agglomeration of zinc oxide complex was not observed in water for 0.25% GFSE film. It could be attributed to repulsive charges amongst nanoparticles and thereby preventing the agglomeration (Fig. A15). The preliminary studies confirmed that the formation of micelles was noticed solely due to addition of GFSE into NaCMC solution (Fig. A16). The elemental mapping of a micelle (Fig. A17) showed that the hydrophobic core consisted of high amount of carbon with low amount of oxygen, probably glycerides from GFSE, while high amount of both sodium and oxygen in the outer surface is from NaCMC polymer.

7.2.9. Zinc release study

Zinc is an essential mineral element, which can accelerate wound healing. It is an added advantage for a wound dressing material, if it releases zinc in a sustained manner to the wound site. Therefore, the zinc release study was investigated and the release profile of ZnO, ZnO control film and GFSE incorporated ZnO control films is shown in Fig. 7.11(a-e). Almost negligible dissolution of synthesized ZnO was observed at pH 7.4 (Fig. 7.11a). However, ZnO control films released a significant amount of zinc within an hour and then the release became almost constant (Fig. 7.11b). At the end of 24 h, the amount of zinc release from ZnO control films was found to be approximately 15 mg/L. The initial fast release of zinc might be attributed to deprotonation of –COOH groups in CA, which could bind with ZnO to form zinc oxide complex. The addition of

various amounts of GFSE (Fig. 7.11c-e) into the control films did significantly decrease the release of zinc compared to ZnO control films. On the other hand, the zinc release was decreased for all the GFSE films. It could be due to metal chelation of polyphenols.

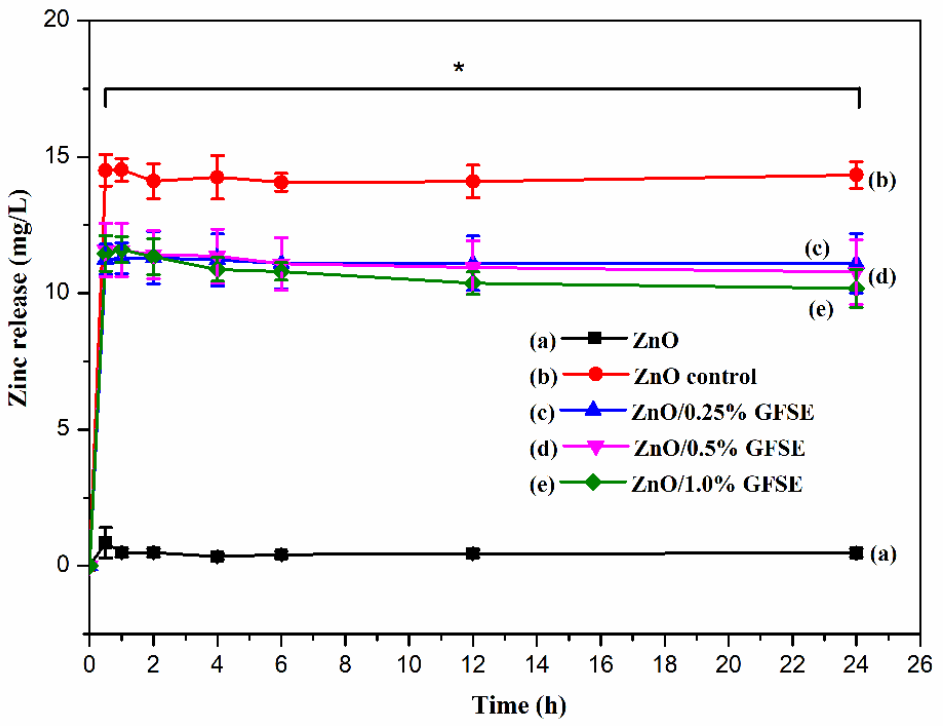

Figure 7.11. Zinc release from (a) ZnO and citric acid crosslinked NaCMC-HPMC hydrogel films of (b) ZnO control, and various GFSE concentrations (v/v) of (c) 0.25% (d) 0.5% and (e) 1.0% in PBS, pH 7.4 at 37°C (*P<0.05 is significantly different compared to GFSE incorporated films).

It is known that polyphenols chelate trace metals such as zinc, iron and copper. Furthermore, it was reported that the presence of procyanidins in GFSE could bind with zinc and thus inhibiting the zinc release (Kim et al., 2011).

7.2.10. Polyphenolic release study

In general, UV-Vis detection method is used to confirm the presence of polyphenolic compounds. As shown in Fig. 7.12A, GFSE in PBS (pH 7.4) exhibits absorption

maxima at 210, 250, 257, 263 and 269 nm. Most of the polyphenolic compounds have absorption maxima at wavelength range of 250-350 nm (Kumar, 2017).

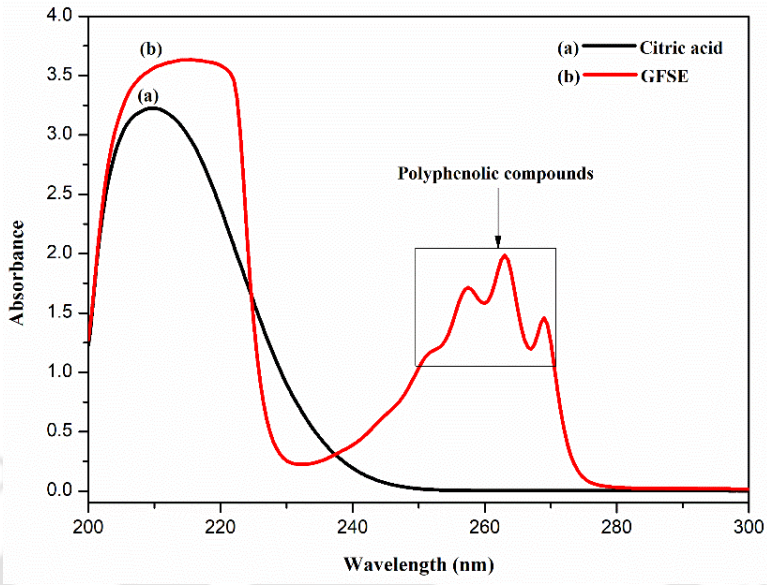

Figure 7.12A. Absorption spectrum of GFSE and citric acid in PBS (pH 7.4) by UV-Vis spectroscopy.

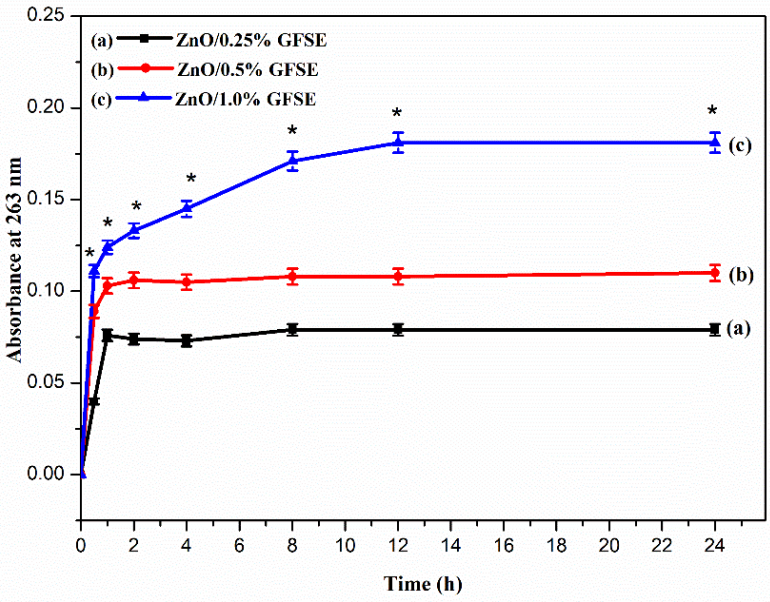

Figure 7.12B. GFSE release from citric acid crosslinked NaCMC-HPMC hydrogel films of (a) ZnO/0.25% GFSE (b) ZnO/0.5% GFSE and (c) ZnO/1.0% GFSE in PBS, pH 7.4 at 37°C (*P<0.05 is significantly different compared to other films).

An absorption band of GFSE at 210 nm is corresponded to characteristic band of CA and thus it further confirmed the presence of CA in GFSE (Krukowski et al., 2017). Since an absorption maximum at 263 nm was observed in the polyphenolic range for GFSE, it was considered to calculate the GFSE release from hydrogel films. GFSE release from various amounts of GFSE added ZnO films is shown in Fig. 7.12B (a-c). Interestingly, the rate of GFSE release was different for all hydrogel films. The absorbance of ZnO/0.25% GFSE and ZnO/0.5% GFSE hydrogel films was almost constant after an hour (Fig. 7.12B(a,b). However, the absorbance of ZnO/1.0% GFSE increased up to 12 h and then became constant (Fig. 7.12B(c)). The increase in number of carboxylic groups upon addition of GFSE might have contributed to strong interaction with polymer matrix (NaCMC and HPMC), resulting in a steady release of polyphenols from ZnO/1.0% GFSE hydrogel films.

7.2.11. Antioxidant activity by DPPH assay

The antioxidant property of hydrogel films was investigated by DPPH free radical scavenging assay (Table 1).

Table 7.1. DPPH radical scavenging activity (%) of citric acid crosslinked NaCMC-HPMC hydrogel films of ZnO control and various GFSE concentrations (v/v) of 0.25%, 0.5% and 1.0% incorporated ZnO control films.

S. No.	Sample	DPPH radical scavenging (%)
1.	ZnO control film	-
2.	ZnO/0.25% GFSE	25.84±2.42*
3.	ZnO/0.5% GFSE	43.12±1.72*
4.	ZnO/1.0% GFSE	79.4±1.04*

*P<0.05 is significantly different amongst each other.

Results of DPPH assay showed that the inhibition of DPPH free radical was found to be 25.84±2.42%, 43.12±1.72% and 79.4±1.04% for ZnO/0.25% GFSE, ZnO/0.5% GFSE and ZnO/1.0% GFSE hydrogel films, respectively. It reveals that GFSE incorporated ZnO control films has the potential to inhibit the free radicals, adding more benefit to the wound dressing materials. A significant release of polyphenols as confirmed by GFSE release study matched with increase in antioxidant activity. The antioxidant property of hydrogel films indicate that the wound healing may accelerate if these films are used as wound dressing materials.

7.2.12. Analysis of antibacterial activity

Bacterial growth on the wound bed delays the wound healing. Therefore, antibacterial activity of hydrogel films was analysed against potent wound pathogens such as *E. coli* and *S. aureus* by zone of inhibition method (Fig. 7.13). All the GFSE incorporated (0.25-1.0% GFSE, v/v) ZnO control films showed higher antibacterial activity against *E. coli* and *S. aureus* than ZnO control films due to release of polyphenolic compounds. Although the release of polyphenolic compounds from GFSE hydrogel films was higher (Fig. 7.12B(a.c)), it did not exhibit significant antibacterial activity against *E. coli* for increasing amounts of GFSE. However, ZnO/1.0% GFSE hydrogel films showed higher antibacterial activity against *S. aureus* than ZnO/0.25% GFSE hydrogel films. The antibacterial action of ZnO complex in ZnO control films might be attributed to surface adsorption, which could lead to increase in porosity of cell membrane followed by seepage cytoplasmic contents (Sirelkhatim et al., 2015).

The difference in antibacterial activity of GFSE against bacterial strains depends on its interaction with bacterial cells' surface (Bordes et al., 2019). Besides, the antibacterial mechanism of polyphenols is not completely deciphered. Several reports explained that polyphenols could modify cell membrane permeability or could bind with enzymes

which induces changes in intracellular activities and thus leakage of essential cellular constituents occurs (Bordes et al., 2019; Cushnie and Lamb, 2011; Taguri et al., 2006).

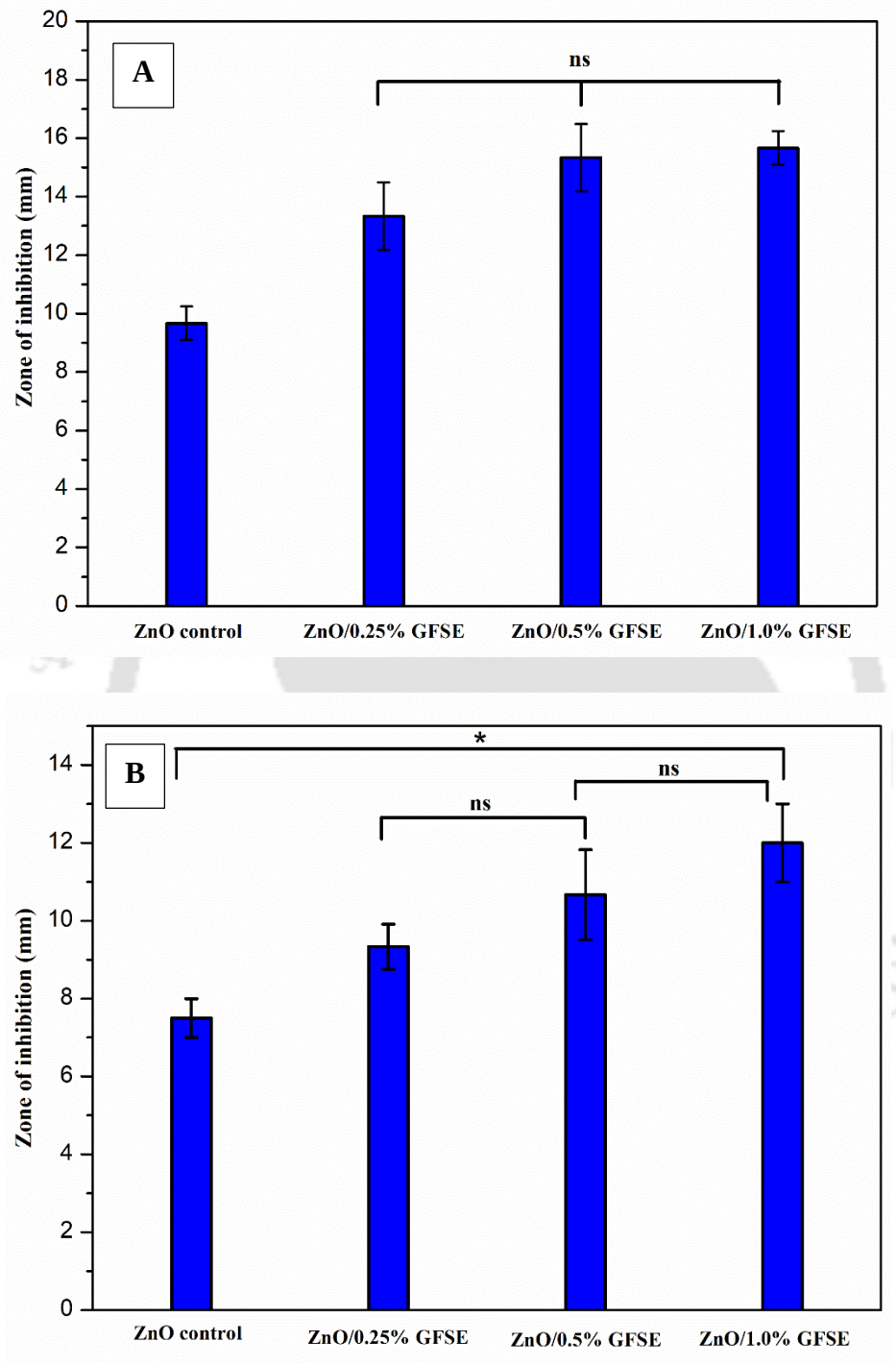

Figure 7.13. Zone of inhibition of citric acid crosslinked NaCMC-HPMC hydrogel films of ZnO control and various GFSE concentrations (v/v) of 0.25%, 0.5% and 1.0% incorporated ZnO control films against (A) *E. coli* and (B) *S. aureus* (*P<0.05 is a significant difference between films; ns is not significant).

7.2.13. Literature comparison

Hydrogel films for wound healing and drug delivery applications prepared from different additives are presented in Table 7.2 for comparison. The SR observed by Namazi et al. (2019), Jaiswal et al. (2019), Poonguzhali et al. (2018), Rakhshaei and Namazi (2017) was higher than the NaCMC-HPMC-ZnO/1.0% GFSE/20% CA hydrogel films while Das et al. (2019), Pooresmaeil and Namazi (2019), Javanbakht and Namazi (2018) reported a lower value. The SR of NaCMC-HPMC-ZnO/1.0% GFSE/20% CA hydrogel films was significantly higher than NaCMC-HPMC/20% CA, NaCMC-HPMC-ZnO/20% CA and NaCMC-HPMC-CuO/20% CA. On contrary to NaCMC-HPMC-ZnO/1.0% GFSE/20% CA hydrogel films, a higher tensile strength and lower elongation (%) were reported by Jaiswal et al. (2019), Rakhshaei and Namazi (2017), Poonguzhali et al. (2018) and Javanbakht and Namazi (2018). Amongst the prepared hydrogel films, elongation (%) was highest for NaCMC-HPMC-ZnO/1.0% GFSE/20% CA hydrogel films while tensile strength was highest for NaCMC-HPMC/20% CA. Antioxidant activity is an important property for a wound dressing material. Since, antioxidants quenches the free radical reactions and promotes wound healing. The NaCMC-HPMC-ZnO/1.0% GFSE/20% CA hydrogel films showed an excellent antioxidant activity, which were not investigated in other studies (Table 7.2). Both the fabricated hydrogel films from the current study and NaCMC/ZnO-MCM-41 films (Rakhshaei and Namazi, 2017) confirmed a strong antibacterial activity against gram negative (*E. coli*) due to the surface charge of nanoparticles. However, the hydrogel films containing citric acid, zinc oxide nanoparticles, graphene oxide-silver nanoparticles, grapefruit seed extract, sulfur nanoparticles and chitosan showed an excellent antibacterial activity against gram positive bacteria such as *Staphylococcus epidermis* or *Staphylococcus aureus* or *Listeria monocytogenes* (Das et al., 2019;

Jaiswal et al., 2019; Namazi et al., 2019; Poonguzhali et al., 2018; Pooresmaeil and Namazi, 2019).

Table 7.2. Comparative study of various polymer (nano)composite hydrogel films for wound healing and drug delivery applications.

S. No	Hydrogel film composition[a]	SR (%)	TS (MPa)	E (%)	AOA	ABA	Biocompatibility	Reference
1.	NaCMC-HPMC/20%CA/MB or TC	163	15	30	-	Yes	-	Dharmalingam and Anandalakshmi (2019)
2.	NaCMC-HPMC-ZnO/20%CA	280	13	20	-	Yes	Yes	Dharmalingam et al. (2020)
3.	NaCMC-HPMC-CuO/20%CA	220	13	18	-	Yes	Yes	Present work
4.	NaCMC-HPMC-ZnO/1.0% GFSE/20% CA	390	8	62	Yes	Yes	-	Present work
5.	NaCMC/HPMC/CA/GFSE (1%)	200	7	46	-	Yes	-	Koneru et al. (2020)
6.	NaCMC/GQD 30%/ECH	100-150	55-60	5-6	-	-	Yes	Javanbakht and Namazi (2018)
7.	PVA/starch/CA	261	2.54	38.55	-	Yes	-	Das et al. (2019)
8.	Oxidized starch/ZnO/EPH	2500-2700	-	-	-	Yes	-	Namazi et al. (2019)
9.	Carrageenan/CS/SNP/GFSE/$CuCl_2$	3750	34.7-41.5	6.6-11	-	Yes	Yes	Jaiswal et al. (2019)
10.	CS/PVP/Nano starch	430-480	35	45	-	Yes	Yes	Poonguzhali et al. (2018)
11.	NaCMC/ZnO-MCM-41/CA	22500-2500	55-60	3-4	-	Yes	Yes	Rakhshaei and Namazi (2017)
12.	PVA/β-CD/GA/GLA/HCl/GO-Ag	120-140%	170	60	-	Yes	-	Pooresmaeil and Namazi (2019)

[a]Refer abbreviations for expansion.

Nature of the polymer, type of crosslinker, size, shape and interaction of nanoparticles with the polymers in the film influenced the SR (%) and mechanical properties as discussed in the literature. From Table 7.2, it can be presumed that the fabricated hydrogel films are comparable with the recent literature in terms of SR, tensile strength, elongation (%), antibacterial activity and biocompatibility.

7.3. Closure

In this chapter, the various properties of NaCMC-HPMC-ZnO/GFSE hydrogel films are discussed. The increase in GFSE concentrations is correlated with higher elongation (%), antibacterial and antioxidant properties of hydrogel films. Further, the effect of GFSE on release of polyphenolic compounds and zinc is discussed. Next chapter (Chapter 8) presents the overall conclusions and important findings of the current work along with scope for the future research.

Chapter 8

Conclusions and scope for future work

In this chapter, the significant conclusions of the current work are briefly presented along with scope for the future work.

8.1. Overall conclusions

The major conclusions drawn on the basis of overall observations and major findings of the research work are as follows:

- It is observed that as CA concentration increases from 5% to 10%, SR, contact angle of water (surface hydrophilicity) and tensile strength of NaCMC-HPMC hydrogel films decreases while the elongation at break (%) increases.
- The average pore diameter of approximately 0.0774 ± 0.011 nm is observed for 20% CA crosslinked NaCMC-HPMC hydrogel films.
- The point of zero charge (pzc) of 5-20% CA crosslinked NaCMC-HPMC hydrogel films is found to be decreased from 5 to 4. Thus, the loading of cationic drug (methylene blue) is higher compared to anionic drug (tetracycline) at pH 7.4.
- It is observed that 5-20% CA crosslinked NaCMC-HPMC hydrogel films release methylene blue in a sustained manner upto 72 h.
- The hydrogel films of 5-20% CA crosslinked NaCMC-HPMC show a significant antibacterial activity after three days of drug release.
- Decrease in crystallinity, SR, initial decomposition temperature, tensile strength of NaCMC-HPMC-ZnO hydrogel films is observed with increase in CA concentrations due to citric acid crosslinking. However, it is found that elongation at break (%) increases with CA content.

- The characteristic peaks of ZnO are absent in NaCMC-HPMC-ZnO hydrogel films due to the formation of zinc oxide complex. According to FETEM-EDX elemental mapping, the formed complex is made up of C, O and Zn suggesting the possible complex formation of CA with ZnO.
- The fabricated NaCMC-HPMC-ZnO hydrogel films release zinc in a sustained manner for 24 h and show significant antibacterial activity against *E. coli* and *S. aureus*.
- The prepared NaCMC-HPMC-ZnO/10% and 20% CA hydrogel films show no cytotoxicity against HaCaT cells.
- The addition of 20% citric acid into CuO nanoflakes produced different nanoparticles of CuO/Cu_2O/Cu in NaCMC-HPMC-CuO hydrogel films.
- The SR of NaCMC-HPMC-CuO hydrogel films is higher than NaCMC-HPMC due to poor crosslinking.
- The presence of nanoparticles of CuO/Cu_2O/Cu in NaCMC-HPMC-CuO/20% hydrogel films decreases the elongation at break (%) as compared to NaCMC-HPMC.
- The prepared NaCMC-HPMC-CuO hydrogel films are biocompatible and shows antibacterial activity against Gram-positive and Gram-negative bacteria.
- The incorporation of GFSE and ZnO into NaCMC-HPMC significantly increases SR and elongation at break (%) compared to NaCMC-HPMC and NaCMC-HPMC- ZnO hydrogel films.
- The antibacterial activity of NaCMC-HPMC-ZnO/1% GFSE is higher than NaCMC-HPMC- ZnO hydrogel films.
- The fabricated NaCMC-HPMC-ZnO/GFSE hydrogel films release zinc and polyphenols in a sustained manner.

All these results strongly commend that the fabricated hydrogel films could find their potential applications in wound healing and drug delivery applications.

8.2. Significance of findings

- The hydrogel films of NaCMC-HPMC/20% CA is loaded with cationic drug (methylene blue). The loading efficiency is significantly (***approximately 23 times***) higher than previous reports.
- First time, ***zinc oxide complex of less than 50 nm*** is synthesized on hydrogel films for wound healing applications.
- The hydrogel films of NaCMC-HPMC-CuO/20% CA containing spherical ***nanoparticles of approximately 2-4 nm of Cu and 5-10 nm*** of Cu_2O are fabricated for wound healing applications.
- First time, ***micellar nanoparticle consists of NaCMC and GFSE with a size of 50-90 nm*** are synthesized.
- The elongation at break (%) of NaCMC-HPMC-ZnO/1% GFSE hydrogel films is significantly higher than previous reports.

8.3. Scope for future work

A few problems relevant to the current topic are discussed below for possible future study.

- Investigation of the polymer nanospheres of NaCMC and HPMC for loading of hydrophilic/hydrophobic drugs would be helpful in cancer therapy.
- It would be interesting to study the zinc oxide complexes for nanomedicine and tissue engineering applications.
- In the present study, a uniform spherical nanoparticles of CuO, Cu_2O and Cu are leached out from 20% CA crosslinked NaCMC-HPMC films. It would be

helpful to produce such kind of nanoparticles without polymers using citric acid for various applications such as cosmetics, sensors and nanofluids in heat transfer.

- It would be fascinating to prepare monodispersed micellar nanoparticles consist of NaCMC and GFSE for targeted drug delivery in cancer therapy.
- The prepared NaCMC-HPMC-ZnO/1% GFSE hydrogel films show high swelling capability, antioxidant activity and antibacterial activity against both Gram positive and Gram negative bacteria. Therefore, it would be very helpful to investigate the hydrogel films as baby diapers.
- The protein adsorption study on fabricated hydrogel films would be useful for tissue engineering applications.
- It would be interesting to study the fabricated hydrogel films to store the perishable foods.

8.4. Closure

In this chapter, significant conclusive remarks based on the thesis along with the scope for future work have been presented.

References

Abd El-Mohdy, H.L., 2007. Water sorption behavior of CMC/PAM hydrogels prepared by γ-irradiation and release of potassium nitrate as agrochemical. React. Funct. Polym. 67, 1094–1102.

Abd El-Rehim, H.A., Hegazy, E.S.A., Diaa, D.A., 2006. Characterization of super-absorbent material based on carboxymethylcellulose sodium salt prepared by electron beam irradiation. J. Macromol. Sci. - Pure Appl. Chem. A 43, 101–113.

Abou-Yousef, H., Kamel, S., 2015. High efficiency antimicrobial cellulose-based nanocomposite hydrogels. J. Appl. Polym. Sci. 132, 1–9.

Ahmed, B., Solanki, B., Zaidi, A., Khan, M.S., Musarrat, J., 2019. Bacterial toxicity of biomimetic green zinc oxide nanoantibiotic: insights into ZnONP uptake and nanocolloid-bacteria interface. Toxicol. Res. (Camb). 8, 246–261.

Ahmed, E.M, 2015. Hydrogel: Preparation, characterization, and applications: A review. J. Adv. Res. 6, 105–121.

Ahrari, F., Eslami, N., Rajabi, O., Ghazvini, K., Barati, S., 2015. The antimicrobial sensitivity of Streptococcus mutans and Streptococcus sangius to colloidal solutions of different nanoparticles applied as mouthwashes. Dent. Res. J. (Isfahan). 12, 44.

Akhtar, N., Metkar, S.K., Girigoswami, A., Girigoswami, K., 2017. ZnO nanoflower based sensitive nano-biosensor for amyloid detection. Mater. Sci. Eng. C 78, 960–968.

Ali, N.H., Amin, M.C.I.M., Ng, S.-F., 2019. Sodium carboxymethyl cellulose hydrogels containing reduced graphene oxide (rGO) as a functional antibiofilm wound dressing. J. Biomater. Sci. Polym. Ed. 30, 629–645.

Alshehri, S.M., Aldalbahi, A., Al-Hajji, A.B., Chaudhary, A.A., Panhuis, M. In Het,

Alhokbany, N., Ahamad, T., 2016. Development of carboxymethyl cellulose-based hydrogel and nanosilver composite as antimicrobial agents for UTI pathogens. Carbohydr. Polym. 138, 229–236.

Anandan, S., Yang, S., 2007. Emergent methods to synthesize and characterize semiconductor CuO nanoparticles with various morphologies--an overview. J. Exp. Nanosci. 2, 23–56.

Andrews, B.A.K., 1989. Non-formaldehyde durable press finishing of cotton with citric acid, in: Book of Papers-American Association of Textile Chemists and Colorists, International Conference & Exhibition.

Arica, M.Y., 2000. Immobilization of polyphenol oxidase on carboxymethylcellulose hydrogel beads: Preparation and characterization. Polym. Int. 49, 775–781.

Augustine, R., Dominic, E.A., Reju, I., Kaimal, B., Kalarikkal, N., Thomas, S., 2014. Electrospun polycaprolactone membranes incorporated with ZnO nanoparticles as skin substitutes with enhanced fibroblast proliferation and wound healing. Rsc Adv. 4, 24777–24785.

Bajpai, A.K., Giri, A., 2003. Water sorption behaviour of highly swelling (carboxy methylcellulose-g-polyacrylamide) hydrogels and release of potassium nitrate as agrochemical. Carbohydr. Polym. 53, 271–279.

Bajpai, S.K., Ahuja, S., Chand, N., Bajpai, M., 2017. Nano cellulose dispersed chitosan film with Ag NPs/Curcumin: An in vivo study on Albino Rats for wound dressing. Int. J. Biol. Macromol. 104, 1012–1019.

Bao, D., Chen, M., Wang, H., Wang, J., Liu, C., Sun, R., 2014. Preparation and characterization of double crosslinked hydrogel films from carboxymethylchitosan and carboxymethylcellulose. Carbohydr. Polym. 110, 113–120.

Bao, Y., Ma, J., Li, N., 2011. Synthesis and swelling behaviors of sodium carboxymethyl cellulose-g-poly(AA-co-AM-co-AMPS)/MMT superabsorbent hydrogel. Carbohydr. Polym. 84, 76–82.

Bao, Y., Ma, J., Sun, Y., 2012. Swelling behaviors of organic/inorganic composites based on various cellulose derivatives and inorganic particles. Carbohydr. Polym. 88, 589–595.

Barros, S.C., da Silva, A.A., Costa, D.B., Cesarino, I., Costa, C.M., Lanceros-Méndez, S., Pawlicka, A., Silva, M.M., 2014. Thermo-sensitive chitosan–cellulose derivative hydrogels: swelling behaviour and morphologic studies. Cellulose 21, 4531–4544.

Barros, S.C., da Silva, A.A., Costa, D.B., Costa, C.M., Lanceros-Méndez, S., Maciavello, M.N.T., Ribelles, J.L.G., Sentanin, F., Pawlicka, A., Silva, M.M., 2015. Thermal–mechanical behaviour of chitosan–cellulose derivative thermoreversible hydrogel films. Cellulose 22, 1911–1929.

Bertoli, A.C., Carvalho, R., Freitas, M.P., Ramalho, T.C., Mancini, D.T., Oliveira, M.C., De Varennes, A., Dias, A., 2015. Theoretical and experimental investigation of complex structures citrate of zinc (II). Inorganica Chim. Acta 425, 164–168.

Boateng, J.S., Matthews, K.H., Stevens, H.N.E., Eccleston, G.M., 2008. Wound healing dressings and drug delivery systems: a review. J. Pharm. Sci. 97, 2892–2923.

Boer, M., Duchnik, E., Maleszka, R., Marchlewicz, M., 2016. Structural and biophysical characteristics of human skin in maintaining proper epidermal barrier function. Adv. Dermatology Allergol. Dermatologii i Alergol. 33, 1.

Bordes, C., Bouarab-Chibane, L., Forquet, V., Lantéri, P., Clément, Y., Leonard, L., Oulahal, N., Degraeve, P., 2019. Antibacterial properties of polyphenols: characterization and QSAR (Quantitative structure--activity relationship) models.

Front. Microbiol. 10, 829.

Bozaci, E., Akar, E., Ozdogan, E., Demir, A., Altinisik, A., Seki, Y., 2015. Application of carboxymethylcellulose hydrogel based silver nanocomposites on cotton fabrics for antibacterial property. Carbohydr. Polym. 134, 128–135.

Buhus, G., Popa, M., Peptu, C., Desbrieres, J., 2007. Hydrogels based on carboxymethylcellulose and poly (vinyl alcohol) for controlled loading and release of chloramphenicol. J Optoelectron. Adv. M. 9, 3445–3453.

Burkert, S., Schmidt, T., Gohs, U., Dorschner, H., Arndt, K.-F., 2007. Cross-linking of poly (N-vinyl pyrrolidone) films by electron beam irradiation. Radiat. Phys. Chem. 76, 1324–1328.

Caló, E., Khutoryanskiy, V. V., 2015. Biomedical applications of hydrogels: A review of patents and commercial products. Eur. Polym. J. 65, 252–267.

Cangul, I.T., Gul, N.Y., Topal, A., Yilmaz, R., 2006. Evaluation of the effects of topical tripeptide-copper complex and zinc oxide on open-wound healing in rabbits. Vet. Dermatol. 17, 417–423.

Cao, X.T., Showkat, A.M., Bach, L.G., Lee, W.K., Lim, K.T., 2014. Preparation and characterization of poly(4-vinylpyridine) encapsulated zinc oxide by surface-initiated RAFT polymerization. Mol. Cryst. Liq. Cryst. 599, 55–62.

Capanema, N.S.V., Mansur, A.A.P., Carvalho, S.M., Carvalho, I.C., Chagas, P., de Oliveira, L.C.A., Mansur, H.S., 2018a. Bioengineered carboxymethyl cellulose-doxorubicin prodrug hydrogels for topical chemotherapy of melanoma skin cancer. Carbohydr. Polym. 195, 401–412.

Capanema, N.S. V, Mansur, A.A.P., Carvalho, S.M., Mansur, L.L., Ramos, C.P., Lage, A.P., Mansur, H.S., 2018b. Physicochemical properties and antimicrobial activity of biocompatible carboxymethylcellulose-silver nanoparticle hybrids for wound

dressing and epidermal repair. J. Appl. Polym. Sci. 135, 45812.

Capanema, N.S. V, Mansur, A.A.P., de Jesus, A.C., Carvalho, S.M., de Oliveira, L.C., Mansur, H.S., 2018c. Superabsorbent crosslinked carboxymethyl cellulose-PEG hydrogels for potential wound dressing applications. Int. J. Biol. Macromol. 106, 1218–1234.

Carrillo-Rodriguez, J.C., Meléndez-Ortiz, H.I., Puente-Urbina, B., Padron, G., Ledezma, A., Betancourt-Galindo, R., 2018. Composite based on poly (acrylic acid-co-itaconic acid) hydrogel with antibacterial performance. Polym. Compos. 39, 171–180.

Chang, C., Duan, B., Cai, J., Zhang, L., 2010. Superabsorbent hydrogels based on cellulose for smart swelling and controllable delivery. Eur. Polym. J. 46, 92–100.

Chang, C., He, M., Zhou, J., Zhang, L., 2011. Swelling behaviors of pH-and salt-responsive cellulose-based hydrogels. Macromolecules 44, 1642–1648.

Charpentier, D., Mocanu, G., Carpov, A., Chapelle, S., Merle, L., Müller, G., 1997. New hydrophobically modified carboxymethylcellulose derivatives. Carbohydr. Polym. 33, 177–186.

Chatterji, P.R., Kaur, H., 1992. Interpenetrating hydrogel networks: 3. Properties of the gelatin-sodium carboxymethylcellulose system. Polymer (Guildf). 33, 2388–2391.

Chaurasiya, S., Udaya Bhanu, J., Thangadurai, P., 2018. Precursor Dependent Structural Phase Evolution in Hydrothermally Prepared Cu_2O Octahedrons and Cu Micro-Flakes and Their Structural and Optical Properties. Trans. Indian Inst. Met. 71, 1185–1191.

Chen, H., An, Y., Yan, X., McClements, D.J., Li, B., Li, Y., 2015. Designing self-nanoemulsifying delivery systems to enhance bioaccessibility of hydrophobic

bioactives (nobiletin): Influence ofhydroxypropyl methylcellulose and thermal processing. Food Hydrocoll. 51, 395–404.

Chen, Z., Meng, H., Xing, G., Chen, C., Zhao, Y., Jia, G., Wang, T., Yuan, H., Ye, C., Zhao, F., 2006. Acute toxicological effects of copper nanoparticles in vivo. Toxicol. Lett. 163, 109–120.

Cho, S.-H., Seo, I.-W., Choi, J.-D., Joo, I.-S., 1990. Antimicrobial and antioxidant activity of grapefruit and seed extract on fishery products. Korean J. Fish. Aquat. Sci. 23, 289–296.

Cho, Y.-S., Kim, S.-K., Ahn, C.-B., Je, J.-Y., 2011. Preparation, characterization, and antioxidant properties of gallic acid-grafted-chitosans. Carbohydr. Polym. 83, 1617–1622.

Chopra, S., Patil, G. V, Motwani, S.K., 2007. Release modulating hydrophilic matrix systems of losartan potassium: optimization of formulation using statistical experimental design. Eur. J. Pharm. Biopharm. 66, 73–82.

Cirillo, G., Kraemer, K., Fuessel, S., Puoci, F., Curcio, M., Spizzirri, U.G., Altimari, I., Iemma, F., 2010. Biological activity of a gallic acid- gelatin conjugate. Biomacromolecules 11, 3309–3315.

Cushnie, T.P.T., Lamb, A.J., 2011. Recent advances in understanding the antibacterial properties of flavonoids. Int. J. Antimicrob. Agents 38, 99–107.

Das, A., Uppaluri, R., Das, C., 2019. Feasibility of poly-vinyl alcohol/starch/glycerol/citric acid composite films for wound dressing applications. Int. J. Biol. Macromol. 131, 998–1007.

Das, R., Das, D., Ghosh, P., Dhara, S., Panda, A.B., Pal, S., 2015. Development and application of a nanocomposite derived from crosslinked HPMC and Au nanoparticles for colon targeted drug delivery. RSC Adv. 5, 27481–27490.

Deepachitra, R., Lakshmi, R.P., Sivaranjani, K., Chandra, J.H., Sastry, T.P., 2015. Nanoparticles embedded biomaterials in wound treatment: a review. J. Chem. Pharm. Sci. 8, 324–329.

Demitri, C., Del Sole, R., Scalera, F., Sannino, A., Vasapollo, G., Maffezzoli, A., Ambrosio, L., Nicolais, L., 2008. Novel superabsorbent cellulose-based hydrogels crosslinked with citric acid. J. Appl. Polym. Sci. 110, 2453–2460.

Deng, J., He, Q., Wu, Z., Yang, W., 2008. Using glycidyl methacrylate as cross-linking agent to prepare thermosensitive hydrogels by a novel one-step method. J. Polym. Sci. Part A Polym. Chem. 46, 2193–2201.

Deng, Y., Handoko, A.D., Du, Y., Xi, S., Yeo, B.S., 2016. In Situ Raman Spectroscopy of Copper and Copper Oxide Surfaces during Electrochemical Oxygen Evolution Reaction: Identification of CuIII Oxides as Catalytically Active Species. ACS Catal. 6, 2473–2481.

Dharmalingam, K, Anandalakshmi, R., 2019. Fabrication, characterization and drug loading efficiency of citric acid crosslinked NaCMC-HPMC hydrogel films for wound healing drug delivery applications. Int. J. Biol. Macromol. 134, 815–829.

Dharmalingam, K., Devivasha B., Kunnumakkara A.B., Anandalakshmi R., 2020. Formation and characterization of zinc oxide complexes in composite hydrogel films for potential wound healing applications. Polym. Compos. Accepted: https://doi.org/10.1002/pc.25538.

Dharmalingam, K., Padmavathi, G., Kunnumakkara, A.B., Anandalakshmi, R., 2019. Microwave-assisted synthesis of cellulose/zinc-sulfate-calcium-phosphate (ZSCAP) nanocomposites for biomedical applications. Mater. Sci. Eng. C 100, 535–543.

Dilaver, M., Yurdakoc, K., 2016. Fumaric acid cross-linked

carboxymethylcellulose/poly(vinyl alcohol) hydrogels. Polym. Bull. 73, 2661–2675.

Ding, C., Zhang, M., Li, G., 2015. Preparation and characterization of collagen/hydroxypropyl methylcellulose (HPMC) blend film. Carbohydr. Polym. 119, 194–201.

Don, T.M., Huang, M.L., Chiu, A.C., Kuo, K.H., Chiu, W.Y., Chiu, L.H., 2008. Preparation of thermo-responsive acrylic hydrogels useful for the application in transdermal drug delivery systems. Mater. Chem. Phys. 107, 266–273.

Du, J., Wong, K.K.Y., 2019. Nanomaterials for Wound Healing: Scope and Advances, in: Theranostic Bionanomaterials. Elsevier, pp. 211–230.

El-Hag Ali, A., Abd El-Rehim, H.A., Kamal, H., Hegazy, D.E.S.A., 2008. Synthesis of carboxymethyl cellulose based drug carrier hydrogel using ionizing radiation for possible use as site specific delivery system. J. Macromol. Sci. Part A Pure Appl. Chem. 45, 628–634.

El-Mohdy, H.L.A., 2014. Radiation initiated synthesis of 2-acrylamidoglycolic acid grafted carboxymethyl cellulose as pH-sensitive hydrogel. Polym. Eng. Sci. 54, 2753–2761.

El-Mohdy, H.L.A., 2007. Water sorption behavior of CMC/PAM hydrogels prepared by γ-irradiation and release of potassium nitrate as agrochemical. React. Funct. Polym. 67, 1094–1102.

El Salmawi, Kariman M, 2007. Application of polyvinyl alcohol (PVA)/carboxymethyl cellulose (CMC) hydrogel produced by conventional crosslinking or by freezing and thawing. J. Macromol. Sci. Part A Pure Appl. Chem. 44, 619–624.

Ethiraj, A.S., Kang, D.J., 2012. Synthesis and characterization of CuO nanowires by a simple wet chemical method. Nanoscale Res. Lett. 7, 1–12.

Farbun, I.A., Romanova, I. V., Terikovskaya, T.E., Dzanashvili, D.I., Kirillov, S.A., 2007. Complex formation in the course of synthesis of zinc oxide from citrate solutions. Russ. J. Appl. Chem. 80, 1798–1803.

Fei, B., Wach, R.A., Mitomo, H., Yoshii, F., Kume, T., 2000. Hydrogel of biodegradable cellulose derivatives. I. Radiation-induced crosslinking of CMC. J. Appl. Polym. Sci. 78, 278–283.

Fekete, T., Borsa, J., Takács, E., Wojnárovits, L., 2016. Synthesis of carboxymethylcellulose/acrylic acid hydrogels with superabsorbent properties by radiation-initiated crosslinking. Radiat. Phys. Chem. 124, 135–139.

Fekete, T., Borsa, J., Takács, E., Wojnárovits, L., 2014. Synthesis of cellulose derivative based superabsorbent hydrogels by radiation induced crosslinking. Cellulose 21, 4157–4165.

Filippov, S., Wang, X.J., Devika, M., Koteeswara Reddy, N., Tu, C.W., Chen, W.M., Buyanova, I.A., 2013. Effects of Ni-coating on ZnO nanowires: A Raman scattering study. J. Appl. Phys. 113, 214302.

Fitzmaurice, S.D., Sivamani, R.K., Isseroff, R.R., 2011. Antioxidant therapies for wound healing: A clinical guide to currently commercially available products. Skin Pharmacol. Physiol. 24, 113–126.

Fu, P.P., Xia, Q., Hwang, H.M., Ray, P.C., Yu, H., 2014. Mechanisms of nanotoxicity: Generation of reactive oxygen species. J. Food Drug Anal. 22, 64–75.

Gajjar, P., Pettee, B., Britt, D.W., Huang, W., Johnson, W.P., Anderson, A.J., 2009. Antimicrobial activities of commercial nanoparticles against an environmental soil microbe, *Pseudomonas putida* KT2440. J. Biol. Eng. 3, 9.

Gao, F., Pang, H., Xu, S., Lu, Q., 2009. Copper-based nanostructures: Promising antibacterial agents and photocatalysts. Chem. Commun. 24, 3571–3573.

Gao, L., Gan, H., Meng, Z., Gu, R., Wu, Z., Zhu, X., Sun, W., Li, J., Zheng, Y., Sun, T., Dou, G., 2016. Evaluation of genipin-crosslinked chitosan hydrogels as a potential carrier for silver sulfadiazine nanocrystals. Colloids Surfaces B Biointerfaces 148, 343–353.

George, S., Pokhrel, S., Xia, T., Gilbert, B., Ji, Z., Schowalter, M., Rosenauer, A., Damoiseaux, R., Bradley, K.A., Mädler, L., 2009. Use of a rapid cytotoxicity screening approach to engineer a safer zinc oxide nanoparticle through iron doping. ACS Nano 4, 15–29.

Ghorpade, V.S., Yadav, A.V., Dias, R.J., 2017. Citric acid crosslinked β-cyclodextrin/carboxymethylcellulose hydrogel films for controlled delivery of poorly soluble drugs. Carbohydr. Polym. 164, 339–348.

Ghorpade, V.S., Yadav, A.V., Dias, R.J., 2016. Citric acid crosslinked cyclodextrin/hydroxypropylmethylcellulose hydrogel films for hydrophobic drug delivery. Int. J. Biol. Macromol. 93, 75–86.

Goh, Y.-F., Shakir, I., Hussain, R., 2013. Electrospun fibers for tissue engineering, drug delivery, and wound dressing. J. Mater. Sci. 48, 3027–3054.

Gorgieva, S., Kokol, V., 2011. Synthesis and application of new temperature-responsive hydrogels based on carboxymethyl and hydroxyethyl cellulose derivatives for the functional finishing of cotton knitwear. Carbohydr. Polym. 85, 664–673.

Grabovac, V., Guggi, D., Bernkop-Schnürch, A., 2005. Comparison of the mucoadhesive properties of various polymers. Adv. Drug Deliv. Rev. 57, 1713–1723.

Güldiken, Ç.G., Karaosmanouglu, O., Sivas, H., Gerçel, H.F., 2020. ZnO microparticle-loaded chitosan/poly (vinyl alcohol)/acacia gum nanosphere-based

nanocomposite thin film wound dressings for accelerated wound healing. J. Appl. Polym. Sci. 137, 48445.

Guo, K., Chu, C.C., 2005. Synthesis and characterization of novel biodegradable unsaturated poly (ester amide)/poly (ethylene glycol) diacrylate hydrogels. J. Polym. Sci. Part A Polym. Chem. 43, 3932–3944.

Guo, S., DiPietro, L.A., 2010. Critical review in oral biology & medicine: Factors affecting wound healing. J. Dent. Res. 89, 219–229.

Gurtner, G.C., Werner, S., Barrandon, Y., Longaker, M.T., 2008. Wound repair and regeneration. Nature 453, 314.

Hamdan, S., Pastar, I., Drakulich, S., Dikici, E., Tomic-Canic, M., Deo, S., Daunert, S., 2017. Nanotechnology-driven therapeutic interventions in wound healing: Potential uses and applications. ACS Cent. Sci. 3, 163–175.

Handore, K., Bhavsar, S., Horne, A., Chhattise, P., Mohite, K., Ambekar, J., Pande, N., Chabukswar, V., 2014. Novel green route of synthesis of ZnO nanoparticles by using natural biodegradable polymer and its application as a catalyst for oxidation of aldehydes. J. Macromol. Sci. Part A Pure Appl. Chem. 51, 941–947.

Hasan, A., Waibhaw, G., Tiwari, S., Dharmalingam, K., Shukla, I., Pandey, L.M., 2017. Fabrication and characterization of chitosan, polyvinylpyrrolidone, and cellulose nanowhiskers nanocomposite films for wound healing drug delivery application, Journal of Biomedical Materials Research - Part A 105, 2391-2404.

Hashem, M., Sharaf, S., Abd El-Hady, M.M., Hebeish, A., 2013. Synthesis and characterization of novel carboxymethylcellulose hydrogels and carboxymethylcellulolse-hydrogel-ZnO-nanocomposites. Carbohydr. Polym. 95, 421–427.

Hebeish, A., Sharaf, S., 2015. Novel nanocomposite hydrogel for wound dressing and

other medical applications. RSC Adv. 5, 103036–103046.

Heggers, J.P., Cottingham, J., Gusman, J., Reagor, L., McCoy, L., Carino, E., Cox, R., Zhao, J.-G., 2002. The effectiveness of processed grapefruit-seed extract as an antibacterial agent: II. Mechanism of action and in vitro toxicity. J. Altern. Complement. Med. 8, 333–340.

Hennink, W.E., van Nostrum, C.F., 2012. Novel crosslinking methods to design hydrogels. Adv. Drug Deliv. Rev. 64, 223–236.

Hoffman, A.S., 2012. Hydrogels for biomedical applications. Adv. Drug Deliv. Rev. 64, 18–23.

Huang, Y.-W., Cambre, M., Lee, H.-J., 2017. The toxicity of nanoparticles depends on multiple molecular and physicochemical mechanisms. Int. J. Mol. Sci. 18, 2702.

Hussain, A., Oves, M., Alajmi, M.F., Hussain, I., Amir, S., Ahmed, J., Rehman, M.T., El-Seedi, H.R., Ali, I., 2019. Biogenesis of ZnO nanoparticles using Pandanus odorifer leaf extract: anticancer and antimicrobial activities. RSC Adv. 9, 15357–15369.

Ibrahim, M.M., Koschella, A., Kadry, G., Heinze, T., 2013. Evaluation of cellulose and carboxymethyl cellulose/poly(vinyl alcohol) membranes. Carbohydr. Polym. 95, 414–420.

Ibrahim, S.M., Abou El Fadl, F.I., El-Naggar, A.A., 2014. Preparation and characterization of crosslinked alginate-CMC beads for controlled release of nitrate salt. J. Radioanal. Nucl. Chem. 299, 1531–1537.

Iohara, D., Okubo, M., Anraku, M., Uramatsu, S., Shimamoto, T., Uekama, K., Hirayama, F., 2017. Hydrophobically modified polymer/α-cyclodextrin thermoresponsive hydrogels for use in ocular drug delivery. Mol. Pharm. 14, 2740–2748.

Jaiswal, L., Shankar, S., Rhim, J.W., 2019. Carrageenan-based functional hydrogel film reinforced with sulfur nanoparticles and grapefruit seed extract for wound healing application. Carbohydr. Polym. 224, 115191.

Jantrawut, P., Bunrueangtha, J., Suerthong, J., Kantrong, N., 2019. Fabrication and Characterization of Low Methoxyl Pectin/Gelatin/Carboxymethyl Cellulose Absorbent Hydrogel Film for Wound Dressing Applications. Materials (Basel). 12, 1628.

Javanbakht, S., Namazi, H., 2018. Doxorubicin loaded carboxymethyl cellulose/graphene quantum dot nanocomposite hydrogel films as a potential anticancer drug delivery system. Mater. Sci. Eng. C 87, 50–59.

Joorabloo, A., Khorasani, M.T., Adeli, H., Mansoori-Moghadam, Z., Moghaddam, A., 2019. Fabrication of heparinized nano ZnO/poly (vinylalcohol)/carboxymethyl cellulose bionanocomposite hydrogels using artificial neural network for wound dressing application. J. Ind. Eng. Chem. 70, 253–263.

Joshi, S.C., 2011. Sol-gel behavior of hydroxypropyl methylcellulose (HPMC) in ionic media including drug release. Materials (Basel). 4, 1861–1905.

Kamoun, E.A., Kenawy, E.R.S., Chen, X., 2017. A review on polymeric hydrogel membranes for wound dressing applications: PVA-based hydrogel dressings. J. Adv. Res. 8, 217–233.

Kanatt, S.R., Makwana, S.H., 2020. Development of active, water-resistant carboxymethyl cellulose-poly vinyl alcohol-Aloe vera packaging film. Carbohydr. Polym. 227, 115303.

Kanmani, P., Rhim, J.W., 2014a. Antimicrobial and physical-mechanical properties of agar-based films incorporated with grapefruit seed extract. Carbohydr. Polym. 102, 708–716.

Kanmani, P., Rhim, J.W., 2014b. Development and characterization of carrageenan/grapefruit seed extract composite films for active packaging. Int. J. Biol. Macromol. 68, 258–266.

Kannan, P.K., Saraswathi, R., 2017. An impedance sensor for the detection of formaldehyde vapor using ZnO nanoparticles. J. Mater. Res. 32, 2800–2809.

Khan, M.I., Behera, S.K., Paul, P., Das, B., Suar, M., Jayabalan, R., Fawcett, D., Poinern, G.E.J., Tripathy, S.K., Mishra, A., 2019. Biogenic Au@ ZnO core--shell nanocomposites kill Staphylococcus aureus without provoking nuclear damage and cytotoxicity in mouse fibroblasts cells under hyperglycemic condition with enhanced wound healing proficiency. Med. Microbiol. Immunol. 208, 609–629.

Kim, B., Kang, B., Vales, T.P., Yang, S.K., Lee, J., Kim, H.J., 2018. Polyphenol-functionalized hydrogels using an interpenetrating chitosan network and investigation of their antioxidant activity. Macromol. Res. 26, 35–39.

Kim, E.-Y., Pai, T.-K., Han, O., 2011. Effect of bioactive dietary polyphenols on zinc transport across the intestinal Caco-2 cell monolayers. J. Agric. Food Chem. 59, 3606–3612.

Kim, S. hee, Chu, C.C., 2000. Pore structure analysis of swollen dextran-methacrylate hydrogels by SEM and mercury intrusion porosimetry. J. Biomed. Mater. Res. 53, 258–266.

Kök, F.N., Wilkins, R.M., Cain, R.B., Arica, M.Y., Alaeddinoğlu, G., Hasirci, V., 1999. Controlled release of aldicarb from lignin loaded ionotropic hydrogel microspheres. J. Microencapsul. 16, 613–623.

Kondaveeti, S., Damato, T.C., Carmona-Ribeiro, A.M., Sierakowski, M.R., Petri, D.F.S., 2017. Sustainable hydroxypropyl methylcellulose/xyloglucan/gentamicin films with antimicrobial properties. Carbohydr. Polym. 165, 285–293.

Korsmeyer, R.W., Gurny, R., Doelker, E., Buri, P., Peppas, N.A., 1983. Mechanisms of solute release from porous hydrophilic polymers. Int. J. Pharm. 15, 25–35.

Koutu, V., Shastri, L., Malik, M.M., 2016. Effect of NaOH concentration on optical properties of zinc oxide nanoparticles. Mater. Sci. Pol. 34, 819–827.

Krasner, D., Kennedy, K.L., Rolstad, B.S., Roma, A.W., 1993. The ABCs of wound care dressings. Ostomy. Wound. Manage. 39, 66–68.

Krukowski, S., Karasiewicz, M., Kolodziejski, W., 2017. Convenient UV-spectrophotometric determination of citrates in aqueous solutions with applications in the pharmaceutical analysis of oral electrolyte formulations. J. Food Drug Anal. 25, 717–722.

Kumar, B.R., 2017. Application of HPLC and ESI-MS techniques in the analysis of phenolic acids and flavonoids from green leafy vegetables (GLVs). J. Pharm. Anal. 7, 349–364.

Lakshmi Prasanna, V., Rajagopalan, V., 2016. A New Synergetic Nanocomposite for Dye Degradation in Dark and Light. Sci. Rep. 6, 1–10.

Lane, M.K.M., Zimmerman, J., 2019. Controlling metal oxide nanoparticle size and shape with supercritical fluid synthesis. Green Chem. 21, 3769–3781.

Lee, Y.-P., Liu, H.-Y., Lin, P.-C., Lee, Y.-H., Yu, L.-R., Hsieh, C.-C., Shih, P.-J., Shih, W.-P., Wang, I.-J., Yen, J.-Y., 2019. Facile fabrication of superporous and biocompatible hydrogel scaffolds for artificial corneal periphery. Colloids Surfaces B Biointerfaces 175, 26–35.

Lehr, C.-M., 2000. Lectin-mediated drug delivery:: The second generation of bioadhesives. J. Control. Release 65, 19–29.

Lenzi, F., Sannino, A., Borriello, A., Porro, F., Capitani, D., Mensitieri, G., 2003. Probing the degree of crosslinking of a cellulose based superabsorbing hydrogel

through traditional and NMR techniques. Polymer (Guildf). 44, 1577–1588.

Li, H., Yang, J., Hu, X., Liang, J., Fan, Y., Zhang, X., 2011. Superabsorbent polysaccharide hydrogels based on pullulan derivate as antibacterial release wound dressing. J. Biomed. Mater. Res. Part A 98, 31–39.

Li, J., Li, Y., Dong, H., 2008. Controlled release of herbicide acetochlor from clay/ carboxylmethylcellulose gel formulations. J. Agric. Food Chem. 56, 1336–1342.

Li, W., Sun, B., Wu, P., 2009. Study on hydrogen bonds of carboxymethyl cellulose sodium film with two-dimensional correlation infrared spectroscopy. Carbohydr. Polym. 78, 454–461.

Li, Y.-S., Han, Y., Qin, J.-T., Song, Z.-Y., Cai, H.-H., Du, J.-F., Sun, S.-F., Liu, Y., 2016. Photosensitive antibacterial and cytotoxicity performances of a TiO_2/carboxymethyl chitosan/poly (vinyl alcohol) nanocomposite hydrogel by in situ radiation construction. J. Appl. Polym. Sci. 133, 44150.

Li, Y., Han, Y., Wang, X., Peng, J., Xu, Y., Chang, J., 2017. Multifunctional hydrogels prepared by dual ion cross-linking for chronic wound healing. ACS Appl. Mater. Interfaces 9, 16054–16062.

Liu, C., Wei, N., Wang, S., Xu, Y., 2009. Preparation and characterization superporous hydroxypropyl methylcellulose gel beads. Carbohydr. Polym. 78, 1–4.

Liu, P., Zhai, M., Li, J., Peng, J., Wu, J., 2002. Radiation preparation and swelling behavior of sodium carboxymethyl cellulose hydrogels. Radiat. Phys. Chem. 63, 525–528.

López-García, J., Lehocký, M., Humpolíček, P., Sáha, P., 2014. HaCaT Keratinocytes Response on Antimicrobial Atelocollagen Substrates: Extent of Cytotoxicity, Cell Viability and Proliferation. J. Funct. Biomater. 5, 43–57.

Lopez, C.G., Rogers, S.E., Colby, R.H., Graham, P., Cabral, J.T., 2015. Structure of

sodium carboxymethyl cellulose aqueous solutions: A SANS and rheology study. J. Polym. Sci. Part B Polym. Phys. 53, 492–501.

Ma, J., Li, X., Bao, Y., 2015. Advances in cellulose-based superabsorbent hydrogels. RSC Adv. 5, 59745–59757.

Ma, J., Zhang, L., Fan, B., Xu, Y., Liang, B., 2008. A novel sodium carboxymethylcellulose/poly (N-isopropylacrylamide)/Clay semi-IPN nanocomposite hydrogel with improved response rate and mechanical properties. J. Polym. Sci. Part B Polym. Phys. 46, 1546–1555.

Mahinroosta, M., Jomeh Farsangi, Z., Allahverdi, A., Shakoori, Z., 2018. Hydrogels as intelligent materials: A brief review of synthesis, properties and applications. Mater. Today Chem. 8, 42–55.

Maity, D., Mollick, M.M.R., Mondal, D., Bhowmick, B., Neogi, S.K., Banerjee, A., Chattopadhyay, S., Bandyopadhyay, S., Chattopadhyay, D., 2013. Synthesis of HPMC stabilized nickel nanoparticles and investigation of their magnetic and catalytic properties. Carbohydr. Polym. 98, 80–88.

Mandal, B., Das, D., Rameshbabu, A.P., Dhara, S., Pal, S., 2016. A biodegradable, biocompatible transdermal device derived from carboxymethyl cellulose and multi-walled carbon nanotubes for sustained release of diclofenac sodium. RSC Adv. 6, 19605–19611.

Marani, P.L., Bloisi, G.D., Petri, D.F.S., 2015. Hydroxypropylmethyl cellulose films crosslinked with citric acid for control release of nicotine. Cellulose 22, 3907–3918.

Meghana, S., Kabra, P., Chakraborty, S., Padmavathy, N., 2015. Understanding the pathway of antibacterial activity of copper oxide nanoparticles. RSC Adv. 5, 12293–12299.

Meng, F., Trivino, A., Prasad, D., Chauhan, H., 2015. Investigation and correlation of drug polymer miscibility and molecular interactions by various approaches for the preparation of amorphous solid dispersions. Eur. J. Pharm. Sci. 71, 12–24.

Mihai, M.M., Dima, M.B., Dima, B., Holban, A.M., 2019. Nanomaterials for Wound Healing and Infection Control. Materials (Basel). 12, 2176.

Mohammed, Y.H., Holmes, A., Haridass, I.N., Sanchez, W.Y., Studier, H., Grice, J.E., Benson, H.A.E., Roberts, M.S., 2019. Support for the safe use of zinc oxide nanoparticle sunscreens: lack of skin penetration or cellular toxicity after repeated application in volunteers. J. Invest. Dermatol. 139, 308–315.

Mohansrinivasan, V., Devi, C.S., Deori, M., Biswas, A., Naine, S.J., 2015. Exploring the anticancer activity of grape seed extract on skin cancer cell lines A431. Brazilian Arch. Biol. Technol. 58, 540–546.

Movassaghian, S., Barzegar-Jalali, M., Alaeddini, M., Hamedyazdan, S., Afzalifar, R., Zakeri-Milani, P., Mohammadi, G., Adibkia, K., 2011. Development of amitriptyline buccoadhesive tablets for management of pain in dental procedures. Drug Dev. Ind. Pharm. 37, 849–854.

Mujtaba, A., Kohli, K., 2016. In vitro/in vivo evaluation of HPMC/alginate based extended-release matrix tablets of cefpodoxime proxetil. Int. J. Biol. Macromol. 89, 434–441.

Mut, A.M., Vlaia, L., Coneac, G., Olariu, I., Vlaia, V., Popoiu, C., Hirjuau, M., Lupuliasa, D., 2018. Novel Topical Chitosan/Hydroxypropylmethylcellulose—Based Hydrogels Containing Fluconazole and Sucrose Esters. Formulation, Physicochemical Characterization. Vitr. Drug Release Permeation. Farm. 66, 59–69.

Namazi, H., Hasani, M., Yadollahi, M., 2019. Antibacterial oxidized starch/ZnO

nanocomposite hydrogel: Synthesis and evaluation of its swelling behaviours in various pHs and salt solutions. Int. J. Biol. Macromol. 126, 578–584.

Namazi, H., Rakhshaei, R., Hamishehkar, H., Kafil, H.S., 2016. Antibiotic loaded carboxymethylcellulose/MCM-41 nanocomposite hydrogel films as potential wound dressing. Int. J. Biol. Macromol. 85, 327–334.

Negut, I., Grumezescu, V., Grumezescu, A.M., 2018. Treatment strategies for infected wounds. Molecules 23, 1–23.

Ni, B., Liu, M., Lü, S., Xie, L., Wang, Y., 2011. Environmentally friendly slow-release nitrogen fertilizer. J. Agric. Food Chem. 59, 10169–10175.

Niaura, G., 2000. Surface-enhanced Raman spectroscopic observation of two kinds of adsorbed OH- ions at copper electrode. Electrochim. Acta 45, 3507–3519.

Nielsen, L.E., 1969. Cross-linking--effect on physical properties of polymers. J. Macromol. Sci. Part C 3, 69–103.

Ogushi, Y., Sakai, S., Kawakami, K., 2007. Synthesis of enzymatically-gellable carboxymethylcellulose for biomedical applications. J. Biosci. Bioeng. 104, 30–33.

Oliveira, R.N., Mancini, M.C., Oliveira, F.C.S. de, Passos, T.M., Quilty, B., Thiré, R.M. da S.M., McGuinness, G.B., 2016. FTIR analysis and quantification of phenols and flavonoids of five commercially available plants extracts used in wound healing. Matéria (Rio Janeiro) 21, 767–779.

Padil, V.V.T., Černík, M., 2013. Green synthesis of copper oxide nanoparticles using gum karaya as a biotemplate and their antibacterial application. Int. J. Nanomedicine 8, 889–898.

Papadimitriou, E., Buckton, G., Efentakis, M., 1993. Probing the mechanisms of swelling of hydroxypropylmethylcellulose matrices. Int. J. Pharm. 98, 57–62.

Parwe, S.P., Chaudhari, P.N., Mohite, K.K., Selukar, B.S., Nande, S.S., Garnaik, B., 2014. Synthesis of ciprofloxacin-conjugated poly (L-lactic acid) polymer for nanofiber fabrication and antibacterial evaluation. Int. J. Nanomedicine 9, 1463–1477.

Peh, K.K., Wong, C.F., 1999. Polymeric films as vehicle for buccal delivery: swelling, mechanical, and bioadhesive properties. J. Pharm. Pharm. Sci. 2, 53–61.

Pekel, N., Yoshii, F., Kume, T., Güven, O., 2004. Radiation crosslinking of biodegradable hydroxypropylmethylcellulose. Carbohydr. Polym. 55, 139–147.

Pfister, L.A., Papaloizos, M., Merkle, H.P., Gander, B., 2007. Hydrogel nerve conduits produced from alginate/chitosan complexes. J. Biomed. Mater. Res. Part A 80, 932–937.

Pinho, E., Soares, G., 2018. Functionalization of cotton cellulose for improved wound healing. J. Mater. Chem. B 6, 1887–1898.

Poonguzhali, R., Basha, S.K., Kumari, V.S., 2018. Fabrication of asymmetric nanostarch reinforced Chitosan/PVP membrane and its evaluation as an antibacterial patch for in vivo wound healing application. Int. J. Biol. Macromol. 114, 204–213.

Pooresmaeil, M., Namazi, H., 2019. Preparation and characterization of polyvinyl alcohol/β-cyclodextrin/GO-Ag nanocomposite with improved antibacterial and strength properties. Polym. Adv. Technol. 30, 447–456.

Popa, M., Bajan, N., Popa, A.A., Verestiuc, L., 2007. Novel supports based on polysaccharides for sustained-release of isosorbide dinitrate. J. Macromol. Sci. Part A Pure Appl. Chem. 44, 483–488.

Pourjavadi, A., Amini-Fazl, M.S., Ayyari, M., 2007. Optimization of synthetic conditions CMC-g-poly (acrylic acid)/Celite composite superabsorbent by

Taguchi method and determination of its absorbency under load. Express Polym. Lett. 1, 488–494.

Pourjavadi, A., Barzegar, S., Mahdavinia, G.R., 2006. MBA-crosslinked Na-Alg/CMC as a smart full-polysaccharide superabsorbent hydrogels. Carbohydr. Polym. 66, 386–395.

Pourjavadi, Ali, Ghasemzadeh, H., Soleyman, R., 2007. Synthesis, characterization, and swelling behavior of alginate-g-poly (sodium acrylate)/kaolin superabsorbent hydrogel composites. J. Appl. Polym. Sci. 105, 2631–2639.

Punnoose, A., Dodge, K., Rasmussen, J.W., Chess, J., Wingett, D., Anders, C., 2014. Cytotoxicity of ZnO nanoparticles can be tailored by modifying their surface structure: a green chemistry approach for safer nanomaterials. ACS Sustain. Chem. Eng. 2, 1666–1673.

Qiu, J., Xu, L., Peng, J., Zhai, M., Zhao, L., Li, J., Wei, G., 2007. Effect of activated carbon on the properties of carboxymethylcellulose/activated carbon hybrid hydrogels synthesized by $γ$-radiation technique. Carbohydr. Polym. 70, 236–242.

Raafat, A.I., Eid, M., El-Arnaouty, M.B., 2012. Radiation synthesis of superabsorbent CMC based hydrogels for agriculture applications. Nucl. Instruments Methods Phys. Res. Sect. B Beam Interact. with Mater. Atoms 283, 71–76.

Raho, R., Nguyen, N.-Y., Zhang, N., Jiang, W., Sannino, A., Liu, H., Pollini, M., Paladini, F., 2020. Photo-assisted green synthesis of silver doped silk fibroin/carboxymethyl cellulose nanocomposite hydrogels for biomedical applications. Mater. Sci. Eng. C 107, 110219.

Rakhshaei, R., Namazi, H., 2017. A potential bioactive wound dressing based on carboxymethyl cellulose/ZnO impregnated MCM-41 nanocomposite hydrogel.

Mater. Sci. Eng. C 73, 456–464.

Rakhshaei, R., Namazi, H., Hamishehkar, H., Kafil, H.S., Salehi, R., 2019. In situ synthesized chitosan--gelatin/ZnO nanocomposite scaffold with drug delivery properties: Higher antibacterial and lower cytotoxicity effects. J. Appl. Polym. Sci. 136, 47590.

Raucci, M G, Alvarez-Perez, M.A., Demitri, C., Giugliano, D., De Benedictis, V., Sannino, A., Ambrosio, L., 2015. Effect of citric acid crosslinking cellulose-based hydrogels on osteogenic differentiation. J. Biomed. Mater. Res. Part A 103, 2045–2056.

Roberts, D E, Mandelkern, L., 1960. The melting temperature of natural rubber networks. J. Am. Chem. Soc. 82, 1091–1095.

Roy, N., Saha, N., Kitano, T., Saha, P., 2012. Biodegradation of PVP-CMC hydrogel film: A useful food packaging material. Carbohydr. Polym. 89, 346–353.

Roy, P.S., Bhattacharya, S.K., 2014. Size-controlled synthesis, characterization and electrocatalytic behaviors of polymer-protected nickel nanoparticles: a comparison with respect to two polymers. RSC Adv. 4, 13892–13900.

Sadeghi, M., Hosseinzadeh, H., 2008. Synthesis and superswelling behavior of carboxymethylcellulose--poly (sodium acrylate-co-acrylamide) hydrogel. J. Appl. Polym. Sci. 108, 1142–1151.

Sahai, A., Goswami, N., Kaushik, S.D., Tripathi, S., 2016. Cu/Cu_2O/CuO nanoparticles: Novel synthesis by exploding wire technique and extensive characterization. Appl. Surf. Sci. 390, 974–983.

Sakai, S., Ogushi, Y., Kawakami, K., 2009. Enzymatically crosslinked carboxymethylcellulose-tyramine conjugate hydrogel: Cellular adhesiveness and feasibility for cell sheet technology. Acta Biomater. 5, 554–559.

Salama, A., El-Sakhawy, M., Kamel, S., 2016. Carboxymethyl cellulose based hybrid material for sustained release of protein drugs. Int. J. Biol. Macromol. 93, 1647–1652.

Sannino, A., Demitri, C., Madaghiele, M., 2009. Biodegradable cellulose-based hydrogels: Design and applications. Materials (Basel). 2, 353–373.

Sannino, A., Esposito, A., De Rosa, A., Cozzolino, A., Ambrosio, L., Nicolais, L., 2003. Biomedical application of a superabsorbent hydrogel for body water elimination in the treatment of edemas. J. Biomed. Mater. Res. - Part A 67, 1016–1024.

Sannino, A., Madaghiele, M., Lionetto, M.G., Schettino, T., Maffezzoli, A., 2006. A cellulose-based hydrogel as a potential bulking agent for hypocaloric diets: An in Vitro biocompatibility study on rat intestine. J. Appl. Polym. Sci. 102, 1524–1530.

Sannino, A, Nicolais, L., 2005. Concurrent effect of microporosity and chemical structure on the equilibrium sorption properties of cellulose-based hydrogels. Polymer (Guildf). 46, 4676–4685.

Sannino, A., Pappada, S., Giotta, L., Valli, L., Maffezzoli, A., 2007. Spin coating cellulose derivatives on quartz crystal microbalance plates to obtain hydrogel-based fast sensors and actuators. J. Appl. Polym. Sci. 106, 3040–3050.

Sannino, A, Pappadà, S., Madaghiele, M., Maffezzoli, A., Ambrosio, L., Nicolais, L., 2005. Crosslinking of cellulose derivatives and hyaluronic acid with water-soluble carbodiimide. Polymer (Guildf). 46, 11206–11212.

Sarkar, D.J., Singh, A., 2017. Base triggered release of insecticide from bentonite reinforced citric acid crosslinked carboxymethyl cellulose hydrogel composites. Carbohydr. Polym. 156, 303–311.

Sarkar, D.J., Singh, A., Gaur, S.R., Shenoy, A. V., 2016. Viscoelastic properties of

borax loaded CMC-g-cl-poly(AAm) hydrogel composites and their boron nutrient release behavior. J. Appl. Polym. Sci. 133, 1–11.

Shafiq, M., Yasin, T., Aftab Rafiq, M., 2014. Structural, thermal, and antibacterial properties of chitosan/ZnO composites. Polym. Compos. 35, 79–85.

Shahbazi, M., Ahmadi, S.J., Seif, A., Rajabzadeh, G., 2016. Carboxymethyl cellulose film modification through surface photo-crosslinking and chemical crosslinking for food packaging applications. Food Hydrocoll. 61, 378–389.

Sharma, P.K., Dutta, R.K., Kumar, M., Singh, P.K., Pandey, A.C., Singh, V.N., 2011. Highly stabilized monodispersed citric acid capped ZnO:Cu2+ nanoparticles: Synthesis and characterization for their applications in white light generation from UV LEDs. IEEE Trans. Nanotechnol. 10, 163–169.

Shen, X., Shamshina, J.L., Berton, P., Gurau, G., Rogers, R.D., 2015. Hydrogels based on cellulose and chitin: Fabrication, properties, and applications. Green Chem. 18, 53–75.

Shi, R., Bi, J., Zhang, Z., Zhu, A., Chen, D., Zhou, X., Zhang, L., Tian, W., 2008. The effect of citric acid on the structural properties and cytotoxicity of the polyvinyl alcohol/starch films when molding at high temperature. Carbohydr. Polym. 74, 763–770.

Shokri, J., Adibkia, K., 2013. Application of cellulose and cellulose derivatives in pharmaceutical industries, in: Cellulose-Medical, Pharmaceutical and Electronic Applications. IntechOpen.

Siddiqi, K.S., ur Rahman, A., Husen, A., 2018. Properties of zinc oxide nanoparticles and their activity against microbes. Nanoscale Res. Lett. 13, 141.

Siddiqui, H., Qureshi, M.S., Haque, F.Z., 2014. One-step, template-free hydrothermal synthesis of CuO tetrapods. Optik (Stuttg). 125, 4663–4667.

Siepmann, J., Peppas, N.A., 2012. Modeling of drug release from delivery systems based on hydroxypropyl methylcellulose (HPMC). Adv. Drug Deliv. Rev. 64, 163–174.

Singh, B., Dhiman, A., 2016. Design of Acacia gum-carbopol-cross-linked-polyvinylimidazole hydrogel wound dressings for antibiotic/anesthetic drug delivery. Ind. Eng. Chem. Res. 55, 9176–9188.

Singla, R., Soni, S., Patial, V., Kulurkar, P.M., Kumari, A., Mahesh, S., Padwad, Y.S., Yadav, S.K., 2017. In vivo diabetic wound healing potential of nanobiocomposites containing bamboo cellulose nanocrystals impregnated with silver nanoparticles. Int. J. Biol. Macromol. 105, 45–55.

Sirelkhatim, A., Mahmud, S., Seeni, A., Kaus, N.H.M., Ann, L.C., Bakhori, S.K.M., Hasan, H., Mohamad, D., 2015. Review on zinc oxide nanoparticles: Antibacterial activity and toxicity mechanism. Nano-Micro Lett. 7, 219–242.

Smith, A.M., Moxon, S., Morris, G.A., 2016. Biopolymers as wound healing materials. Wound Heal. Biomater. 2, 261–287.

Sotiriou, G.A., Watson, C., Murdaugh, K.M., Darrah, T.H., Pyrgiotakis, G., Elder, A., Brain, J.D., Demokritou, P., 2014. Engineering safer-by-design silica-coated ZnO nanorods with reduced DNA damage potential. Environ. Sci. Nano 1, 144–153.

Straccia, M.C., D'Ayala, G.G., Romano, I., Laurienzo, P., 2015. Novel zinc alginate hydrogels prepared by internal setting method with intrinsic antibacterial activity. Carbohydr. Polym. 125, 103–112.

Straccia, M.C., Romano, I., Oliva, A., Santagata, G., Laurienzo, P., 2014. Crosslinker effects on functional properties of alginate/N-succinylchitosan based hydrogels. Carbohydr. Polym. 108, 321–330.

Svintsitskiy, D.A., Chupakhin, A.P., Slavinskaya, E.M., Stonkus, O.A., Stadnichenko,

A.I., Koscheev, S. V., Boronin, A.I., 2013. Study of cupric oxide nanopowders as efficient catalysts for low-temperature CO oxidation. J. Mol. Catal. A Chem. 368–369, 95–106.

Swanzy, J., 2017. Zinc oxide complexes, U.S. Patent 9,657,036.

Taguri, T., Tanaka, T., Kouno, I., 2006. Antibacterial spectrum of plant polyphenols and extracts depending upon hydroxyphenyl structure. Biol. Pharm. Bull. 29, 2226–2235.

Tan, Y.M., Lim, S.H., Tay, B.Y., Lee, M.W., Thian, E.S., 2015. Functional chitosan-based grapefruit seed extract composite films for applications in food packaging technology. Mater. Res. Bull. 69, 142–146.

Tang, H., Chen, H., Duan, B., Lu, A., Zhang, L., 2014. Swelling behaviors of superabsorbent chitin/carboxymethylcellulose hydrogels. J. Mater. Sci. 49, 2235–2242.

Thanh, N.T.K., Maclean, N., Mahiddine, S., 2014. Mechanisms of nucleation and growth of nanoparticles in solution. Chem. Rev. 114, 7610–7630.

Tran, T.H., Okabe, H., Hidaka, Y., Hara, K., 2017. Removal of metal ions from aqueous solutions using carboxymethyl cellulose/sodium styrene sulfonate gels prepared by radiation grafting. Carbohydr. Polym. 157, 335–343.

Ullah, F., Othman, M.B.H., Javed, F., Ahmad, Z., Akil, H.M., 2015. Classification, processing and application of hydrogels: A review. Mater. Sci. Eng. C 57, 414–433.

Venkatesha, N.J., Ramesh, S., 2018. Citric acid-assisted synthesis of nanoparticle copper catalyst supported on an oxide system for the reduction of furfural to furfuryl alcohol in the vapor phase. Ind. Eng. Chem. Res. 57, 1506–1515.

Vijayakumar, V., Samal, S.K., Mohanty, S., Nayak, S.K., 2019. Recent advancements

in biopolymer and metal nanoparticle-based materials in diabetic wound healing management. Int. J. Biol. Macromol. 122, 137–148.

Wach, R.A., Mitomo, H., Nagasawa, N., Yoshii, F., 2003. Radiation crosslinking of carboxymethylcellulose of various degree of substitution at high concentration in aqueous solutions of natural pH. Radiat. Phys. Chem. 68, 771–779.

Wach, R.A., Mitomo, H., Yoshii, F., Kume, T., 2001. Hydrogel of biodegradable cellulose derivatives. II. Effect of some factors on radiation-induced crosslinking of CMC. J. Appl. Polym. Sci. 81, 3030–3037.

Wang, L., Dong, W., Xu, Y., 2007a. Synthesis and characterization of hydroxypropyl methylcellulose and ethyl acrylate graft copolymers. Carbohydr. Polym. 68, 626–636.

Wang, M., Xu, L., Hu, H., Zhai, M., Peng, J., Nho, Y., Li, J., Wei, G., 2007b. Radiation synthesis of PVP/CMC hydrogels as wound dressing. Nucl. Instruments Methods Phys. Res. Sect. B Beam Interact. with Mater. Atoms 265, 385–389.

Wang, W., Liu, Z., Liu, Y., Xu, C., Zheng, C., Wang, G., 2003. A simple wet-chemical synthesis and characterization of CuO nanorods. Appl. Phys. A 76, 417–420.

Wang, Y., Shi, X., Wang, W., Wang, A., 2013. Synthesis, characterization, and swelling behaviors of a pH-responsive CMC-g-poly(AA-co-AMPS) superabsorbent hydrogel. Turkish J. Chem. 37, 149–159.

Welch, C.M., 1988. Tetracarboxylic Acids as Formaldehyde-Free Durable Press Finishing Agents: Part I: Catalyst, Additive, and Durability Studies. Text. Res. J. 58, 480–486.

Wen, X., Bao, D., Chen, M., Zhang, A., Liu, C., Sun, R., 2015. Preparation of CMC/HEC Crosslinked Hydrogels for Drug Delivery. BioResources 10, 8339–8351.

Weng, L., Zhang, L., Ruan, D., Shi, L., Xu, J., 2004. Thermal gelation of cellulose in a NaOH/thiourea aqueous solution. Langmuir 20, 2086–2093.

Wongrakpanich, A., Mudunkotuwa, I.A., Geary, S.M., Morris, A.S., Mapuskar, K.A., Spitz, D.R., Grassian, V.H., Salem, A.K., 2016. Size-dependent cytotoxicity of copper oxide nanoparticles in lung epithelial cells. Environ. Sci. Nano 3, 365–374.

Wu, Z., Yang, H., Archana, G., Rakshit, M., Ng, K.W., Tay, C.Y., 2018. Human keratinocytes adapt to ZnO nanoparticles induced toxicity via complex paracrine crosstalk and Nrf2-proteasomal signal transduction. Nanotoxicology 12, 1215–1229.

Xiao, C., Li, H., Gao, Y., 2009. Preparation of fast pH-responsive ferric carboxymethylcellulose/poly(vinyl alcohol) double-network microparticles. Polym. Int. 58, 112–115.

Xiao, J., Chen, S., Yi, J., Zhang, H.F., Ameer, G.A., 2017. A Cooperative Copper Metal–Organic Framework-Hydrogel System Improves Wound Healing in Diabetes. Adv. Funct. Mater. 27.

Yadollahi, M., Namazi, H., Aghazadeh, M., 2015. Antibacterial carboxymethyl cellulose/Ag nanocomposite hydrogels cross-linked with layered double hydroxides. Int. J. Biol. Macromol. 79, 269–277.

Yang, C.Q., 1993. Effect of pH on nonformaldehyde durable press finishing of cotton fabric: FT-IR spectroscopy study: Part I: Ester crosslinking. Text. Res. J. 63, 420–430.

Yang, C.Q., Wang, X., 1996. Formation of cyclic anhydride intermediates and esterification of cotton cellulose by multifunctional carboxylic acids: An infrared spectroscopy study. Text. Res. J. 66, 595–603.

Yu, J., Yang, G., Li, Y., Yang, W., Gao, J., Lu, Q., 2014. Synthesis, Characterization,

and swelling behaviors of acrylic acid/carboxymethyl cellulose superabsorbent hydrogel by glow-discharge electrolysis plasma. Polym. Eng. Sci. 54, 2310–2320.

Zare-Akbari, Z., Farhadnejad, H., Furughi-Nia, B., Abedin, S., Yadollahi, M., Khorsand-Ghayeni, M., 2016a. PH-sensitive bionanocomposite hydrogel beads based on caborboxymethyl cellulose/ZnO nanoparticle as drug carrier. Int. J. Biol. Macromol. 93, 1317–1327.

Zarrindokht Emami-Karvani, 2012. Antibacterial activity of ZnO nanoparticle on Gram-positive and Gram-negative bacteria. African J. Microbiol. Res. 5, 1368–1373.

Zhang, H., Zhai, D., He, Y., 2014. Graphene oxide/polyacrylamide/carboxymethyl cellulose sodium nanocomposite hydrogel with enhanced mechanical strength: Preparation, characterization and the swelling behavior. RSC Adv. 4, 44600–44609.

Zhang, J., Xu, Y., Liu, T., Min, J., Ma, Y., Song, Y., Lu, J., Mi, W., Wang, Y., Li, H., 2019. In vivo construction of lymphoid node by implantation of adipose-derived stromal cells with hydroxypropyl methyl cellulose hydrogel in BALB/c nude mice. Organogenesis 15, 85–99.

Zhong, Y., Wang, J., Yuan, Z., Wang, Y., Xi, Z., Li, L., Liu, Z., Guo, X., 2019. A mussel-inspired carboxymethyl cellulose hydrogel with enhanced adhesiveness through enzymatic crosslinking. Colloids Surfaces B Biointerfaces 179, 462–469.

Appendix

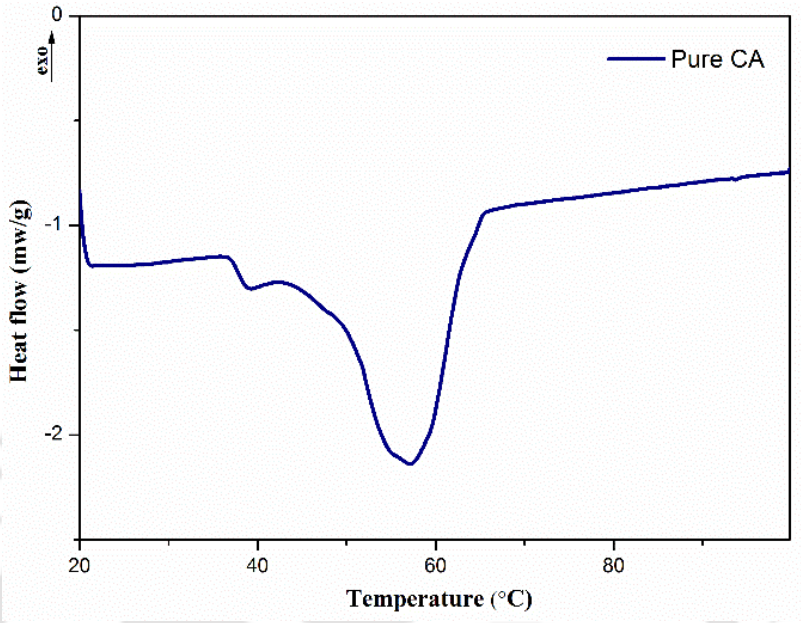

Figure A1. DSC curve of pure citric acid (CA).

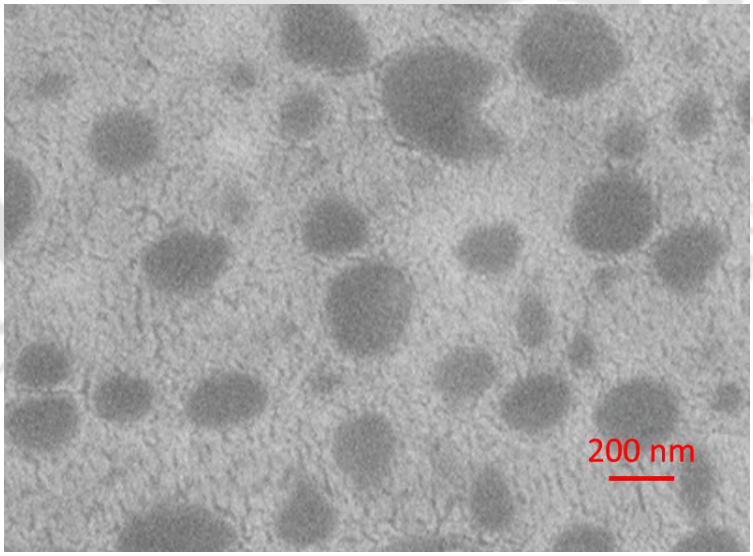

Figure A2. The presence of nanopores at higher magnifications (50 KX) for cryofixed NaCMC-HPMC/20% CA hydrogel films.

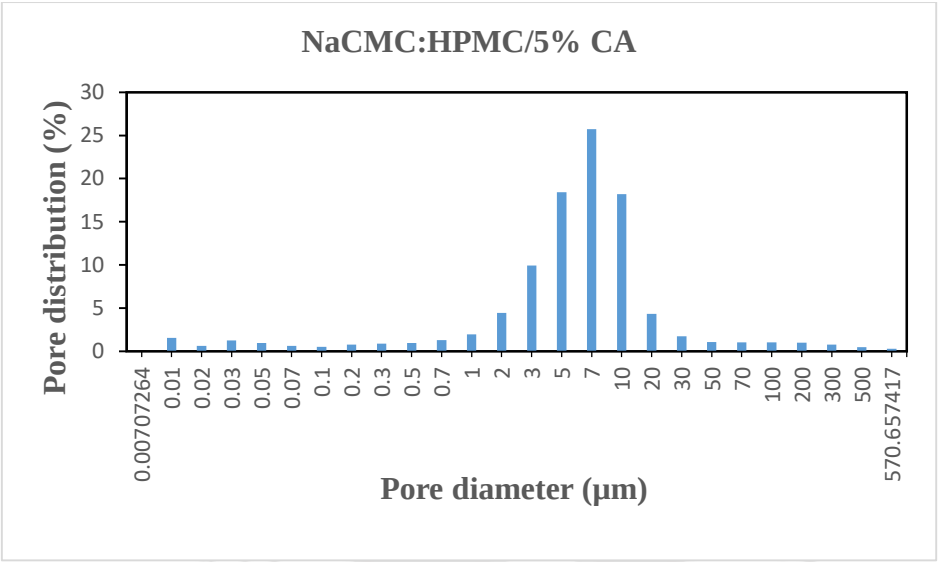

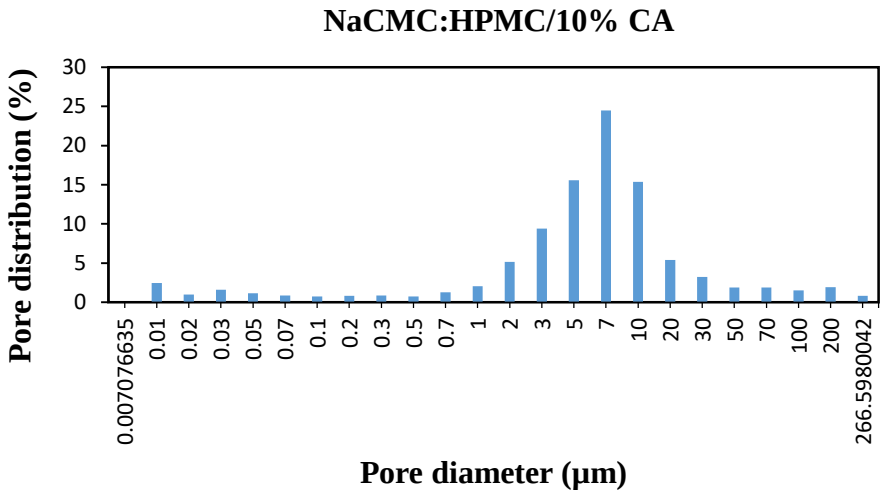

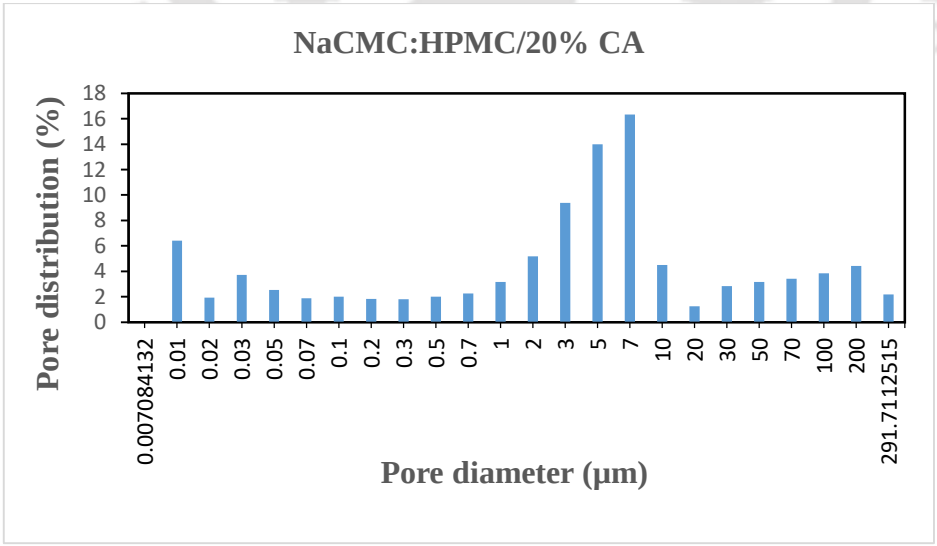

Figure A3. The pore distribution (%) vs. pore diameter (µm) of CA crosslinked hydrogel films.

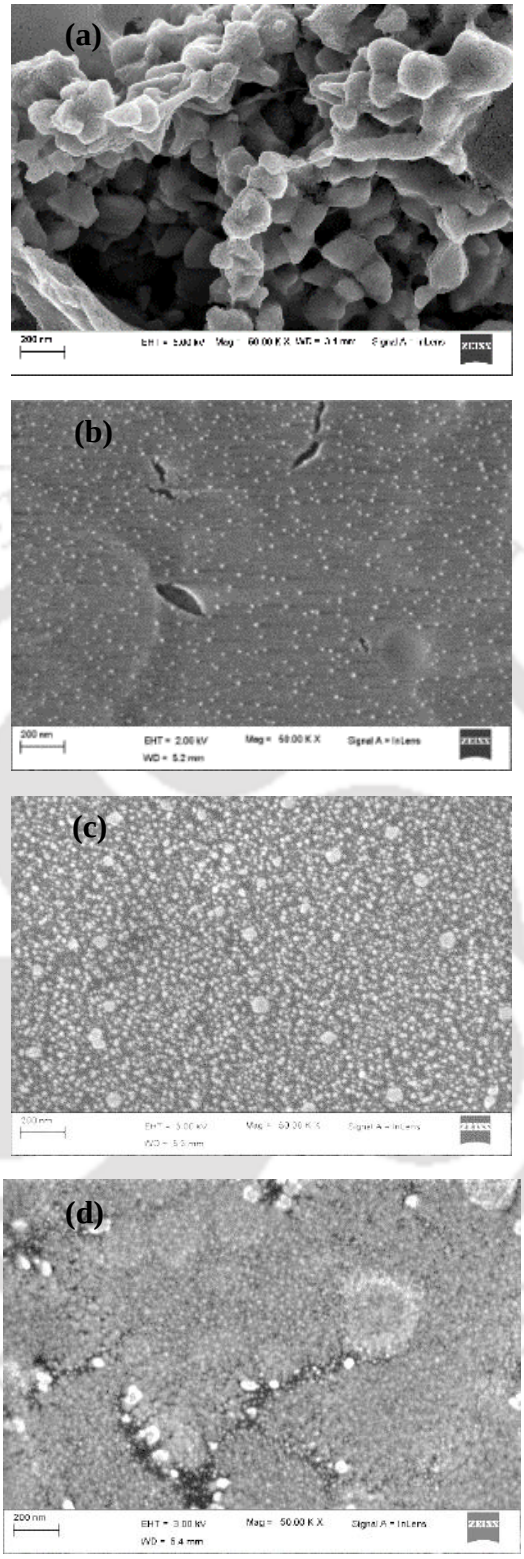

Figure A4. FESEM images of extracted nanoparticles from NaCMC-HPMC-ZnO hydrogel films of (a) control, and crosslinked with (b) 5% CA (c) 10% CA and (d) 20% CA at a magnification of 50KX (a-d).

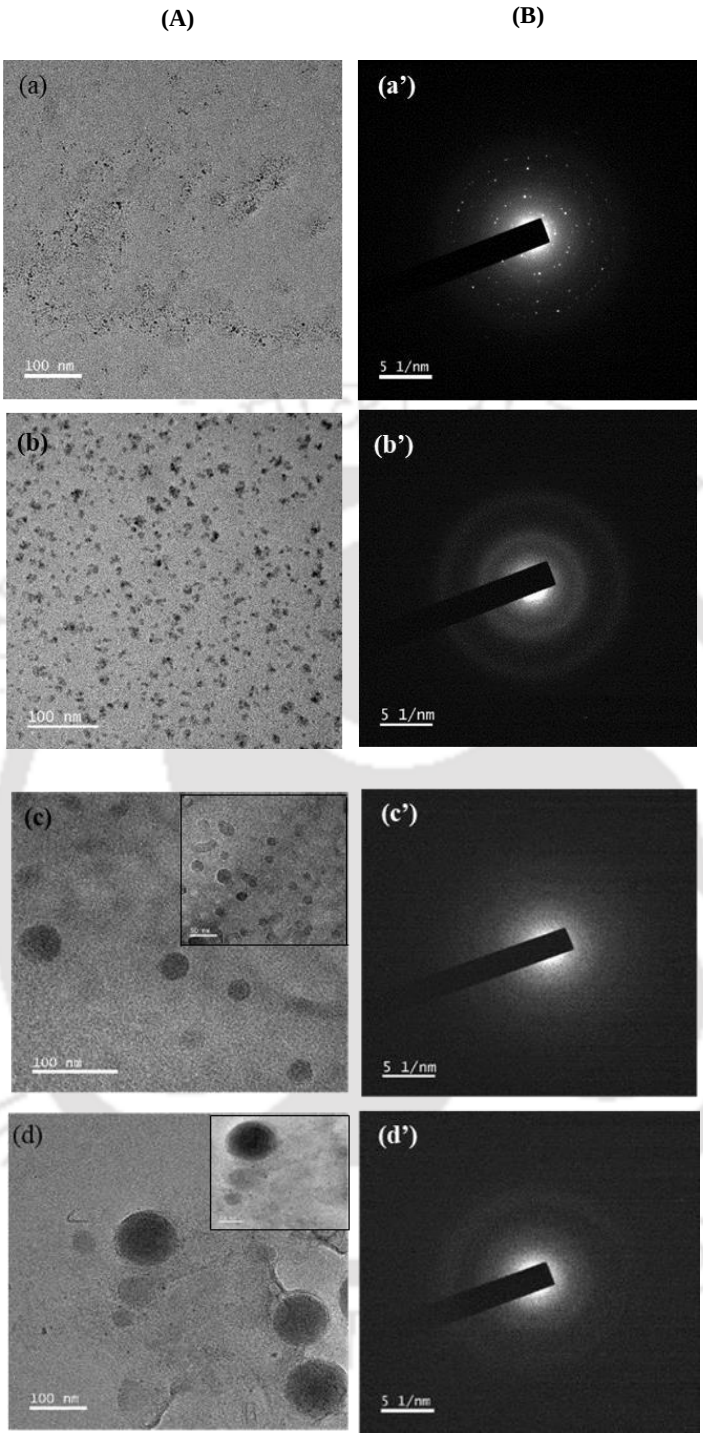

Figure A5. (A) FETEM images, (B) SAED of different weight ratios of ZnO NPs and citric acid (a, a') 1:1 (b, b") 1:2 (c, c') 1:4 (d, d') 1:8. Inset figure shows higher magnifications at 50 nm.

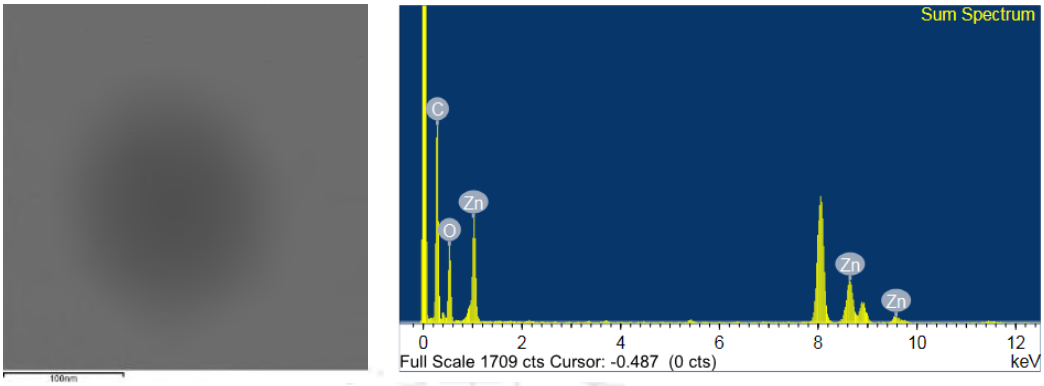

Elem...	Weight%	Atomic%
C K	59.61	76.35
O K	19.48	18.73
Zn K	20.91	4.92
Totals	100.00	

Figure A6. EDX spectra of 1:4 weight ratios of ZnO NPs and citric acid by FETEM.

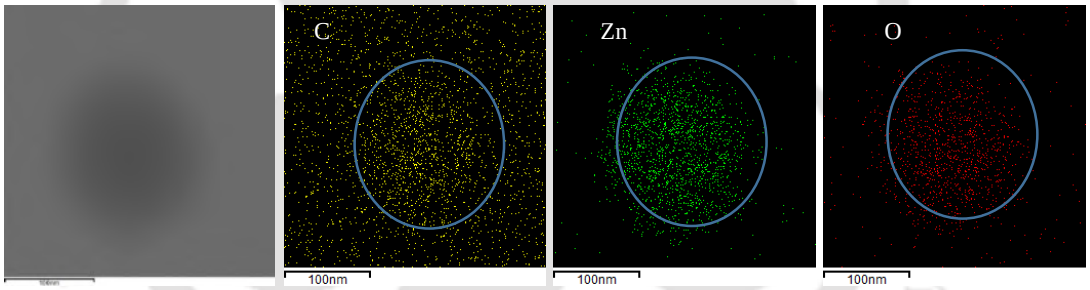

Figure A7. Elemental mapping of 1:4 weight ratios of ZnO NPs and citric acid by FETEM.

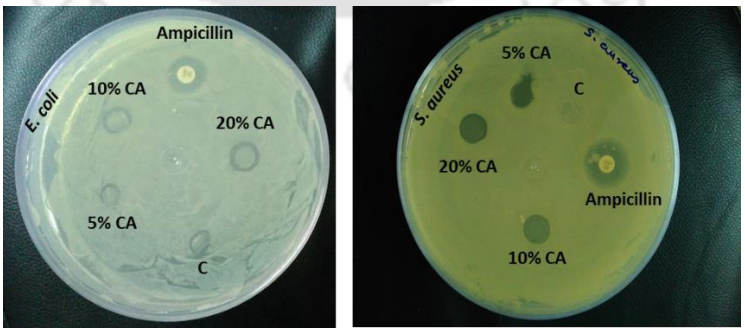

Figure A8. Zone of inhibition of control films and CA crosslinked films against *E. coli* and *S. aureus.*

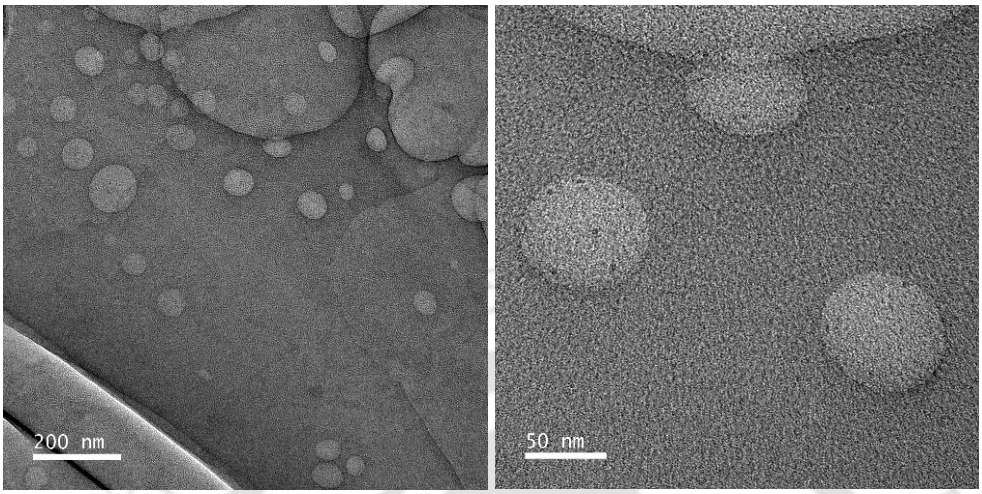

Figure A9. FETEM images of polymer nanospheres of NaCMC-HPMC-ZnO/5% CA at different magnifications.

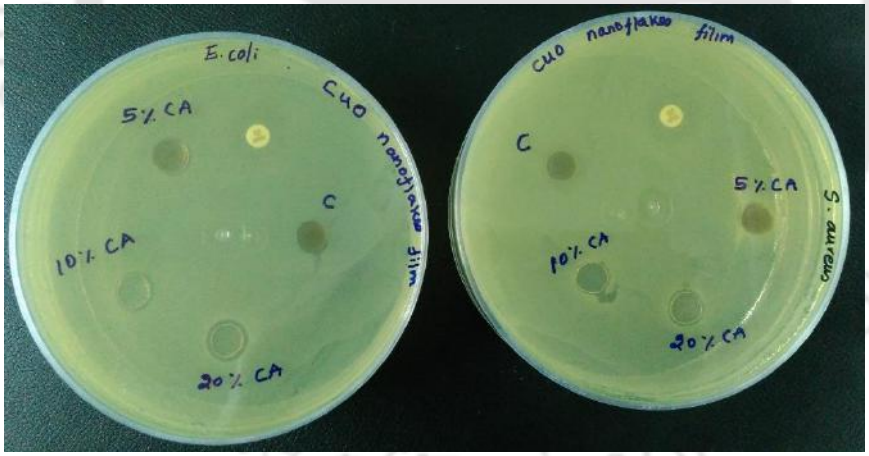

Figure A10. Zone of inhibition of control films and different citric acid (CA) concentrations (5-20%) for *S. aureus* and *E. coli.*

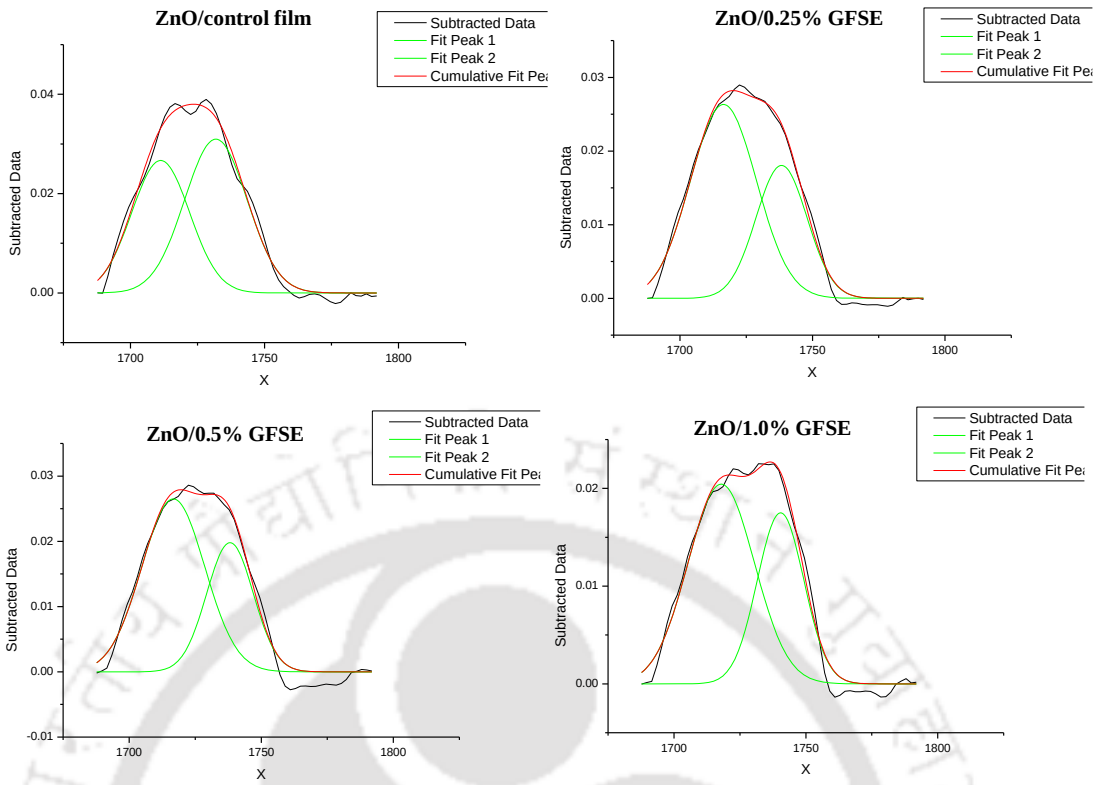

Figure A11. FTIR peak fitting from 1680-1790 cm^{-1} for ester bond.

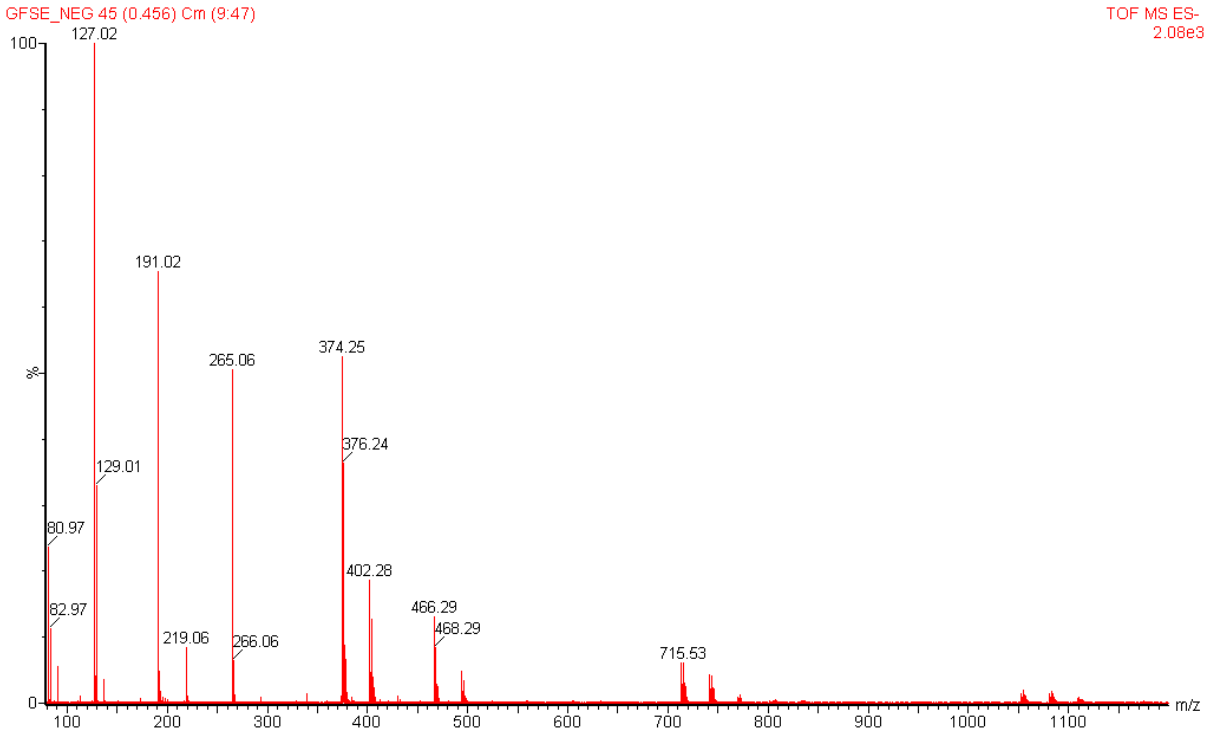

Figure A12. ESI-Q-TOF-MS profiles of GFSE at negative ion mode. The precursor m/z of citric acid and monoglycerides was observed at m/z of 190.99 and 265.03, respectively.

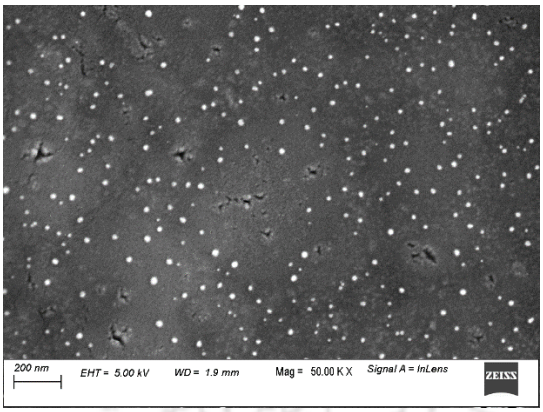

Figure A13. NaCMC-HPMC hydrogel films incorporated with 0.25% GFSE (v/v) without addition of ZnO and citric acid.

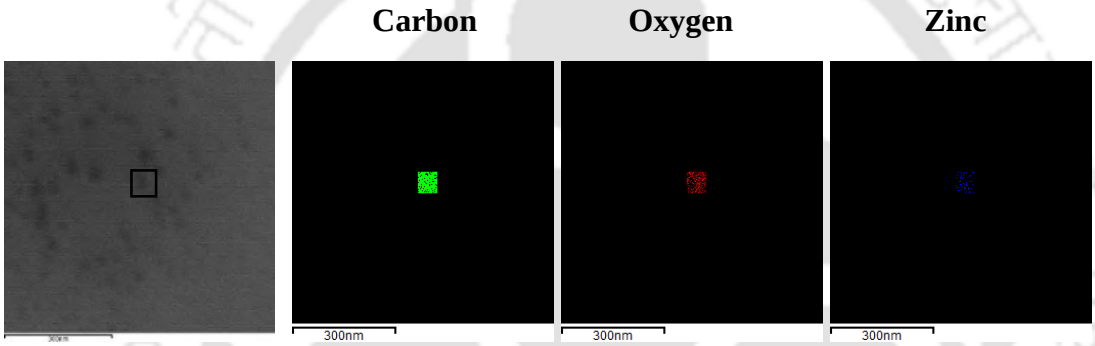

Figure A14. Elemental mapping of zinc oxide complex by FETEM-EDX

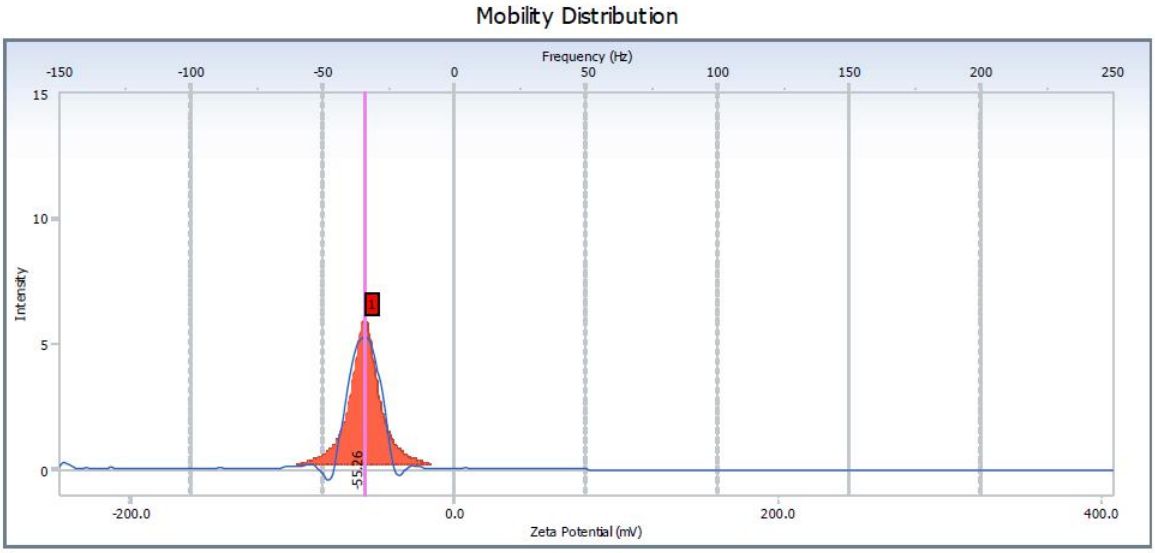

Figure A15. Zeta potential of nanoparticles leached out from 1% GFSE nanocomposite films in water.

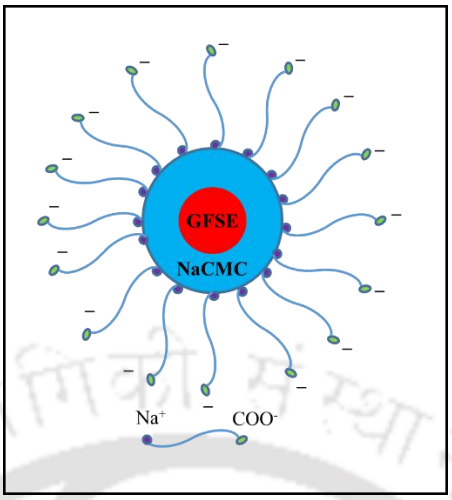

Figure A16. Possible micelle (nanoparticle) structure.

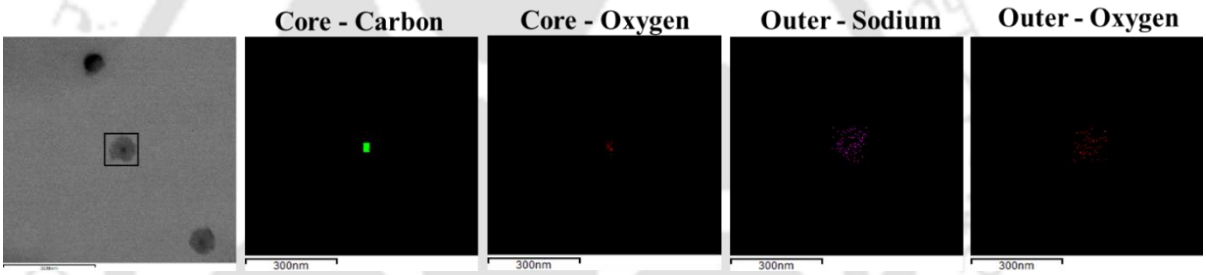

Figure A17. Elemental mapping of a micelle by FETEM-EDX.

Table A1. FTIR absorption bands assignment to the ester region (1680-1790 cm^{-1}) of ZnO/control films and various GFSE incorporated hydrogel films.

Sample name	Peak 1 (carboxylic group)		Peak 2 (ester bond)	
	λ (cm^{-1})	Absorption	λ (cm^{-1})	Absorption
ZnO/control film	1711.27599	0.02667	1731.85808	0.03096
ZnO/0.25% GFSE	1716.41108	0.02632	1737.32415	0.01804
ZnO/0.5% GFSE	1716.71121	0.0265	1738.17793	0.01979
ZnO/1.0% GFSE	1717.90781	0.02043	1740.42407	0.0175

List of Publications based on thesis

1. **K. Dharmalingam** and R. Anandalakshmi, Functionalization of cellulose-based hydrogel films with zinc oxide complex and grapefruit seed extract for potential applications in treating chronic wounds, Polymer, 202, (2020), 122620.

2. **K. Dharmalingam**, Devivasha Bordoloi, Ajaikumar B. Kunnumakkara and R. Anandalakshmi, Preparation and characterization of cellulose-based nanocomposite hydrogel films containing CuO/Cu2O/Cu with antibacterial activity, Journal of Applied Polymer Science, 137, (2020), e49216.

3. **K. Dharmalingam**, Devivasha Bordoloi, Ajaikumar B. Kunnumakkara and R. Anandalakshmi, Formation and characterization of zinc oxide complexes in composite hydrogel films for potential wound healing applications, Polymer Composites, (2020), 41, 2274-2287.

4. Aditya Koneru, **K. Dharmalingam*** and R. Anandalakshmi, Cellulose based nanocomposite hydrogel films consisting of sodium carboxymethylcellulose – grapefruit seed extract nanoparticles for potential wound healing applications. International Journal of Biological Macromolecules, 148 (2020) 833-842. (*****Equal contribution).

5. **K. Dharmalingam** and R. Anandalakshmi, Fabrication, characterization and drug loading efficiency of citric acid crosslinked NaCMC-HPMC hydrogel films for wound healing drug delivery applications, International Journal of Biological Macromolecules, 134 (2019) 815-829.

6. Abhishek Roy, **K. Dharmalingam**, Aaro Idhayan and R. Anandalakshmi, Recent advancements in preparation and application of CMC-based hydrogels: A review (Under review).

7. Abhishek Roy, **K. Dharmalingam** and R. Anandalakshmi, Studies on structural intricacies of citric acid binding with ZnO nanoparticles and CuO nanoflakes using isothermal titration calorimetry (Submitted).

Other publications

1. **K. Dharmalingam**, R. Anandalakshmi and Shashank Shekhar, Microwave-induced solid dispersion of curcumin in HPMC matrix using water as hydration carrier, Journal of Dispersion Science and Technology, (2020), Accepted (in press): https://doi.org/ 10.1080/01932691.2020.1770608.

2. Pankaj Jha, **K. Dharmalingam**, Takahisa Nishizu, Nakako Katsuno, R. Anandalakshmi, Effect of amylose-amylopectin ratios on physical, mechanical and thermal properties of starch based bionanocomposite films incorporated with CMC and nanoclay, Starch-Stärke (2019) 1900121.

3. **K. Dharmalingam**, Ganesan Padmavathi, Ajaikumar B. Kunnumakkara, R. Anandalakshmi, Microwave-assisted synthesis of cellulose/zinc-sulfate-calcium-phosphate (ZSCAP) nanocomposites for biomedical applications, Materials Science & Engineering C 100 (2019) 535–543.

4. **K. Dharmalingam**, D. Pamu, R. Anandalakshmi, Comparison of solid state synthesis of zinc calcium phosphorous oxide (ZCAP) ceramics under conventional and microwave heating methods, Materials Letters 212 (2018) 207–210.

5. Abshar Hasan, Gyan Waibhaw, Sakshi Tiwari, **K. Dharmalingam**, I. Shukla and Lalit M. Pandey, Fabrication and characterization of chitosan, polyvinylpyrrolidone, and cellulose nanowhiskers nanocomposite films for wound healing drug delivery application, Journal of Biomedical Materials Research Part A (2017) 105A 2391–2404.

6. Jahnu Saikia, **K. Dharmalingam**, Venugopal T Bhat, Vibin Ramakrishnan, Electric field modulation of supramolecular assembly of catalytic peptides with high enantioselectivity (under preparation).

7. Vivek Prakash, Sajitha Sasidharan, **K. Dharmalingam**, Vibin Ramakrishnan, Biodegradable alternatives for heavy metal sequestration (Under preparation).

Book Chapter

1. **K. Dharmalingam**, R. Anandalakshmi, Polysaccharide Based Films for Food Packaging Applications. In: *Advances in Sustainable Polymers: Processing and Applications*, Springer, Singapore, (2019) 183-207.

2. **K. Dharmalingam**, Abhishek Roy, R. Anandalakshmi, Essential oil in Active Food Packaging System. In: *Biopolymer-Based Food Packaging: Innovations and Technology Applications*, John Wiley & Sons, Inc. (Submitted).
3. Abhishek Roy, **K. Dharmalingam**, R. Anandalakshmi, Silver and ZnO Nanoparticles in Food Packaging. In: *Biopolymer-Based Food Packaging: Innovations and Technology Applications*, John Wiley & Sons, Inc. (Submitted).

Conference Proceedings

1. Mrinal Bhowmik, Sayan Halder, **K. Dharmalingam**, R. Anandalakshmi, P. Muthukumar, Evaluation of Thermo-Kinetic and Absorption Characteristics of Pure Desiccants and Desiccant Mixtures, 10th International Conference on Materials Processing and Characterizations (ICMPC-2020), February 21- 23, 2020. Accepted in Materials Today: Proceedings. https://doi.org/10.1016/j.matpr.2020.02.430.

2. **K. Dharmalingam** and R. Anandalakshmi**,** Influence of Citric acid on NaCMC-HPMC-ZnO Hydrogel Films for Wound Healing Applications, International Conference on Advanced Materials Research (AMRC 2019), September 26-27, 2019, National University of Singapore, Singapore.

3. **K. Dharmalingam** and R. Anandalakshmi, Solid dispersion of quercetin in HPMC matrix by microwave irradiation, Sophisticated Instruments in Modern Research, ICSIMR-2017, June 30 – July 1, 2017, Indian Institute of Technology Guwahati, India.

4. **K. Dharmalingam** and R. Anandalakshmi, Rapid microwave-assisted synthesis and characterization of zinc sulfate calcium phosphate/cellulose bionanocomposites, International Conference on Nanoscience and Technology (ICONSAT 2016), Feb 29 – March 2, 2016, IISER-Pune.

DOCTORAL COMMITTEE

Chairman: Prof. G. Pugazhenthi, Department of Chemical Engineering

Advisor: Dr. R. Anandalakshmi, Department of Chemical Engineering

Members: Dr. Partho Sarathi Gooh Pattader, Department of Chemical Engineering

Dr. S. Senthilkumar, Department of Biosciences and Bioengineering